C.P. No. 901

C.P. No. 901

MINISTRY OF AVIATION

AERONAUTICAL RESEARCH COUNCIL

CURRENT PAPERS

A Survey of Unsteady Hypersonic Flow Problems

By

B. M. Wood

LONDON: HER MAJESTY'S STATIONERY OFFICE

1966

Price £1 6s. 6d. net

C.P. No.901*

March, 1965

A Survey of Unsteady Hypersonic Flow Problems

- By -
B. M. Wood

SUMMARY

After giving general information on hypersonic flows, flight conditions and vehicles, the report reviews work on the analysis of unsteady hypersonic flows, analytical studies of the dynamic stability of hypersonio vehicles, and experimental and analytical work on flutter at hypersonic speeds. On this basis it then examines the need for research and suggests lines that research should follow.

The chief conclusion is that the quasi-steady analysis of unsteady hypersonic flows may be adequate for the practical purposes of dynamic stability and flutter analysis. It is suggested that research should be directed to finding the degree of inaccuracy involved in quasi-steady estimates of the unsteady aerodynamic forces, and the sensitivity of dynamic stability and flutter analyses to inaccuracies in these forces.

In structure, the report consists of the general survey and conclusions, together with a number of Appendices which review various aspects in detail and which give the information and references on which the statements in the general survey are based.

CONTENTS/

---

*Replaces N.P.L. Aero Memo. 19 - A.R.C.26 757
Some of the statements in this document may be of a tentative character, and the paper does not necessarily carry the authority of the Aerodynamics Division, N.P.L.

CONTENTS

APPENDICES

Detailed Reviews

4.2.1/

C O N T E N T S (Contd.)

Introduction

This report is concerned with hypersonic flows around bodies undergoing pitching and plunging oscillations and around bodies or parts of bodies undergoing flutter. It brings together information on the methods of analysis applicable to these unsteady flows, and on the practical problems of dynamic stability and flutter of hypersonic vehicles where an understanding of such flows may be needed. It is intended that the report should give a basis for the planning of research and some conclusions are drawn from the information presented about the kind of work which would be of value or of interest.

The report is divided into a general survey and four Appendices, which give detailed information and references. The first of the Appendices gives some background information on hypersonic flows, flight conditions, and vehicles, and the other three are reviews of particular fields of work - the theoretical analysis of unsteady hypersonic flows; analytical studies of the dynamic stability of hypersonic vehicles in level flight, and the oscillatory behaviour of vehicles in re-entry or exit trajectories; and information from experimental and analytical studies of flutter at hypersonic speeds.

The general survey, which forms the first part of the document, summarises the information given in the Appendices, and presents general conclusions about the kinds of research work that should be considered. If detailed information, and evidence for the conclusions are not required, only the first part needs to be read (i.e., pp. 3-9).

General/

General Survey and Conclusions

Theoretical and experimental investigations of unsteady flows have formed an important part of aerodynamic research at subsonic and supersonic speeds - principally because of the need to calculate the forces due to unsteady flows around bodies or parts of bodies for analyses of the dynamic stability or flutter of aircraft. Vehicles are already flying at hypersonic speeds for short periods on re-entering the atmosphere from ballistic or orbital flights, and there are possible extensions to more controllable re-entry vehicles and to aircraft which will cruise at hypersonic speeds. These developments have already led to some investigations of unsteady flow at hypersonic speeds; but changes in the fluid dynamic characteristics, together with differences in the flight conditions and the forms of the vehicles from those designed for flight at lower speeds make it difficult to decide what kinds of investigation would be most relevant or fruitful. Because of this, when it was decided that the Helium Tunnel at the National Physical Laboratory would be suitable for the study of unsteady flows at hypersonic speeds, it seemed important to review the information at present available to provide a basis for the planning of a research programme.

1. Hypersonic Flight Conditions

There is no clear boundary marking the change from flow at high supersonic speeds to flow at hypersonic speeds; instead there is a growth in the importance of certain features of the flow which are of negligible importance or are absent at supersonic speeds. Some of these features arise from the "fluid dynamic" behaviour of the gas and are related to the high Mach number, and others arise from the fact that the gas has a high velocity and large energy.

A Mach number of about five is usually taken as marking the lower boundary of the hypersonic flow regime. As the Mach number increases above five different approximate solutions of the flow equations become necessary because, in general, linearisation of the equations is no longer possible, potential flow can no longer be assumed, and the thickness and rate of change of thickness of boundary layers lead to problems arising from the interaction of the boundary layer with the external flow. When the flow velocity is large (IO 000 fps), because of the large energy of the flow, high temperatures are generated at stagnation points or when the gas is decelerated in passing through shock waves, and problems arise from the excitation of vibrational modes of polyatomic gas molecules, dissociation and ionisation, and the ideal gas conditions no longer apply.

The forms of vehicle used for flight at hypersonic speed bring new theoretical problems throughout the speed range but these problems can be most acute for hypersonic conditions. There are two main kinds of flight operation - re-entry from orbit or from space and cruising flight at hypersonic speeds, and different types of vehicle are used for each. In re-entry flight the vehicle must dissipate the large amount of energy which it has when it first enters the atmosphere and, at present, it seems likely to have the form of a bluff body, or a slender blunted body with a large drag and a lift/drag ratio around unity. For cruising conditions the vehicle can be designed for efficient lifting flight, and it may have the form of a very slender wing/body combination or a slender lifting body. Analysis must deal, then, with-the flow around bluff bodies and with interaction effects between surfaces on the wing/body combinations. It must also deal with slender bodies with blunted noses and lifting surfaces of thin section with blunt leading edges, because noses or leading edges that are

effectively/

effectively sharp at hypersonic Mach numbers are difficult to make and give rise to very severe heating problems.

2. The Analysis of Unsteady Hypersonic Flows

All analyses of unsteady hypersonic flows assume that the physical and chemical effects of high temperatures in real gases and the flow changes that result from them can be calculated on a quasi-steady basis after the unsteady flow for an ideal gas has been found. The analyses also assume, in the usual way, that the flow can be considered as separable into a boundary layer, in which viscous effects are important, and an external flow, in which they can be neglected - though corrections must be made to calculations of the inviscid flow to allow for the thickness of the boundary layer. The first assumption is justified, for the types of unsteady flow being considered here, by comparisons between the characteristic times of such processes as dissociation and ionisation and those of any flow unsteadiness that is likely to occur in practice. It seems possible that the second assumption may need some investigation: although analyses of simple flows similar to boundary layers with a fluctuating external velocity suggest that boundary layers can be analysed as if they respond in a quasi-steady manner for fluctuations having the characteristic times likely in practice, available experimental evidence suggests that this may not be true.

The methods available for the analysis of unsteady inviscid flows can be divided into three groups:

(i) First there are third order piston theory and Newtonian impact theory: so far these have been the methods most widely used. Although there are flow conditions in which either of these theories can be physically sound, in many oases their use is empirical or semi-empirical. They are attractive because they give simple relations between the pressure and downwash at a point on a body surface.

(ii) In the second group hypersonic small disturbance theory provides a basis (a), at small incidences, for the use of a variational method to find unsteady flows around pointed slender three-dimensional bodies for values of the parameter $M_\infty\delta$ (where δ is the thickness ratio) up to a limit near unity; and (b) for applying the shook expansion method to the calculation of unsteady flows around thin, sharp, two-dimensional sections and, when $M_\infty\delta$ exceeds a minimum value near unity, around pointed, slender, three-dimensional bodies. (The limits on the values of $M_\infty\delta$ for slender bodies are not exact but are related to the error that is acceptable in the calculation - this is the sense in which $M_\infty\delta > 1$, and $M_\infty\delta < 1$ will be used in the rest of this section).

(iii) Thirdly, there are methods of analysis in which an unsteady flow is considered as a small perturbation of a known steady flow such as the solution of a bluff body flow or a characteristics solution for a more general body shape. These methods have been applied to some simple flows and, in principle, they could be used for any flows where a suitable steady flow solution was available. In practice, their use may be limited because of the complexity of the analysis or the length of time necessary for computation, but they may be the only methods for dealing with many important kinds of flow and they need to be investigated more extensively.

Judged on the basis of the assumptions and approximations made in their development, the first two groups of methods seem to be adequate to deal with a number of simple flows. Piston theory (at lower hypersonic Mach numbers,

and/

and values of $M\delta < 1$) and shock expansion theory seem adequate for two-dimensional sections and for wings with supersonic leading edges. Shock expansion theory and the variational method should, in principle, deal satisfactorily with slender bodies whose cross-sections are everywhere convex though, in practice, there can be difficulties if the conditions at the nose are not given by a known solution, and if the cross-section is not circular and the incidence is not small. At sufficiently high Mach numbers Newtonian theory will give good results for surfaces that are convex, but it is liable to be considerably in error on surfaces that are concave, and on control surfaces or flared sections lying within the shock layer of the body.

For steady conditions, experimental evidence supports these conclusions, For unsteady conditions the evidence is more limited. since very few direct measurements of derivatives have been made, and the results which have been obtained from flutter tests are inconclusive because of the experimental uncertainties. It would seem likely from the nature of the theories that, when used within their limiting conditions, they would agree quite well with experiments: but the size of the differences between measured aerodynamic damping derivatives and calculated values suggest (as has been mentioned above) that it may not be possible to assume a quasi-steady response of the boundary layer to fluctuations of the external flow.

But these comparatively simple methods of analysis cannot be used, at present, for many of the kinds of flows which are likely to ooour in practice. In particular, they cannot be used for two-dimensional sections, swept wings, or slender bodies, above the incidence for shook detachment; for slender bodies where $M\delta < 1$, at large incidences; for blunted, thin, two-dimensional sections and blunted slender bodies; for bluff bodies; and for bodies on which it is necessary to consider interaction effects between surfaces. It is possible that a satisfactory semi-empirical method of analysis can be developed for the blunted thin section and blunted slender body by using a suitable bluff body solution for the nose region combined with the shock expansion method downstream but, in general, for most of these flows, it will probably be necessary to use a small perturbation method for small amplitude motions and a quasi-steady analysis for large amplitudes. Because of this, there will necessarily be a very close relationship between the development of unsteady analyses and the development of suitable steady analyses. It is likely that, even when a satisfactory unsteady analysis has been developed, the need to develop the results in a form suitable for use in flutter calculations will remain a major problem, espeoially as flutter may involve longitudinal bending distortions of vehicles.

3. The Dynamic Stability of Hypersonic Vehicles

The practical importance of unsteady flows is to be found in the investigation of dynamic stability and flutter of vehicles and, in order to assess the need for accuracy in the analysis of unsteady hypersonic flows, it is necessary to have information on the stability and flutter characteristics of the vehioles.

Dynamic stability has been investigated by extending the classical analysis of aircraft stability to flight at very high speeds and constant altitude, and by examining the oscillatory behaviour of vehicles in re-entry flight. It appears that the form of the vehicle and its aerodynamic characteristics at hypersonic speeds only effect the stability characteristics in details, the qualitative behaviour being determined by the high speed of

flight/

flight and the altitude at which it takes place. For example, although a full analysis that will give the correct behaviour at extreme altitudes requires the inclusion of terms to account for changes in the air density, gravity force, and other factors with altitude, and takes account of the effective rate of pitch due to the curvature of the flight path, the behaviour of the vehicle is dominated by the large values of the ratio of vehicle density to air density at which flight is possible. The longitudinal motion of the vehicle still exhibits two oscillatory normal modes, as at lower speeds. One mode involves, predominantly, changes of speed and altitude, and the other involves, predominantly, pitching oscillations. The second mode has a comparatively short period at the lower altitudes of hypersonic flight, and, under these conditions, it might involve unsteady flow effects. Because of the large values of relative density characteristic of hypersonic flight, the frequency parameters of normal modes are small and the rates of decay of the oscillations are low. Qualitatively, the changes in the lateral behaviour of vehicles at hypersonic speeds are similar to the changes in the longitudinal behaviour. The frequency parameters involved are likely to be rather higher than for the longitudinal motion, but they will still be considerably smaller than those at lower speeds.

Analyses of the longitudinal oscillatory behaviour of vehicles in re-entry flight show no essential differences from the behaviour in the case of level flight. At a given point in the trajectory, the frequency of the oscillatory pitching motion is the same as it would be for level flight at the same speed and altitude, and the criteria for convergence of the motion can be shown to be the same in the two cases apart from the inclusion in the re-entry case of terms that are dependent on the drag of the vehicle, and the rate of increase of air density.

It is possible to set an approximate upper limit of 0·01 on the values of frequency parameter likely to be found in hypersonic stability analyses. For values of the parameter in this range it should be possible to treat the flow as quasi-steady, although accurate estimates of the aerodynamic damping may need rather careful examination of the boundary layer behaviour. The results of stability investigations do not show any conditions in which a very accurate knowledge of unsteady aerodynamic forces would be of critical importance for normal stability analyses, especially as artificial control of the stability would probably be used in normal conditions. Nevertheless, if vehicles are designed for emergency manual control, or if it is required to analyse the uncontrolled motion of a re-entry vehicle, accurate values of aerodynamic forces might be important.

4. Flutter of Hypersonic Vehicles

The kinds of flutter likely to occur at hypersonic speeds are determined chiefly by the form of the vehicles. From general technical considerations, it seems that the most likely form of flutter involving the whole vehicle structure will be either that of a slender body in bending modes, or of a slender wing/body combination involving flexure, torsion, and camber modes of the wing, and bending modes of the body. Panel flutter could, also, be a problem over those areas of the body surfaces where dynamic pressures can be high but the simple, conventional flexure/torsion flutter of lifting surfaces is only likely to be encountered on certain kinds of control surface.

There have been some analytical and experimental investigations of the flutter of low aspect ratio wings with chordwise flexibility, and of rigid cones with pitching and plunging flexibilities, but the majority of investigations

have/

have been concerned with the flutter of two-dimensional sections with pitching and plunging freedoms, and the closely allied problem of cantilever wings with root flexibilities in pitching and flapping. The studies of flutter of two-dimensional sections have shown the effects of an altitude parameter μM_∞, a thickness parameter $M_\infty \delta$, and a mean incidence parameter $M_\infty \alpha_s$, where μ is the mass ratio of the section, δ is the thickness ratio, and α_s is the mean incidence. For sharp sections with similar profiles, the same pitching axis position, and the same density and mass distributions, and ratios of the natural frequency in plunge to that in pitch of less than one (which is the usual condition), flutter speed is approximately proportional to $\sqrt{\mu M_\infty}$ for $M_\infty \delta$ and $M_\infty \alpha_s$ constant; decreases with increasing $M_\infty \delta$ for μM_∞ and $M_\infty \alpha_s$ constant, and it can decrease with increasing $M_\infty \alpha_s$ for μM_∞ and $M_\infty \delta$ constant. The profile shape of a sharp-nosed section only has a large effect if it causes a large change in the centre of pressure position (e.g., a change from a double wedge to a single wedge section), but blunting the nose of a section at constant μM_∞ increases the flutter speed up to a limit of blunting that depends on the Mach number; further blunting reduces the flutter speed or causes divergence before the section flutters. It seems possible that the effects of strong nose shock waves, the entropy variations that result from these, and real gas effects may increase the flutter speed over the value which it would have if these effects were absent. Finally, when aerodynamic non-linearities are significant, theoretical investigations have shown that there exists a range of speeds within which flutter can be started by disturbances of a finite size - the larger the disturbance the lower the flutter speed.

The limited investigations of the effects of chordwise bending modes on the flutter of low aspect ratio wings serve to show that these can be important (though the effects depend on the characteristics of the particular structure) and that flutter of a slender wing involving only longitudinal bending modes is possible. The flutter analysis and experiment on a rigid cone with pitching and plunging flexibilities suggest that the flutter speed/altitude parameter for a given cone is independent of Mach number.

There do not seem to have been any investigations of panel flutter at hypersonic speeds, but, since structural limitations ensure that the displacements are very small so that the hypersonic parameter $M_\infty \delta$ (where δ is a measure of the displacement) remains small, some deductions about panel flutter behaviour can be made from the results of investigations at lower Mach numbers. On this basis, panel flutter seems unlikely to be influenced by fluid dynamic effects of high Mach numbers, except by those arising from the thickness of the boundary layers; but critical conditions could arise in practice because strong shock waves will increase the values of local dynamic pressures above those for the free stream, and the stiffness and end loadings of panels will increase as a result of aerodynamic heating of the structure.

The investigations of flutter that have been examined are all concerned with rather special cases; nevertheless, they all suggest that purely fluid dynamic effects at high Mach numbers will not have a large Influence on the likelihood of flutter. For example, for a two-dimensional section, although leading edge blunting and a large mean incidence can cause reductions in the flutter margin at high Mach numbers, present information suggests that, for flight at constant pressure, and when the effect of aerodynamic heating on structural stiffness is ignored, the transonic flight régime remains as the most critical. On the other hand, flutter could be a danger at hypersonic speeds because aerodynamic heating could alter the stiffness of a structure and for some flight paths, particularly during re-entry, high dynamic pressures occur when the heating

rate/

rate is also high, and because for acme parts of the structure local dynamic pressures can be several times greater than free stream values.

The frequency parameter at which flutter will occur is determined to a large extent by the natural frequencies of the vehicle structure and by the flight speed at which flutter occurs. An upper limit of 0·5, baaed on body length, has been suggested as probable for flutter involving slender body bending modes and. the limit for other forma of flutter is likely to be of the same order. For frequency parameters near this upper limit it would be necessary to take account of unsteady effects in calculation of the aerodynamic damping forces if accurate values of these were required. The flutter investigations for hypersonic speeds that have been reviewed do not examine the need for accurate values of aerodynamic forces, but acme studies for lower speeds have suggested that, under certain conditions, if aerodynamic damping terms are small, they have very little influence on flutter speeds and frequencies.

5. Discussion and Conclusions

The essential point to emerge from this review is the need to establish whether or not quasi-steady analyses of unsteady flows will be adequate for the practical problems of vehicle dynamic stability and flutter at hyperacnio speeds. From the evidence available it seems likely that auoh analyses will be adequate, but a definite answer to the question will depend, first, on the sensitivity cf analyses Of dynamic stability and flutter to small errors in the aerodynamic forces, especially to errors in the aerodynamic damping; and, secondly, on the size of errcra in the estimates of unsteady aerodynamic forces due to the assumption of quasi-steadiness at the frequency parameters to be met in practice. These points suggest two lines for further research:

(i) Investigations of the sensitivity of dynamic stability and flutter analyses to errcra in the estimations of the aerodynamic forces involved;

(ii) Investigations of the errors involved in quasi-steady estimates of unsteady aerodynamic forces at hypersonic speeds.

A number of steps would be involved in the second investigation. In the first place, in those simple cases where an adequate unsteady analysis already exists it would be a fairly straightforward matter to find the error involved in assuming quasi-steady conditions. Secondly, it would be possible to Investigate more complex flows experimentally by comparing unsteady measurements with quasi-steady predictions derived either from steady analyses, or from suitable steady-state measurements. But, finally, it would be necessary to develop methods of unsteady analysis to deal with more complex shapes, so that it would be possible to establish the limits of quasi-steady analyses with greater generality.

There is a second general point to be made. Studies of unsteady flows should, in the main, be carried cut as part of more general studies either of methods of theoretical analysis or of the flow field around a body for both steady and unsteady conditions. At hypersonic speeds, methods for the theoretical analysis of unsteady flows are closely related to those for steady flows, and their limitations are likely to be similarly related; an understanding of the full flow field - in particular, of the behaviour of the boundary layer and the effect of more bluntness - will be Important for the application of theories and the interpretation of results.

Recommendations for specific research projects are given in Sections 2.4 and 4.3 in the Appendices.

APPENDICES/

APPENDICES

Detailed Reviews

APPENDIXI: Review of Hypersonic Flight Conditions

1.1 Characteristics of Hypersonic Flows[1,2,3,4]

The term 'hypersonic' is used of flows above about M = 5, when certain features of the flow, which are unimportant at lower Mach numbers, begin to grow in significance. These characteristic features are separable into changes in the fluid dynamics of a gas which result from the high Mach number, and physical and chemical effects which result from the high speed and. consequent high energy of the flow. Because of the high energy of the flow, high temperature will be generated where the gas is brought to rest at stagnation points and where it is decelerated in boundary layers and in passing through shock waves - particularly if these are strong. These temperatures can be high enough to cause excitation of vibrational degrees of freedom of polyatomic gas molecules, dissociation and ionisation. The hydrodynamic properties of the flow are affected by the resultant changes in the ratio of specific heats of the gas, in the specific heats themselves, and by the relaxation phenomena involved. When still higher temperatures are generated, radiation from the hot gas provides an additional means of energy transfer.

Because of the high Mach number, certain simplifications can be made in the fluid dynamic analysis of flow in comparison with analysis at lower Mach numbers but certain complications must be met as well. The principal simplifications are that, for slender bodies, longitudinal disturbances of the flow can be neglected in comparison with lateral disturbances and certain flows, particularly those over bluff bodies, become independent of the Mach number when this is high enough.

The principal complications are that the range of thickness ratios for which analyses based on linearization of the equations of motion of the fluid can be applied becomes very small, that strong, curved shock waves can be present, causing entropy variations in the flow so that potential flow theory cannot be applied, and that, because of the thickness and rate of growth of the boundary layer and the sensitivity of the external flow to small changes of direction, interactions between the boundary layer and the external flow can be important.

Further complications are found in the analysis of flows that occur in practice because of the finite thickness of nominally sharp leading edges and the use of blunt leading edges to reduce heat transfer. The analysis of hypersonic flow past a bluff shape is, itself, very complex, involving all flow regimes - subsonic, transonic, supersonic and hypersonic. Downstream of a blunt leading edge, the gas which has passed. through the very strong, highly curved, shock set up by the leading edge, forms a layer of high entropy and vorticity adjacent to the body. The analysis of the flow in the entropy layer and the analysis of the interactions between the body shape, the flow in this layer and the external flow have not yet been carried out in a completely satisfactory way.

1.2 Hypersonic Vehicles

Hypersonic vehicles can be separated into two main groups: those vehicles intended to fly efficiently within the atmosphere at hypersonic speeds,

and/

and those vehicles intended for re-entry flight from orbit or from space. General discussions of the design problems involved are given in Refs. 5 to 8.

The first group of vehicles includes the hypersonic cruise vehicles, for which the useful Mach number range may be $5 < M < 7$, the re-usable booster for space vehicles, for which the Mach number range may extend to $M = 13$, and the one-stage-to-orbit vehicle. All of these vehicles seem likely to be of slender form with leading edges highly swept to reduce both shock wave drag and aerodynamic heating of the leading edges, either a slender-body/slender-wing configuration using favourable interference effects between wing and body to give maximum aerodynamic efficiency (Fig.1(a) and Ref. 8) or a development of the caret wing. The latter, in its simplest form, is a body which has a concave lower surface with an inverted V cross-section: the lower surface is designed to support a plane shock between its edges - most of the lift is generated on the lower surface and the upper surfaces can be shielded from the flow in the cruise attitude (Fig. 1(b) and Refs. 9 and 10).

The common characteristics of the re-entry group of vehicles are that they are unpowered and must dissipate large amounts of kinetic energy during the period of re-entry. The form of the vehicle depends on the way in which it is designed to dissipate this energy, and the degree of control of the trajectory that is required. The simplest form is a blunt body designed to follow a ballistic trajectory. For such a body, most of? the energy is transferred to the gas in the shook layer ahead of the body and is dissipated in the wake. Peak body surface temperatures are high, but the heating period is short. As speeds increase above escape speed, a ballistio re-entry trajectory rapidly becomes unacceptable because deceleration rates become too high, re-entry must be initiated with very great accuracy, and there is little control of the landing point after re-entry has started. In consequence, lifting bodies with a high drag and moderate lift/drag ratio (in the range between 0·5-1·0) offer significant improvements in the control of deceleration rates and of the trajectory. For these vehicles, peak temperatures will be lower than for the ballistic vehicle, but heating times will be longer and a greater amount of heat will be absorbed by the structure. Suitable vehicles would either be bluff bodies modified to produce small amounts of lift or slender bodies which could be operated at high incidence at the start of re-entry, (Fig. 2(a) and (b), Refs. 7 and 8). A third possible re-entry vehicle is represented by the Rogallo wing, which would be a lightweight inflatable structure of heat resistant material cooled by radiation (Fig. 2(c), Refs. 5 and 10).

1.3 Flight Envelopes for Hypersonic Vehicles

For any particular hypersonic vehicle there is a flight corridor of altitudes and speeds within which flight is possible. For flight at a given speed the lower altitude band of this corridor is determined by the maximum values of dynamic pressure and stagnation or recovery temperature that the structure can withstand, and the upper altitude band is set by the wing loading of the vehiale and the maximum lift coefficient that it can attain. At comparatively low speeds (5000 ft/sec) the wing loading and lift coefficient define a dynamic pressure below which flight is not possible, but for speeds that are a significant fraction of orbit81 speed, account must be taken of the centrifugal lift developed on the vehicle. We then have

$$W\left(1 - \frac{U^2}{gR}\right) = \tfrac{1}{2}\rho U^2 S C_L \qquad \ldots (1.1)$$

where,

where W is the weight of the vehicle; S is the lifting area; R is the radius of the flight path from the earth's centre. Thus when the speed is high flight is possible at lower values of dynamic pressure than when the speed is lcw.

The actual limits of the flight corridor depend on the design of the vehicle, but Fig. 3 has been prepared to indicate the range of flight conditions within which hypersonic vehicles may normally be expected to operate. The minimum value of the parameter W/SC_L has been taken to be 15 lb/ft^2: only vehicles involving light weight lifting structures are likely to give values of less than this; and the maximum value of dynamic pressure has been taken as 1000 lb/ft^2. The lines in Fig. 3 representing the altitudes and speeds for these constant parameters define a flight corridor in terms of minimum lift and maximum dynamic pressure. Two bands are shown representing the speeds and altitudes at which the-stagnation temperature will be 2000°R and 4000°R. A limit on stagnation temperature of 2000°R will permit flight in only a restricted region; a limit of 4000°R permits a flight corridor extending to orbital speed.

Superimposed on the flight corridors defined by dynamic pressure, stagnation temperatures and lift in Fig. 3 are shown lines of constant Reynolds number and constant values of the viscous interaction parameters, χ. The values of Reynolds number per foot that are likely to be met suggest that, at the higher speeds and altitudes, laminar boundary layers will extend over much of the vehicle surface, and flow separations will be more easily provoked than at lower speeds, where much of the boundary layer is turbulent. The parameter χ indioates the importance cf interactions between the boundary layer and the external flow and is defined by the equation:

$$\chi \equiv M^3 (c_\infty / Re_x)^{\frac{1}{2}} \qquad \ldots (1.2)$$

where c_∞ is the constant in the viscosity relation

$$\frac{\mu}{\mu_\infty} = c_\infty \frac{T}{T_\infty}$$

and is usually close to unity. The value of c_∞ has been taken as unity in Fig. 3. Values of χ of $O(0{\cdot}5)$ and greater suggest that these interactions will have significant effects on pressure distributions for sharp-nosed bodies (Appendix II, Seotion 2.2).

Fig. 4 shows some possible trajectories for super-circular ballistic re-entry (re-entry velocity is greater than circular orbital velocity), super circular lifting re-entry, lifting exit, and expandable structure lifting re-entry (W/SC_L < 15): these are superimposed on the flight corridors defined in Fig. 3. The ballistic trajectory shows very high values of dynamic pressure and stagnation temperature illustrating the severity of the conditions for this form of re-entry which was mentioned before. The super circular lifting re-entry trajectory shows a condition of high dynamic pressure and stagnation temperature in the early stages of re-entry, when the Mach number is very high, but the lifting exit trajectory shows a maximum dynamic pressure below the hypersonic speed range.

APPENDIX II/

APPENDIX II Review of Theoretical Analysis of Unsteady Hypersonic Flows

Despite the complexity of the real flow situation outlined, in Section 1, it is assumed that real gas effects and boundary layer behaviour cause modifications to the flow for an inviscid perfect gas which can be estimated when that flow is known. This assumption is inherent in all the methods of analysis that are available; it appears justified in the conditions which are considered here, but it will be discussed later in this section.

2.1 Methods of Analysis

The methods used for the analysis of inviscid unsteady hypersonic flows fall into three groups. In the first group there are two methods used widely on a semi-empirical basis because of their simplicity. One of these is based on Lighthill's piston theory, and the other on Newtonian theory. In the second there are methods based on the application of hypersonic small disturbance theory - the variational method, and the shook-expansion method. And, in the third there are two methods based on analyses which consider the unsteady flow quantities 8s small perturbations of the steady flow field: these methods have not, as yet, been much used.

2.1.1 Piston theory and Newtonian impact theory

Piston theory and Newtonian impact theory have been used fairly widely: piston theory for flutter analysis on wings, impact theory for the estimation of pressures and overall forces on bodies. The methods are attractive because, in the simple forms in which they are usually employed, they give direct relationships between the local downwash and pressure on a body surface.

Piston theory is closely related to hypersonic small disturbance theory which is considered in 2.1.2, but it is discussed separately here since the term has been used mainly to describe a particular relationship between the downwash and the pressure on a surface and this relationship has been extended, on a semi-empirical basis, to high Mach numbers.

Piston theory in its original form[14] applies on surfaces with small lateral curvature and supersonic edges, for $M^2 >> 1$ and $M\delta << 1$, where δ is a measure of the maximum surface slope and is usually taken to be the largest of the thickness ratio, mean incidence, and dimensionless amplitude of tune dependent motion. In practice $M > 2{\cdot}5$ appears to be the lower Mach number limit for reasonable accuracy.

According to the theory, the pressure at a point on the surface can be related to the streamwise slope and normal velocity of the surface $z(x,y,t)$ by the expression

$$p = \rho_{aw} = \left(\frac{\gamma - 1}{2} \frac{w}{a_\infty} \right)^{\frac{2\gamma}{\gamma-1}} \qquad \ldots (2.1)$$

where $w = U \frac{\partial z}{\partial x} + \frac{\partial z}{\partial t}$, and p, ρ and a are the local pressure, density and speed of sound, and p_∞, ρ_∞ and a_∞ are their free stream values. Equation (2.1) gives the pressure acting on a piston moving with a velocity w into a gas in a one-dimensional channel, under isentropic conditions (i.e., for $w/a_\infty << 1$).

In/

In practice, equation (2.1) is replaced by the approximation given by the leading terms in the binomial expansion of the bracket. Expressed in non-dimensional terms, this expansion is

$$C_p = \frac{2\delta}{M} w_0 + \frac{(\gamma+1)}{2} \delta^2 w_0^2 + \frac{(\gamma+1)}{6} M\delta^3 w_0^3 + \ldots \qquad \ldots (2.2)$$

where $C_p = \dfrac{p - p_\infty}{\frac{1}{2}\gamma p_\infty M^2}$, $w_0 = \dfrac{w}{U\delta}$, and δ is the measure of maximum surface slope defined above.

When equation (2.2) is used to calculate the lift distribution on an aerofoil it shows the effects both of thickness and mean incidence. Fig. 39, from Ref. 57, shows that the predicted thickness effect agrees well with that found by experiment, and by the more exact theory of Van Dyke. Appendix IV shows that changes in lift distribution due to thickness and mean incidence can have an important influence on the flutter of an aerofoil section.

From its derivation, equation (2.1) only applies for isentropic conditions, and, for a compression, this requires that $w/a_\infty \ll 1$ (or $M\delta \ll 1$). But it is shown by Lighthill[14] that equation (2.2) gives a good approximation to the one-dimensional piston pressure up to $w/a_\infty \simeq 1$ and, on this basis, piston theory has been used for flutter studies well into the hypersonic Mach number range considered in this report (e.g., Ref. 61).

For values of $M\delta > 1$, Miles[15], Raymond[16] and East[17] have suggested that piston theory be extended on a semi-empirical basis by substituting shock-wave relationships for equation (2.1) for compression surfaces. The methods suggested are based on the expressions for one-dimensional-shock flow in front of a piston moving at a speed $w > a_\infty$. These expressions are:

$$\left.\begin{aligned} \frac{a}{a_\infty} &= \left(\frac{p\rho_\infty}{p_\infty \rho}\right)^{\frac{1}{2}} \\ \frac{p-p_\infty}{p_\infty} &= \mu \\ \frac{p}{\rho_\infty} &= \frac{1 + [(\gamma+1)/2\gamma]\mu}{1 + [(\gamma-1)/2\gamma]\mu} \end{aligned}\right\}, \qquad \ldots (2.3)$$

where

$$\mu = \gamma\left(\frac{w}{a_\infty}\right)\left\{\frac{\gamma+1}{4}\left(\frac{w}{a_\infty}\right) + \left[\left(\frac{\gamma+1}{4}\right)^2\left(\frac{w}{a_\infty}\right)^2 + 1\right]^{\frac{1}{2}}\right\}$$

Miles[15] suggests two ways in which these relationships could be used:

(1) Where the shock wave movement due to the unsteady disturbances is small, equations (2.3) should be used to calculate the local flow conditions due to the steady state surface slope, and the values of ρ and a from this calculation should then be used in (2.1) with the unsteady disturbance w' to calculate the unsteady pressure disturbance.

(2)/

(2) Where the shock wave movement is likely to be significant, it would be necessary to perturb the first of equations (2.3).

The second method is essentially that followed by East[17] and Raymond[16]. Although the relationships suggested by Raymond are developed in a way different from that used by East and Miles the results can be shown to be equivalent. In Ref. 15 expressions are given which are derived for the second method when it is assumed that a strong shock wave exists (so that $p/p_\infty \gg 1$). For a strong shock wave equations (2.3) reduce to

$$\left.\begin{aligned} \frac{p}{p_\infty} &= \frac{\gamma(\gamma+1)}{2}\left(\frac{w}{a_\infty}\right)^2 \\ \frac{p}{\rho_\infty} &= \frac{(\gamma+1)}{(\gamma-1)} \\ \frac{a}{a_\infty} &= \sqrt{\frac{\gamma(\gamma-1)}{2}}\left(\frac{w}{a_\infty}\right) \end{aligned}\right| \qquad \ldots (2.4)$$

and, from equations (2.4), the perturbation pressure is given by:

$$p' = (\gamma+1)\rho_\infty a_\infty M\theta w' \qquad \ldots (2.5)$$

where w' is the perturbation downwash and θ is the mean inclination of the surface to the free stream direction (θ is still small, though $M\theta$ is large, so that $\tan\theta \simeq \theta$).

This form of shock wave piston theory is soundly based in that it can still be assumed that flow disturbances in the x- and y-directions are small in comparison with those in the s-direction and that the action of the surface on the flow at a point can be given by the flow in front of a piston moving in a one-dimensional channel, but it assumes that the shock wave strength is always directly related to the piston speed by equation (2.3). In fact, equation (2.3) is derived with the assumption of a uniform piston speed and. the relationships should be modified to take account of the compression and expansion waves set up by the accelerations and decelerations of the piston corresponding to the shape of the surface profile. These effects could be included[18] but the point relation between the pressure and the surface slope and normal velocity would be lost.

The first method suggested by Miles[15], that the strong shock relations should be used to calculate the local flow conditions in which equation (2.1) is applied, is similar to the suggestion in Ref. 57 that account could be taken of steady state entropy gradients and even real gas effects by applying simple piston theory in the local conditions established by a steady state calculation. Strictly, the method is applicable only where the flow conditions are little effected by the unsteady disturbance (e.g., for panel flutter calculations). For this case, the method seems to be soundly based if the local Mach number is still high enough but its use in such conditions suggests the need for an investigation of the pressure on a piston moving in a one-dimensional channel in a fluid with large entropy gradients.

Unsteady/

Unsteady Newtonian theory is discussed by Hayes and Probstein', by Zartarian[19] and by Zartarian and Saurwein[20]. The theory can be shown to apply in the limits $M \to \infty$, $\gamma \to 1$, when $\varepsilon \to \infty$, where ε is the density ratio aoross the shook at the body surface. The theory assumes that there are no interactions between fluid particles, that the only change in the velocity of a particle impinging on a body surface takes place normal to the surface, and that, after impact, the particle follows the surface of the body within an infinitesimally thin shock layer. The pressure at a point at the surface of the shock layer can be found directly from the change in the component of the fluid momentum normal to the body *surface,* so that the pressure coefficient at the surface of the shook layer is given by:

$$C_p = \frac{p - p_\infty}{\frac{1}{2}\rho_\infty U^2} = 2\left(\frac{u_n - q_n}{U}\right)^2 \qquad \ldots (2.6)$$

where q_n is the normal velocity of the body surface point arising from any motion of the body, and any time-dependent distortion of the surface, and u_n is the component of the free-stream velocity normal to the surface. It is clear from the assumptions in the theory that it can be applied only where the flow impinges directly on the surface: it can give no information about surfaces shielded from the flow and the pressures on such surfaces are assumed to be negligible.

A fully rational theory[1,20] requires a calculation of the pressure differences across the shock layer necessary to account for the accelerations of the fluid particles following the body surface. This would involve an analysis of the structure of the shock layer, and a consideration of the complications that can occur in the behaviour of the layer. But, since corrections for these effects would introduce very great complications, the theory, as it has been empirically applied, assumes that the pressure at the body surface is the same as that at the surface of the shock layer and, in this form, it is sometimes known as Newtonian impact theory.

Under steady conditions the simple theory has been found to give reasonably satisfactory results on convex surfaces where the Mach number is high enough for the shook to be close to the surface, provided that the expression (2.6) is factored to give the correct value of the C_p at the stagnation point or the leading edge of the body. The accuracy of impact theory in these circumstances is, apparently, due in part to the oancelling of opposing errors: the pressure behind the shook is higher than the impact theory value, but the pressure difference across the shock layer due to the centrifugal effect compensates *for* this (Ref. 2).

Examples of the use of Newtonian impact theory for unsteady flow analysis are to be found in Befs. 21, 22 and 23. In Ref. *21* Tobak and Wehrend compare the results of impact theory analysis for a cone with first and second order potential flow solutions and, for the stiffness derivative, with exact values over the Mach number range from 3·0 to 5·0. The impact theory values appear to be a limit which the exact values approach with increasing Mach number, but the cone is an especially favourable case for the application of Newtonian theory. East[17] has shown that, in the limits $M \to \infty$, $\gamma \to 1$, the expressions from Newtonian impact theory and from strong shook piston theory are the same.

The/

The simplicity of the theory makes it attractive for practical applications but it has serious limitations which may not always be obvious in advance. It has already been pointed cut that it gives no information about pressures on surfaces shielded from the mainstream flow; it is found to be seriously in error on concave surfaces; and it is unreliable wherever the effects of a finite shock layer thickness may be important, e.g., over much of a slender body at small incidence (Figs. 11, 12 & 13) and on control surfaces and flared sections on slender bodies which operate within the nose shock.

2.1.2 Hypersonic small disturbance theory

The second group of methods makes use of the result from small disturbance theory that, for slender bodies at high enough Mach number, the flow in a lamina of fluid normal to the body axis can be considered as independent of flow in adjacent laminae. This result is implicit in the assumptions of piston theory, but it has been established formally, and with more general applicability, in hypersonic small disturbance theory. Since the theory brings out important characteristics of hypersonic flow, it will be discussed first, before considering how its results are applied to the calculation of unsteady flows.

Small disturbance theory is concerned with flows involving velocity disturbances which are small relative to the free-stream velocity, i.e., with the flows past slender bodies in two dimensions or three dimensions, or with planar bodies with supersonic leading edges and small lateral curvature. At low enough Mach numbers, linearisation of the equations of motion is possible for the flow around such bodies, but at hypersonic Mach numbers the velocity disturbances are not small in comparison with the speed of sound and the pressure disturbances are not small in comparison with the free-stream static pressure, so that the flow equations cannot be linearised. Despite the fact that the equations are essentially non-linear, some valuable information on the flow conditions can be obtained and the equations themselves can be simplified by making use of the fact that the velocity disturbances are small relative to the free-stream velocity, and the pressure disturbances are small relative to the free-stream dynamic pressure.

As full discussions of the theory are given by Van Dyke[4] and Hayes and Probstein[1], it will only be briefly outlined here and illustrated by the general flow equations.

Consider a slender, pointed body in a hypersonic stream at only a small angle to the free-stream direction. The shock waves make only small angles with the free-stream direction and, because of this, it can be assumed that velocity disturbances in this direction are small in comparison with those normal to it and the lateral extent of the flow field is small in comparison with the body length. The scale of smallness involved is, in general, of the same order as the thickness ratio or the angle of incidence of the body.

Take an axis system with origin at the nose of the body, and the x-axis in the direction of the free stream; let U be the free-stream velocity and u, v and w be the disturbance velocity components in the x, y and z directions. Let the larger of the thickness ratio and the angle of incidence be denoted by 6, and apply the transformations:

$$u = \delta u' \qquad x = \delta^{-1} x' \qquad \ldots (2.7)$$

Then/

Then the transformed velocity component u' will be of the same order of magnitude as the components v and w, and gradients of flow quantities in terms of x' will be of the same order of magnitude as those in the y and z directions. Substituting these transformed quantities into the equations of continuity, momentum and entropy (with isentropic conditions along the streamlines) we obtain

$$\frac{\partial \rho}{\partial t} + U\delta \frac{\partial \rho}{\partial x'} + \frac{\partial(\rho v)}{\partial y} + \frac{\partial(\rho w)}{\partial z} = -\delta^2 \frac{\partial(\rho u')}{\partial d}, \quad \ldots (2.8)$$

$$\frac{\partial u'}{\partial t} + us \frac{\partial u'}{\partial x'} + v \frac{\partial u'}{\partial y} + w \frac{\partial u'}{\partial z} + \frac{\partial p}{\rho \partial x'} = -\delta^2 u' \frac{\partial u'}{\partial x'}, \quad \ldots (2.9)$$

$$\frac{\partial v}{\partial t} + us \frac{\partial v}{\partial x'} + v \frac{\partial v}{\partial y} + w \frac{\partial v}{\partial z} + \frac{1}{\rho} \frac{\partial p}{\partial y} = -\delta^2 u' \frac{\partial v}{\partial x'}, \quad \ldots (2.10)$$

$$\frac{\partial w}{\partial t} + us \frac{\partial w}{\partial x'} + v \frac{\partial w}{\partial y} + w \frac{\partial w}{\partial z} + \frac{1}{\rho} \frac{\partial p}{\partial z} = -\delta^2 u' \frac{\partial w}{\partial x'}, \quad \ldots (2.11)$$

and

$$\frac{\partial s}{\partial t} + U\delta \frac{\partial s}{\partial x'} + v \frac{\partial s}{\partial y} + w \frac{\partial s}{\partial z} = -\delta^2 u' \frac{\partial s}{\partial x'}. \quad \ldots (2.12)$$

where S is the entropy, and is given by $S = C_v \log(p/\rho^\gamma)$ + constant, where C_v is the specific heat at constant volume. If the right-hand sides of these equations are neglected as they are of second order of smallness, the equations for v, w, p and p are decoupled from that for u'. The significance of this is seen more clearly if the equations are now transformed to axes fixed in the fluid, for if

$$\left.\begin{aligned} \bar{t} &= t \\ \bar{x}' &= x' - U\delta t \end{aligned}\right\} \quad \ldots (2.13)$$

and

$$\left.\begin{aligned} \frac{\partial}{\partial x'} &= \frac{\partial}{\partial \bar{x}'} \\ \frac{\partial}{\partial t} &= \frac{\partial}{\partial \bar{t}} - U\delta \frac{\partial}{\partial \bar{x}'} \end{aligned}\right\}, \quad \ldots (2.14)$$

then equations (2.8) to (2.12) become:

$$\frac{\partial \rho}{\partial \bar{t}} + \frac{\partial(\rho v)}{\partial y} + \frac{\partial(\rho w)}{\partial z} = 0 \quad \ldots (2.15)$$

$$\frac{\partial u'}{\partial \bar{t}} + v \frac{\partial u'}{\partial y} + w \frac{\partial u'}{\partial z} + \frac{1}{\rho} \frac{\partial \rho}{\partial \bar{x}} = 0 \quad \ldots (2.16)$$

$\frac{\partial v}{\partial t}$ /

$$\frac{\partial v}{\partial t} + v\frac{\partial v}{\partial y} + w\frac{\partial v}{\partial z} + \frac{1}{\rho}\frac{\partial p}{\partial y} = 0 \qquad \ldots (2.17)$$

$$\frac{\partial w}{\partial t} + v\frac{\partial w}{\partial y} + w\frac{\partial w}{\partial z} + \frac{1}{\rho}\frac{\partial p}{\partial z} = 0 \qquad \ldots (2.18)$$

$$\frac{as}{at} + v\frac{as}{\partial y} + w\frac{as}{\partial z} = 0 \qquad \ldots (2.19)$$

It can be seen that the equations (2.15) and (2.17) to (2.19) are the equations for the unsteady flow of a fluid in two dimensions.

Since the boundary conditions at the shock wave and the body transform in a similar way to the equation3 of motion, the flow around a slender two-dimensional body becomes the problem of flow around an expanding and contracting piston in motion in two dimensions, and the flow past a thin two-dimensional section becomes that of a piston moving in one dimension. The link with piston theory in the twc-dimensional case is obvious, but the actual piston theory relations and the point relationship between piston velocity and pressure do not follow unless isentropic flow is assumed in front of the piston.

A similar argument to that just used justifies the use of strip theory on surfaces at hypersonic speeds if the flow is attached at the leading edge of the surface'. It can be shown that the transformations

$$\left.\begin{aligned} y &= \delta^{-1}Ay' \\ \text{and} \qquad v &= \delta A^{-1}v' \end{aligned}\right\} \qquad \ldots (2.20)$$

where A is the aspect ratio of the surface, make spanwise disturbances and gradients in the flow of the same order as those normal to the surface. If these transformations are applied in equations (2.15) to (2.19), and terms of order δ^2A^{-2} are neglected, one-dimensional piston theory is shown, formally, to be applicable on such surfaces.

It can be seen that no assumptions about the time-dependent terms have been made in the development of the theory. There are two limitations that must be observed. The first is that the downwash components due to the unsteadiness must remain small, of $O[\delta]$ so that, for a sinusoidal unsteadiness giving a non-dimensional displacement $\delta_0 = h/\ell$ at a point, it is necessary that

$$\frac{\omega\ell\delta_0}{U} << 1 \qquad \ldots (2.21)$$

where $\omega = 2\pi f.$

The second limitation is that the wavelength of the unsteady disturbance should be large in comparison with spacial extent of propagation of a point disturbance in the time that it takes the body to pass any point in the fluid. Since δ, which is a measure of the surface slope of the body, is of the same order as the Mach angle, $U\delta$ is of order 'a' where 'a' 13 the speed of sound in the fluid. Then, at the tail of the body the maximum extent Of propagation

of/

of a disturbance is of order $\delta\ell (\simeq a\ell/U)$. Consequently, the second limitation can be expressed by

$$\lambda >> \delta\ell$$

or

$$\lambda/\ell >> 6 \qquad \ldots (2.22)$$

where- λ is the wavelength of the disturbance.

Sychev has shown, in Ref. 25, that a form of small disturbance theory can be developed for bodies at large incidence in hypersonic flow, provided that the flow on the leeward side of the body can be neglected. From this development of the theory it can be shown that on the windward side of the body the flow in a lamina of fluid normal to the axis of the body can be considered as independent of the flow in adjacent laminae. The form that the equations take will be illustrated, as before, by considering the general equations of motion of the fluid. The equations are presented this time in non-dimensional form as, for this case, the development can be seen more clearly.

The axes ξ, η, ζ, are taken with origin at the nose of the body and the ξ-axis in the mean direction of the principal body axis and the ζ-axis in the plane of the &-axis and the flow direction (Fig. 6). The independent variables are made non-dimensional by the transformations:

$$\bar{\xi} = \frac{\xi}{b}, \quad \bar{\eta} = \frac{\eta}{\delta b}, \quad \bar{\zeta} = \frac{\zeta}{\delta b}, \quad \bar{t} = \frac{tU \cos \alpha}{b} \qquad \ldots (2.23)$$

where b is the body length, δ is a ratio representing the maximum surface slope, a is the angle of incidence of the body and U is the flow velocity of the free stream.

The dependent variables are made non-dimensional by the transformations:

$$\frac{U \cos \alpha + u}{u \cos a} = 1 + \bar{u}, \quad \bar{v} = \frac{v}{U \sin a}, \quad \bar{w} = \frac{w}{U \sin a}$$

$$P = \frac{P}{\rho_\infty U^2 \sin^2 a}, \quad \text{and} \quad \bar{\rho} = \frac{P}{\rho_\infty} \qquad \ldots (2.24)$$

where u, v, w are the velocity perturbations in the ξ, η, ζ directions. Then the general equations of fluid motion become

$$\frac{\rho_\infty u \cos a}{b} \frac{\partial \bar{u}}{\partial \bar{t}} + \frac{\rho_\infty u \cos \alpha}{b} \frac{\partial \bar{p}}{\partial \bar{\xi}} + \frac{\rho_\infty U \sin \alpha}{b\delta} \frac{\partial(\bar{\rho v})}{\partial \bar{\eta}} + \frac{\rho_\infty U \sin \alpha}{b\delta} \frac{\partial(\bar{\rho w})}{a4}$$

$$= - \frac{\rho_\infty U \cos a}{b} \frac{\partial(\bar{\rho u})}{\partial \bar{\xi}}, \qquad \ldots (2.25)$$

$$\frac{U^2 \cos^2 \alpha}{b}$$

$$\frac{U^2\cos^2\alpha}{b}\frac{\partial\bar{u}}{\partial\bar{t}} + \frac{U^2\cos^2\alpha}{b}\frac{\partial\bar{u}}{\partial\bar{\xi}} + \frac{U^2\sin\alpha\cos\alpha}{b\delta}\bar{v}\frac{\partial\bar{u}}{\partial\bar{\eta}} + \frac{U^2\sin\alpha\cos\alpha}{b\delta}\bar{w}\frac{\partial\bar{u}}{\partial\bar{\zeta}}$$

$$+ \frac{\rho_\infty U^2\sin^2\alpha}{\rho_\infty b}\frac{\partial\bar{p}}{\partial\bar{\xi}} = -\frac{U^2\cos^2\alpha}{b}\bar{u}\frac{\partial\bar{u}}{\partial\xi}, \qquad \ldots (2.26)$$

$$\frac{U^2\sin\alpha\cos\alpha}{b}\frac{\partial\bar{v}}{\partial\bar{t}} + \frac{U^2\cos\alpha\sin\alpha}{b}\frac{\partial\bar{v}}{\partial\bar{\xi}} + \frac{U^2\sin^2\alpha}{b\delta}\bar{v}\frac{\partial\bar{v}}{\partial\bar{\eta}} + \frac{U^2\sin^2\alpha}{b\delta}\bar{w}\frac{\partial\bar{v}}{\partial\bar{\zeta}}$$

$$+ \frac{\rho_\infty U^2\sin^2\alpha}{\rho_\infty b\delta}\frac{\partial\bar{p}}{\partial\bar{\eta}} = -\frac{U^2\cos\alpha\sin\alpha}{b}\bar{u}\frac{\partial\bar{v}}{\partial\bar{\xi}}, \qquad \ldots (2.27)$$

$$\frac{U^2\sin\alpha\cos\alpha}{b}\frac{\partial\bar{w}}{\partial\bar{t}} + \frac{U^2\cos\alpha\sin\alpha}{b}\frac{\partial\bar{w}}{\partial\bar{\xi}} + \frac{U^2\sin^2\alpha}{b\delta}\bar{v}\frac{\partial\bar{w}}{\partial\bar{\eta}} + \frac{U^2\sin^2\alpha}{b\delta}\bar{w}\frac{\partial\bar{w}}{\partial\bar{\zeta}}$$

$$+ \frac{\rho_\infty U^2\sin^2\alpha}{\rho_\infty b\delta}\frac{\partial\bar{p}}{\partial\bar{\zeta}} = -\frac{U^2\cos\alpha\sin\alpha}{b}\bar{u}\frac{\partial\bar{w}}{\partial\bar{\xi}}, \qquad \ldots (2.28)$$

$$\frac{u\cos\alpha}{b}\frac{as}{\partial\bar{t}} + \frac{u\cos\alpha}{b}\frac{as}{\partial\bar{\xi}} + \frac{U\sin\alpha}{b\delta}\bar{v}\frac{as}{\partial\bar{\eta}} + \frac{U\sin\alpha}{b\delta}\bar{w}\frac{as}{\partial\bar{\zeta}}$$

$$= -\frac{u\cos\alpha}{b}\bar{u}\frac{as}{\partial\bar{\xi}}; \qquad \ldots (2.29)$$

these equations reduce to

$$\delta\cot\alpha\frac{\partial\bar{\rho}}{\partial\bar{t}} + \delta\cot\alpha\frac{\partial\bar{\rho}}{\partial\bar{\xi}} + \frac{\partial(\bar{\rho}\bar{v})}{\partial\bar{\eta}} + \frac{\partial(\bar{\rho}\bar{w})}{\partial\bar{\zeta}} = -6\cot a\frac{\partial(\bar{\rho}\bar{u})}{\partial\xi}, \qquad \ldots (2.30)$$

$$\delta\cot\alpha\frac{\partial\bar{u}}{\partial\bar{t}} + \delta\cot\alpha\frac{\partial\bar{u}}{\partial\bar{\xi}} + \bar{v}\frac{\partial\bar{u}}{\partial\bar{\eta}} + \bar{w}\frac{\partial\bar{u}}{\partial\bar{\zeta}} + \delta\tan\alpha\frac{\partial\bar{p}}{\partial\bar{\xi}} = -\delta\cot\alpha\,\bar{u}\frac{aii}{\partial\bar{\xi}}, \qquad (2.31)$$

$$\delta\cot\alpha\frac{\partial\bar{v}}{\partial\bar{t}} + \delta\cot\alpha\frac{\partial\bar{v}}{\partial\bar{\xi}} + \bar{v}\frac{\partial\bar{v}}{\partial\bar{\eta}} + \bar{w}\frac{\partial\bar{v}}{\partial\bar{\zeta}} + \frac{\partial\bar{p}}{\partial\bar{\eta}} = -6\cot\alpha\,\bar{u}\frac{\partial\bar{v}}{\partial\bar{\xi}}, \qquad \ldots (2.32)$$

$$\delta\cot\alpha\frac{\partial\bar{w}}{\partial\bar{t}} + \delta\cot\alpha\frac{\partial\bar{w}}{\partial\bar{\xi}} + \bar{v}\frac{\partial\bar{w}}{\partial\bar{\eta}} + \bar{w}\frac{\partial\bar{w}}{\partial\zeta} + \frac{\partial\bar{p}}{\partial\bar{\zeta}} = -\delta\cot\alpha\,\bar{u}\frac{\partial\bar{w}}{\partial\bar{\xi}}, \qquad \ldots (2.33)$$

$$\delta\cot\alpha\frac{as}{\partial\bar{t}} + \delta\cot\alpha\frac{as}{\partial\bar{\xi}} + \bar{v}\frac{as}{\partial\bar{\eta}} + \bar{w}\frac{as}{\partial\bar{\zeta}} = -\delta\cot\alpha\,\bar{u}\frac{as}{\partial\bar{\xi}}. \qquad \ldots (2.34)$$

But/

But

$$\bar{u} \cot \alpha = \frac{u \cot \alpha}{u \cos \alpha} \qquad \ldots (2.35)$$

and, on the windward side of the body, the disturbances are confined between the body and the shock wave, which lies close to the body, and consequently u is of order δv or δw, and ucota is of order δ $\left(\text{cot a is of order } \frac{u \cos \alpha}{w}\right)$.

The right-hand sides of equations *(2.30)* to *(2.34)* are, then, of order δ^2 and can be neglected if 6 is small. If the equations are now transformed to axes parallel to the original axes and moving in the +ve ξ direction with velocity $V_\infty \cos \alpha$, and the substitutions:

$$\frac{\partial}{\partial \bar{\xi}} = \frac{\partial}{\partial \bar{\xi}'}$$

$$\frac{\partial}{\partial \bar{t}} = \frac{\partial}{\partial t'} - \frac{\partial}{\partial \xi'} \qquad \ldots (2.36)$$

are made, equations *(2.30)* to (2.34) transform to

$$\delta \cot a \frac{\partial \bar{\rho}}{\partial \bar{t}'} + \frac{\partial(\bar{\rho v})}{\partial \bar{\eta}} + \frac{\partial(\bar{\rho w})}{\partial \bar{\zeta}} = 0 \quad , \qquad \ldots (2.37)$$

$$6 \cot a \frac{\partial \bar{u}}{\partial t'} + \bar{v} \frac{\partial \bar{u}}{\partial \bar{\eta}} + \bar{w} \frac{\partial \bar{u}}{\partial \bar{\zeta}} + \delta \tan \alpha \frac{\partial \bar{p}}{\partial \bar{\xi}'} = 0, \qquad \ldots (2.38)$$

$$\delta \cot \alpha \frac{\partial \bar{v}}{\partial t'} + \bar{v} \frac{\partial \bar{v}}{\partial \bar{\eta}} + \bar{w} \frac{\partial \bar{v}}{\partial \bar{\zeta}} + \frac{\partial \bar{p}}{\partial \bar{\eta}} = 0, \qquad \ldots (2.39)$$

$$6 \cot \alpha \frac{\partial \bar{w}}{\partial \bar{t}'} + \bar{v} \frac{\partial \bar{w}}{\partial \bar{\eta}} + \bar{w} \frac{\partial \bar{w}}{\partial \bar{\zeta}} + \frac{\partial \bar{p}}{\partial \bar{\zeta}} = 0, \qquad \ldots (2.40)$$

$$6 \cot a \frac{as}{\partial \bar{t}'} + \bar{v} \frac{as}{\partial \bar{\eta}} + \bar{w} \frac{as}{\partial \bar{\zeta}} = 0, \qquad \ldots (2.41)$$

and the problem reduces to that of an expanding, contracting and translating piston in two dimensions.

In the original derivation by Sychev, he states that the equations are valid only for a body with all transverse dimensions small in comparison with its length. In fact, there seems no reason why the results should not apply in two-dimensional flow and for swept wings on a strip basis, provided the flow remains attached at the leading edge. But, clearly, there is a range of bodies which have significant lateral dimensions on which the flow detaches at the leading edge at moderate angles of attack, or is never attached, and in these cases the theory will not apply.

It/

It was pointed cut at the beginning of the discussion of Sychev's extension of small disturbance theory that the theory only applied for the windward side of bodies. It can be shown for two-dimensional bodies that the pressures on the leeward side are small enough in comparison with those on the windward side for their neglect to introduce errors of the same size as the other terms neglected in the theory.

2.1.3 The variational method

Some special steady flow problems are solved according to small-disturbance theory in Ref. 24, but there does not appear to have been any attempt to solve equations (2.15) and (2.17) to (2.19) directly for unsteady conditions. Nevertheless, general conclusions about the nature of the hypersonic flow around slender bodies derived from small-disturbance theory have been used as a basis for applying a variational method to the solution of some unsteady problems and the shock-expansion method to the solution of others. The fullest account of this work is given in Refs. 19, 20 and 26, and there are shorter accounts in Refs. 13 and 27.

The results of the small-disturbance theory analysis have shown that the flow around a slender three-dimensional body becomes the problem of flow around an expanding, contracting and translating piston in two dimensions, and the flow around a thin two-dimensional section simplifies, in the same way, to a one-dimensional problem. In Ref. 19 it is suggested that a variational method should be used to solve the equivalent two-dimensional flow problem for a slender body (the method could also be used for the equivalent one-dimensional flow for a thin section, but the interest in this case is trivial). The method assumes that the flow can be considered as isentropic, but this is considered to be a reasonable approximation for values of $M\delta < 1$. This conclusion is based on the fact that analyses which assume isentropic conditions (e.g., 3rd order piston theory) give satisfactory results on two-dimensional sections up to the value $MS \simeq 0{\cdot}7$ (corresponding to $M\theta_N \simeq 0{\cdot}7$ for a double wedge and $M\theta_N \simeq 1{\cdot}4$ for a biconvex section) and the entropy rise across the nose shock from a wedge is considerably greater than that for a cone with the same value of $M\theta_N$.

For general flow under isentropic conditions the variational method starts from a consideration of the integral

$$I = \int_{t_1}^{t_2} \int_{V(t)} \rho \left[\tfrac{1}{2}q^2 - \frac{d\phi}{dt} - E(\rho) \right] dV\, dt \equiv \int_{t_1}^{t_2} \int_{V(t)} p\, dV\, dt \qquad \ldots (2.42)$$

applied to the conditions set up in the stationary fluid by the motion of the body. The integral is taken over the disturbed volume of the fluid between two fixed times t_1 and t_2 at which conditions are known. ρ is the fluid density, q is the fluid velocity, ϕ is the fluid velocity potential function, $E(\rho)$ is the internal energy per unit volume, $\frac{d}{dt} \equiv \frac{\partial}{\partial t} + u \frac{\partial}{\partial x} + v \frac{\partial}{\partial y} + w \frac{\partial}{\partial z}$, and p is the fluid pressure. (Clearly, the first integral in (2.42) reduces to $\int_{t_1}^{t_2} \int_{V(t)} -\rho \left[\tfrac{1}{2}q^2 + \frac{\partial \phi}{\partial t} + E(\rho) \right] dV\, dt$ for this case, but the form given is more closely related to the form used in more general formulations of the variational principle for fluids). The conditions for the first integral in (2.42) to be a

minimum/

minimum are that its variations for small variations in the values of p, q and ϕ should be zero. These conditions can be shown to lead to the equations of continuity, irrotationality and momentum for the flow, so that the problem of finding the flow by solving the equations of motion for the fluid can be changed into that of finding a function for p which makes the integral in equation (2.42) a minimum.

For isentropic conditions, p can be expressed in terms of the velocity potential, ϕ, in the form

$$\frac{p}{p_\infty} = \left[1 - \frac{(\gamma-1)}{a_\infty^2}\left(-\frac{\partial\phi}{\partial t} + \tfrac{1}{2}q^2\right)\right]^{\gamma/(\gamma-1)} \qquad (2.43)$$

where a_∞ is the free-stream speed of sound. Using this expression, equation (2.42) can be written in the form

$$I \equiv \int_{t_1}^{t_2}\int_{V(t)} p\, dV\, dt = \int_{t_1}^{t_2}\int_{V(t)} p_\infty\left[1 - \frac{(\gamma-1)}{a_\infty^2}\left(\frac{\partial\phi}{\partial t} + \tfrac{1}{2}q^2\right)\right]^{\gamma/(\gamma-1)} dV\, dt, \qquad (2.44)$$

and the problem becomes that of finding a function for ϕ such that the variation in I is zero for small variations in ϕ. This problem can be solved in an approximate manner by assuming a finite series for ϕ which satisfies the boundary conditions (including the known conditions at t_1 and t_2) and in which the coefficients are determined by the condition that the variation in I for small variations in each coefficient must be zero.

When this general method is applied to the case of flow around a two-dimensional piston in Ref. 19 it is shown that the statement of the variational principle must be modified slightly to take account of the fact that the conditions at time t_2 are not known. The modified statement has the form

$$\Delta\int_{t_1}^{t_2}\int_{V(t)} p\, dV\, dt + \int_{V(t_2)} [\rho\Delta\phi]_{t=t_2} dV = 0 \qquad \ldots(2.45)$$

where $\Delta\int_{t_1}^{t_2}\int_{V(t)} p\, dV\, dt$ is the small variation in the integral for a small variation in p (or ϕ), and $\Delta\phi$ is the corresponding small variation in ϕ. The variations must be taken so that $\Delta\phi = 0$ at the outer wave from the piston, the boundary conditions at the piston are unaltered, and at time t_1 the disturbed volume is zero or the flow is known everywhere and the variations are correspondingly restrained. When both p and ρ are expressed in terms of the velocity potential equation (2.45) can be written as:

$$\Delta\int_{t_1}^{t_2}\int_{S(t)}\left[1 - \frac{(\gamma-1)}{a_\infty^2}\left(\frac{\partial\phi}{\partial t} + \tfrac{1}{2}\left(\frac{\partial\phi}{\partial y}\right)^2 + \tfrac{1}{2}\left(\frac{\partial\phi}{\partial z}\right)^2\right)\right]^{\gamma/(\gamma-1)} dy\, dz\, dt$$

$$+ \frac{\gamma}{a_\infty^2}\int_{S(t_2)}\left\{\left[1 - \frac{(\gamma-1)}{a_\infty^2}\left(\frac{\partial\phi}{\partial t} + \tfrac{1}{2}\left(\frac{\partial\phi}{\partial y}\right)^2 + \tfrac{1}{2}\left(\frac{\partial\phi}{\partial z}\right)^2\right)\right]^{1/(\gamma-1)}\Delta\phi\right\}_{t=t_2} dy\, dz \qquad \ldots (2.46)$$

where S(t) is the disturbed area in the two-dimensional problem. Zartarian[19]/

Zartarian[19] gives examples of solutions using this method for simple shapes for which known solutions are available (e.g., flow past cylindrical and elliptic cones and ogival shapes), and shows that good agreement with more exact solutions is obtained even for small numbers of terms in the series for ϕ. It is shown in Ref. 26 that some more complex cross-section shapes can be dealt with by using suitable co-ordinate transformations to give simpler forms. Because of the limitation to approximately isentropic conditions, the variational method is limited to bodies at small angles of Incidence although the small-disturbance theory still applies up to large incidences.

2.1.4 The shock-expansion method

The shock-expansion method for calculating the flow field around bodies in high-speed flow was developed for steady flow conditions[28,29,30,31]. Its use for the calculation of unsteady flows is based on the fact that the results of the small-disturbance theory analysis can be interpreted as meaning that the flow in any given lamina of fluid whose plane is (approximately) normal, to the longitudinal axis of a body (or to the mean chord of a wing section) is independent of the flow in adjacent laminae. Because of this independence, the flow at a given station along the body depends only on the body shape that has been 'seen' by the lamina at that station. In general, the lamina 'sees' the body shape as an expanding and contracting piston with translational velocity, and the analysis of the flow is independent of the fact that the translational velocity may be the result of incidence and camber on a body in steady motion, or the pitching and translation of a body in unsteady motion. Consequently, according to small disturbance theory, the flow at a given station on a body in unsteady motion is the same as that for a body of the same cross-section, with an appropriate axial distortion; and the flow at a series of points along a body in unsteady motion can be found by a series of appropriate steady flow calculations. The shock expansion method is suitable for carrying out these equivalent steady flow calculations, for small-amplitude motions at Mach numbers for which real gas effects are not important, gives closed form expressions for the overall force and pitching moment.

In the simplest form, the shock-expansion method for two-dimensional flow, the oblique shock relations are applied to the wedge flow at the leading edge of the section to give the conditions just behind the shook wave and the conditions on the surface downstream are considered as given by applying the Prandtl-Meyer expansion relation along the surface from the leading edge condition. The Prandtl-Meyer relation in this case is given by

$$\frac{\partial p}{\partial s} = \frac{2\gamma p}{\sin 2\beta_L} \cdot \frac{\partial \theta}{\partial s}, \qquad \ldots (2.47)$$

where S is the distance measured along the body surface, p and β_L are the local values of pressure and of the parameter $\beta = \sqrt{M^2-1}$, and θ is the local inclination of the surface to the free-stream direction. For a thin section this can be integrated to give the expression:

$$\frac{p(x)}{p_N} = \left\{ 1 + \left(\frac{\gamma-1}{2} \right) M_N [\theta(x) - \theta_N] \right\}^{2\gamma/(\gamma-1)}, \qquad \ldots (2.48)$$

where the subscript N denotes conditions at the leading edge.

This/

This simple form of the method ignores the effect of the reflection of disturbances from the body surface at the shock wave and from regions of entropy gradient in the flow, and. the picture of the flow as consisting of a straight shock wave from the nose followed by a simple expansion is not in general adequate for the whole field. The significance of these reflections has been examined. in Ref. 28 and it is found that, at the body surface, the reflected disturbances tend to cancel each other for the condition $\gamma > 1{\cdot}3$. Since this condition holds for most flows of practical interest, the simple theory is adequate to give surface pressure information.

For thin two-dimensional sections undergoing small-amplitude sinusoidal distortions about zero mean incidence in flow3 of sufficiently high Mach numbers, the expressions for the nose shock conditions and for the Prandtl-Meyer relation can be simplified and, as a result, a closed-form expression for the lift distribution can be developed. For a symmetrical section the expression is[19]:

$$\frac{p_\ell - p_u}{p_\infty} \simeq 2e^{ikt}\left\{\frac{2\gamma}{(\gamma+1)}\left[(\bar{\beta}M)^2 - 1\right] + 1\right\}\left\{1 + \frac{(\gamma-1)}{2}\bar{M}_N\,\bar{\Delta}(x)\right\}^{2\gamma/(\gamma-1)} \times$$

$$\times \left\{\eta_C - \frac{dg(0)}{dx} + ikg(0)\right\} e^{-ikx} +$$

$$+ \gamma\bar{M}_N\left[m\bar{\Delta}(x) - 1\right]\left[\frac{dg(0)}{dx} + ikg(0)\right] e^{-ikx} + \left[\frac{dg}{dx} + ikg\right]\Big] \quad \ldots \quad (2.49)$$

where g(x) is the complex amplitude of the time-dependent motion; η and m are the rates-of change of pressure and Mach number at the nose with change of nose angle; M_N is the value of the Mach number at the nose for zero distortion; $\bar{\beta}$ is the value of the shock inclination angle for zero distortion; and $\bar{\Delta}(x)$ is the turning angle of the flow from the nose due to thickness alone.

For conditions where the simplified expressions for the nose conditions and the expansion could not be applied, where the amplitude was not small, or when real gas effect3 became important, numerical methods would have to be employed.

The shock-expansion method can be applied to slender three-dimensional bodies for which $M\delta$ is greater than a limit around unity (the limit is not rigid; errors become greater as unity is approached) because it can be shown for such bodies that the flow on the body surface is locally two-d' imensional in planes normal to the body surface and tangential to the streamlines[29,30,31], and as a consequence of this, the Prandtl-Meyer relation can be applied along the surface streamlines. The surface streamlines can be shown to follow closely the surface geodesics through the nose. A geodesic is a line on a surface such that at any point its projection on the tangent plane at that point has zero curvature; it is determined by the geometry of the surface so that once the initial direction of the surface streamlines is known the expansion conditions can, in principle, be determined from the geometry of the surface. The condition3 at the nose of the body must, of course, be found from the flow over a cone hating the same cross-section as the body at the nose. This presents a limitation for the application of the method since the flow is known only for cones with certain simple cross-sections at small angles of yaw.

For/

For bodies of revolution at small incidence and amplitudes of motion it can be assumed that the surface streamlines remain the meridian lines throughout the motion and a closed form expression can be developed for the surface pressure distribution. But for bodies of other cross-sections, or for large amplitudes of motion, both the nose shock conditions and the surface geodesics become difficult to determine.

Because of the Sychev extension of small-disturbance theory to large incidences, unsteady shock expansion theory can be applied, for two- and three-dimensional bodies, to oscillations about a large mean incidence, and, in a step-wise manner, to large amplitude oscillations - provided the shock remains attached throughout the motion.

2.1.5 Small perturbation analyses

The last methods of analysis that will be discussed both assume, as a starting point, that the steady flow is known in a suitable form and that the unsteady motion of the body is small enough for the disturbances set up by it to be small in comparison with the steady flow quantities.

The first method, put forward by Kennett[32], considers the case of flow in the neighbourhood of the stagnation point of a bluff body of revolution.

The equations of the flow are derived in terms of a curvilinear co-ordinate system based on the body surface, as shown in Fig. 7. It is assumed that the density in the shock layer is constant, that the body motion does not produce any density changes, and that the flow perturbations caused by the unsteady motion are small in comparison with the steady flow quantities. The flow equations are re-expressed in terms of the steady flow quantities and the unsteady perturbations, and they are then linearised in the perturbations. The following set of equations is obtained:

$$\frac{\partial u'}{\partial t} + \frac{1}{1 + K_b y}\left(u_o \frac{\partial u'}{\partial x} + u' \frac{\partial u_o}{\partial x}\right) + v_o \frac{\partial u'}{\partial y} + v' \frac{\partial u_o}{\partial y} + \frac{1}{\rho_o (1+K_b y)} \frac{\partial p'}{\partial x}$$

$$+ \frac{K_b}{1 + K_b}(u_o v' + v_o u') = O(q'^2), \qquad \ldots (2.50)$$

$$\frac{\partial v'}{\partial t} + \frac{1}{1 + K_b y}\left(u_o \frac{\partial v'}{\partial x} + u' \frac{\partial v_o}{\partial x}\right) + v_o \frac{\partial v'}{\partial y} + v' \frac{\partial v_o}{\partial y} + \frac{1}{\rho_o} \frac{\partial p'}{\partial y}$$

$$\frac{2K_b}{1 + K_b y} u_o u' = O(q'^2), \qquad \ldots (2.51)$$

$$\frac{\partial w'}{\partial t} + \frac{u_o}{1 + K_b y} \frac{\partial w'}{\partial x} + v_o \frac{\partial w'}{\partial y} + \frac{1}{r\rho_o} \frac{\partial p}{\partial \phi} + \frac{u_o w'}{(1+K_b y) r} \frac{\partial r}{\partial x} + \frac{w' v_o}{r} \frac{\partial r}{\partial y} = O(q'^2), \quad (2.52)$$

and/

and $$r\frac{\partial u'}{\partial x} + u'\frac{\partial r}{\partial x} + (1+K_b y)r\frac{\partial v'}{\partial y} + v'\left[(1+K_b y)\frac{\partial r}{\partial y} + rK_b\right] + (1+K_b y)\frac{\partial w'}{\partial \phi} = O(q'^2), \quad \ldots (2.53)$$

where $u_0 + u'$ is velocity component in x-direction (see Fig. 7)
$v_0 + v'$ is velocity component in y-direction
w' is velocity component in ϕ-direction
ρ_0 is the steady flow density
K_b is the body surface curvature in the meridianal (x,y)-plane
q' is u', v', or w', whichever is the greater.

The terms in equations (2.50) - (2.53) are next subjected to an order of magnitude analysis starting from the assumption that for hypersonic flow

$$\varepsilon_0 = \frac{P0}{\rho_\infty} >> 1$$

and using the results of steady flow analyses to conclude that

$$\left.\begin{aligned} &\frac{u_0}{U} = O(i), \qquad \frac{p_0}{\rho_0 U^2} = O(1), \\ &\frac{v_0}{U} = O(\varepsilon_0^{-1}), \quad \text{and} \quad \frac{A}{R_0} = O(\varepsilon_0^{-1}), \end{aligned}\right\} \quad \ldots (2.54)$$

where Δ is the shock stand-off distance and R_0 is the nose radius of curvature.

It is also established that if

$$\frac{u'}{U} = O(K) << 1, \quad \frac{v'}{v_0} << 1, \quad \frac{p'}{\rho_0} << \text{and} \quad \frac{w'}{u_0} << 1, \quad \ldots (2.55)$$

where K is a measure of the order of magnitude of the perturbations, then

$$\frac{v'}{U} = O\left(\frac{K}{\varepsilon_0}\right), \quad \frac{p'}{\rho_\infty U^2} = O(K), \quad \text{and} \quad \frac{w'}{U} = O(K). \quad \ldots (2.56)$$

When the equations (2.52) - (2.55) are non-dimensionalised. and terms of order K/ε_0 are neglected then the following dimensional equations are obtained:

$$\left[u_0\frac{\partial}{\partial x} + v_0\frac{\partial}{\partial y} + \left(iw + \frac{\partial u_0}{\partial x}\right)\right]\tilde{u} + \left(\frac{\partial u_0}{\partial y}\right)\tilde{v} = O(\varepsilon_0^2) + O\left(\frac{K}{\varepsilon_0}\right), \quad \ldots (2.57)$$

$$\frac{\partial \tilde{p}}{\partial y} - 2\rho_0 u_0 K_b \tilde{u} = O(\varepsilon_0^2) + O\left(\frac{K}{\varepsilon_0}\right), \quad \ldots (2.58)$$

$$\left[u_0\frac{\partial}{\partial x}\right/$$

$$\left[\frac{\partial}{\partial x} + v_o \frac{\partial}{\partial y} + \left(iw + \frac{u_o}{r_b}\frac{\partial r_b}{\partial x}\right)\right] ; = O(\varepsilon_o^2) + O\left(\frac{K}{\varepsilon_o}\right), \quad \ldots (2.59)$$

$$\text{and} \quad \left(\frac{\partial r_b}{\partial x} + r_b \frac{\partial}{\partial x}\right)\tilde{u} + r_b \frac{\partial \tilde{v}}{\partial y} + \frac{\partial \tilde{w}}{\partial \phi} = O(\varepsilon_o^2) + O\left(\frac{K}{\varepsilon_o}\right) \quad \ldots (2.60)$$

where r_b is the body radius of revolution, and simple harmonic motion has been assumed with

$$\begin{aligned} u'(x,y,\phi;t) &= \tilde{u}(x,y,\phi)e^{iwt}, \\ v'(x,y,\phi;t) &= \tilde{v}(x,y,\phi)e^{iwt}, \\ w'(x,y,\phi;t) &= \tilde{w}(x,y,\phi)e^{iwt}, \\ \text{and} \quad p'(x,y,\phi;t) &= \tilde{p}(x,y,\phi)e^{iwt}. \end{aligned} \quad \ldots (2.61)$$

From the equations (2.57) - (2.60) it can be seen that (2.57), (2.59) and (2.60) can be combined to give a single equation for $\tilde{u}$. When $\tilde{u}$ is known $\tilde{p}$ can be found by integrating equation (2.58).

The boundary conditions at the body and shock are analysed and simplified in a similar way. Five boundary conditions are obtained because another unknown, the shock wave position, must be introduced.

To illustrate the application of the analysis, Kennett considers the case of a spherical cap in plunging sinusoidal motion. He takes as a basis an approximate flow field and relations originally derived by Hayes, and is able to find a solution for $\tilde{u}$ in the form of a series in y, the co-ordinate normal to the body surface with coefficients dependent on the frequency parameter - so that, for small frequency parameters, only a few terms are required. The solution is considered to be valid within 10% up to the point where the surface slope is 45" and this corresponds to the range of applicability of the constant density assumption.

Kennett regards the results of his analysis as a first-order correction to the results from quasi-steady Newtonian theory in which it is assumed that the shook and body move together, and the perturbation pressure behind the shook is the perturbation pressure on the body. He finds that the shock amplitude is given by

$$\bar{Y}_s = \frac{\tilde{Y}_s}{R_o} = \bar{Y}_b\left[1 + \left(\frac{ik}{5}\right)\left(\frac{\xi - \sin\xi\cos\xi}{\sin^2\xi}\right)\right], \quad \ldots (2.62)$$

where $\xi = \frac{x}{R_o}$, R_o = radius of spherical cap

and $\bar{Y}_b = \frac{\tilde{Y}_b}{R_o}$ is the dimensionless amplitude of the body surface displacement.

The pressure is given by

$$\bar{p}_b = \frac{\tilde{p}}{\frac{1}{2}\rho_\infty U^2} = \bar{p}_{o_b} + \left\{4ik\cos\xi + 4\sin^2\xi\frac{\bar{Y}_b}{\bar{Y}_s} - 5\tfrac{3}{9}\sin^2\xi\right\}\bar{Y}_s. \quad \ldots (2.63)$$

The/

The cut-of-phase component of $\bar{Y}_s$ is plotted in Fig. 8 and the cut-of-phase component of $\bar{p}_b$ is plotted in Fig. 9 in comparison with the quasi-steady Newtonian result. At practical values of $k\bar{\lambda}$ where $\bar{\lambda} = \tilde{\lambda}/R_o$ is the non-dimensional amplitude of the cap plunging motion, it is clear that the cut-of-phase component of the shock wave motion will be negligible over the range of applicability of the analysis. The cut-of-phase component of the pressure is small for quasi-steady Newtonian theory; the present theory provides a correction of the order of 5% at the limit of its application.

The analysis by Holt[33] can be applied to those parts of the flow around a body where supersonic conditions exist, and a characteristic analysis has been carried cut. Starting from an established flow field and known characteristic directions, Holt expresses the flow equations in terms of a cc-ordinate system based on the given characteristic directions and introduces small perturbations of the flow quantities. If squares and products of the perturbation quantities are neglected, the equations become linear equations for the perturbations with coefficients determined by the steady flow solution. Holt applied this analysis to the simple case of isentropic flow over an axisymmetric conical afterbody in Ref. 33. More recently, Kawamura and Tsien[34] applied the method of analysis to an axisymmetric body to determine the stability derivatives, but this is for, effectively, steady state conditions.

The small perturbation methods of solution can be valid only when the conditions are such that the hypersonic similarity parameter for the body motion, $M\delta$ (where δ is the change in surface slope due to the motion), is small, so that disturbances to the flow quantities are sufficiently small. In general, numerical solutions will be necessary, but this is unlikely to be an important drawback since a numerical solution of the steady flow held will usually have been necessary in the conditions for which the methods are best used.

2.2 The Influence of Real Gas Effects and Viscosity

It was pointed cut in Appendix I that, in many hypersonic flows, temperatures will be generated in the gas which are sufficient to cause excitation of vibrational degrees of freedom of pclyatcmic gas molecules, dissociation, and ionisation; and that these effects can give rise to significant modifications to the flow. Fortunately, the characteristic times involved in these reactions will usually be very short in comparison with the characteristic time of any flow unsteadiness likely to be met in practice. For example, the relaxation time for dissociation of oxygen for flow in the stagnation region of a blunt body at $M = 15$ at 200 000 ft is of the order of 2×10^{-4} seconds, whereas the maximum frequency for any unsteady motion involving the structure of a vehicle is unlikely to be as high as 100 cycles per second, and will, usually, be very much less than this. Consequently, although the effects of these changes in the gas can complicate analysis, they can usually be dealt with on a quasi-steady basis.

The effects of viscosity are not as clearly defined. The first effects that must be considered exist already in steady flow and arise from the fact that boundary layers are in general very much thicker than at lower Mach numbers because of the rise in the temperature of the gas as a result of its deceleration in the layer, and the smaller unit Reynolds numbers associated with high altitude flight. The thickness of the boundary layer can be such that it exerts a significant influence on the external 'inviscid' flow. A measure of this influence is usually given by the size of the parameter χ defined by:

$$\chi = M^3 (c_\infty / Re_x)^{\frac{1}{2}} \qquad \ldots (2.64)$$

where/

where c_∞ is the constant in the viscosity relation:

$$\frac{\mu}{\&a} = c_m \frac{T}{T_\infty}$$

and can often be taken as unity; and Be, is the Reynolds number based on the distance from the leading edge.

For $\chi >> 1$, a condition which can occur close to a sharp nose Or leading edge, the streamline inclination induced by the boundary layer can be larger than that due to the body surface inclination: this is termed a 'strong interaction'. But, over most Of the body and especially when the nose is not very sharp, the effect Of the boundary layer can usually be considered as being a small perturbation of the inviscid flow.

The boundary layer on an oscillating body does not seem to have been examined directly, and the only analytical evidence on its behaviour appears to be a study by Lighthill[35], for an incompressible fluid, of the response Of a boundary-layer-type flow to fluctuations Of velocity in the external flow and a study by Moore[36] of the compressible boundary layer on an accelerated plate. The scale Of unsteadiness can be measured by a frequency parameter $\omega_0 x/v_0$, where $\omega_0 = 2\pi f_0$ and f_0 is the frequency of the fluctuations v_0 is the mean external velocity, and x is the distance from the leading edge of the surface. Lighthill's analysis suggests that the boundary layer can be treated by a quasi-steady Or first order unsteady theory for $\omega_0 x/v_0 << 0{\cdot}6$.

Moore's analysis shows that the scale of unsteadiness can be measured by parameters of the form $\frac{x}{v_0^2}\frac{dv_0}{at}, \frac{x^2}{v_0^3}\frac{d^2v_0}{at?}, \ldots$ for a sinusoidal Velocity variation, the first parameter in this sequence would be equivalent to the frequency parameter in Lighthill's work. Moore concludes that the flow can be analysed on a first-order unsteady basis for small values of the unsteadiness parameters.

These results suggest that, for most conditions where unsteady hypersonic flows are likely to occur, the thickness of the boundary layer and, consequently, its effect on unsteady aerodynamic forces, can be found by assuming that it responds in a quasi-steady manner to changes in the external flow conditions, since the frequency parameters will be considerably less than the limiting value proposed by Lighthill. This conclusion obviously requires investigation, especially in view of some anomalies in experimental results which are mentioned in (2.3) and there are some oases (for example, panel flutter) where frequency parameters could be higher than the limit suggested.

2.3 Experimental Verification of Theoretical Analyses

There have been very few reports of experimental measurements Of unsteady forces at hypersonic speeds. Those reports which show comparisons with theoretical calculations are References 17, 37, 38 and 39. In the report by Maas[39] the comparisons are not very informative because of the uncertainties in the measurements and. the lack of clarity about what theoretical methods are being used. The comparisons in the other reports are clearer, but there are only scanty results. Because Of this situation it is necessary to Consider the accuracy of the methods of analysis under steady conditions to get some

indication/

indication of their reliability, even though results of their use under steady conditions cannot be conclusive evidence of their value when the flow is unsteady.

In Figs. 10 and 11 third order piston theory predictions for the pressure distribution on a biconvex parabolic arc section aerofoil are shown compared with the distribution from a characteristics solution, which should be accurate for the inviscid flow. For a two-dimensional section the correction for boundary layer growth should be straightforward and need not be considered in this comparison. At $M = 3'5$, in Fig. 10, the agreement is quite close, though third-order piston values are consistently low; at $M = 10$, in Fig. 11, the errors are much greater. The departures from the characteristics result are greatest in the regions of the nose and trailing edge over which $M\theta > 1$ (θ is the surface slope). The error in the prediction of the oentre of pressure for a single surface would be quite large, but this does not necessarily mean that the oentre of pressure for the section is similarly in error, since this depends on the increment of pressure difference with incidence and not the overall distribution.

Calculations by Newtonian impact theory are compared with characteristic results for the same biconvex section at $M = 10$ and ∞ for zero incidence, and at $M = 10$ for an incidence of $19{\cdot}9^\circ$ in Figs. 11, 12 and 13. Results are shown for equation (6) and for this expression modified to give the correct pressure at the leading edge. The unmodified equation always gives values of pressure that are considerably lower than the accurate values. The modified equation is inadequate at $M = 10$, $\alpha = 0^\circ$ (Fig. 11); even at $M = \infty$ it is considerably in error beyond the one third chord point (Fig. 12). For the section at an incidence of $19{\cdot}9^\circ$, the theory is being tested under very favourable conditions, since there should be only a thin shook layer over the lower surface of the section. Even for this case (Fig. 13), there are appreciable errors in the pressure distribution given by the modified expression.

Results for two-dimensional shook-expansion theory are given in Figs. 14 and 15. In Fig. 14, pressure distributions on the same 1% aerofoil section as before are given for the characteristics calculation, for the shock expansion method, and for a simplified version of the shook expansion method applicable to slender bodies at high Mach number (this slender aerofoil method corresponds to the expressions used to derive equation (2.49)). There is close agreement of the methods. In Fig. 15, the effect of real gas thermodynamics on the pressure distributions are shown. When caloric and thermal imperfections of the gas are fully considered in the shock expansion method, the results differ very little from the characteristics result, consequently the characteristics results have not been included in Fig. 15. The results from the slender aerofoil method use an average value of γ throughout the field. Above an incidence of about 10° it is clear that the departures from perfect gas behaviour become significant, especially for the slender aerofoil method.

Figs. 16 and 17 illustrate the use of *generalised* shock expansion theory on an ogival body of revolution. In Fig. 16 comparison is made with both characteristics results and with experiment. At adequate values of $M\delta = Md/\ell$ agreement with the characteristics results is seen to be good, and Fig. 17 shows that the agreement with experiment is also good if account is taken of the boundary layer. (In Ref. 29 it is argued on physical grounds that, provided the boundary layer flow is largely hypersonic, and the conditions governing the application of two-dimensional shock expansion theory to a three-dimensional body are satisfied; the boundary layer flow along geodesics can also be calculated using two-dimensional relationships). In Figs. 19-23 results are given for the application of shock expansion theory to more complex slender

bodies 26./

bodies[26]. The shape of these bodies (Fig. 18) is such that there are no direct solutions for the conical shock at the nose and conditions have to be determined by perturbing the solution for a circular cone; calculation of the general geodetics of the surface is too complex to be practicable and pressure distributions are found by the shock expansion method only along top, bottom and side geodesics; the distribution on the rest of the surface is found by assuming that the distribution at a given section is the same as for a cone which is locally tangent to the body (this distribution is known from the solution found for the nose). Two bodies are considered. They have identical cross-sections but one is straight and the other cambered so that it is equivalent, according to small disturbance theory, to the straight body undergoing a uniform rate of pitch. For the straight body, the pressures predicted are found to be consistently lower than those measured, though the shape of the distribution is predicted, Fig. 19. About half the difference between theory and measurement can be accounted for by the effect of the boundary layer (Fig. 20). The incremental pressure distributions with incidence are found to be quits closely predicted except on the leeward side of the body when separation, or a thickening of the boundary layer, appears to take place (Fig. 21). Similar results are found for the cambered body. The difference in the calculated and measured basic pressure distributions are of the same order as those for the straight model (Fig. 22) and the incremental pressure distributions with incidence are, again, well predicted (Fig. 23). It was not possible to assess the accuracy of the incremental pressures due to camber because this would have involved comparisons of pressures measured on the two models and slight differences between the models and in the tunnel conditions meant that this was not possible.

Figs. 24 and 25, from Reference 19, show comparisons between flutter derivatives for two-dimensional sections calculated by second-order piston theory, third-order piston theory, and by shock expansion theory. From the steady state comparisons it is to be expected that third-order piston theory will be increasingly in error as $M_\infty\theta_N$ increases beyond unity, and this is shown by these figures. But the figures also show that the errors for some sections (the biconvex section) need not be very large either in the derivatives or in the oentre of pressure position, up to quite high values of the parameter $M\theta_N$, and consequently piston theory may remain valuable for flutter calculations well beyond the theoretical limits for its application.

Results of unsteady measurements are shown in Figs. 26 to 29. Figs. 26 and 27, from Ref. 17, show results of measurements on a $9\frac{1}{2}^\circ$ semi-angle, single-wedge section in a gun tunnel in air at $M \simeq 9{\cdot}7$. The aerodynamic damping and stiffness were found from measurements of the change due to the air flow in the rate of decay and in the frequency of oscillations in pitch of the model, which was mounted on a spring support. Fig. 26 shows the results of the stiffness measurements. The results are compared with calculation by strong shock piston theory with an empirical correction for nose bluntness effects. The theory gives good agreement with experiment for the sharp leading edge model, though there is some deterioration for axes positions at the nose and trailing edge. The bluntness correction makes agreement worse, on the whole, for the blunt leading edge models. There is a significant change in stiffness with the bluntness for most axis positions. Fig. 27 shows the results for aerodynamic damping and similar comparisons with theory. The differences between theory and experiment vary greatly with axis position and it seems clear that there must be large effects occurring which are not accounted for by the theory. The effect of blunting also varies greatly with axis position.

Fig. 28 shows the results reported in Ref. 37 of similar experiments on a double-wedge aerofoil in a helium tunnel. Again, the large difference

between/

between theory and. experiment is to be noted, though it should be understood that for high Mach numbers the actual aerodynamic damping respresented by these values is low. The result for a sharp-nosed single wedge oscillating about the trailing edge is included from Ref. 17: because, at high Mach numbers, pressures on the rear half of a double wedge are very low, the results can be compared with those of Ref. 37. There seems to be agreement between the results from the two sets of experiments.

The results of Refs. 17 and 37 are too few in number, and there are too many uncertainties about experimental conditions and Interferences in the flow (e.g., it is pointed out in Ref.17 that the shock waves from the model support are likely to have a large influence on the flow over the model for forward axis positions) for definite conclusions to be drawn. It appears that the influence of bluntness is much greater than is predicted by simple corrections based on induced pressure measurements on flat plates[17]. The influence of the boundary layer may be greater than is predicted on the assumption that it behaves in a quasi-steady manner, for it appears that a correction based on this assumption would account for less than half the difference between theory and experiment shown in Fig. 28.

Fig. 29, from Ref. 38, shows a comparison between the aerodynamic. damping on a bluff body found by experiment, and the value predicted by Newtonian impact theory. The experimental results were found from free oscillation measurements. The theoretical and experimental values do not agree closely, but the theoretical values are of the right order of magnitude and have the right sign.

2.4 Discussion and Conclusions

The methods that have been described provide for the analysis of only a small part of the unsteady hypersonic flows that may be met in practice. This fact becomes evident when the attempt is made to set down what practical flow problems can be dealt with, and what work remains to be done.

Piston theory, shock expansion theory, and the variational method provide means that are physically and analytically valid for calculating surface pressures in a range of simple inviscid flows. For wings of thin sharp section which are two-dimensional or have only moderate sweep (the condition $\delta A^{-1} \ll 1$ is satisfied) third-order piston theory can be applied for Mach numbers and incidences such that $M\delta$ or Ma < about 0·9, and δ or $\alpha \gg 1/M^2$, and shock expansion theory can be applied for $M\delta > 1{\cdot}0$ and for incidenoes up to the value for shock detachment, though numerical computation may become necessary for large values of flow turning angle at the nose.

For low aspect ratio wings of thin, sharp section, for $M\delta$ and $M \cos A \leqslant 1$ (where A = sweep angle of the leading edge), the variational method should be applicable, though its use for the flow round such a cross-section has not been examined. Only small incidences could be *considered,* because the method depends on the fact that the flow in a fluid lamina can be considered as isentropic.

For pointed slender bodies, the variational method can be applied for $M\delta \leqslant 1$ and for small incidenoes, and the generalized shook expansion method can be applied for MS > 1 and for large incidences. There may, however, be limitations on application of the methods arising from the shape of the body cross-se&ion, or from the difficulty of determining the nose starting conditions for the shock expansion method.

During/

During panel flutter the surface displacements remain very small because of the physical constraints involved, and piston theory applied in the flow conditions set up by the body should remain valid.

Although these methods are valid for inviscid flows, the accuracy with which surface pressures could be found in a real flow would depend on the accuracy with which corrections for the boundary layer influence could be found, and the degree of interaction between the boundary layer and the external flow.

There remain a large range of flows for which these methods are not valid. In fact, wing sections with sharp leading edges and pointed slender bodies are not likely to be used at high Mach numbers because of the large heating rates which a pointed leading edge or nose would experience, and the high structure temperatures that would occur. The flows around slender wing sections and bodies with leading edge or nose blunting, which would be employed to reduce temperatures and heating rates in these regions, present a range of new problems because, at high Mach numbers, the flow around a body is significantly affected by even small degrees of blunting, and the assumptions of small disturbance theory are not necessarily any longer applicable.

Beside the leading edge blunting problem there remain the problems of two-dimensional and swept sections at incidences greater than that for shock detachment; the problems of low aspect ratio wings for $M \cos A > 1$, and at large incidence; the problems of slender bodies at moderate Incidence for $M\delta < 1$, and for incidences above shock detachment for $M\delta < 1$ and $M\delta > 1$; the problem of-bluff body shapes; and the problems presented by the complex flows with interaction effects that will occur round real vehicle shapes.

There have been attempts to deal with the nose bluntness problem empirically or semi-empirically. East[17] obtained a correction for nose bluntness to apply to the wedge pressures calculated by strong shock piston theory, from experimental measurements of the overpressure generated on a flat plate by blunting. From the results in Ref. 17 of comparisons with experiment, the correction does not seem to be a satisfactory one. In Ref. 57, it is suggested that the effects of nose blunting might be allowed for by using Newtonian theory to find the pressures on the blunt nose of an aerofoil, and piston theory where the surface slope became small enough. This proposal does not seem very sound since it ignores, for example, the effect of the nose blunting and strong nose shock on the flow downstream. When used in a flutter test to calculate flutter speeds for comparison with experimental results (Section 4.2.1 and Ref. 60), the method gives results which correspond qualitatively to the experimental results, but which are in error by 15-20%.

It seems probable that the problem of leading edge bluntness on slender bodies will split into two parts with a rather undefined boundary between them. On the one hand there will be the problem of slender bodies with small amounts of blunting. This one might hope to deal with by modifications of the shock expansion and variational methods since the departures from the basic sharp leading edge flow can be expected to be small. The modifications would involve some treatment of the overpressure due to the blunt leading edge, perhaps through developments of the blast wave analogy (Chernyi[2]), and of the effect of the entropy layer from the nose.

On the other hand, there will be the problem of slender bodies with a large degree of blunting: for such bodies it may be necessary to know the details of the flow over the nose, and the results of small-disturbance theory

will/

will no longer apply and a simple expansion from conditions downstream of the nose would not exist. In this case, it will be necessary to apply Kennett's small-perturbation analysis to a suitable bluff body flow solution to find the nose conditions, and apply Holt's small perturbation analysis to a characteristics solution of the steady flow downstream of the nose. Such analysis will apply, of course, only for small amplitude motions of the body.

The results of small-disturbance theory will still apply for low aspect ratio wings with sharp sections for which $M \cos A > 1$, and for pointed slender bodies for which $M\delta < 1$ at moderate incidence, and consequently, unsteady flows around such bodies can be found from calculation of an equivalent series of steady flows. But the only way of calculating the equivalent steady flows would seem to be the characteristics method - though some simplification of the process may be brought about by applying the linearized characteristics method of Ferri[40].

Newtonian impact theory provides a simple method for estimating the aerodynamic forces on wings and bodies at incidences above those for shook detachment, but the predictions made are necessarily unreliable. A satisfactory method of dealing with these flows, for small amplitude motions of the bodies, seems likely to involve the application of a small-perturbation analysis to a satisfactory steady flow solution. Similar conclusions apply to the problems of bluff bodies, and real vehicle shapes: in both cases analyses have been made using Newtonian impact theory but these, obviously, have only limited value and a small-perturbation analysis is required - if an adequate steady solution exists.

In those oases where it has been suggested that a small-perturbation analysis applied to a steady solution is likely to be the only way in which a satisfactory unsteady flow analysis can be made, it has been made clear that the method can only be applied for small-amplitude disturbances. There seems to be no alternative to a quasi-steady analysis of the flow around a body is undergoing large amplitude displacements. In practical oases this will certainly be adequate for most cases since such motions are unlikely to involve large frequency parameters.

APPENDIX III/

APPENDIX III Review of the Dynamic Stability of Hypersonic Vehicles

For the purpose of this review, information is required on the changes in the dynamic behaviour of vehicles at very high speeds resulting from the changed flight conditions, and on the likely order of magnitude of frequency parameters characterising the unsteady motions. Sufficient information can be obtained on these points from generalized studies without entering into details of the behaviour of particular configurations and, in consequence, this section is concerned, in the main, only with such generalized studies.'

The equations expressing the dynamic behaviour of a flight vehicle are changed both by the high speed and altitude, and by the kind of mission being flown, since re-entry or exit flight differs from steady flight at constant altitude. The high speed and altitude of flight modify the equations of motion firstly by the introduction of new terms. It may be necessary to take account of the curvature of the flight path and the rotation of the axis system by introducing terms for the 'centrifugal lift' and a constant rate of pitch, and, in level flight at high altitude, variations in altitude due to oscillatory motions can be large enough to make it necessary to introduce terms expressing changes in the air density, gravity force, 'centrifugal lift', and rate of pitch. Second, the equations need modification because of changes in the relative magnitudes of the terms involved, and because the aerodynamic forces may be non-linear with changes of attitude even for moderate amplitudes, so that the aerodynamic coefficients cannot be considered as constant.

For vehicles in re-entry or exit trajectories changes in speed and flight path angle along the 'steady' trajectory must be considered. The changes in speed could involve changes in the aerodynamic coefficients as well as in the dynamic pressure, and. the rates of change could be large enough, in the time scale of the motions involved, for this to be Important.

Also, large amplitude motions both for re-entry and for level flight, and flight at large angles of attack, as in the case of a slender body flying a high drag lifting re-entry trajectory (Appendix I Section 2), may require analysis.

In most of the analyses which have been made it has been assumed that the aerodynamic forces are linear with displacements. Comparison of the results of these analyses with the results of the few which include non-linear effects indicates that the qualitative picture is not greatly affected by non-linearities. The longitudinal behaviour has been studied most intensively, but there is no reason to expect that the effects of the flight conditions on the lateral behaviour will be very different.

3.1 Longitudinal Behaviour of Hypersonic Vehicles

3.1.1 Steady flight at constant altitude

Nonweiler[52] discusses the changes in the equations of motion necessary in considering very high speed flight. He shows that the major distinguishing feature of flight in these conditions which affects the solution of the stability equations is the high value of the relative density of the aircraft,

$$\left(\mu \equiv \frac{m}{\ell S b}\right) \qquad \ldots (3.1)$$

where/

where m is vehicle mass; ρ is air density; S and b are representative areas and lengths of the vehicle.

If μ is very large, then the terms C, D and E in the stability quartic (Duncan, Ref. 41, Chapter 5):

$$A\lambda^4 + B\lambda^3 + C\lambda^2 + D\lambda + E = 0 \qquad \ldots (3.2)$$

are very much larger than the terms A and B and it is possible to give fairly simple expressions for the roots of the quartic in terms of the coefficients:

$$\lambda_{1,2} \simeq -\frac{D \pm (D^2-4EC)^{\frac{1}{2}}}{2C}$$

$$\lambda_{3,4} \simeq \tfrac{1}{2}\left(\frac{D}{C} - \frac{B}{A}\right) \pm i\left(\frac{C}{A}\right)^{\frac{1}{2}} \qquad \ldots (3.3)$$

which, if the dominant terms only are retained, become

$$\lambda_{1,2} \simeq -\left[C_D \pm i(8K_L^2 - C_D^2)^{\frac{1}{2}}\right]$$

$$\lambda_{3,4} \simeq \tfrac{1}{2}\left\{-\tfrac{1}{2}\left(C_D + C_{L_\alpha}\right) + \frac{C_{m_q}}{i_B} \pm i\left[-\frac{C_{m_\alpha}}{i_B} K_L \left(\frac{V^2}{gb}\right)\right]^{\frac{1}{2}}\right\} \qquad \ldots (3.4)$$

where C_D is the drag coefficient;

C_{L_α} is the rate of change of lift coefficient with angle of attack: $(\partial C_L/\partial\alpha)$;

C_{m_α} is the rate of change of pitching moment coefficient with angle of attack: $(\partial C_m/\partial\alpha)$;

C_{m_q} is the rate of change of pitching moment coefficient with pitching velocity parameter $\frac{\theta b}{V}$: $\left(\frac{\partial C_m}{\partial \dot{\theta} b/V}\right)$;

i_B is the non-dimensional form of the pitching moment of inertia about the centre of gravity, IB : $I_B/\rho Sb^3$;

$K_L = \frac{C_L}{2} + \frac{m}{\rho SR}$ and R is the radius of the flight path.

The first pair of roots represent the usual phugoid type of oscillation and the second pair represent the usual predominantly pitching oscillation, provided the aircraft is statically stable, i.e., provided that

$$C_{m_\alpha} < 0. \qquad \ldots (3.5)$$

The/

The real and imaginary parts of the first pair of roots in equation (3.3) are both of order unity so that the period and the time constant of the rate of decay of the phugoid oscillation are both of the same order of magnitude as the natural unit of time

$$\tau = \frac{m}{\rho U S} = K_L \left(\frac{b}{2g} \right)^{\frac{1}{2}} \left(\frac{U^2}{gb} \right)^{\frac{1}{2}} \quad \cdots (3.6)$$

which is large at high speeds, provided that K_L is not very small, because of the size of the term $\left(\frac{U^2}{gb} \right)^{\frac{1}{2}}$, the Froude number. In the second pair of roots, representing the pitching oscillation, the real part is again of order unity, but the imaginary part is, usually, large. The period of the pitching oscillation is given by:

$$T_p = \tau \cdot \frac{2\pi}{\left(\frac{C}{A} \right)^{\frac{1}{2}}} = K_L \left(\frac{b}{g} \right)^{\frac{1}{2}} \cdot \left(\frac{U^2}{gb} \right)^{\frac{1}{2}} \frac{2\pi}{\left[\frac{C_{m_\alpha}}{i_b} \cdot K_L \left(\frac{U^2}{gb} \right) \right]^{\frac{1}{2}}}$$

$$= 2\pi \left(\frac{b . i_B . K_L}{g \, C_{m_\alpha}} \right)^{\frac{1}{2}} \quad \cdots (3.7)$$

so that it depends on KL, and becomes large only at high altitudes where K_L is large, and does not become very small because of the limit on the value of KL set by structural limitations on speed at low altitudes. The time constant of the rate of decay of the pitching oscillation becomes, then, very long in comparison with the period, And the oscillation is poorly damped. Assuming likely values of C_{m_α} and i_B, Nonweiler estimates that, for K_L of order 0·01, which he considers a likely lower limit, the period of the pitching oscillation will be 2 or 3 seconds, and the time to half amplitude will occupy a few periods; for KL of order unity, the period will be 20 to 30 seconds, and the time to half amplitude would be several minutes; and for K_L large, which would correspond to conditions close to a high altitude orbit, the time to half amplitude could be an hour.

The phugoid motion is very lightly damped and, in the time occupied by a few cycles of the pitching motion, is equivalent to the motion of a system with two degrees of freedom in neutral equilibrium. This characteristic of the phugoid motion, coupled with the small damping of the pitohing motion, could present novel control problems since pilot or automatic action to control the pitching motion could cause drift in the speed and altitude.

The qualitative conclusions of Nonweiler are confirmed by the detailed analysis of Etkin[43] and Rangi[44] for a vehicle with hypothetical characteristics flying at a constant altitude. The analysis takes account of the effects of using a rotating axis system, and of changes in the radius of the flight path, which are neglected by Nonweiler. Because of the additional terms which these factors introduce, the stability equation is a quintic, giving three normal modes, two oscillatory and one non-oscillatory. The characteristics of the oscillatory modes are shown in Figs. 30(a), (b) and (c) with some particulars of the hypothetical

vehicle./

vehicle. (The difference between the damping curves for the phugoid motion for the vehicle with air-breathing engine, and for the vehicle with rocket engine, is a result of the assumed variation of thrust with altitude for the sirbreathing vehicle.)

The values of frequency parameter given by Etkin's analysis can be used to estimate the order of magnitude of the maximum frequency parameters that are likely to be met in practice, except for vehicles with very low wing loadings. This result arises from the fact that it can be shown, by a dimensional argument, that the frequency parameter of the pitching oscillations of a vehicle is independent of vehicle size and speed, and is dependent only on the aerodynamic characteristics, the altitude, the weight loading, and the inertia properties. The hypothetical vehicle is sufficiently representative in these respects.

In general terms, the frequency of the pitching oscillations of a vehicle is given by:

$$f \propto \sqrt{\frac{M_\alpha}{I_B}} \qquad \text{... (3.8)}$$

where M_α is the aerodynamic stiffness in pitch and I_B is the vehicle moment of inertia.

Then, if the aerodynamic coefficients are independent of speed,

$$f \propto \sqrt{\frac{\rho U^2 Sb}{mK_y^2}}$$

where K_y is the radius of gyration of the vehicle, and the frequency parameter

$$k = \frac{2\pi f b}{U} \propto \sqrt{\frac{\rho S b^3}{mK_Y^2}} . \qquad \text{... (3.9)}$$

From equation (3.9) it can be concluded that the frequency parameter is independent of the velocity of the vehicle, and depends only on the vehicle characteristics and the altitude. It decreases with altitude.

For geometrically and inertially similar bodies, since

$$S \propto b^2,$$

$$m \propto \sigma b^3 \quad \text{where } \sigma \text{ is the vehicle density,}$$

and $$K_y \propto b,$$

it follows from equation (3.9) that

$$k \text{ cc } \sqrt{\rho/\sigma} . \qquad \text{... (3.10)}$$

From equation (3.10), it can be concluded that the frequency parameter is independent of the vehicle size, and inversely proportional to the square root

of/

of the vehicle density or density ratio, or for bodies of the same size it varies inversely as the square root of the weight loading. The vehicle considered by Etkin has a weight loading of 30 lb/ft^2; this is rather low for practical vehicles so that, by this criterion, the frequency parameters in Ref. 43 are probably higher than would usually be found except for vehicles using lightweight lifting structures. An estimate from Etkin's results of the frequency parameters for vehicles using a lightweight surface is complicated by the change in the form of the vehicle, but one would expect from equation (3.10) that it would be of the order of the square root of the ratio of the weight loading of the lifting surfaces in the two cases, and this ratio would be of the order of three to one.

The argument in the preceding paragraphs sets an upper limit (from Ref. 43) of 0·01 for the frequency parameter of the pitching oscillations of most vehicles at hypersonic flight speeds, rising to 0·03 or more for a vehicle using a lightweight lifting structure.

3.1.2 Re-entry flight

A general analysis of the stability of a vehicle moving in a steady re-entry or exit trajectory, comparable to that of Etkin for the case of steady orbital flight, has not yet been carried out. Such an analysis would be difficult because of the time dependence of U, ρ and γ (the flight path angle) in the steady trajectory, and the dependence of the aerodynamic coefficients on Mach number.

Refs. 45 to 4.8 give analyses, of increasing generality, of the problem of the pitching oscillations of a vehicle about a mean re-entry trajectory. The papers are chiefly concerned with the history of the pitching oscillations following re-entry with an initial angle of incidence and/or pitching rate, but, in the course of the analyses, the condition which governs whether the oscillation grows or decays is derived. The equations are simplified by the omission of terms which are small or have a small effect on the pitching oscillations, and they are expressed in terms of wind axes since this makes it simpler to handle a large, changing mean angle of attack.

It is assumed that the equations of motion of the vehicle can be separated into a set representing motion along the steady trajectory and a set representing pitching oscillations about this trajectory. This assumption is confirmed in the paper by Fine 49 in which the full equations are solved numerically, and it is shown that pitching oscillations up to amplitudes of 10° have a very small effect on the mean flight path and speed of the vehicle if its static margin is large.

Among the analyses available, the most general solution of the oscillation equations is given by Sommer and Tobak in Ref. 48. The solution which they obtain enables the history of the oscillation to be calculated for an arbitrary trajectory under the assumptions that the drag is independent of the angle of attack, but the other aerodynamic forces very linearly with angle of attack, and all the aerodynamic coefficients are independent of Mach number, except the pitching moment coefficient.

The equation describing the pitching oscillations derived in Ref. 48 is

$$\ddot{\alpha} + pi(t)\dot{\alpha} + f_2(t)\alpha = 0 \qquad \ldots (3.11)$$

where a is the oscillatory angle of attack and

$f_1(t)/$

$$f_1(t) = C_{L_\alpha} \frac{\rho US}{2m} - (C_{m_q} + C_{m_{\dot\alpha}}) \frac{\rho USb^2}{2I_B}$$

$$f_2(t) = -C_{m_\alpha} \frac{\rho U^2 Sb}{2I_B} + \frac{d}{dt}\left(C_{L_\alpha} \frac{\rho US}{2m}\right) - \frac{C_{m_q} C_{L_\alpha}}{I_B m} \left(\frac{\rho USb}{2}\right)^2$$

where $C_{m_{\dot\alpha}}$ is the rate of change of pitching moment coefficient C_m with time rate of change of angle-of-attack parameter, $\dot\alpha b/U$.

Comparison of this equation with that for the short period motion of an aircraft in level flight (Ref. 42: Section 6.7) shows that the equations are the same, apart from the time dependence of U and ρ and the factor $\frac{d}{dt}\left(C_{L_\alpha} \frac{\rho US}{2m}\right)$ in the stiffness term $f_2(t)$. The factor $\frac{d}{dt}\left(C_{L_\alpha} \frac{\rho US}{2m}\right)$ can be shown to be negligible in comparison with the other terms (Refs. 47 and 49) so that it is to be expected that the frequency at a given altitude will be close to that for level flight. This is confirmed by Kistler and Capalongan in Ref. 51 where they give the results of analogue studies of the motion of hypervelocity vehicles.

From the solution of equation (3.11), it can be shown that the requirement for convergence of the oscillations is that

$$K \equiv \frac{1}{C_D}\left[-C_{L_\alpha} + \left(\frac{b}{\sigma}\right)^2 (C_{m_q} + C_{m_{\dot\alpha}})\right] < -1 + \left(\frac{mg}{C_D S}\right) \sin\gamma \left[\frac{1}{q} + \frac{\beta}{g\rho} + \frac{1}{g\rho \sin\gamma} \frac{C'_{m_\alpha}(s)}{C_{m_\alpha}(s)}\right]$$

... (3.12)

where q is the free-stream dynamic pressure $\frac{1}{2}\rho_\infty U^2$,

s is distance along the flight path,

β is density parameter in $\rho = \rho_0 e^{-\beta h}$,

γ flight path angle to local horizontal,

$$C'_{m_\alpha} = \frac{\partial(C_{m_\alpha})}{\partial s}.$$

The parameter K occurs also in the equation for the short period motion of an aircraft in level flight (Ref. 42: Section 6.7). The convergence criterion is then

$$K < 0. \qquad \ldots (3.13)$$

It can be shown from equation (3.12) that the conditions of re-entry flight introduce a destabilising influence from decelerating effect of the drag of the vehicle, and a stabilizing effect from the rate of increase of air density.

After they have established the equations of motion of a vehicle and the convergence criterion, equation (3.12), Sommer and Tobak examine the oscillation histories of a range of lifting and non-lifting vehicles for a range of entry conditions to give examples of the significance of the damping

criterion./

criterion. Figs. 31 and 32 are taken from the report to show the behaviour of non-lifting vehicles: although the report is principally concerned with manned vehicles for which the peak acceleration is 11·5g, which limits the initial flight path angle to a maximum of 4°, one case of an unmanned trajectory with $\gamma_i = 22°$ and the peak deceleration reaching 60g, is included for comparison.

The conditions assumed for calculating the steady trajectories are

(a) constant aerodynamic coefficients

(b) $\bar{U}_i = \dfrac{U_i}{\sqrt{gR_i}} = 1$ corresponding to entry from circular orbit at about 80 miles. Ui = initial speed: $\sqrt{gR_i}$ ≡ circular orbital speed.

(c) $h_i = 400\,000$ ft = initial altitude

(a) $\rho = \rho_0 e^{-\beta h}$ $\rho_0 = 0{\cdot}0027$ slugs/f+? $\beta = \dfrac{1}{23\,500}$ ft^{-1}

(e) W/CDS = 30 lb/ft^2.

Fig. 31 shows graphs of critical values of the parameter K,

$$K_{crit.} = -1 + \left(\frac{W}{C_D S}\right) \sin\gamma \left[\frac{\beta}{g\rho} + \frac{1}{q}(1 - \bar{u}^2)\right], \qquad \ldots \quad (3.14)$$

where $\bar{u}$ = ratio of horizontal component of flight velocity to circular orbital speed. Equation (3.14) is the form in which the convergence criterion is obtained for the condition of constant aerodynamic coefficients. The significance of the curves can be seen from an examination of one of them - the $\gamma_i = 22°$ trajectory. Divergent oscillations occur when the value of K for the vehicle is greater than $K_{crit.}$, thus for a vehicle with K = -0·4, this trajectory shows stable oscillations down to 110 000 ft, divergent oscillations from 110 000 ft to 70 000 ft and then convergent oscillations again.

The condition of small γ_i differs from the condition of yi = 22° since it does not need as large a negative value of K to prevent divergent oscillations, and a region of divergence is likely to start at a greater altitude and, for small negative values of K, to persist for a longer time.

Fig. 32 shows graphs of the growth of oscillations along a re-entry trajectory h decreasing, α_0 being the amplitude of the oscillation and α_i the initial amplitude of oscillation. For K = -2 convergence is found for large and small γ_i; for K = 0 a region of divergence is found, as indicated in Fig. 31, but the rate of growth is so small that the final amplitudes remain small fractions of the initial amplitude; for K = +2 there is a region of rapid divergence for all values of γ_i and, because of the greater altitude range over which divergence occurs, the vehicles operating at small entry angles reach an amplitude ratio of 1 at a significantly greater altitude than for the case of $\gamma_i = 22°$.

Figs. 33 and 34 show the effects of small amounts of lift. It was mentioned in Appendix I that the use of lift in re-entry can reduce the maximum rate of deceleration considerably and Fig. 33 shows that the effect of lift

is/

is to reduce further the range of values of K for which divergence occurs, but to increase the altitude at which divergence starts when it does occur. Fig. 34 shows that, as in the non-lifting case, K = 0 does not show serious divergence, but K = +2 does.

Confirmation of the qualitative validity of the simplified analyses of re-entry which have been discussed is provided in Ref. 53, where the results are presented of a 6-degree of freedom numerical analysis, using experimentally determined aerodynamic forces, of the re-entry motion of a blunt uncontrolled vehicle. This analysis shows; in particular,-that provided the lift-curve slope C_{L_α} of the body is positive, the motion converges even for zero value of $(C_{m_q} + C_{m_{\dot{\alpha}}})$.

3.1.3 The effect of aerodynamic non-linearities

In Ref. 51, Kistler and Capalongan give the results of studies, using analogue computers, in which they considered the effects of aerodynamic non-linearities on the longitudinal dynamic motions of hypervelocity, high-altitude vehicles. They found that reasonable accuracies could be obtained using linear aerodynamics if the coefficients were determined at the trim point of the vehicle, and provided the perturbations were small. For large perturbations accuracies began to drop rapidly. The study included level flight and shallow re-entry conditions and one of the conclusions of the report was that artificial damping of the vehicles would be necessary, and this might well overshadow any non-linear aerodynamic damping characteristics.

Laitone and Coakley, in Ref. 50, examine the effect of aerodynamic non-linearities on the pitching oscillations of a vehicle flying in a re-entry trajectory. The results do not affect the conclusions that have been drawn about small amplitude motions, but they show that a steady limit cycle oscillation can exist and that conditions are possible in which oscillations will grow if the initial disturbance exceeds a certain amplitude.

3.2 The Lateral Behaviour of the Hypersonic Vehicle

In Ref. 52 Nonweiler has also examined, qualitatively, the lateral dynamic behaviour of a hypersonic vehicle. The analysis is carried out in the same way as for the longitudinal behaviour: the approximate roots for the stability equation are found under the assumption that terms involving the relative density, μ, are large. The roots show the usual modes: normally, two non-oscillatory modes and one oscillatory, the 'dutch roll'. An examination of the factors governing the modes shows that it should not be difficult to ensure convergence of the non-oscillatory modes and damping of the dutch roll even for slender bodies at high incidences. But the period of the lateral oscillation is likely to be rather shorter than that of the pitching oscillation for slender bodies at high incidence - typically 3 seconds for a value of KL of unity, but since such bodies are not likely to be operating at large incidences for low values of K_L at low altitude, the maximum values of frequency parameter will probably remain of the same order as those for the longitudinal pitching oscillation.

The longitudinal behaviour of a hypersonic vehicle flying a re-entry path has been found to be not essentially different from that of the same vehicle in level flight and it is reasonable to suppose that the same result would be found for the lateral behaviour. The rate of decay of the lateral oscillation

will/

will be affected by a stabilising influence from the rate of increase of air density and a destabilising influence from the drag of the vehicle, as is the case for the longitudinal pitching motion.

3.3 Discussion and Conclusions

For hypersonic vehicles in level flight maximum frequency parameters are likely, in general, to be small, with values of the order 0·01. The rate of decay of the pitching oscillation due to aerodynamic damping is low and artificial augmentation of the damping is likely to be necessary and, as a result of this, the aerodynamic damping of a vehicle is not likely to be a significant design criterion for normal operation.

For re-entry flight the position is similar. The frequencies of pitching oscillation at a given altitude are the same as those for level flight at that altitude. The rate of decay can be greater or smaller, depending on the specific case, since additional factors are brought into play, but for practical vehicles it is small. The convergence factor K is unlikely to be negative and the worst case occurs when it is close to zero and CD is large - for this case divergence of the motion occur towards the end of the trajectory but the final amplitude is small (Figs. 32 and 34).

There are some cases for which fairly accurate values of aerodynamic damping might be important. The most likely cases are when it is necessary to know accurately the motion of an uncontrolled re-entry vehicle because of requirements of heat shielding or parachute deployment, and when it is necessary to design for emergency manual control of a vehicle. Since it has been shown [54] that oscillatory motions with low or even negative damping can be manually controlled, emergency manual control appears to be a feasible design objective.

APPENDIX IV Review of Flutter of Hypersonic Vehicles

Differences between the flutter behaviour of vehicles flying at hypersonic speeds and the behaviour at lower speeds will be due to changes in the nature of the air flow at hypersonic speeds and the changes in the stiffnesses of the vehicle structure which result from heating of the structure. This report is mainly concerned with the effects of changes in the nature of the flow but the importance of the second factor should be borne in mind and is illustrated in a general way by Fig. 35(a), (b) and (c) from Ref. 55. In Fig. 35(c) the lower line represents the value of the speed parameter $U/b\omega_\alpha$ along the flight profile, and the upper line represents the values of $U/b\omega_\alpha$ at which flutter could occur. Its importance is emphasised by the fact that for some flight profiles the maximum heating rate can be combined with the maximum value of dynamic pressure on the trajectory - as in the case of the supercircular lifting re-entry trajectory shown in Fig. 4.

4.1 Types of Flutter and Values of Flutter Frequency Parameter

The types of flutter than can be expected on hypersonic vehicles are discussed in Refs. 5 and 6. These discussions and the conclusions presented here can, of course, only be deductions from the likely structures of the vehicles based on general technical considerations. On this basis, flutter involving vibration modes of the main structure is likely to be met only on slender vehicles for hypersonic cruise, and lifting re-entry vehicles having high L/D and, if it occurs, it seems likely to be of a form involving the longitudinal bending modes of the body, even for the winged vehicles. The slenderness of the wing, and the degree of integration of wing and body, make it unlikely that vibration of the wing can be considered in isolation from the response of the body. Simple bending-torsion flutter could occur for certain types of control surface. Panel flutter could occur on lifting surfaces, heat shields, and in inlet and propulsion ducts for power units, where panels are heavily loaded, aerodynamically and thermally. Membrane flutter and large amplitude distortions could be met if lightweight structures are used to give lift or drag in re-entry. It is suggested in Ref. 12 that, for slender bodies, using representative values of the overall structural frequencies, an upper limit of 3000 rad.ft/sec can be set on the product ωb where $\omega = 2\pi f$, b is a representative length and f is a frequency, so that at $M = 5$, $U \simeq 5000$ ft/sec, the maximum value of frequency parameter will be about 0·6, but values are likely to be much lower than this in most practical cases.

For bending-torsion flutter of control surfaces it seems likely, again using representative frequencies, that the maximum value of ωb will be around 600 rad.ft/sec, giving maximum frequency parameters around 0·1. And, in a similar way, it can be deduced for panel flutter that frequency parameters based on a representative length of the order of the wavelength of the panel mode, will be in the range of values up to 0·5.

4.2 Flutter Investigations

Most of the reports of analytical and experimental work on flutter at hypersonic speeds that have been published have been concerned with the standard basic case of flutter of a two-dimensional section with pitching and plunging flexibilities, or the closely comparable case of flutter of a rigid half sing with root flexibility in pitching and plunging or flapping, both of which are related to the bending/torsion flutter of wings. There has been a much smaller amount of work on flutter of low aspect ratio wings with chordwise-bending as well as torsional and spanwise-bending modes of vibration, and with

flutter of slender bodies. No information has been found on panel flutter at hypersonic speeds, but it seems reasonable to assume that, because the deflections involved will remain very small, the values of the hypersonic similarity parameter $M\delta$ will be small and, consequently, tentative conclusions about hypersonic panel can be drawn on the basis of extrapolations from results at lower Mach numbers. No relevant information has been found on membrane flutter.

4.2.1 Bending-torsion flutter of wings

Chawla[56] has used piston theory to third-order terms in the steady displacements and *to first-order* terms in flutter disturbances to carry out a parametric survey of the flutter of the typical section at supersonic speeds. He presents the solutions of the flutter determinant in a way which enables the effects of a number of parameters to be distinguished. The results are for Mach numbers less than 5, but the trends shown should continue to apply up to Mach numbers at which piston theory becomes invalid.

Morgan, Runyan and Huckel[57] start with a general discussion of the methods for predicting unsteady airloads in flutter calculations at high Mach numbers. They investigate the effect of thickness in some detail through comparisons between linear and nonlinear theories, and show the effects of frequency ratio, centre of gravity and elastic axis positions, and aerofoil shape. Finally, they consider refinements to the aerodynamic analyses to allow for strong shook waves, changes in specific heats and other real gas effects, *and* to provide a means to deal with blunt-nosed bodies.

Runyan and Morgan[58] give comparisons between theoretical and experimental flutter results for two rigid rectangular wings with a root mounting giving. pitching and flapping flexibilities, and some results showing the effect of aerodynamic heating on the flutter of a solid wing.

Zartarian and Hsu[26] have used third-order piston theory to investigate the flutter of the typical section about a non-zero mean incidence, and the effects of aerodynamic nonlinearities on flutter of the section at zero mean incidence.

Hanson[59] gives the results of an extensive experimental investigation of thickness and nose bluntness effects. Many of the results are for Mach numbers below those considered in this report, but they are useful here because they show the trend of the flutter altitude parameter with Mach number, and enable the values at high Mach number to be compared with the values in the critical transonic flutter condition. The thickness effects are compared with piston theory results.

Goetz[60] extends the experimental investigation of bluntness effects in Hanson's report to a Mach number of 15, *and* compares the results with predictions by Newtonian piston theory[54] and Newtonian theory.

Young[61] gives the results of an experimental investigation of the effects of thickness and mean incidence. These investigations show that there are a number of aerodynamic parameters affecting the flutter Of the section.

Chawla[56] derives the following expressions for the flutter speed and frequency using piston theory:

$$\left/ \frac{V_f}{b\omega_\alpha} \right. .$$

$$\frac{V_f}{b\omega_\alpha} = \mu M \bar{L}_2 \left[\frac{4\bar{x}_\alpha^2 \bar{\omega}_f^2 + (1-\bar{\omega}_f)^2(1-\zeta^2)\bar{r}_\alpha^2}{\mu M[2\bar{x}_\alpha \bar{L}_2 - \bar{L}_4(1-\zeta^2)] - \bar{M}_4 \bar{L}_2 + \bar{L}_4^2} \right]^{\frac{1}{2}} \quad \ldots (4.1)$$

$$\bar{\omega}_f^2 = \frac{\bar{r}_\alpha^2 \bar{L}_2 + \bar{M}_4 \bar{\omega}_h^2}{\bar{r}_\alpha^2 \bar{L}_2 + \bar{M}_4 - 4\bar{x}_\alpha \bar{L}_4} \quad \ldots (4.2)$$

where
$$\bar{L}_2 = MkL_2$$
$$\bar{L}_4 = MkL_4 \quad \ldots (4.3)$$
$$\bar{M}_4 = MkM_4$$

and F = aerodynamic force on section $= -4\rho bU^2 k^2 \{(L_1 + iL_2)\frac{h}{b} + (L_3 + iL_4)\alpha\}$

M_o = aerodynamic moment about pitching axis

$$= -4\rho b^2 U^2 k^2 \{(M_1 + iM_2)\frac{h}{b} + (M_3 + iM_4)\alpha\}. \quad \ldots (4.4)$$

For simple harmonic motion, and piston theory aerodynamics

$$\left.\begin{aligned} L_1 = M_1 = 0, \quad M_2 = L_4 \\ b = (1/k)L_2, \quad M_3 = (1/k)M_2 = (1/k)L_4 \end{aligned}\right\} \quad \ldots (4.5)$$

and, taking a double-wedge section as typical,

$$\bar{L}_2 = 1 + \frac{(\gamma+1)}{4}[(M\alpha_s)^2 + (M\delta)^2]$$

$$\bar{L}_4 = (1-2\bar{x}_\alpha)\left\{1 + \frac{(\gamma+1)}{4}[(M\alpha_s)^2 + (M\delta)^2 1\right\} - \frac{(\gamma+1)}{4}(M\delta)$$

$$\bar{M}_4 = 4(\tfrac{1}{3} - \bar{x}_\alpha + \bar{x}_\alpha^2)\left\{1 + \frac{(\gamma+1)}{4}[(M\alpha_s)^2 + (MS)"]\right\} - 2(1-\bar{x}_\alpha)\frac{(\gamma+1)}{4}(M\delta) \ldots (4.6)$$

where δ is the thickness ratio of the section, and α_s is the mean incidence. These results show three aerodynamic parameters: μM, an altitude parameter; $M\delta$, a thickness parameter, and $M\alpha_s$, a mean incidence parameter. This result is specifically for a double-wedge section, but Chawla shows that the results are the same for more general sections, though the thickness parameter applies only within a family of shapes, of course. The significance of $M\delta$ and Ma, is in agreement with the results of hypersonic small-disturbance theory (Appendix II) and of experiment, which show that these are similarity parameters for hypersonic flows.

Besides the parameters from Chawla's analysis, other factors have been found to be significant. These are profile shape, the effect of strong leading-edge shock waves, leading-edge bluntness, and aerodynamic nonlinearities. The effects of changes of μM, $M\delta$, $M\alpha_s$ and these other parameters on flutter of the section will now be discussed.

(i)/

(i) Altitude parameter. μM

Figs. 36 and 37, reproduced from Ref. 56, show the relationships between flutter speed, frequency ratio and altitude parameter (μM) for a flat plate, two-dimensional section. The dependence of flutter speed on altitude is obscured in some degree by the form of the parameter μM, since M is dependent on V_f. The relationship is a little clearer if the μM is re-expressed as

$$\mu M = \frac{m}{4b^2} \cdot \frac{V_f}{\sqrt{\gamma \rho p}} \cdot \quad \ldots (4.7)$$

Then, from the graphs, it is clear that, for a given altitude (P and p fixed) and frequency ratio, there will be a unique flutter speed and, since μM increases with altitude independently of any change in the flutter speed (because of the changes in ρ and p), the flutter speed itself must also increase with altitude. The relationship of flutter speed and altitude can be expressed more explicitly, in an approximate form, by making use of the fact that, in Fig. 36, V_f can be shown to vary approximately as $(\mu M)^{\frac{1}{2}}$*. Using this relationship it is possible to write, for the flutter speeds at two altitudes

$$\frac{V_{f_2}}{V_{f_1}} = \left[\frac{(\mu M)_2}{(\mu M)_1} \right]^{\frac{1}{2}} \quad \ldots (4.8)$$

and, if equation (4.8) is squared, and the following substitutions are made:

$$M = \frac{V_f}{a} ; \quad \mu = \frac{\rho_o \mu_o}{\rho} \quad \ldots (4.9)$$

where suffix o refers to a reference altitude,

$$\text{then} \quad \frac{V_{f_2}}{V_{f_1}} \simeq \frac{(a_1 \rho_1)}{(a_2 \rho_2)} \quad \ldots (4.10)$$

$$\text{and} \quad \frac{M_{f_2}}{M_{f_1}} = \frac{(a_1^2 \rho_1)}{(a_2^2 \rho_2)} = \frac{p_1}{p_2} . \quad \ldots (4.11)$$

If, then, the changes of ρ and a with altitude are known, curves of flutter speed and Mach number against altitude can be plotted. Such curves are shown in Fig. 38(a) and (b). In Fig. 38(b) use is made of the fact that, for 35 330 ft < h < 105 000 ft, $a_2/a_1 \simeq 1$, and

$$\frac{V_{f_2}}{V_{f_1}} = \frac{M_{f_2}}{M_{f_1}} \simeq \frac{p_1}{p_2} . \quad \ldots (4.12)$$

The/

*This result can also be seen from equation (4.1) since

$\mu M[2\bar{x}_\alpha \bar{I}_2 - \bar{I}_4(1-\zeta^2)] \gg (-\bar{M}_4 \bar{I}_2 + \bar{I}_4^2)$ for μM large.

The theoretical deduction that μM is a parameter affecting flutter has not been directly investigated, but some confirmation of it can be found in the results of the experiments by Hanson[59] and Goetz[60]. These results are given in Figs. 42 and 51. They show that, for a given aerofoil at a given Mach number, the results at widely different values of μ and a show the same values of the parameter $b\omega_\alpha\sqrt{\mu}/a$ at flutter. Since

$$\frac{b\omega_\alpha\sqrt{\mu}}{a} = \frac{b\omega_\alpha\sqrt{\mu}\,M_f}{V_f} \qquad \ldots (4.13)$$

the constancy of this parameter is equivalent, for a fixed Mach number, to the relation

$$V_f \propto \sqrt{\mu M} \qquad \ldots (4.14)$$

found by Chawla (equation (4.8)).

Fig. 44, derived from the results of both Hanson and Goetz, for pointed leading-edge sections, shows that the use of the parameter $\frac{V_f}{b\omega_\alpha}\sqrt{\mu M}$ correlates results from models of different thickness at different Mach numbers, but having the same value of $M\delta$, provided $M > 2$, which is a normal lower limit for the use of piston theory, in any case. This figure will be discussed again in a later section, but it seems to support quite well the theoretical result for the significance of μM.

(ii) Thickness parameter $M\delta$

The paper by Morgan, Runyan and Huckel[57] gives a comparison between measurements of the lift and centre of pressure position on a 5% thick double-wedge aerofoil in steady flow at $M = 6.86$, and calculations by linear theory, which does not include thickness effects, and by third-order piston theory and a second-order solution due to Van Dyke for flow round an oscillating two-dimensional aerofoil, which do include these effects. The results are reproduced in Fig. 39. There is little difference in the lift coefficient up to an incidence of about 12 degrees, but there is a considerable error in the prediction of the centre of pressure position by linear theory. Since the centre of pressure position is an important flutter parameter (see, for example, Ref. 62, Section 6.5c) it is to be expected that the thickness of an aerofoil may have an important influence on its flutter behaviour at high Mach numbers.

The effect of thickness is shown by the theoretical flutter boundaries of Fig. 40, taken from Ref. 57, from which a comparison can be made between those theories that take account of thickness and linear theory which does not. For the particular value of bending-pitching frequency ratio the influence of thickness is destabilising. The effect of thickness depends, to some extent, on frequency ratio and on the positions of the elastic axis and centre of gravity positions - this is shown in Fig. 41(a)-(d), also from Ref. 57, but, in general, for $\omega_h/\omega_\alpha < 1$[56] the influence of thickness is found to be destabilising. Chawla[56] gives similar results.

These theoretical predictions are supported by the experimental results of Hanson[59] and Young[61], which are shown in Fig. 42. The two sets of results are

plotted/

plotted together only for convenience; strictly, the results of Young are not comparable with those of Hanson since Young's measurements were made on a wing of aspect ratio 2·9 with pitching and plunging freedoms, whereas Hanson's measurements were on a wing of aspect ratio 1·0 with pitching and. flapping freedoms, and parameters like frequency ratio and axis position were significantly different for the two sets.

Runyan and Morgan[58] give experimental evidence of the inadequacy of linear theory in results for the flutter of a double-wedge wing and a thin plate wing with root flexibility. The results are given in Fig. 43. They show clearly that three-dimensional linear theory, which takes account of tip effects, is quite inadequate to predict the experimental results.

All of these results show the destabilising effect of increasing thickness for particular conditions. Chawla's analysis suggested a general relationship between flutter speed, Mach number, and thickness since the result of his analysis using piston theory showed that, if other parameters in the problem were the same, the flutter speed depended directly on the product $M\delta$. This conclusion can be supported experimentally for $M > 2$ by the results given by Hanson[59] and Goetz[60]. The models in these tests were constructed so that they mere identical in mass and mass distribution. and in axis position; only the wedge thickness varied. In Fig. 44 the parameter $\frac{V_f}{b\omega_\alpha}\sqrt{\frac{1}{\mu M}}$ is plotted against $M\delta$. Since Chawla has shown that V_f is proportional to $\sqrt{\mu M}$, the effect of this variable should be eliminated from the flutter speed parameter used. It can be seen that the results do collapse quite well on to a single curve, confirming the significance of both parameters MS and μM.

(iii) Incidence

Chawla[56] investigates theoretically the effect of the incidence parameter Ma, on flutter of a double-wedge section. Some results are given in Fig. 45. Under the conditions given in the figure, with $M\delta = 0{\cdot}25$, an Initial angle of attack giving Ma, = 0·25 has a small stabilising effect for $0 < \omega_h/\omega_\alpha < 1{\cdot}0$ and a small destabilising effect for $\omega_h/\omega_\alpha > 1{\cdot}0$. For a zero thickness aerofoil, Chawla found that an initial angle of attack reduces the flutter speed by a constant amount: for Ma, = 0·25 the multiplying factor is 0·982.

Zartarian and Hsu[26] investigate theoretically the effect of initial incidence at considerably greater values of $M\alpha_s$ for a wing with $\delta = 0{\cdot}05$. The result is shown in Fig. 46. Up to Mu, = 0·25, the value of the flutter velocity parameter is reduced by a factor of about 0·99; for Ma, = 0·50, which represents only a moderate incidence even at $M = 5$, there is a reduction by a factor of 0·95.

These results receive confirmation from the experimental investigation of Young[61], from which Fig. 47 is reproduced. Both theory and experiment show a decrease in the flutter speed parameter with incidence and show agreement on the amount. The results indicate some effect of thickness: for $M\alpha_s = 0{\cdot}10$ and $M\delta = 1{\cdot}1$, the theoretical reduction factor is about 0-93; for $M\alpha_s = 0{\cdot}10$ and $M\delta = 1{\cdot}5$, the factor is 0·95.

The good agreement on the effect of incidence on flutter speed between theory and experiment in Ref. 61, is not repeated for the effect on flutter

frequency./

frequency. Theoretical calculations show slight increases with $M\alpha_s$, but experimental results show slight reductions.

(iv) Profile

The effects of profile shape were investigated in Ref. 57 by calculating the stability boundaries at $M = 5$ for four aerofoils: a 4% thick symmetrical double wedge; a 4% thick NACA 65 A004 profile; a flat plate; and a 4% thick single wedge. The results are reproduced in Fig. 48. The first two profiles have almost coincident boundaries at high values of frequency ratio, but they diverge below $\omega_h/\omega_\alpha \simeq 1{\cdot}0$: thickness in these cases is destabilising in comparison with the flat plate except above $\omega_h/\omega_\alpha \simeq 1{\cdot}2$. The single wedge is less stable than the flat plate throughout the ω_h/ω_α range but the boundary curve is very similar to that for the flat plate.

(v) Local flow conditions

The third-order piston theory, and Van Dyke's second-order theory used in Ref. 57, assume isentropic conditions. They do not take account of the presence of strong shock waves, of entropy variations, and of effects of high temperature such as the reduction of the ratio of specific heats. It is suggested in Ref. 57 and by Miles[15] that, for a small displacement motion like flutter, account could be taken of these effects by applying piston theory for the unsteady displacements in the local flow conditions found by a steady flow analysis. The effect of trying to take local flow conditions into account in this way is not clear from the evidence available. In Ref. 57 the flutter of a 4% thick double-wedge aerofoil is considered, using standard shock wave relations to calculate the local Mach number, density, and velocity: the results are shown in Fig. 49. In this case, the effect of the local flow conditions is stabilising; the size of the effect depends on the values of ω_h/ω_α, and increases with Mach number. On the other hand, a similar calculation carried out for the conditions of the experiments of Ref. 61, showed no significant differences from third-order piston theory results. There is no obvious explanation for this difference. The frequency ratios in Ref. 61 are close to 0·4, and a ratio of 0·4 in Fig. 45 shows large differences between "local flow" and third-order piston calculations; the only difference in the conditions lies in the axis position which, for Ref. 58, is at mid-chord, and for Fig. 45 is at 40% chord.

(vi) Bluntness

It was pointed out in Appendix II that, under hypersonic flow conditions, even small degrees of blunting can have significant effects on the flow over a body and that large degrees of blunting are likely to be used on the noses of vehicles and the leading edges of lifting surfaces to reduce the rate of heating. In Ref. 57 an attempt is made to assess the effect of nose blunting on the flutter of an aerofoil by using Newtonian impact theory to calculate pressures over the blunt nose region up to the point where the surface slope becomes small enough for piston theory to be applicable, and using piston theory over the remainder of the surface. The results are shown in Fig. 50, where they are compared with a calculation by piston theory. It is seen that Newtonian piston theory usually predicts greater stability than does piston theory alone. Piston theory is inapplicable, strictly, to the blunt nose region of the section, and this result indicates that it is liable to give conservative results when used on an empirical basis for calculations on blunt-nosed bodies.

Experiments/

Experiments indicate that, up to certain limits of bluntness and Mach number, nose blunting can have a stabilising effect on a simple section. Results on the effect of nose blunting are given in Hanson[59] and Goetz[60]. Fig. 51 summarises the results from both papers for one set of models. The significant thickness effect in these tests is assumed to be related to the thickness/chord ratio of the basic pointed wedge section, which has been subjected to blunting. All the sections used in the tests have the same chord, so that the thickness and chord of the wedge section on which the section is based increase with blunting (see sketch, Fig. 51). Up to about 10, nose blunting is stabilising up to a nose radius of at least 3% chord. For a nose radius of 6% of the chord divergence was met at values of the altitude parameter greater than the flutter values for the 3% aerofoil. There is a marked increase in the altitude parameter when the blunting is increased from 1% to 3% at $M = 15{\cdot}4$.

Goetz gives theoretical calculations by Newtonian theory, and by Newtonian-piston theory, for flutter at $M = 15{\cdot}4$. Both calculations predict satisfactorily the increased stability for a nose radius of 1% as compared with a sharp edge, and the decrease of stability when the radius is further increased to 3%. The theoretical calculations are shown compared with the experimental results in Fig. 52. The greater measure of agreement of the Newtonian theory calculation with experiment for nose radii of 1% and 3% seems likely to be fortuitous, since the error that the calculation shows for a nose radius of zero indicates that it does not satisfactorily predict the pressure distribution on the flat surfaces of the aerofoil.

The experiments also show a reduction in the flutter frequency with increasing nose radius. This is small for the increase to 1%, but large for the increase from 1% to 3%. This effect is not found in any marked degree in the theoretical results.

(vii) Aerodynamic non-linearities

Most of the flutter analyses that have been discussed so far have used piston theory to third order in the steady displacements, but only to first order in the unsteady displacements, so that the flutter equations were linear. This means that allowance is made for the effects of mean incidence and thickness, but that it is assumed that body surface slopes due to the oscillatory motions are much less than those due to thickness and mean incidence, and that $M\alpha_0 \ll 1$. Since, at large Mach numbers, the condition $M\alpha_0 \ll 1$ may not apply even for α_0 very small, it is important to investigate how the flutter of a section is altered when aerodynamic nonlinearities are considered for the oscillatory displacements.

Zartarian and Hsu[26] investigate the effect of aerodynamic non-linearities by carrying out a flutter analysis on a two-dimensional section with third-order piston theory applied to the flutter displacements. It is assumed that the actual displacements are still small, so that structural non-linearities do not appear. The flutter equations are then obtained in the form (terms allowing for non-zero mean incidence are included.):

$$\zeta_1 h_u'' + \zeta_2 h_u' + \zeta_3 h_u + \zeta_4 \alpha_u'' + \zeta_5 \alpha_u' + \zeta_6 \alpha_u = -\{\zeta_7 h_u'^2 + \zeta_8 h_u' \alpha_u' + \zeta_9 h_u' \alpha_u$$

$$+ \zeta_{10} \alpha_u'^2 + \zeta_{11} \alpha_u' \alpha_u + \zeta_{12} \alpha_u^2 + \zeta_{13} h_u'^3 + \zeta_{14} h_u'^2 \alpha_u' + \zeta_{15} h_u'^2 \alpha_u + \zeta_{16} h_u' \alpha_u'^2$$

$$+ \zeta_{17} h_u' \alpha_u' \alpha_u + \zeta_{18} h_u' \alpha_u^2 + \zeta_{19} \alpha_u'^3 + \zeta_{20} \alpha_u'^2 \alpha_u + \zeta_{21} \alpha_u' \alpha_u^2 + \zeta_{22} \alpha_u^3 \quad \ldots (4.15)$$

where/

where h_u and α_u are the flutter displacements in plunge and pitch, and the primes denote the operator $\frac{1}{\omega_\alpha}\frac{d}{dt}$. The coefficients ζ_n involve the characteristics of the section, the mean incidence, Mach number, and frequency parameter: there are two sets of coefficients, one for the plunge equation, the other for the pitch equation. These non-linear equations are first simplified under the assumption that, if the non-linearities are small, information on the orders of magnitude of terms can be obtained from the solution of the linearized problem, and certain terms in the non-linear equations can then be neglected because of their smallness. It is also assumed that the mean incidence is zero. An approximate analysis of the simplified equations is then carried out. It is assumed, first, that if the section is flying at a speed close to the flutter speed predicted by a linearized analysis, and is subjected to a disturbance, it will stabilize to a finite periodic motion and that this motion can be represented by

$$h_u = \sum_{n=-\infty}^{\infty} h_n e^{in\omega t} \qquad h_0 = 0; \quad h_{-n} = h_n^*$$

$$a_u = \sum_{n=-\infty}^{\infty} \alpha_n e^{in\omega t} \qquad a_0 = 0; \quad \alpha_{-n} = \alpha_n^* \qquad \ldots (4.15)$$

where h_n^* and α_n^* are the complex conjugates of h_n and α_n. h_n and a_n are allowed to be complex so that it is possible to allow phase angles between the degrees of freedom, but h_u and α_u can be shown to be real. For simple harmonic motion (single frequency) $|h_n|$ and $|\alpha_n|$ are equal to one half of the corresponding amplitudes.

It is then assumed that the fundamental harmonic of the two component motions dominant in the flutter motion, and the equations are found which ensure that these components are balanced. Finally, if it is further assumed, on the basis of a linearized analysis, that the phase angle between the h_u and α_u motions is very small, the equations for the motion become

$$h_1\left\{\left(-\zeta_1 \frac{\omega^2}{\omega_\alpha^2}\right) + \frac{i\omega}{\omega_\alpha}(\zeta_2 + \alpha_1^2\zeta_{18}) + (\zeta_3)\right\} + \alpha_1\left\{\left(-\zeta_4 \frac{\omega^2}{\omega_\alpha^2}\right) + \frac{i\omega}{\omega_\alpha}(\zeta_5 + \alpha_1^2\zeta_{21})\right.$$

$$\left. + (\zeta_6 + 3\alpha_1^2\zeta_{22})\right\} = 0 \qquad \ldots (4.16)$$

where the coefficients ζ_n are given below.

h_n motion/

	h_u motion	α_u motion
ζ_a	$\mu M K_\alpha^2 \mu$	$\mu M K_\alpha^2 \bar{X}_\alpha$
ζ_2	$K_\alpha Y$	$K_\alpha\left\{(1-2\bar{x}_0)Y - \frac{\nu+1}{6}(M\delta)\right\}$
ζ_3	$\mu M K_\alpha^2 \left(\frac{\omega_h}{\omega_\alpha}\right)^2$	0
ζ_4	$\mu M K_\alpha^2 \bar{X}_\alpha$	$\mu M K_\alpha^2 r_\alpha^2$
ζ_5	$K_\alpha\left\{(1-2\bar{X}_0)Y - \frac{\nu+1}{6}(M\delta)\right\}$	$K_\alpha\left\{\left(\frac{4}{3} - 4\bar{x}_0 + 4\bar{x}_1^2\right)Y - \frac{\nu+1}{3}(1-2\bar{x}_0)M\delta + \frac{\nu+1}{45}(M\delta)^2\right\}$
ζ_6	Y	$\mu M K_\alpha^2 r_\alpha^2 + \left\{(1-2\bar{x}_0)Y - \frac{\nu+1}{6}(M\delta)\right\}$
ζ_{18}	$\frac{\nu+1}{4} M^2 K_\alpha$	$\frac{\nu+1}{4} M^2 K_\alpha (1-2\bar{x}_0)$
ζ_{21}	$\frac{\nu+1}{4} M^2 K_\alpha (1-2\bar{x}_0)$	$\frac{\nu+1}{4} M^2 K_\alpha \left(\frac{4}{3} - 4\bar{x}_0 + 4\bar{x}_0^2\right)$
ζ_{22}	$\frac{\nu+1}{12} M^2$	$\frac{\nu+1}{12} M^2 (1-2\bar{x}_0)$

where

$$\left.\begin{aligned} K_\alpha &= \omega_\alpha b/U \\ Y &= 1 + \frac{\nu+1}{12}(M\delta)^2 \end{aligned}\right\}.$$

A "flutter" speed and frequency can then be found from these equations in the usual way if a value is assumed for a_1. It can be shown that equations (4.16) are the same as the linearized equations for flutter about a large mean incidence α_s if α_1 is replaced by α_s. Since α_1 is, in fact, one half of the amplitude of the motion, it follows from this analysis that the flutter speed and frequency for an oscillation of large amplitude are the same as for the linearized flutter about a mean angle of attack $\alpha_s = \alpha_1$. Fig. 46, *then,* shows a boundary for the non-linear flutter case, es well as for the large

mean incidence case; but, for the non-linear case, it represents not a speed above which small disturbances will grow, but the size of the α_1 component of an unstable limit cycle oscillation for the corresponding speed. If the section is flying at a speed corresponding to some horizontal line of the figure and is subjected to a disturbance, the resultant motion of the wing will grow if the amplitude of the initial disturbance is greater than the value of α_1 given by the curve (and h_1), but it will decay if it is less.

There has been no direct experimental investigation of the results of this non-linear analysis. In Ref. 61, where the values of Mach number would make non-linear effects likely, some cases of limited-amplitude flutter after a slow initial growth were experienced, and there were other oases where finite-amplitude initial disturbances were necessary before flutter occurred, but this behaviour could be the result of friction or structural non-linearities.

Comparison of Theory and Experiment

The results available suggest that piston theory for sharp-nosed sections may give predictions of flutter as adequate as other methods up to quite high values of $M\delta$ and Ma; this is suggested especially by the results in Young's report[61] where $M\delta_{max} \simeq 1{\cdot}5$ and $M\alpha_s \simeq 1{\cdot}7$.

For blunt nose sections, it can be concluded from Goetz's results[60] that Newtonian theory may be adequate to predict flutter speed, but it can be used only on an empirical basis; and that the Newtonian-piston theory, suggested in Ref. 57, is likely to be no more adequate than Newtonian theory in the simple form proposed - possibly this is because it does not take account of the effects of the strong shock wave set up by the blunt nose, since attempts to take account of such effects (Ref. 57 and. Fig. 49) suggest that they reduce the flutter speed. Both theories are conservative in their predictions.

One point emerges from this review which is not strictly relevant to its purpose, but which it may be useful to make. This is, that it is difficult to assess the adequacy of aerodynamic theories for flutter analyses from comparisons between experimental results and theoretical. predictions of flutter speed and frequency, because of the structural uncertainties in the experimental conditions. Greater attention needs to be paid to defining these conditions. Such uncertainties are shown most clearly in Hanson's report[59], where the choice of structural modes to be used in the analysis has a considerable effect on the agreement between theory and experiment, but it is not clear which choice is more appropriate structurally; and in Young's report[61], where the level of structural damping assumed in the analysis made a very large difference to the agreement of theory and experiment on flutter frequency.

4.2.2 The flutter of slender configurations

It was pointed out earlier that flutter of the main structure of a hypersonic vehicle was likely to involve chordwise bending modes of the wings, and bending modes of the body. Information on flutter of these kinds is meagre. The general forms of the equations involved are established in Ref. 62: for slender bodies they are considered in Chapter 7 and for low aspect ratio lifting surface flutter with chordwise bending modes in Chapter 8. But the aerodynamic problems involved tare not examined. What can be established. from the available references is that chordwise bending modes can be important in the flutter of low aspect ratio surfaces, so that aerodynamic theories must provide adequate pictures of the pressure distribution[64,65] and that the free-free flutter of a

slender/

slender delta involving predominantly lengthwise modes, is possible[65]. And some information can be found on the adequacy of available theories giving the aerodynamic load's on slender bodies for flutter analysis from experiments on the flutter of slender rigid cones on pitching and plunging flexible supports[63]

(i) Low aspect ratio wings

Ref. 65 examines the flutter of rectangular low aspect ratio cantilever wings with bending and torsion modes, and one chordwise deformation mode of vibration, using piston theory. The report considers the cases of a solid biconvex section and a section of the same shape built up to have a uniform mass distribution. The results of the analyses are summarised in Figs. 53 and 54 - they show clearly the importance of the chordwise mode. For the built-up wing the critical value of the flutter speed parameter, and the adequacy of an analysis using only bending and torsion modes, depend very much on the chordwise frequency ratio f_3/f_2. The two-mode analysis is markedly unconservative for values of the frequency ratio less than 1·4; for values of the ratio between 1·4 and 2·5 the two-mode analysis is conservative. For the solid section wing the variation of the speed parameter with frequency ratio is less marked, and an analysis using only bending and torsion modes is unconservative throughout the range of chordwise frequency ratios.

Ref. 64 describes a method for the flutter analysis of a low aspect ratio wing which includes camber deflections. The method uses piston theory. , In Fig. 55 (Ref. 58) results using this method are compared with theoretical predictions neglecting camber deflections, and with experiment. As might be expected from the results of Ref. 65, the comparison suggests that the importance of including camber modes of deflection depends on the particular conditions; for the 60° leading-edge sweep model the accuracy of the theoretical prediction using camber modes is no greater than for a two-mode analysis; but for the 45" model, the two-mode analysis shows much larger errors.

Ref. 65 also gives a much simplified analysis of a slender delta wing in free-free flutter: the delta wing was a flat plate with uniform mass distribution and only longitudinal bending modes were included. The analysis was generalised to include a range of apex angles using piston theory and slender body theory: piston theory was assumed to apply in the range $2 \leqslant M \leqslant 7$ for supersonic leading edges for which $M \geqslant \operatorname{cosec} \varepsilon$, where a is the semiapex angle of the delta; and slender body theory was applied for semiapex angles up to ME < 0·5. There was no simple theory that could be applied for the range $0.5 < M\varepsilon < 1$. The first three longitudinal elastic modes were used in the analysis. The fact that the mass distribution was uniform meant, in the piston theory analysis, that there was no coupling between the rigid body modes of pitching and plunging and the elastic modes; and for the slender body theory analysis, that coupling occurred only in the virtual inertia terms, which were negligible for large enough values of the density ratio parameter. Throughout the range of the analysis by slender body theory, divergence was found to occur before flutter; for the piston theory analyses flutter was found in all cases, and the predominant mode in the instability depended on the density ratio. For small values of density ratio the predominant mode was the fifth mode (the third elastic mode); for large values of the density ratio, it was the fourth mode (the second elastic mode). The results of the analyses are summarized in Fig. 56 for large values of density ratio. E_2 is an effective stiffness based on the frequency of the second elastic mode and the mass per unit area of the plate. The piston theory analyses show values of critical dynamic pressure parameter that are constant with apex angle at a given Mach number down to an apex angle given by $M \sin \varepsilon = 1$; and values of critical pressure parameter that increase with Mach number. The slender body analyses show values of critical dynamic

pressure/

pressure both for divergence and for flutter (if it could occur) that decrease with apex angle. The marks on the curves show the limits of application of slender body theory at the Mach number shown, from the criterion $M < 0{\cdot}5$.

Ref. 65 goes on to discuss the extension of the analyses to cases with spanwise deformations, and to wing body combinations. It points cut that, for these cases, the modes and frequencies will be dependent on the semiapex angle ε and that, for low values of ε, the mode frequencies will be close together, which would make it necessary to include a greater number of modes in the analysis.

(ii) The flutter of slender bodies

It has been shown in Refs. 66 and 78 that a feasible technique can be developed for measuring the aerodynamic stiffness and damping on flexible slender models oscillating in longitudinal bending modes, and it is shown in Ref. 67 that flutter tests on such models are also possible using admittance techniques. The tests in these references were all carried out at Mach numbers less than 3, and consequently do not provide information relevant to this review, but they are noted because the techniques are relevant to the flutter problems being discussed.

The only information related to the flutter of slender bodies at hypersonic speeds comes from analyses and experimental results on a support giving flexibility in plunging and pitching. These results have direct, relevance to the possible use of slender cones as control devices mounted at the wing tips of hypersonic vehicles, and also provide a simple test of the use of available aerodynamic theories.

Ref. 57 considers the flutter of a 15° conical shell with pitching and plungingflexibilities. The aerodynamic forces for the analysis are found assuming quasi-steady conditions and using a theory due to von Kármán . The forces on each section of the cone are assumed to be those on the corresponding section of a continuous cone with overall downwash, w, equal to the downwash at the section, and the forces on this corresponding cone are found by the von Kárman theory. Since the theory is only valid for $w/a < 1$, where a is the speed of sound, the calculation is limited to $M < 7{\cdot}5$. The results are shown in Fig. 57.

Ref. 63 gives the results of experiments on a series cf models of a 7·5° semiangle conical shell. The models had variations of axis position, c.g. position, and frequency ratio, and measurements were made over the range $M = 1{\cdot}6$ to $15{\cdot}4$. The majority of the results are for Mach numbers of 1·6, 2·0 and. 3·0, but the experimental and theoretical results suggest that this kind of flutter may be relatively independent of Mach number. This conclusion is suggested most clearly by Fig. 58, which shows the results of tests on one model and. a comparison of the results with theoretical predictions. The experimental results for the low Mach number tests are seen to group quite closely together and the single result at $M = 15{\cdot}4$ falls in closely with them (the fact that the test medium is helium for the high Mach number should not be very significant for this comparison, as the pressure distribution is likely to be the same as for air. The theoretical curves from Van Dyke's second-order slender body theory[68], and for Newtonian theory, also agree closely. Van Dyke's theory must be applied in a quasi-steady manner, but it appears to give closer agreement with experiment than other theories used in the report, for the low Mach number tests; Newtonian theory should give satisfactory results on a cone shape at $M = 15$.

The/

The conclusion drawn from Fig. 58 is supported by the results shown in Fig. 59 for a geometrically similar cone with different axis Position and c.g. position, at M = 2, 3 and 6·83. There is rather more scatter of the experimental points, but there is still a strong suggestion that the flutter of the cone is not greatly affected by Mach number. Calculations by Newtonian theory and by shock expansion theory were made for the M = 6·83 case, but only poor agreement was obtained. The shock expansion result is not shown in Fig. 58.

The failure of the analysis using shock expansion theory in Ref. 63 may be related to the fact that the flow is predominantly conical, despite the unsteady components, and such flows violate a condition for the use of shock expansion theory for three-dimensional bodies.

For the flutter cases in both Figs. 58 and 59 the analysis was found to be affected by the inclusion of a factor from the drag of the cone. The qualitative effect of this is shown by one curve in each Figure.

The large variations of flutter parameter shown in Fig. 57 for axes around the mid-length are not shown in Figs. 58 and 59. This may be related to the particular theory used since the results of applying von Karman s theory in Ref. 63 also showed a dependence of critical flutter parameter on Mach number. But direct comparisons are not possible because of the different characteristics of the cones used: the frequency ratio of $\omega_h/\omega_\alpha = 0{\cdot}5$, used in the investigations for Fig. 57, was not investigated in Ref. 63 and, in fact, Figs. 58 and 59 suggest that flutter would not have been possible at a frequency ratio of 0·5 for the models used in those investigations.

4.2.3 Panel flutter

There appear to be no published results of investigations of panel flutter at hypersonic speeds but, since it can be assumed from structural considerations that displacements will remain very small, the hypersonic similarity parameter for the displacements, $M\delta$, will remain small, and consequently it is reasonable to draw tentative conclusions about panel flutter at hypersonic speeds by extrapolation from experiments and piston theory analyses for lower Mach numbers. This is the basis on which this section has been written. Surveys of information on panel flutter at lower Mach numbers are given in Refs. 74 and 76.

(i) Flat panels

Analyses for Mach numbers between 2 and 5 indicate that the effects of changes in the fluid dynamics of a perfect gas due to increased Mach number do not cause a significant change in the critical thickness ratio for flutter This is illustrated by Figs. 60 and 61, from Refs. 69 and 70, for a buckled two-dimensional panel clamped front and rear, and for a rectangular panel simply supported on all four edges. These results show, for Mach numbers greater than about 1·2, a small increase in critical thickness with increasing Mach number. But there are two effects occurring in real flight situations which could make panel flutter a significant problem at hypersonic speeds. These effects are the large increases of dynamic pressure which can occur in the local flow conditions on vehicles, especially on the lifting surfaces of vehicles at large angles of attack and in intake ducts; and aerodynamic heating effects, which would lower the elastic stiffness and could set up compressive stresses in panels, or even cause buckling. Typical local flow conditions which could occur are shown in Fig. 62 from Ref. 71. The significance of the conditions can be gauged from the critical dynamic Pressure parameter λ found by Hedgepeth in Ref. 70:

$\lambda/$

$$\lambda = \frac{2q\ell^3}{\sqrt{M^2-1}} \cdot \frac{12(1-\nu^2)}{Et^3} \qquad \ldots (4.17)$$

where, for a panel of given shape and loading conditions, λ has a fixed value. It follows that:

$$\left(\frac{t^3}{\ell^3}\right)_{crit} \propto \frac{q}{\sqrt{M^2-1}}, \quad \text{or} \quad \left(\frac{t^3}{\ell^3}\right)_{crit} \propto \frac{q}{M} \quad \text{for } M \text{ large.} \qquad \ldots (4.18)$$

Then from Fig. 62, at M = 20 and $\alpha = 27°$ (as an example) it can be seen that the local q/M can be as much as 20 times the free-stream value. Theoretical predictions of the effect of compressive stress on the flutter of panels confirm a reduction in flutter dynamic pressure with compressive stress up to the point at which the panel buckles[72,75].

At low supersonic Mach numbers above M= 1·4 the boundary layer does not appear to have very much effect on the flutter characteristics75 but the very thick boundary layers at hypersonic Mach numbers may have a greater influence.

(ii) Cylindrical shells

Early analyses had suggested that large thicknesses were needed to prevent flutter of cylindrical shells[76] and that the flutter critical thickness increased quite rapidly with Mach number.

Practical experience has suggested that these results were pessimistic and this has been confirmed by recent theoretical and experimental work. Early theoretical investigations, which had not included the effects of material damping or of damping effects from the boundary layer, had found that the critical mode of flutter of a finite cylinder was one with no circumferential nodes. But more recent results published in Ref. 74 show that this mode of flutter is strongly affected by both material damping and aerodynamic damping and, as a result, the critical mode becomes one with circumferential nodes and the critical thickness and dependence on Mach number are considerably reduced. These results are illustrated by Figs. 64 and 65. The results were confirmed by the results of experiments reported in Ref. 74.

It can be concluded, then, that for cylindrical shells, as for flat panels, the perfect fluid dynamic effects of high Mach number are not likely to cause any important changes in the flutter conditions, but there will be important effects in practice from heating of the structure causing reductions in material properties and compressive stresses, from the local flow conditions, and from the influence of the thick boundary layers. It seems likely that the effect of the thick hypersonic boundary layers will still be stabilising but some investigation of this is needed.

4.3 Discussion and Conclusions

From the information which has been collected in this review, it seems likely that the principal causes of any degradation of flutter behaviour on vehicles operating at hypersonic speeds will be the degradation of the stiffness properties of the structure and the high local values of dynamic pressure, rather than any large changes in fluid dynamic behaviour.

Most/

Most of the information relates to the pitching and plunging flutter of a two-dimensional section, or the similar problem of the bending-torsion flutter of a cantilever wing. There is still a need, in this field, to investigate the use of theories applicable to Mach numbers higher than the piston theory range, and to find an adequate method for estimating the aerodynamic forces on a section with a blunt leading edge; experimentally, there is a need for studies that explicitly take account of possible non-linear behaviour, and for further studies on the effects of incidence. But this kind of flutter is likely to be of comparatively minor importance for hypersonic vehicles, and there is a great need for more analytical and experimental work on the flutter of low aspect ratio wings and slender bodies, on panel flutter, and on membrane behaviour.

Work on slender bodies and low aspect ratio wings is likely to be analytically complex. For pointed slender bodies and wings with supersonic leading edges, shock expansion theory should give suitable estimates of the aerodynamic forces but its use in flutter analyses may be complicated. For blunted nose bodies an adequate aerodynamic analysis does not exist (Appendix II). Experimental work on these bodies and wings could include tests on rigid bodies flexibly mounted to give a simple check on theories, but would need to be extended to the use of flexible models.

In the case of panel flutter, a theoretical investigation of the use of piston theory in a steady flow field with large entropy gradients would be useful since these are the conditions which usually apply downstream of the strong nose shock on a hypersonic vehicle, and experiments would need to be carefully planned to show what fluid dynamic effects, if any, require special investigation.

All the experimental results which have been reviewed show clearly the need in future experimental flutter studies for very careful control of the experimental conditions if reliable and precise information is to be obtained on the merits of aerodynamic theories used in flutter analyses.

Finally, the point should be made that the values of aerodynamic damping coefficients at hypersonic speeds tend to be low, flutter frequency parameters tend to be small, and the density ratios at which flight takes place are high. In these conditions the importance of aerodynamic damping in flutter analyses may become negligible (Ref. 62, Section 6-6) and it would then be possible to use quasi-static air forces and the calculation of these forces would be correspondingly simplified. Clearly, this is a matter which should be investigated.

Nomenclature/

Nomenclature

(Some terms are not included in this index if they are used only locally)

---

a	local speed of sound
a_∞	free-stream value of speed of sound
A	aspect ratio of wing (span/mean chord)
b	representative length of a body ($\frac{1}{2}\bar{c}$ for a wing, ℓ for a body)
$\bar{c}$	mean chord of a wing
C_D	drag coefficient of a body [Drag/$\frac{1}{2}\rho U^2 S$]
CL	lift coefficient of a body [Lift/$\frac{1}{2}\rho U^2 S$]
C_{L_α}	rate of change of lift coefficient with angle of attack: $\partial C_L/\partial\alpha$
C_m	pitching moment coefficient
C_{m_α}	rate of change of pitching moment coefficient with angle of attack: $\partial C_m/\partial\alpha$
$C_{m_{\dot{\alpha}}}$	rate of change of pitching moment coefficient with time rate of change of angle of attack parameter, $\frac{\dot{\alpha}b}{U}$: $\frac{\partial C_m}{\partial(\dot{\alpha}b/U)}$
C_{m_q}	rate of change of pitching moment coefficient with pitching velocity parameter, $\frac{\theta b}{U}$: $\frac{\partial C_m}{\partial(\dot{\theta}b/U)}$
C_p	pressure coefficient $\frac{P - P_\infty}{\frac{1}{2}\rho_\infty U^2}$
d	maximum body diameter
E	Young's Modulus
E_2	effective stiffness based on frequency of second elastic mode
f	frequency of oscillation
f_i	frequency of natural mode : i = 1 for first mode, etc.
g	gravitational constant
$\bar{g}$	structural damping factor
h	altitude

h/

h displacement of section in plunge (flutter)

i_B non-dimensional form of I_B : $\frac{I_B}{\rho S b^3}$

I_B pitching moment of inertia of a body about its centre of gravity

k frequency parameter $\frac{2\pi f b}{U}$

X convergence factor for pitching oscillations of a vehicle flying on a re-entry path defined by equation (3.12)

X_{crit} critical value of X in equation (3.14)

K_L $\frac{C_L}{2} + \frac{m}{\rho S R}$

x_Y pitching radius of gyration of a body about its oentre of gravity

ℓ body length

ℓ panel length - in flutter studies

L/D ratio of lift to drag

L_i, L_i see definitions of derivatives (i = 1 to 4)

m mass of vehicle - Appendix III

m mass per unit span of two-dimensional section

m mass of wing or cone

m mass/unit area Of panel

} Appendix IV

M free stream or flight Mach number U/a_∞

M_f flutter Mach number

M_δ Mach number of boundary layer in approximate calculation of boundary layer damping in Figs. 64 to 65.

M_i, M'_i see definitions of derivatives (i = 1 to 4)

n number of circumferential nodes in the flutter of a cylindrical shell

N_x mid-plane stress in panel (Fig. 63)

p local pressure .

p_∞ free-stream static pressure

$\bar{p}$/

$\bar{p}$ non-dimensional pressure: $\bar{p} = \dfrac{p}{\rho_\infty U^2 \sin^2\alpha}$ (equation (2.24))

$\bar{p}_b$ amplitude of oscillatory non-dimensional pressure at body surface: $\dfrac{\tilde{P}_b}{\frac{1}{2}\rho U_\infty^2}$ (Fig. 9 and equation (2.63))

Δp incremental pressure

q fluid velocity in variational method (equation (2.42))

q dynamic pressure $q = \frac{1}{2}\rho_\infty U^2$

r radial co-ordinate (Fig. 7)

r_b local radius of body (Fig. 7)

$\bar{r}_a$ radius of gyration of a wing section in semi-chords: $\bar{r}_\alpha = \sqrt{\dfrac{I_\alpha}{mb^2}}$

R radius of flight path from centre of earth

R_i initial value of radius in re-entry problem } Appendix III

R cylindrical shell radius - Appendix IV

R_0 radius of spherical cap nose - Fig. 7

Re Reynolds number based on U and ℓ

Re_x Reynolds number based on distance from leading edge

s distance along flight path in re-entry problem

S entropy - Appendix II

S representative area of vehicle - Appendices III and IV

t time

t' transformed quantity (equation (2.13))

$\bar{t}$ non-dimensional value of t, (equation (2.23)) } Appendix II

$\bar{t}'$ transformed quantity (equation (2.36))

t thickness of panel or shell - Appendix IV

T local temperature (°R)

T_∞ free-stream temperature

T_σ stream temperature immediately behind shook wave

u/

u	disturbance velocity in x-direction or in ξ-direction
u'	transformed quantity (equation (2.7))
$\bar{u}$	non-dimensional value of u (equation (2.24))
u	horizontal component of vehicle velocity in re-entry problem
$\bar{u}$	ratio of u to $\sqrt{gR_i}$, the circular orbital speed at radius R_i
U	free-stream velocity or flight speed
$\bar{U}$	$U/(gR)^{\frac{1}{2}}$
U_i	initial flight speed at re-entry
$\bar{U}_i$	$U_i/(gR_i)^{\frac{1}{2}}$
v	disturbance velocity component in y-direction or in ~-direction
$\bar{v}$	non-dimensional value of v (equation (2.24))
v	disturbed volume of fluid in variational problem (equation (2.42))
V_f	flutter speed
w	downwash velocity at surface
w	disturbance velocity component in z-direction or in ζ-direction
$\bar{w}$	non-dimensional value of w (equation (2.24))
W	weight of vehicle
x,y,z	co-ordinate axes (Fig. 5)
x'	transformed quantity (equation (2.7))
$\bar{x}'$	transformed quantity (equation (2.13))
$\bar{x}$	normalised co-ordinate x/ℓ or x/c
$\bar{x}_\ell$	normalised co-ordinate $x/$(nose length)
$\bar{x}_o$	distance, in chord lengths, that the elastic axis of a section lies behind the leading edge
$\bar{x}_p$	value of $\bar{x}$ at centre of pressure
$\bar{x}_a$	distance, in chord lengths, that the c.g. of a section lies behind the elastic axis
$\bar{Y}_s$	dimensionless amplitude of shock displacement Y_s/R_o
	Y_s amplitude of displacement + curvilinear co-ordinates (Fig. 7 and equation (2.64))

α instantaneous angle of attack

α_0 amplitude of oscillatory angle of attack

α_s mean angle of attack

β $\sqrt{M^2-1}$

γ ratio of specific heats

γ flight path angle to local horizontal

γ_i flight path angle at start of re-entry

} Appendix III

δ quantity specified by the largest of the thickness ratio, mean incidence of body or surface, and the dimensionless amplitude of the time-dependent motion - Appendix II
the thickness ratio of aerofoil section - Appendix IV

$\bar{\delta}$ apparent boundary layer thickness - wall to 99% free-stream velocity point (Figs. 64 and 65)

A prefix denoting a small variation of a quantity in the variational problem (Appendix IV)

ε semi-apex angle of delta wing

ε_0 density ratio across shock wave

ζ cc-ordinate axis (Fig. 6)

$\bar{\zeta}$ non-dimensional value of ζ (equation (2.23))

} Appendix II

ζ = ω_h/ω_f (Appendix IV)

η co-ordinate axis (Fig. 6)

$\bar{\eta}$ non-dimensional value of η (equation (2.23))

θ steady surface slope measured from chordline or body axis

θ_N value of θ at the nose

κ order of magnitude of perturbations

μ relative density of vehicle (equation (3.1))

μ mass ratio of wing

= $m/4b^2\rho$ for tnc-dimensional section; m is mass per unit span b = $\bar{c}/2$

= $m/4b^2s\rho$ for a wing; m is mass of wing b = $\bar{c}/2$
s = span of wing

μ local viscosity

μ_∞ viscosity of free stream

ν	Poisson's ratio - Appendix IV
ξ	co-ordinate axis (Fig. 6)
$\bar{\xi}$	non-dimensional value of ξ (equation 2.23))
$\bar{\xi}'$	transformed value of $\bar{\xi}$ (equation(2.36))
ρ	density
ρ_∞	free-stream density
$\bar{\rho}$	non-dimensional value of ρ (equation (2.24))
σ	vehicle density
τ	natural unit of time (equation(j.9))
ϕ	velocity potential
ϕ	angular co-ordinate in Figs. 7 and 18
χ	viscous interaction parameter in equation (1.2)
ω	circular frequency radians/sec = $2\pi f$
ω_i	circular frequency of the ith mode
ω_f	circular flutter frequency
$\bar{\omega}_f$	ω_f/ω_α
ω_h	circular bending or plunging frequency
ω_α	circular torsional frequency

Definitions of flutter parameters

$\frac{V_f}{b\omega_\alpha}$	dimensionless flutter speed
$\frac{b\omega_\alpha\sqrt{\mu}}{a}$	flutter altitude parameter
$\frac{V_f}{b\omega_\alpha\sqrt{\mu}}$	flutter speed/altitude parameter

Definitions/

Definitions of derivatives

$$L_2 = \frac{\ell_{\dot{z}}}{2k}$$

$$L_3 = \frac{(\ell_\theta - 4k^2 \ell_{\ddot{\theta}})}{2k^2}$$

$L_2 = kL_3$ for piston theory

$$L_4 = -\frac{"B}{k}$$

$$M_2 = -\frac{m_{\dot{z}}}{2k}$$

$$M_3 = -\frac{(m_\theta - 4k^2 m_{\ddot{\theta}})}{k^2}$$

$M_2 = kM_3$ for piston theory

$$M_4 = -\frac{2m_{\dot{\theta}}}{k}$$

where Lift $= 4\rho_\infty U_\infty^2 \, b \, k^2 e^{i\omega t} \left[\frac{h}{b} (L_1 + iL_2) + \alpha_0 (L_3 + iL_4) \right]$

and pitching moment $= -4\rho U_\infty^2 \, b^2 k^2 e^{i\omega t} \left[\frac{h}{b} (M_1 + iM_2') + \alpha_0 (M_3 + iM_4) \right]$

The quantities L_3', L_4', M_1', M_2', M_3', M_4' refer to the leading-edge axis ($\bar{x}_0 = 0$).

Acknowledgements

The author wishes to acknowledge the help received in the preparation of this report from discussions with colleagues at the National Physical Laboratory. He wishes to acknowledge with particular gratitude the help, advice and encouragement received from Mr. N. C. Lambourne.

References/

References (Appendix I)

No.	Author(s)	Title, etc.
1	Hayes, W. A. and Probstein, R. F.	Hypersonic flow theory. Academic Press. 1959
2	Chernyi, G. G.	Introduction to hypersonic flow. Academic Press. 1961
3	Lees, Lester	Hypersonic flow. Presented at 5th International Aeronautical Conference. IAS Preprint 554.
4	Campbell, W. F. and Meyer, R. F.	Hypersonics, Pt. II. Nat. Research Council Canada Report No.DME/NAE. 1961(4).
5	Snaring, T. M. and Ketter, D. J.	Future dynamic aerothermoelastic considerations from vehicle requirement viewpoint. Proceedings of Symposium on Aerothermoelasticity, October, 1961. ASD TR-61-645.
6	Laidlow, W. R. and Wykes, J. H.	Potential aerothermoelastic problems associated with advanced vehicle design. ASD TR-61-645. Proc. of Symposium on Aerothermoelasticity, October, 1961.
7		Aerodynamics of space vehicles. NASA Sp.23. December, 1962.
8	Eggers, A. J. Jr.	Some considerations of aircraft configurations suitable for long range hypersonic flight. Proceedings of 11th Symposium of Colston Research Society, 1959. Butterworths.
9	Nonweiler, T.	Delta wings of shapes amenable to exact shock-wave theory. A.R.C.22 644 March, 1961.
10	Peckham, D. H.	On three-dimensional bodies of delta planform which can support plane attached shock waves. A.R.C. C.P.640. March, 1962.
11	Penland, J. A.	A study of the aerodynamic characteristics of a fixed geometry paraglider configuration and three canopies with simulated variable canopy inflation at Mach No. of 6. NASA TN.O-1022.

References (Appendix II)/

References (Appendix II)

No.	Author(s)	Title, etc.
12	Ashley, Holt and Zartarian, Garabed	Theoretical hypervelocity unsteady aerodynamics. Proceedings of Symposium on Aerothermoelasticity. ADS TR-61-645.
13	Ashley, Holt and Zartarian, Garabed	Thickness and boundary layer effects. AGARD Manual on Aeroelasticity, Vol.II, Chap.9.
14	Lighthill, M. J.	Oscillating aerofoils at high Mach number. J.Ae.Sci. Vol.20, pp.402-406, June, 1953.
15	Miles, J. w.	Unsteady flow at hypersonic speeds. Hypersonic flow. Proceedings of 11th Symposium of the Colston Research Society, Bristol 1959. p.180 Butterworths Scientific Publications.
16	Raymond, Joseph L.	Piston theory applied to strong shocks and unsteady flow. J.Fl.Mech. Vol.8, Pt.4. 1960. pp.509-513.
17	East, R. A.	A theoretical and experimental study of oscillating wedge shaped aerofoils in hypersonic flow. University of Southampton AASU Rep. No.228.
18	Mahony, J. J.	A critique of shock expansion theory. J.Aero.Sci. Vol.22, No.10. 1955. pp.673-680.
19	Zartarian, Garabed	Unsteady airloads on pointed airfoils and slender bodies at high Mach numbers. Wright Air Development Center. WADC TR-59-583.
20	Zartarian, Garabed and Sauerwein, Harry	Further studies on high speed unsteady flow. ASD-TDR-62-463. September, 1962.
21	Tobak, Murray and Wehrend, William R.	Stability derivatives of cones at supersonic speed. NACA TN 3788. September, 1956.
22	Margolis, K.	Theoretical evaluation of the pressures, forces and moments at hypersonic speeds acting on arbitrary bodies of revolution undergoing separate and combined angle-of-attack and pitching motions. NASA TN D-652. June, 1961.
23	Reid, Robert C. Jr. and Mayo, Edward E.	Equations for the Newtonian static and dynamic aerodynamic coefficients for a body of revolution with en offset center-of-gravity location. NASA TN D-1085. June, 1963.
24	Van Dyke, Milton D.	A study of hypersonic small disturbance theory. NACA Report 1194. 19%.

25/

No.	Author(s)	Title , etc.
25	Sychev, V. V.	Three-dimensional hypersonic flow past slender bodies at high angles of attack. PMM Vol.24, No.2, 1960. pp.205-212.
26	Zartarian, Garabed and Hsu, Pao Tan	Theoretical and experimental studies on airloads related to hypersonic aeroelastio problems of general slender configurations. ASD Tech. Report 61-7. April, 1961.
27	Zartarian, Garabed, Hsu, Pao Tan and Ashley, Holt	Dynamic airloads and aeroelastio problems at entry Mach numbers. Journal of Aerospace Sciences, Vol.28, No.3. March, 1961. pp.209-222.
28	Eggers, A. J. Jr., Syvertson, Clarence A. and Kraus, Samuel	A study of inviscid flow about airfoils at high supersonic speeds. NACA Report 1123. 1953.
29	Eggers, A. J. Jr. and Savin, Raymond C.	A unified two-dimensional approach to the calculation of three-dimensional hypersonic flows, with application to bodies of revolution. NACA Report 1249. 1955.
30	Eggers, A. J. Jr., Savin, Raymond C. and Syvertson, Clarence A.	The generalized shock-expansion method and its application to bodies travelling at high supersonic speeds. J.Aero.Sci., Vol.22, No.4. April, 1955. pp.231-238.
31	Savin, Raymond C.	Application of the generalized shook-expansion method to inclined bodies of revolution travelling at high supersonic speeds. NACA TN 3349. April, 1955.
32	Kennett, H.	Some steady and unsteady inviscid hypersonic flows past bluff bodies. AFOSR 1031 MIT Fluid Dynamics Research Lab. Rep. 61-1.
33	Holt, Maurice	A linear perturbation method for stability and flutter calculations on hypersonic bodies. Journal of the Aerospace Sciences, Vol.26, No.12. December, 1959. pp.787-793.
34	Kawamura, Ryuma and Tsien, Fu-Hsing	Aerodynamic stability derivatives of axi-symmetric body moving at hypersonic speeds. Presented at 3rd Int. Congress of Aero Sciences, August, 1962. Stockholm.
35	Lighthill, M. J.	The response of laminar skin friction and heat transfer to fluctuations in the stream velocity. Proc.Roy.Soc.(London), Series A, Vol.224. July, 1954.

No.	Author(s)	Title. etc.
36	Moore, F. K.	Aerodynamic effects of boundary layer unsteadiness. 6th Anglo-American Aeronautical Conference September, 1957 Royal Aeronautical Society, 1959.
37	Olik-Ruckemann, K. and LaBorge, J. G.	Oscillatory experiments in a helium hypersonic wind tunnel. National Research Council of Canada Aero Rep.LR335. March, 1962.
38	Dayman, B. Jr., Nelson, D. A. and Jaffe, P.	Measurement of pitch damping at large angles of oscillation for proposed Mars atmosphere-entry vehicles. Institute of Aerospace Sciences IAS Paper 63-79.
39	Maas, Walter Leo	Experimental determination of pitching moment and damping coefficients of a cone in low density hypersonic flow. University of California Institute of Engineering Research Tech. Rep. HE-150-190. October, 1961
40	Ferri, A.	General theory of high speed aerodynamics Section G Chapter 6. Vol.VI. High speed aerodynamics and jet propulsion. Oxford University Press.

References (Appendix III)

No.	Author(s)	Title, etc.
41	Duncan, W. J.	The principles of the control and stability of aircraft. Cambridge University Press.
42	Etkin, Bernard	Dynamics of flight. John Wiley & Sons, Inc.
43	Etkin, Bernard	Longitudinal dynamics of a lifting vehicle in orbital flight. J.Ae./Sp.Sci. Vol.28, No.10. October, 1961. pp.779-788.
44	Rangi, R. S.	Non-linear effects in the longitudinal dynamics Of a lifting vehicle in a circular orbit. UTIA Tech. Note No.40. AFOSR 210. October, 1960.
45	Fredrich, Hans R. and Dore, Frank J.	The dynamic motion of a missile descending through the atmosphere. J.Ae.Sci. Vol.22, No.9. September, 1955. pp.628-632.
46	Allen, Julian H.	Motion of a ballistic missile angularly misalined with the flight path upon entering the atmosphere and its effect upon aerodynamic heating, aerodynamic loads and miss distance. NACA Tech. Note 4048. October, 1957.
47	Tobak, Murray and Allen, Julian H.	Dynamic stability of vehicles traversing ascending and descending paths through the atmosphere. NACA Tech. Note 4275. July, 1958.
48	Sommer, Simon C. and Tobak, Murray	Study of the oscillatory motion of manned vehicles entering the earth's atmosphere. NASA Memo 3-2-59A. April, 1959.
49	Fine, J. M.	The stability of flight paths of lifting vehicles during entry into planetary atmospheres. UTIA Tech. Note No.48. July, 1961.
50	Laitone, E. V. and Coakley, T. J.	Non-linear dynamic stability of space vehicles entering or leaving an atmosphere. Paper No. ICAS-20. 3rd International Congress in Aeronautical Sciences, Stockholm, August, 1962.
51	Kistler, E. L. and Capalongan, F. F.	Some studies of the dynamic motions of hypervelocity, high altitude vehicles. Proceedings of National Specialists meeting on Dynamics and Aeroelasticity, Forth Worth, Texas. November 6-7, 1958.

52./

No.	Author(s)	Title, etc.
52	Nonweiler, T.	The control and stability of glider aircraft at hypersonic speeds. A.R.C.21 301 7th October, 1959.
53	Peterson, Victor L.	Motions of a short 10° blunted cone entering a Martian atmosphere at arbitrary angles of attack and arbitrary pitching rates. NASA TN D-l 3.26. May, 1962.
54	Taylor, Lawrence W. Jr. and Day, Richard E.	Flight controllability limits and related human transfer functions as determined from simulator and free flight tests. NASA TN D-746. May, 1961.

References (Appendix IV)/

References (Appendix IV)

No.	Author(s)	Title. etc.
55	Bisplinghoff, R. L.	Some structural and aeroelastic considerations of high-speed flight. 19th Wright Brothers Lecture. J.Ae.Sci. Vol.23, No.4. April, 1956. pp.289-329.
56	Chawla, Jagannath P.	Aeroelastic instability at high Mach number. J.Ae.Sci. Vol.25, No.4. April, 1958. pp.246-258.
57	Morgan, Homer G., Runyan, Harry L. and Huckel, Vera	Theoretical considerations of flutter at high Mach numbers. J.Ae.Sci. Vol.25, No.6. June, 1958. pp.371-381.
58	Runyan, Harry L. and Morgan, Homer G.	Flutter at very high speeds. NASA TN D-942. August, 1961.
59	Hanson, Perry W.	Aerodynamic effects of sane configuration variables on the aeroelastic characteristics of lifting surfaces at Mach numbers from 0•7 to 6•86. NASA TN D-984. November, 1961.
60	Goetz, Robert C.	Effects of leading-edge bluntness on flutter characteristics of some square-planform double-wedge airfoils at a Mach number of 15•4. NASA TN D-1407. October, 1962.
61	Young, Lou S.	Effects of angle of attack and thickness ratio on flutter of a rigid unswept diamond-airfoil section wing at a Mach number of IO-O. NASA TN D-1380. August, 1962.
62	Bisplinghoff, R. L. and Ashley, Holt	Principles of aeroelasticity. John Wiley & Sons Inc. 1962.
63	Sewall, John L., Hess, Robert W. and Watkins, Charles E.	Analytical and experimental investigations of flutter and divergence of spring mounted cone configurations at supersonic speeds. NASA TN D-1021. April, 1962.
64	Morgan, Homer G. Huckel, Vera and Runyan, Harry L.	Procedure for calculating flutter at high supersonic speeds, including camber deflections, and comparison with experimental results. NACA TN 4335. September, 1958.

65./

No	Author(s)	Title, eto.
65	Dugundji, John, and Crisp, John 0. C.	On the aeroelastic characteristics of low aspect ratio wings with chordwise deformations. Unpublished U.S. Report.
66	Hanson, Perry W, and Doggett, Robert V.	Aerodynamic damping of a 0•02 scale Saturn SA-1 Model vibrating in the first free-free bending mode. NASA TN D-1956. September, 1963.
67	Asher, Gifford W. and Watanabe, Roy K.	Admittance techniques in high speed flutter model testing. Part I. WADD Tech. Report 61-31. July, 1961.
68	Van Dyke, Milton D.	A study of second order supersonic flow theory. NACA Report 1081. 1952.
69	Sylvester, Maurice A.	Experimental studies of flutter of buckled rectangular panels at Mach numbers from 1•2 to 3•0 including effects of pressure differential and of panel width length ratio. NASA TN D-833. May, 1961.
70	Hedgepeth, John M.	Flutter of rectangular simply supported panels at high supersonic speeds. J.Ae.Sci. Vol.24, No.8. pp.563-573. August, 1957.
71	Shirk, Miohael H. and Olsen, James J.	Recent panel flutter research and application. Paper presented at 17th Structures and Materials Panel Meeting of AGARD. A.R.C.26 337.
72	Dixon, Sidney C., Griffith, George E. and Bohon, Herman L.	Experimental investigation at a Mach number of 3'0 of the effects of thermal stress and buckling on the flutter of four-bay aluminium alloy panels with length-width ratios of IO. NASA TN D-921. October, 1961.
73	Hess, Robert W. and Gibson, Frederick W.	Experimental investigation of the effects of compressive stress on the flutter of a curved panel and a flat panel at supersonic Mach numbers. NASA TN D-1306. October, 1962.
74	Fung, Y. C.	Some recent contributions to panel flutter research. AIAA Journal, Vol.1, No.4. April, 1963.

75./

No.	Author(s)	Title, etc.
75	Look, M. H. and Fung, Y. C.	Comparative experimental end theoretical studies of the flutter of flat panels in a low supersonic flow. AFOSR TN 670. May, 1961.
76	Fung, Y. C.	Guggenheim Aeronautical Laboratory, California Institute of Technology. A summary of the theories and experiments on panel flutter. AFOSR TN 60-224. GALCIT Report. May, 1960.
77	Isaacs, R. P.	Transtability flutter of supersonic aircraft panels. U.S. Air Force Project Rand P-101. (Quoted in Fig. 55).
78	Hanson, Perry W. and Doggett, Robert V. Jr.	Wind tunnel measurements of aerodynamic damping derivatives of a launching vehicle vibrating in free-free bending modes at Ma h numbers from 0·70 to 2·87, and comparisons with theory. NASA TN D-l 391. October, 1962.

PB.

FIG. I

(a) Slender wing/body combination

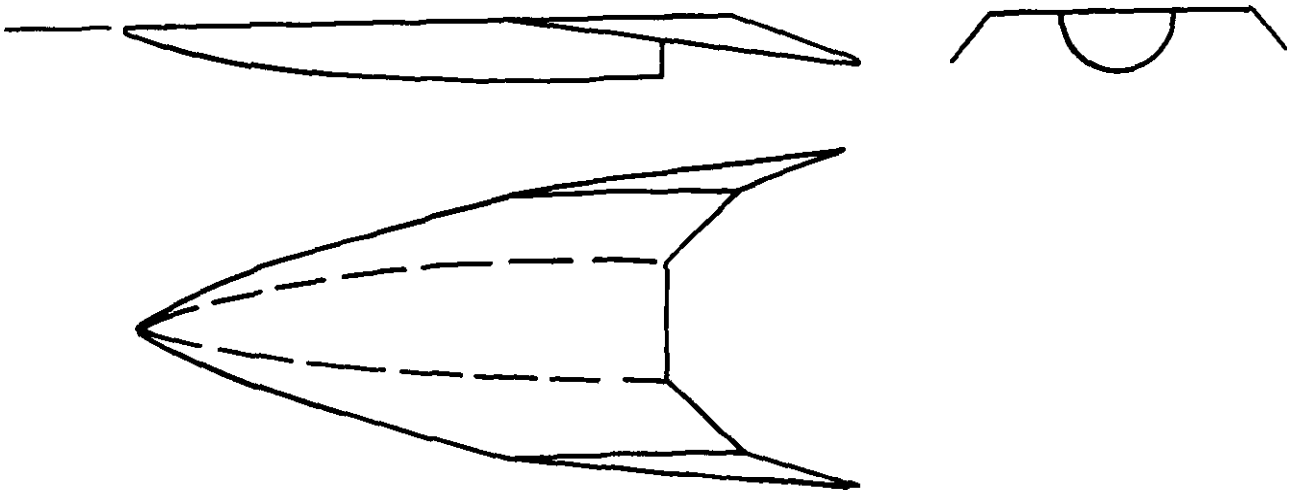

(b) Caret wing

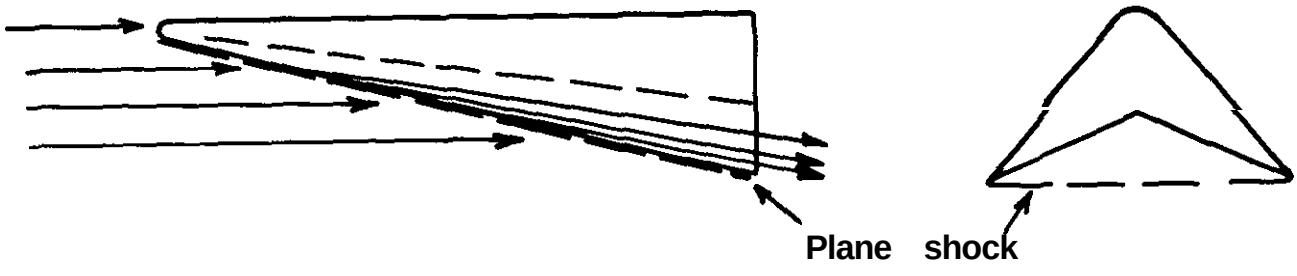

Hypersonic cruise configurations

FIG 2

(a) Bluff reentry shapes :
L/D ≃ 1/2 (Ref. 6)

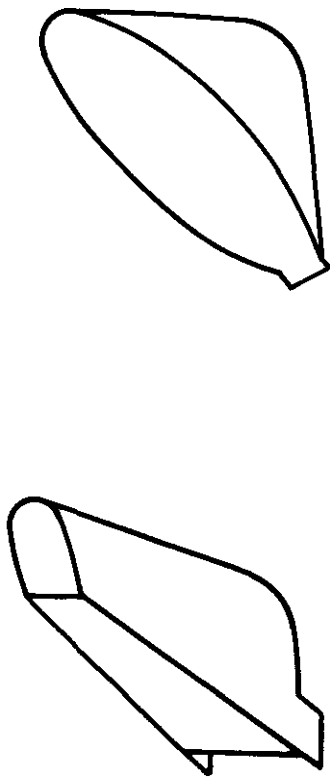

(b) Blunted slender reentry shape:
L/D ≃ 1 (Ref. 6)

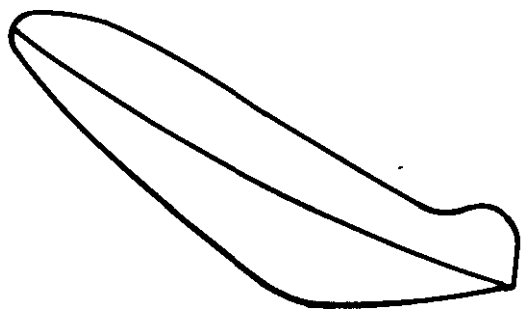

(c) Rogollo wing (Ref. 11)

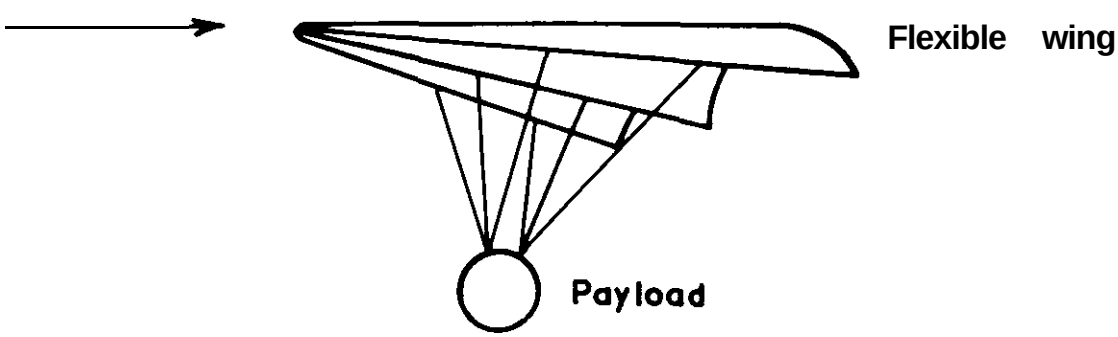

Reentry vehicles

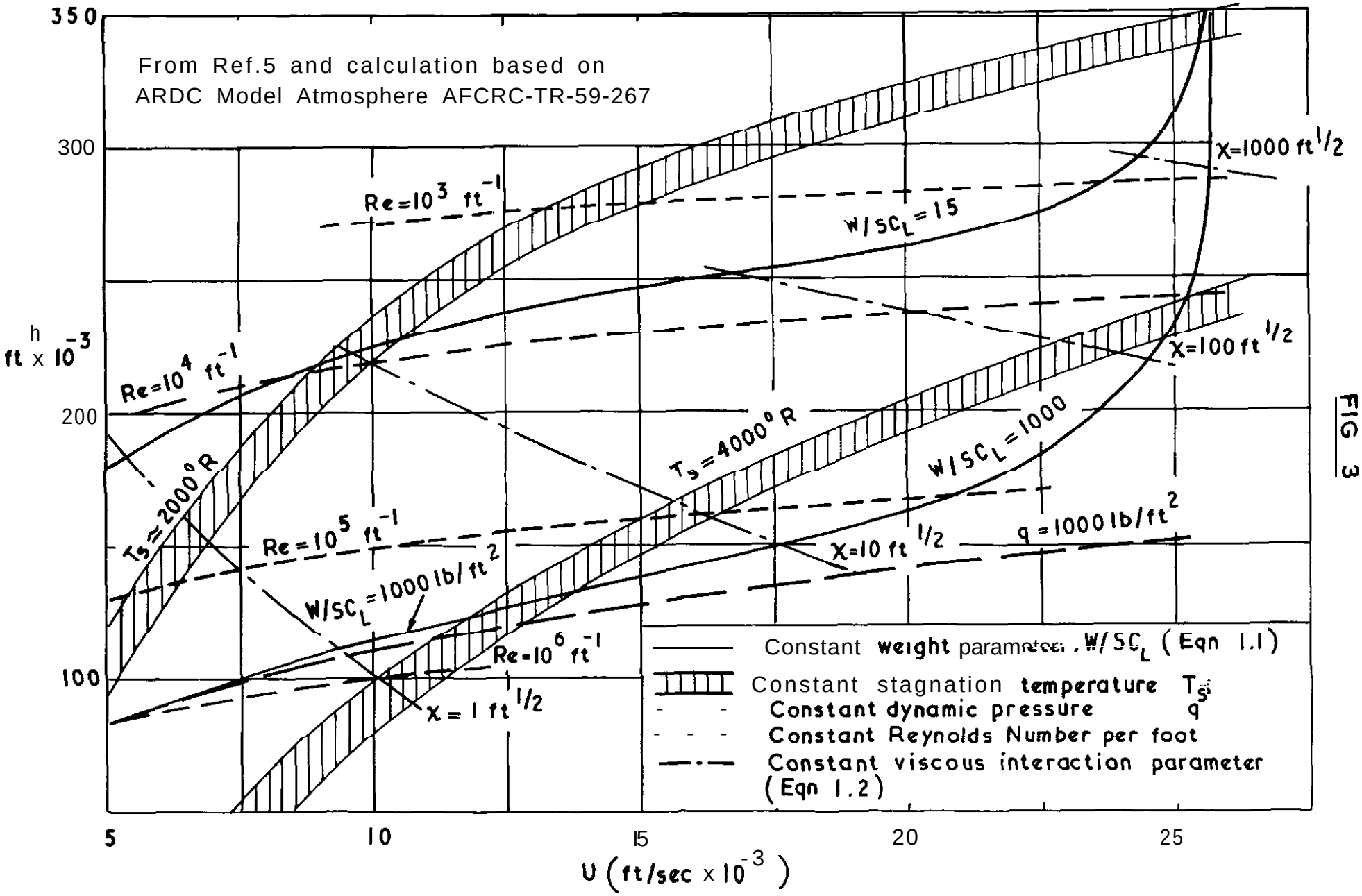

FIG 3

Hypersonic flight conditions

Reproduced from Ref. 5

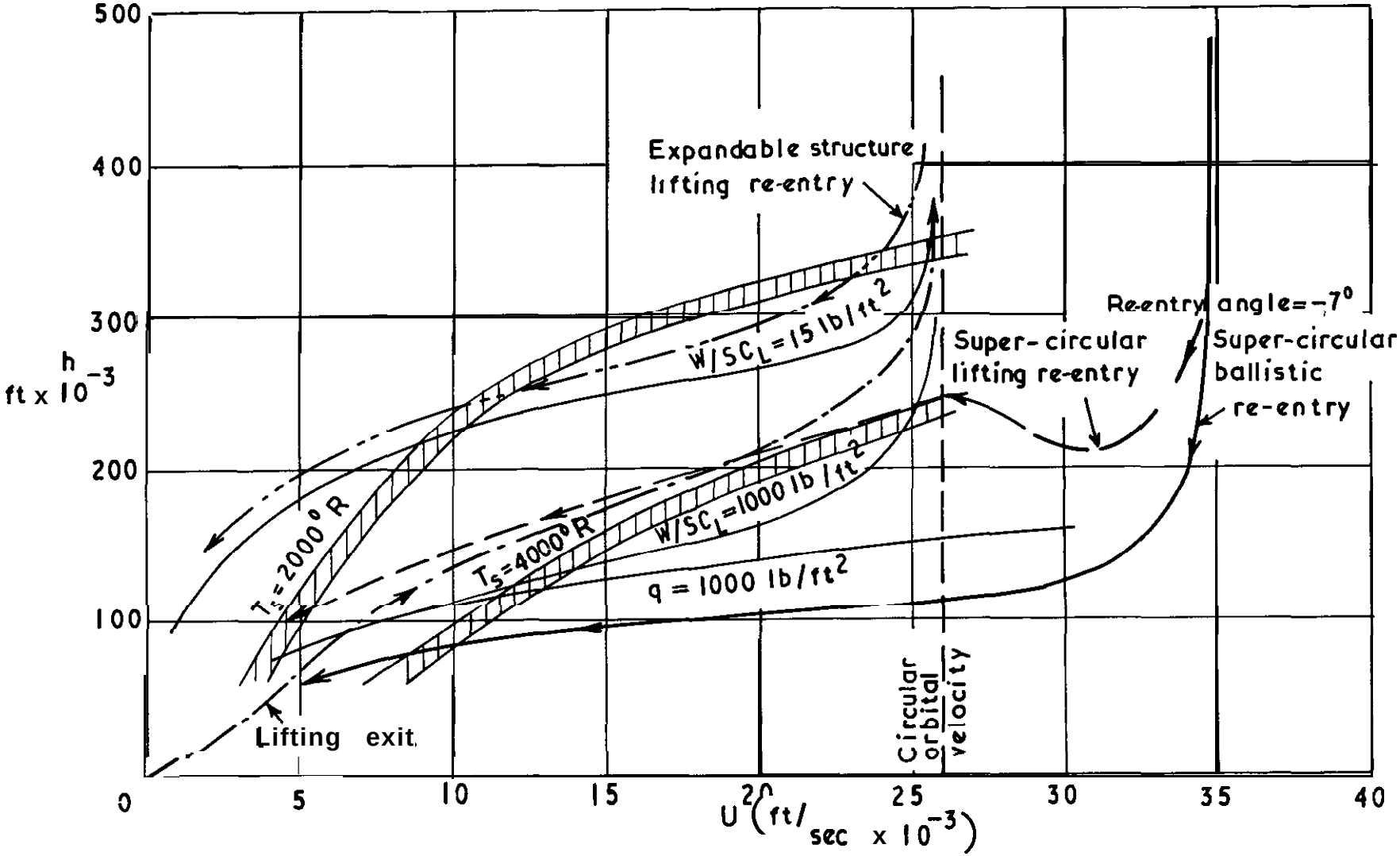

FIG 4

Re-entry and exit trajectories

FIGS. 5-7

FIG 5

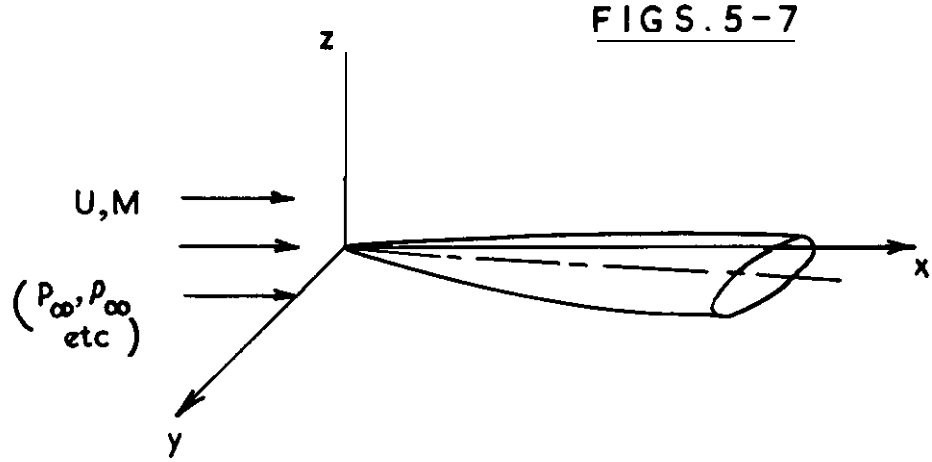

Axis system for thin pointed body in a hypersonic air stream

FIG. 6

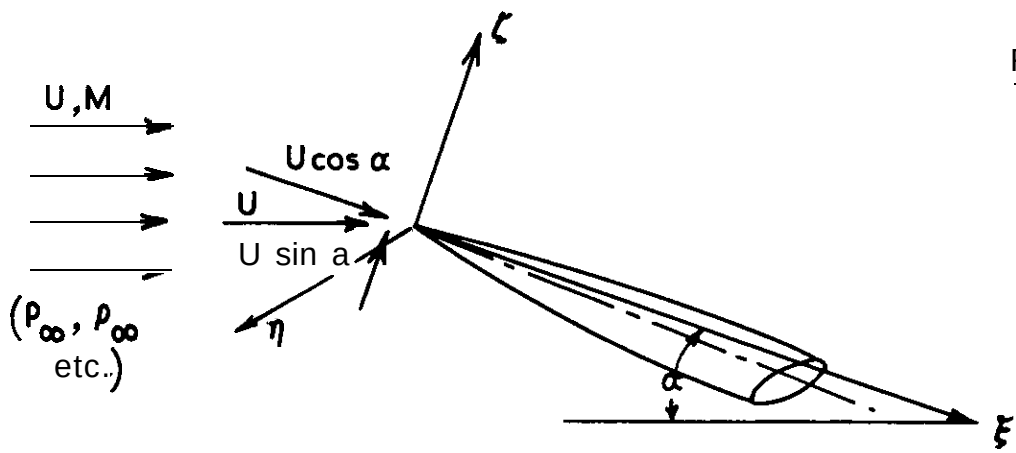

Axis system for thin pointed body at large incidence

FIG.7

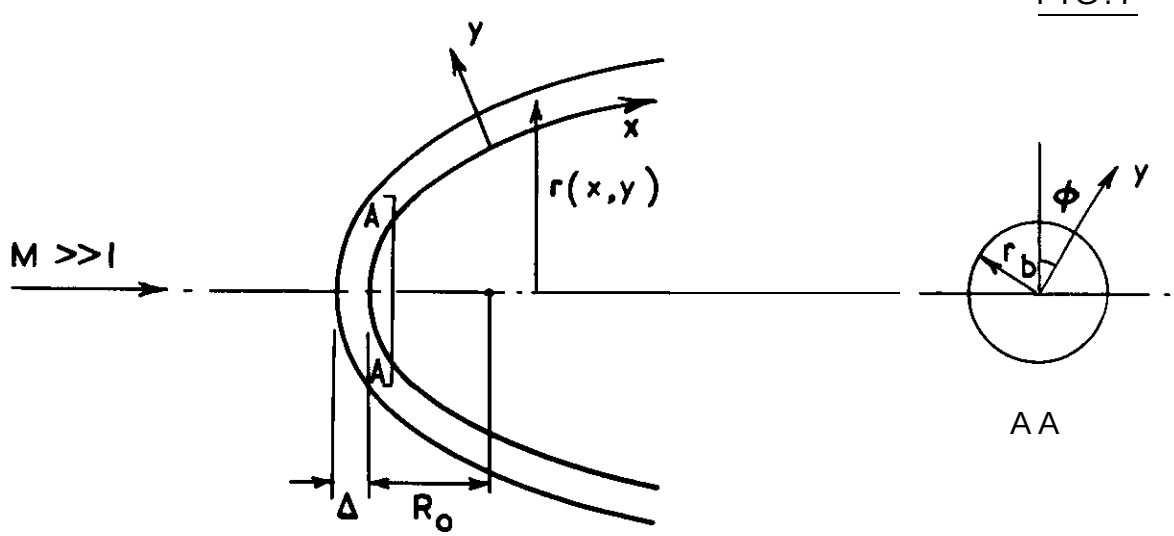

Orthogonal curvilinear coordinates for the constant density shock layer

FIG. 8

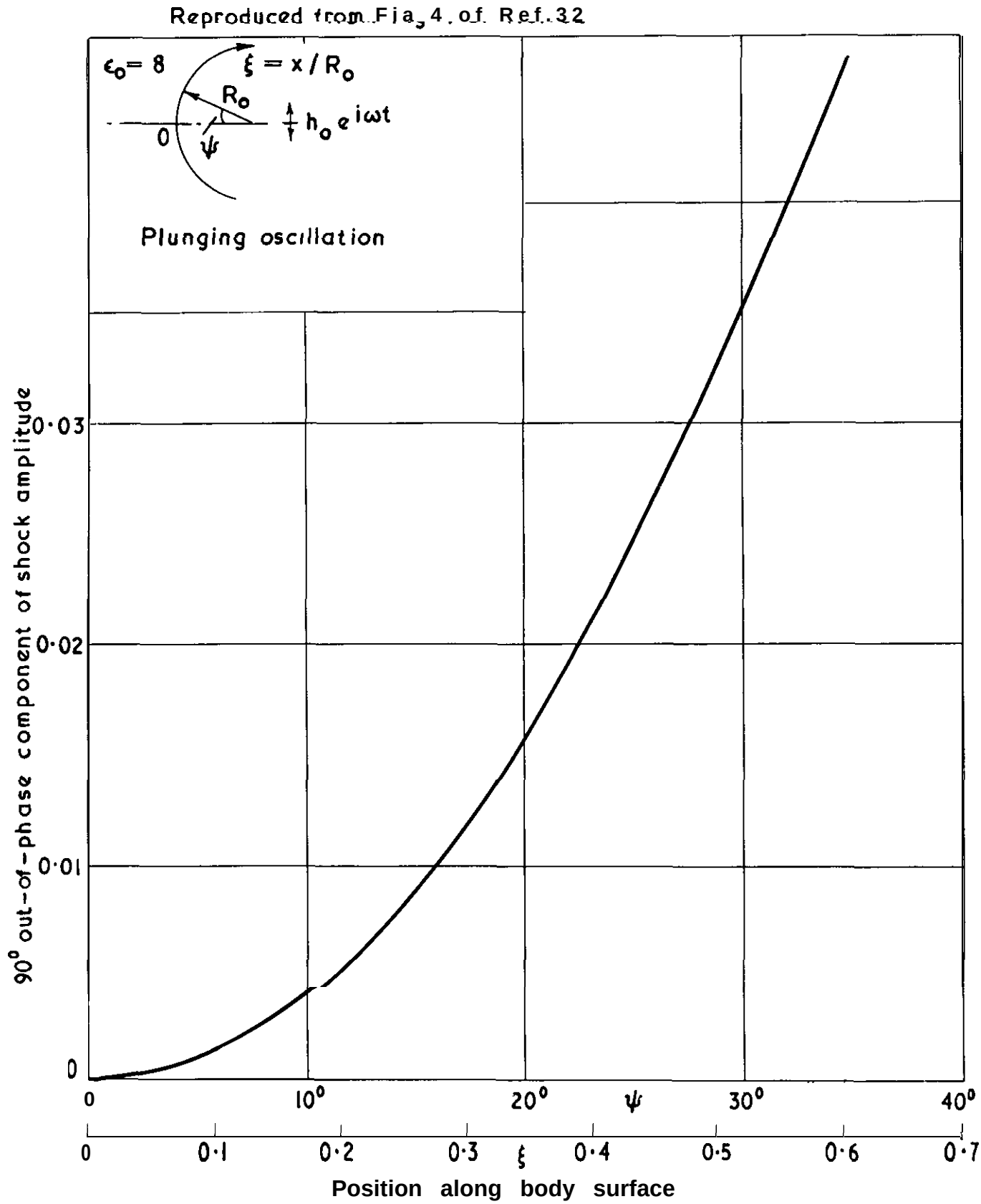

90° out-of-phase component of shock around a plunging spherical cap from constant density solution

FIG. 9

Reproduced from Fig. 5 in Raf. 32

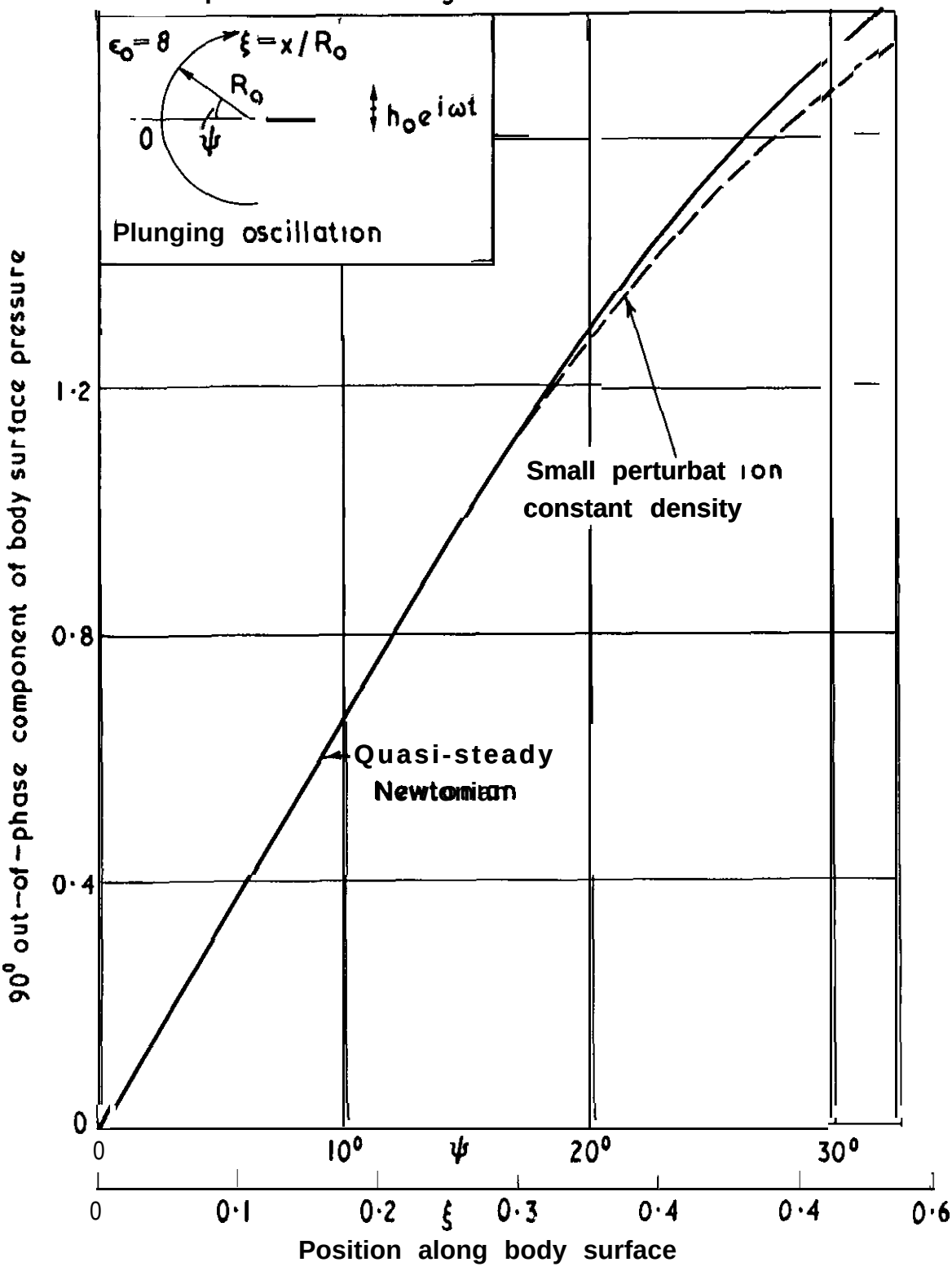

90^0 out-of-phase component of surface pressure on plunging sherical cap from the constant density solution

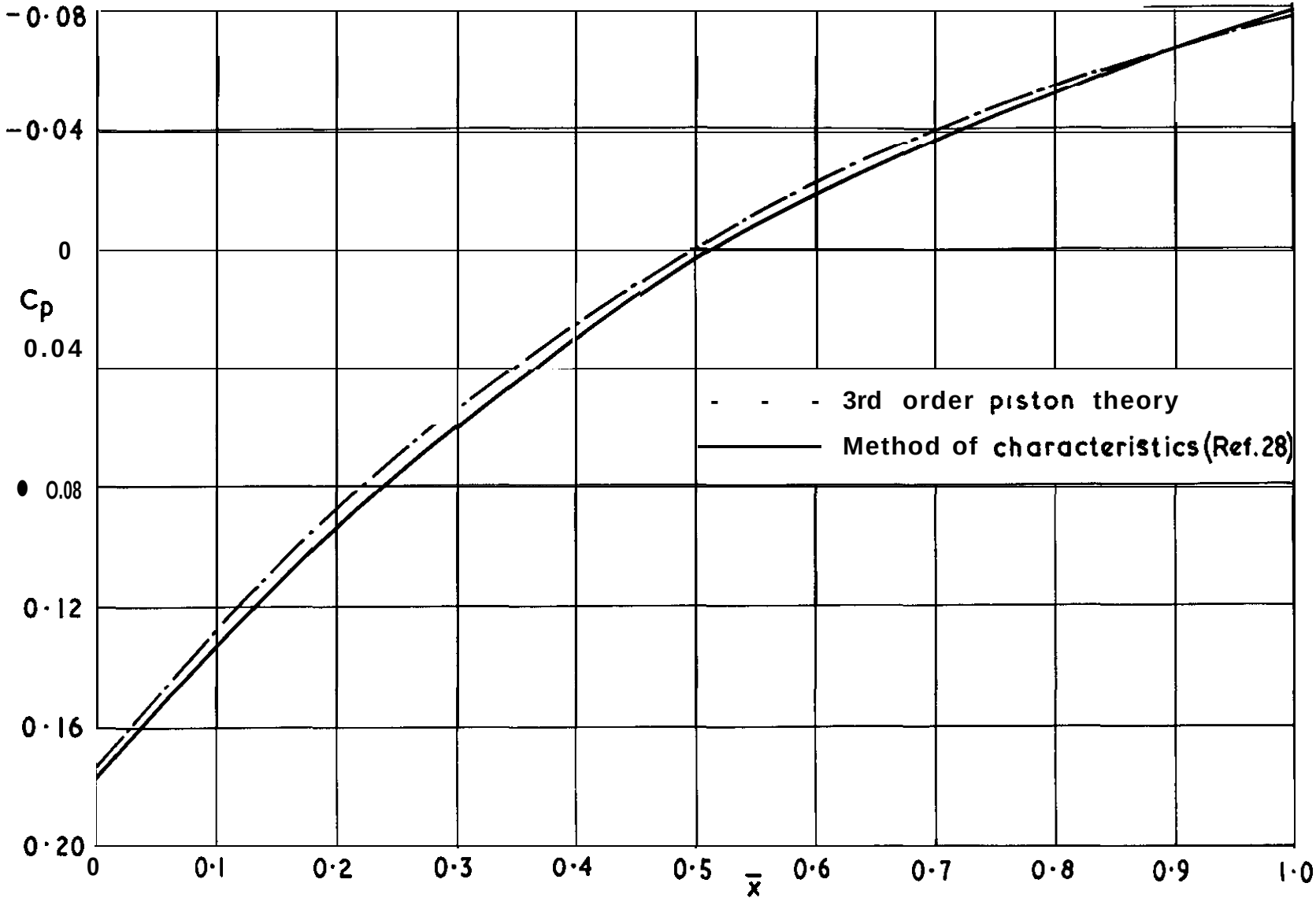

FIG. 10

Pressure distribution on a 10% thick biconvex aerofoil section ($M = 35$, $\alpha_s = 0^\circ$

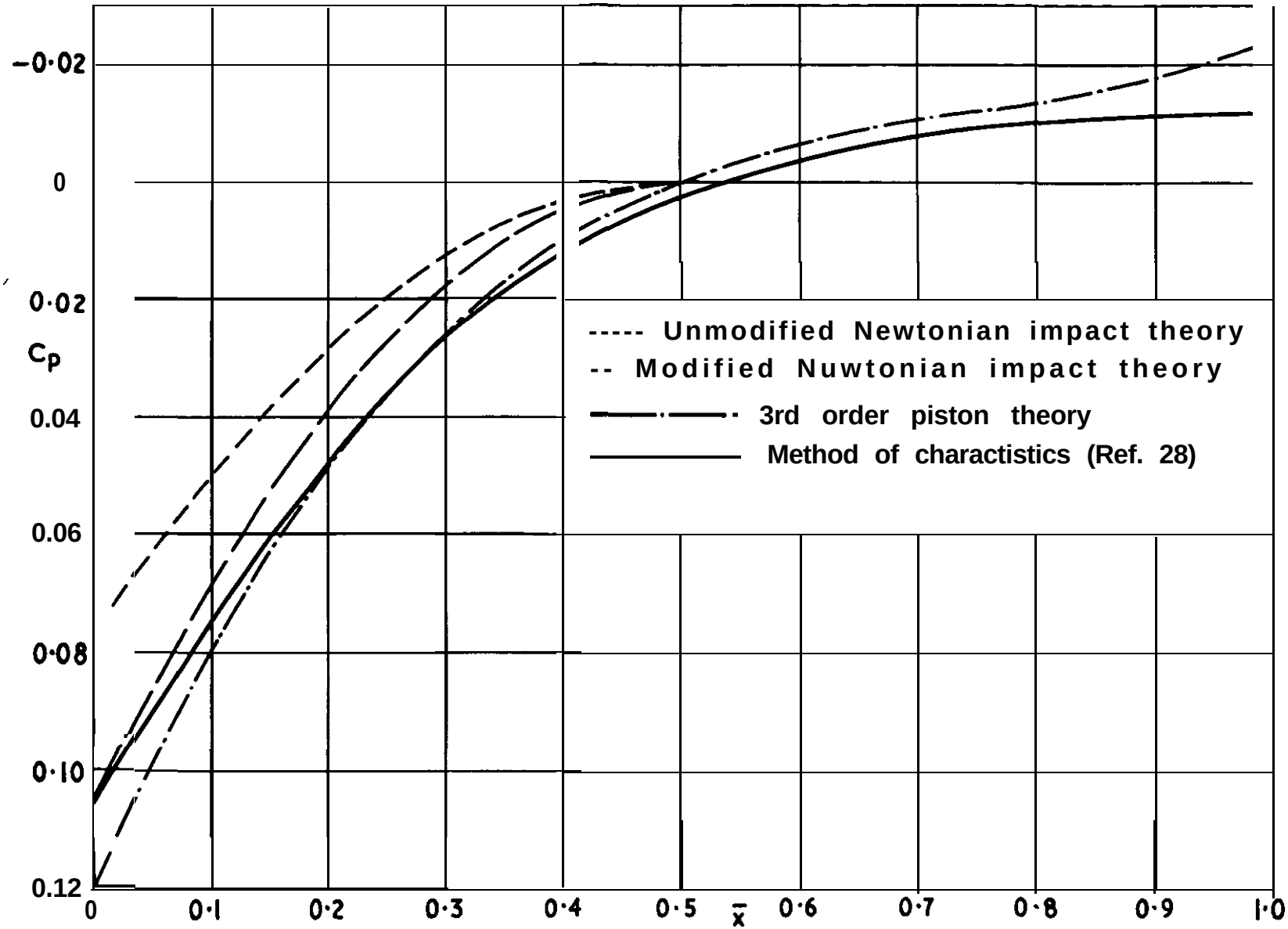

FIG.

Pressure distribution on a 10% thick biconvex aerofoil section ($M = 10$, $\alpha_s = 0^\circ$)

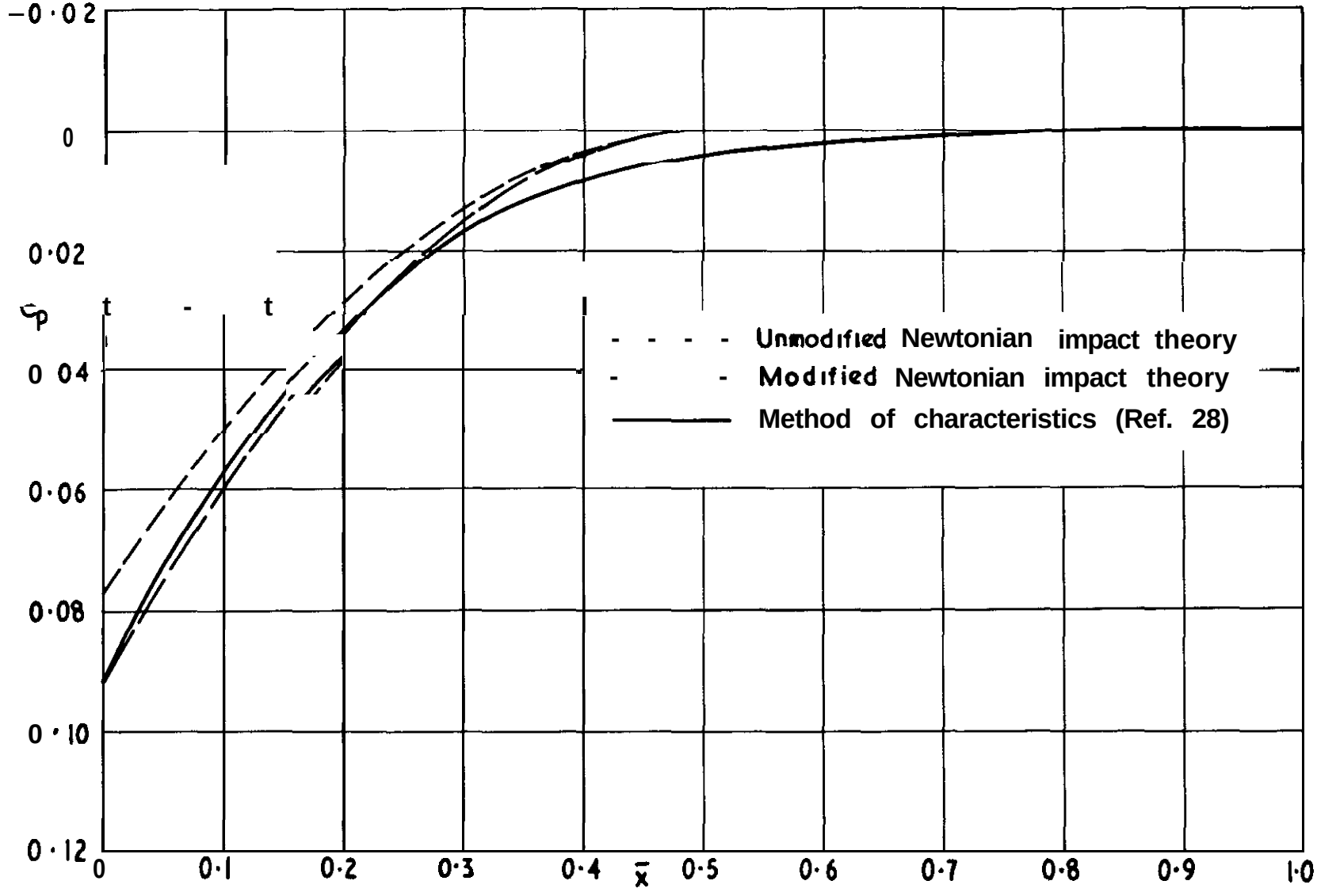

Pressure distribution on a 10% thick biconvex aerofoil section ($M = \infty$, $a = 0^0$)

FIG. 12

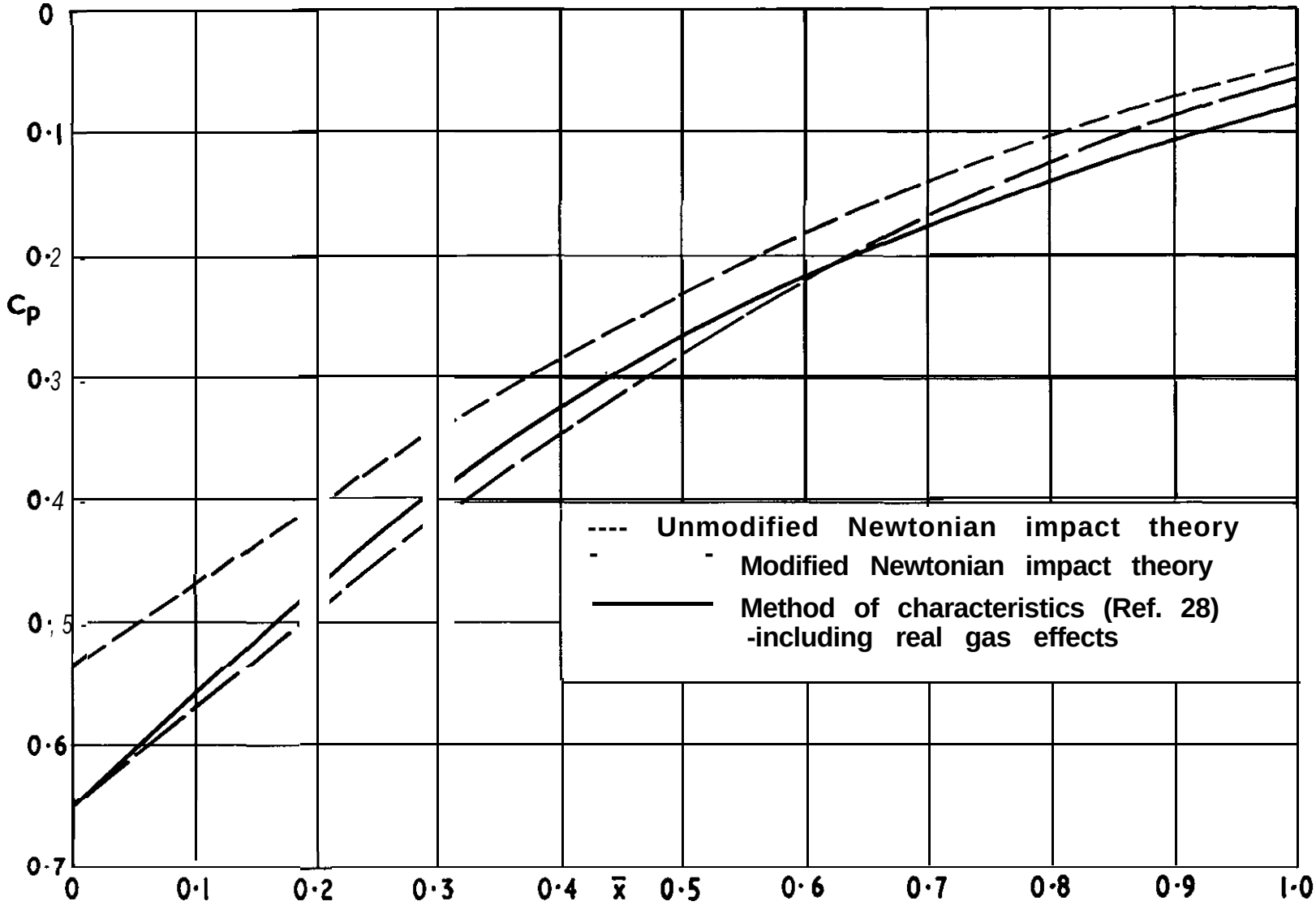

FIG 13

Pressure distribution on lower surface of a 10% thick biconvex aerofoil section

$(M = 10,\ T_\infty = 500^0\,R,\ \alpha = 19{\cdot}9^0)$

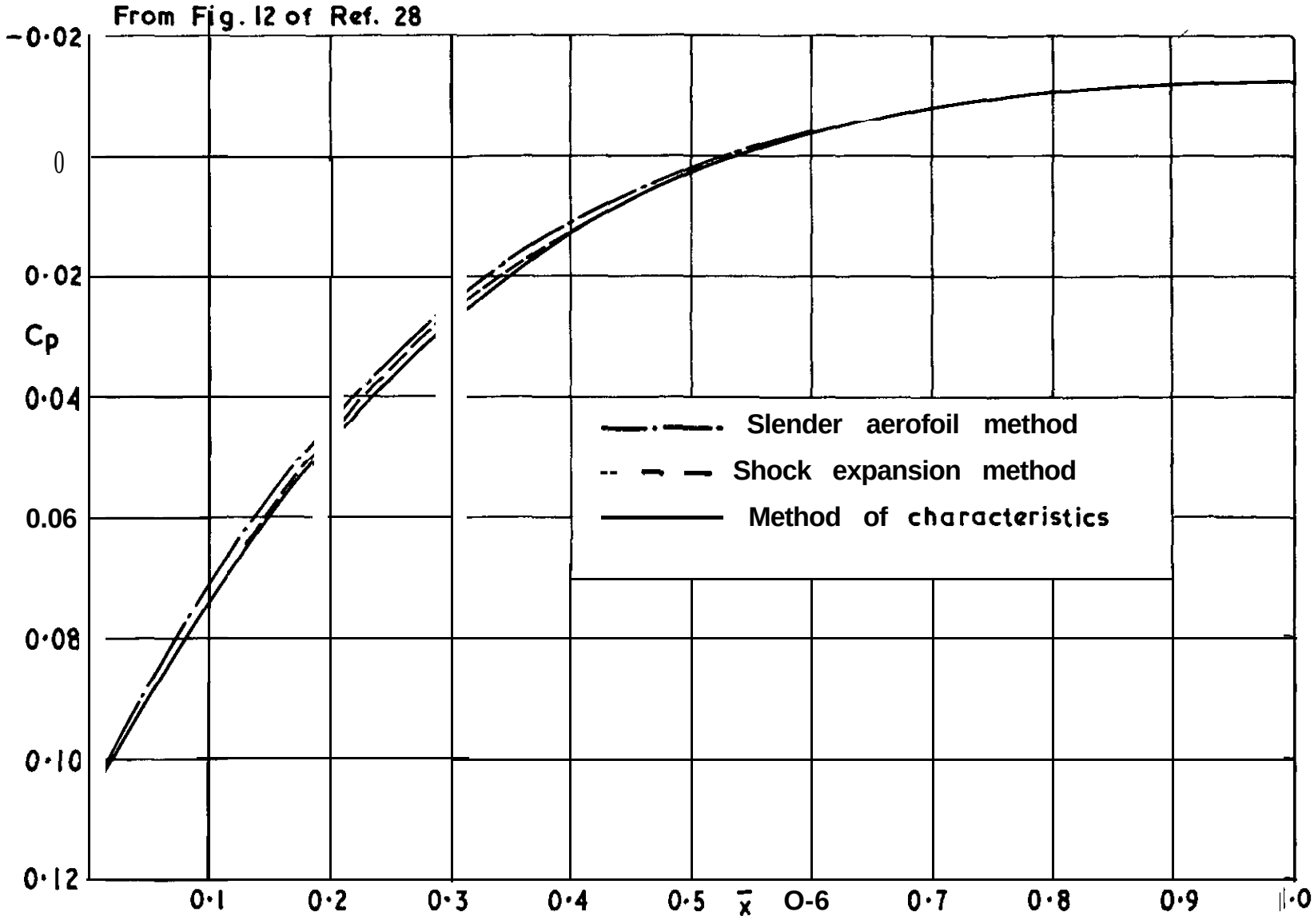

FIG. 14

Pressure distribution on 10% thick biconvex aerofoil section ($M = 10$, $\alpha_s = 0^0$)

FIG. 15 (a)

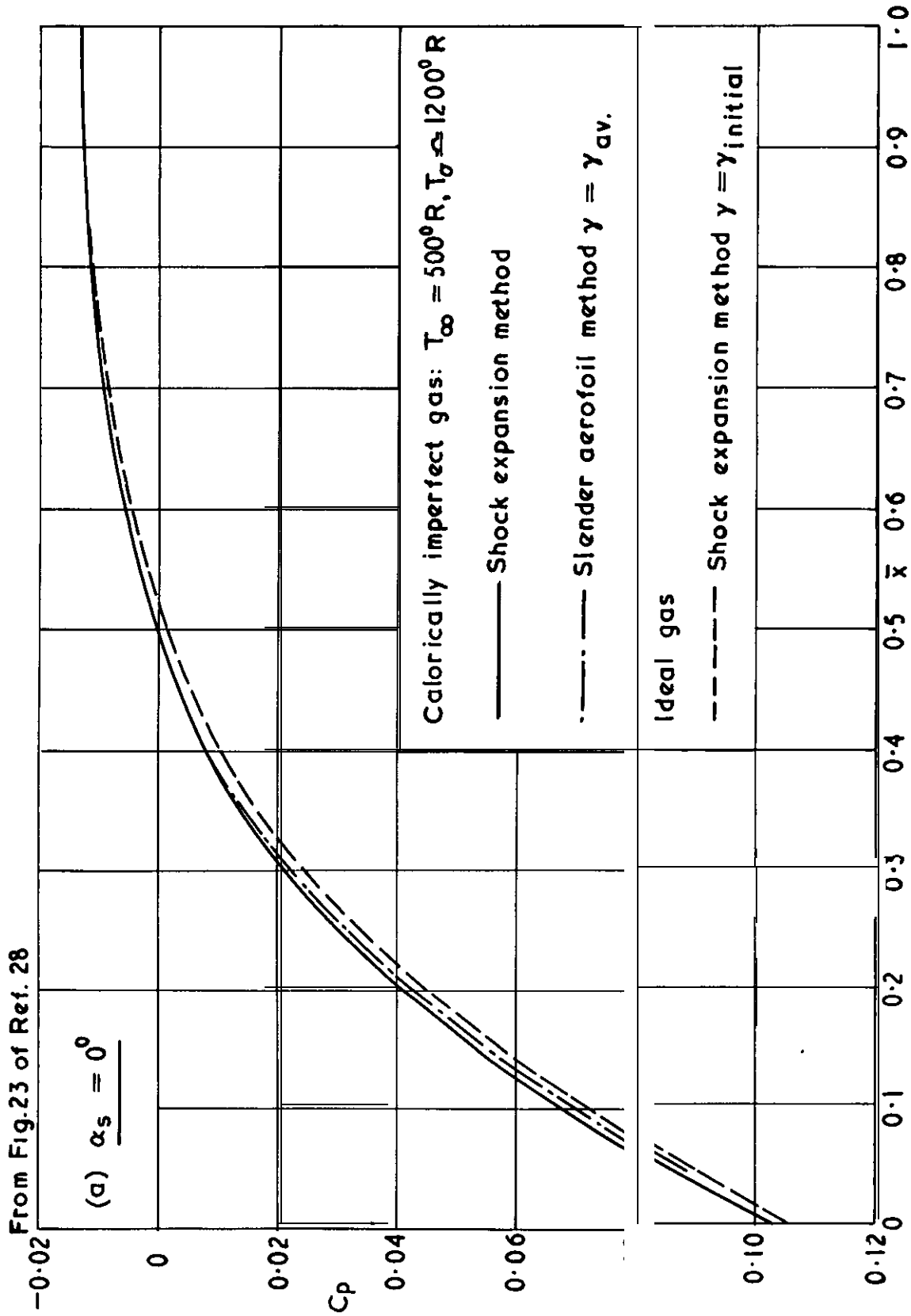

Pressure distribution on lower surface of 10% thick biconvex aerofoil section at various angles of attack — showing real gas effects ($M = 10$. $T_\infty = 500^0R$)

FIG. 15 (b)

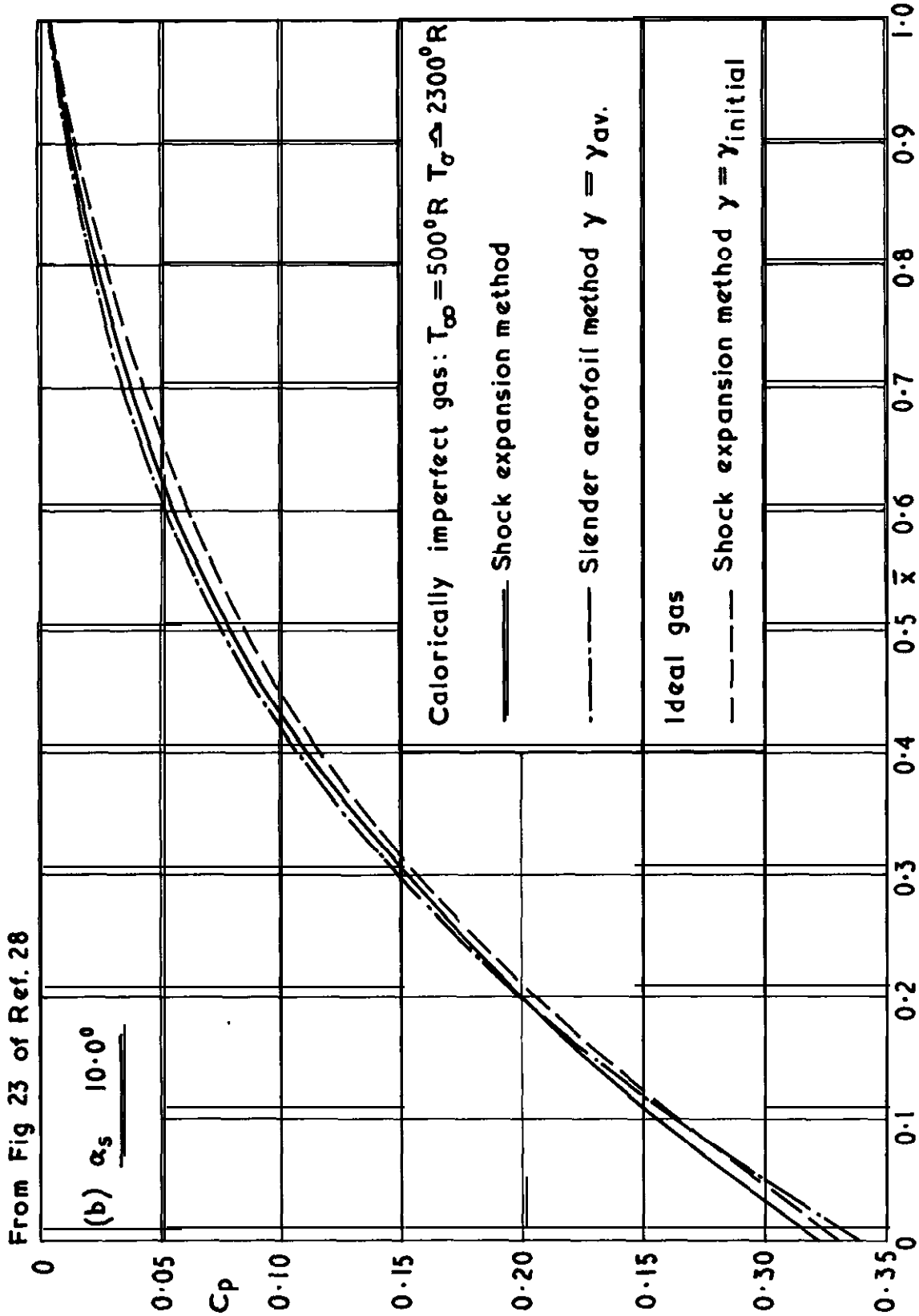

Pressure distribution on lower surface of 10% thick biconvex aerofoil section at various angles of attack showing real gas effects ($M = 10$. $T_\infty = 500°R$)

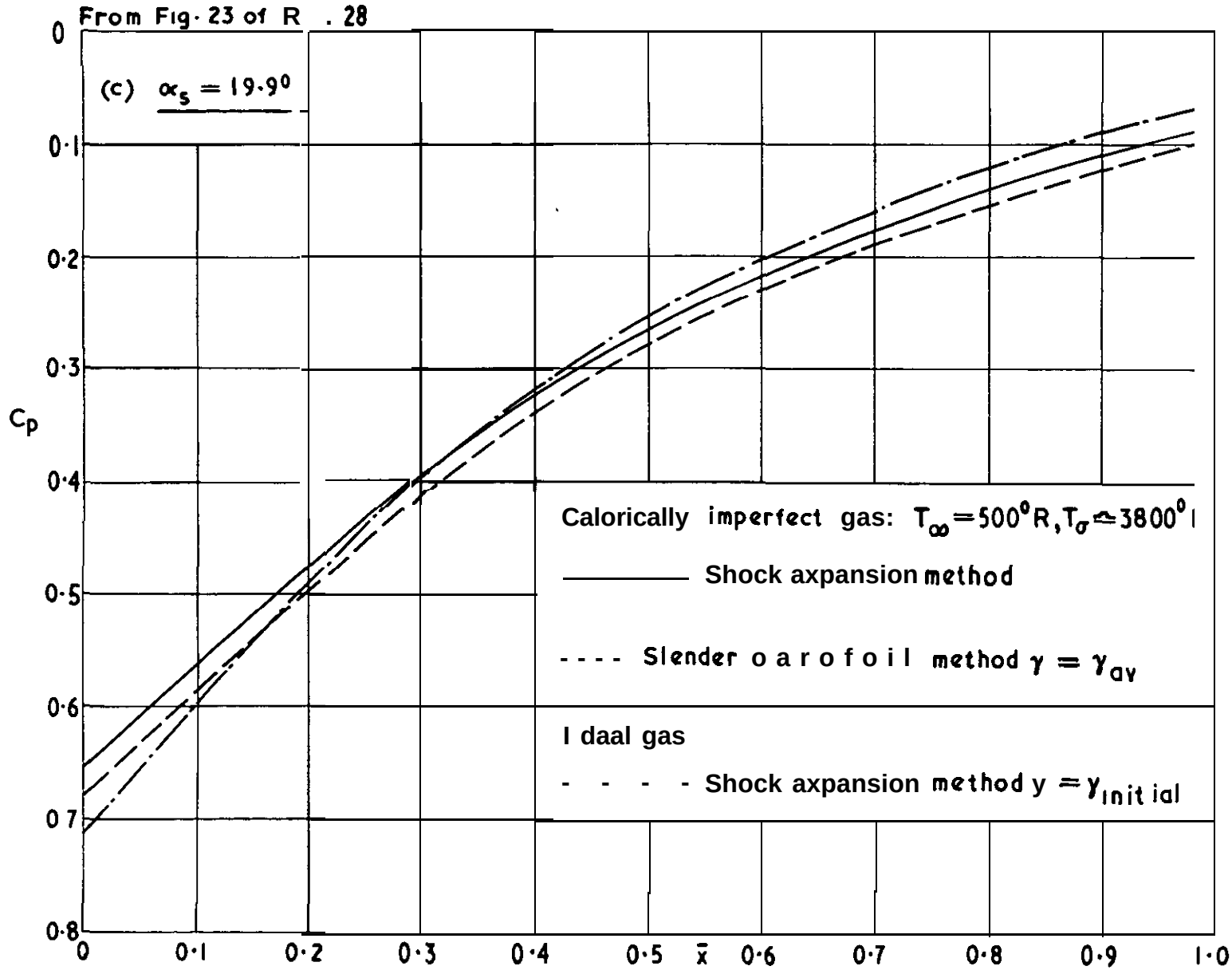

FIG. 15(c)

Prossora distribution on lower surface of 10% thick biconvax aarofoil section at various anglas of attack-showing raal gas effects (M = IO. $T_\infty = 500^0 R$)

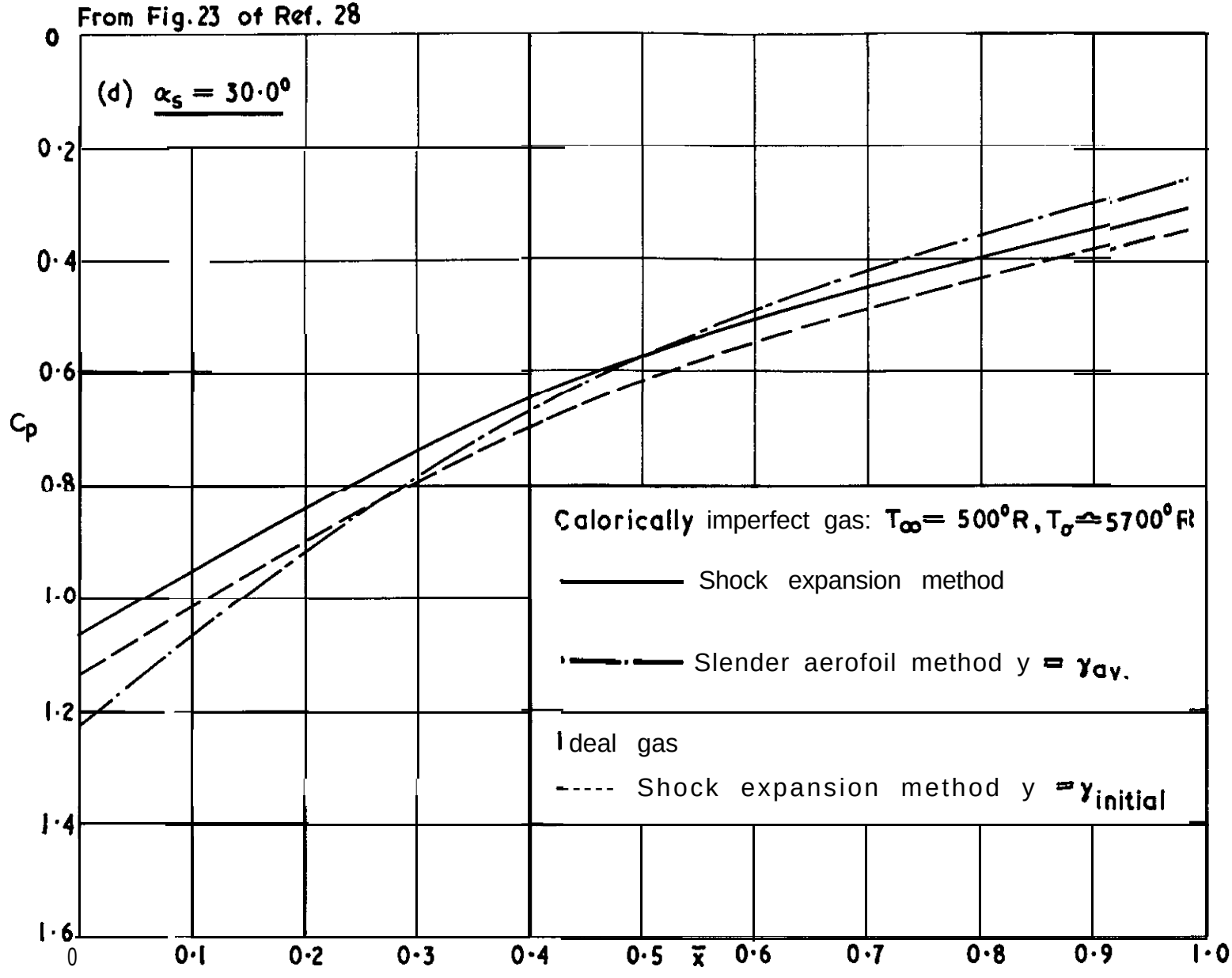

FIG. 15(d)

Pressure distribution on lower surface of 10% thick biconvex aerofoil section at various angles of attack — showing real gas effects ($M = 10$, $T_\infty = 500^0$ R

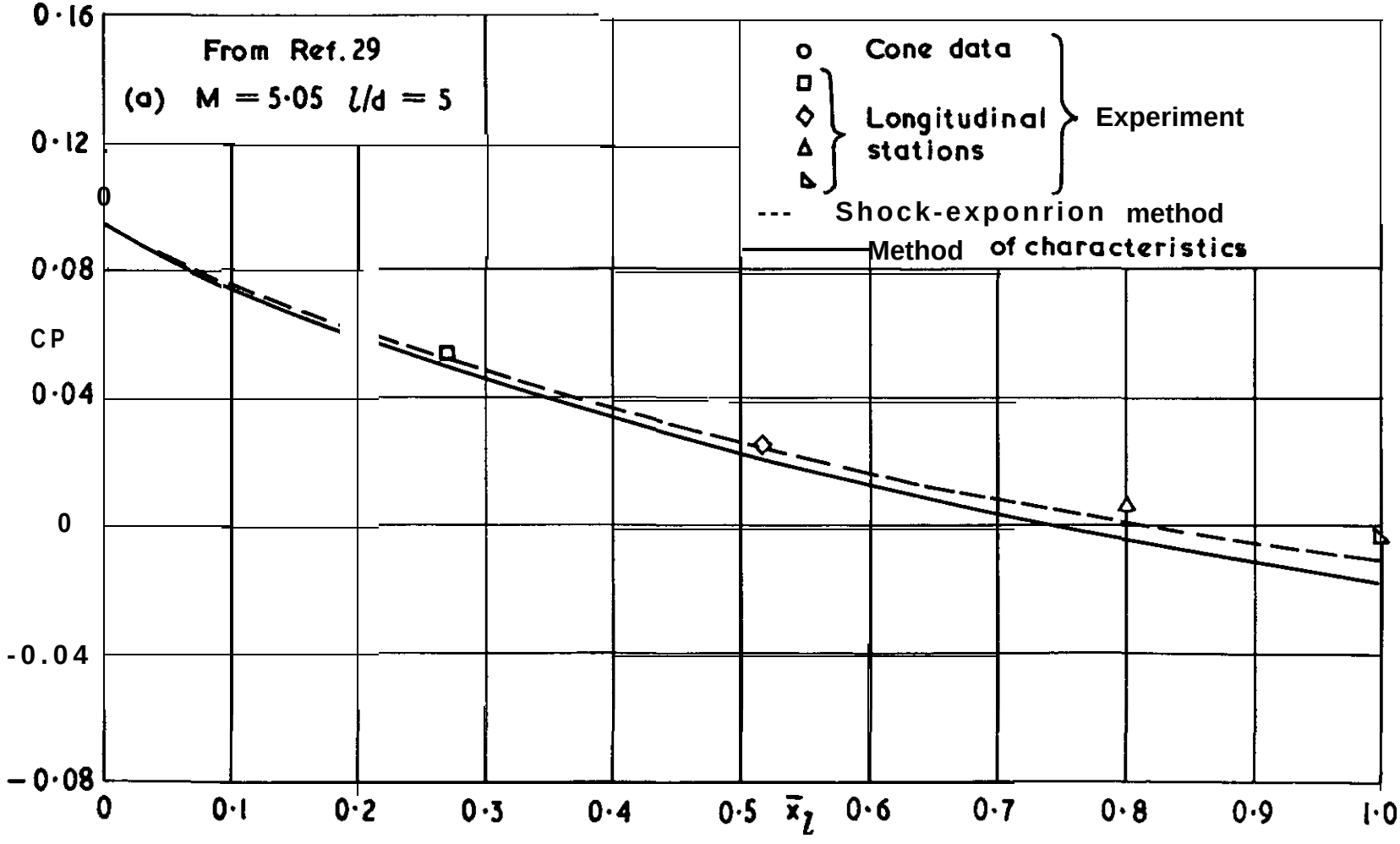

FIG. 16 (a

Pressure distribution on circular arc ogives at as $= 0^0$

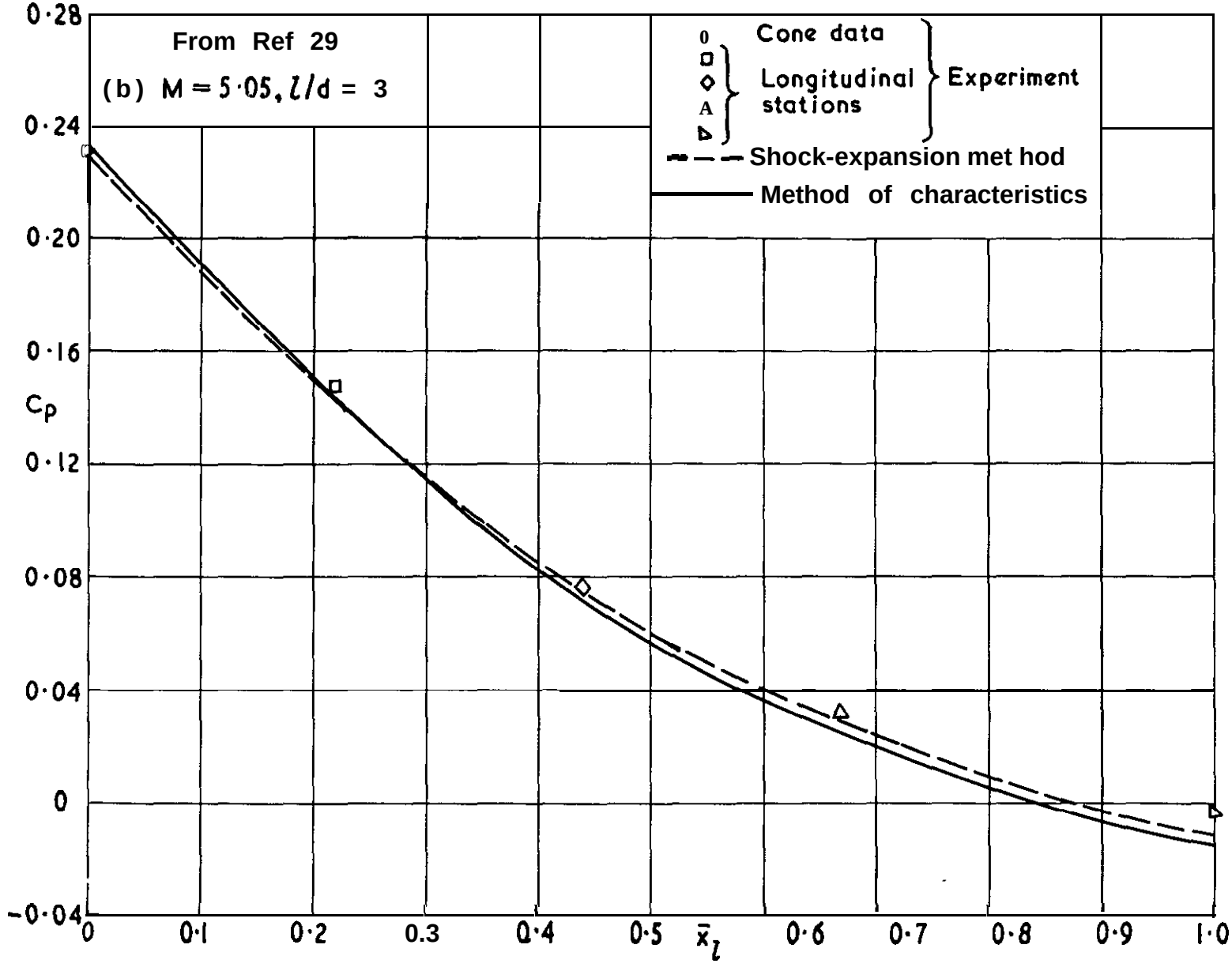

FIG. 16 (b)

Pressure distribution on circular arc ogives at $\alpha_s = 0^0$

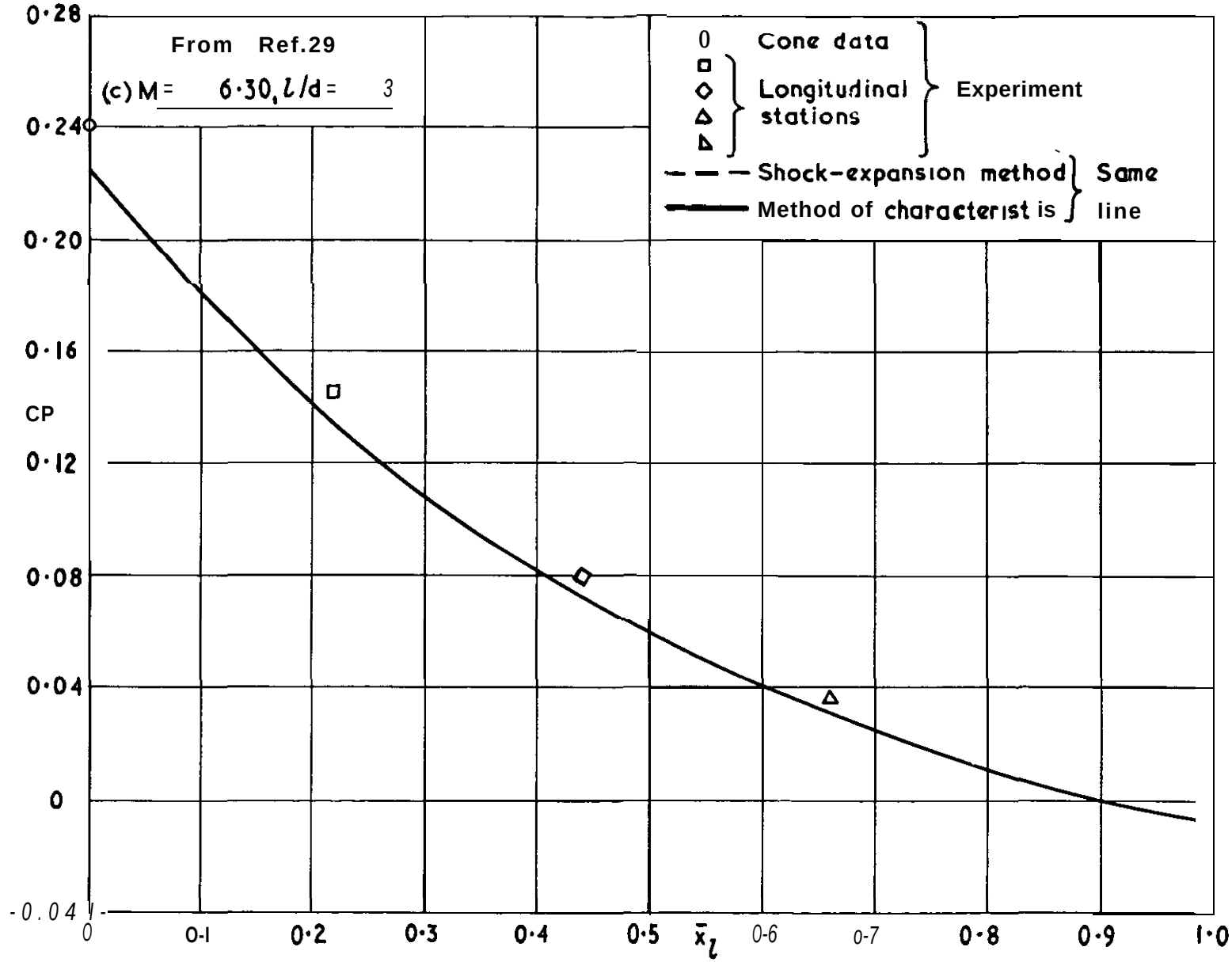

FIG. 16 (c)

Pressure distribution on circular arc ogives at $x_s = 0^0$

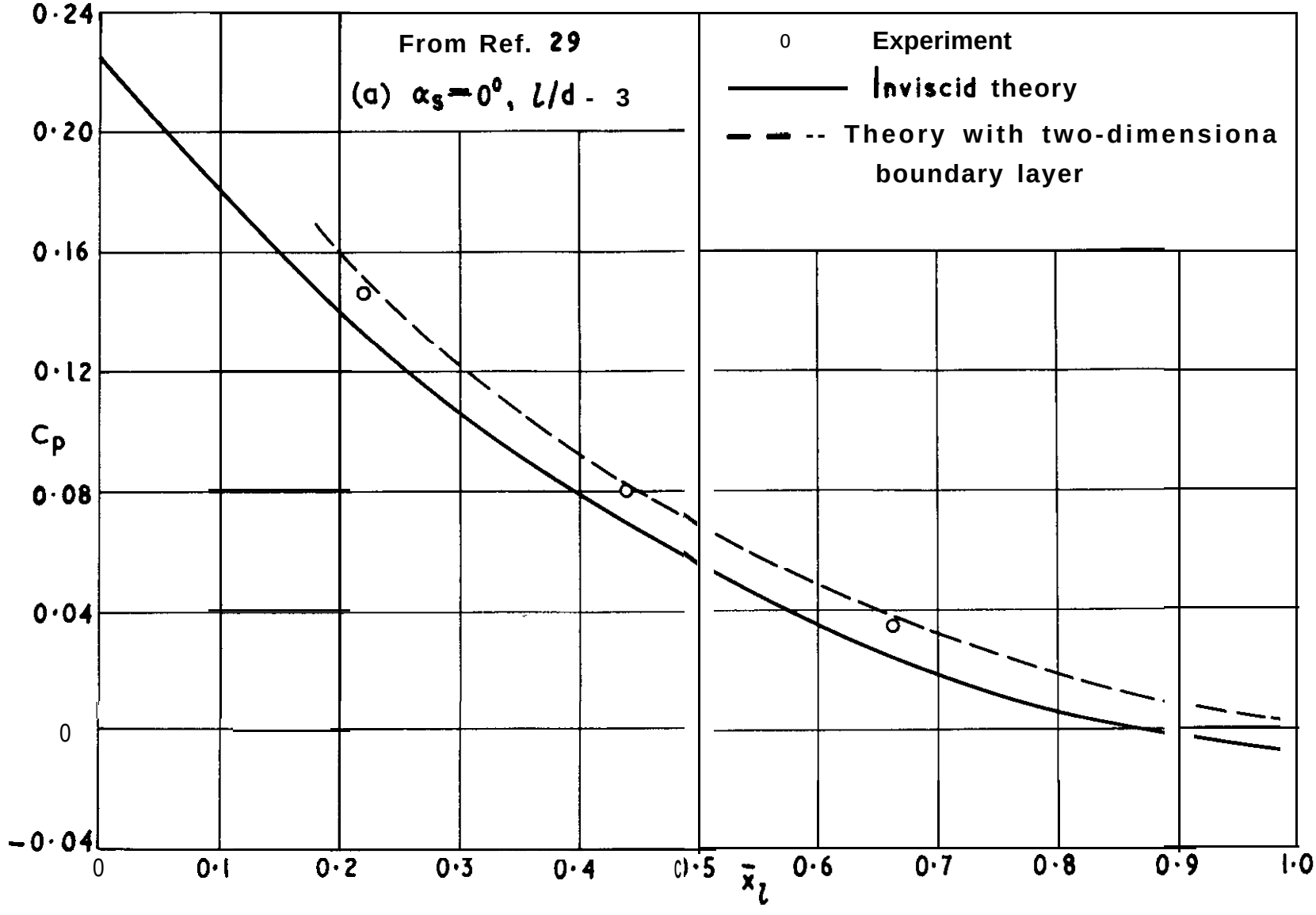

FIG. 17(a)

Effect of boundary layer on pressures on circular arc ogives at M = 6·30

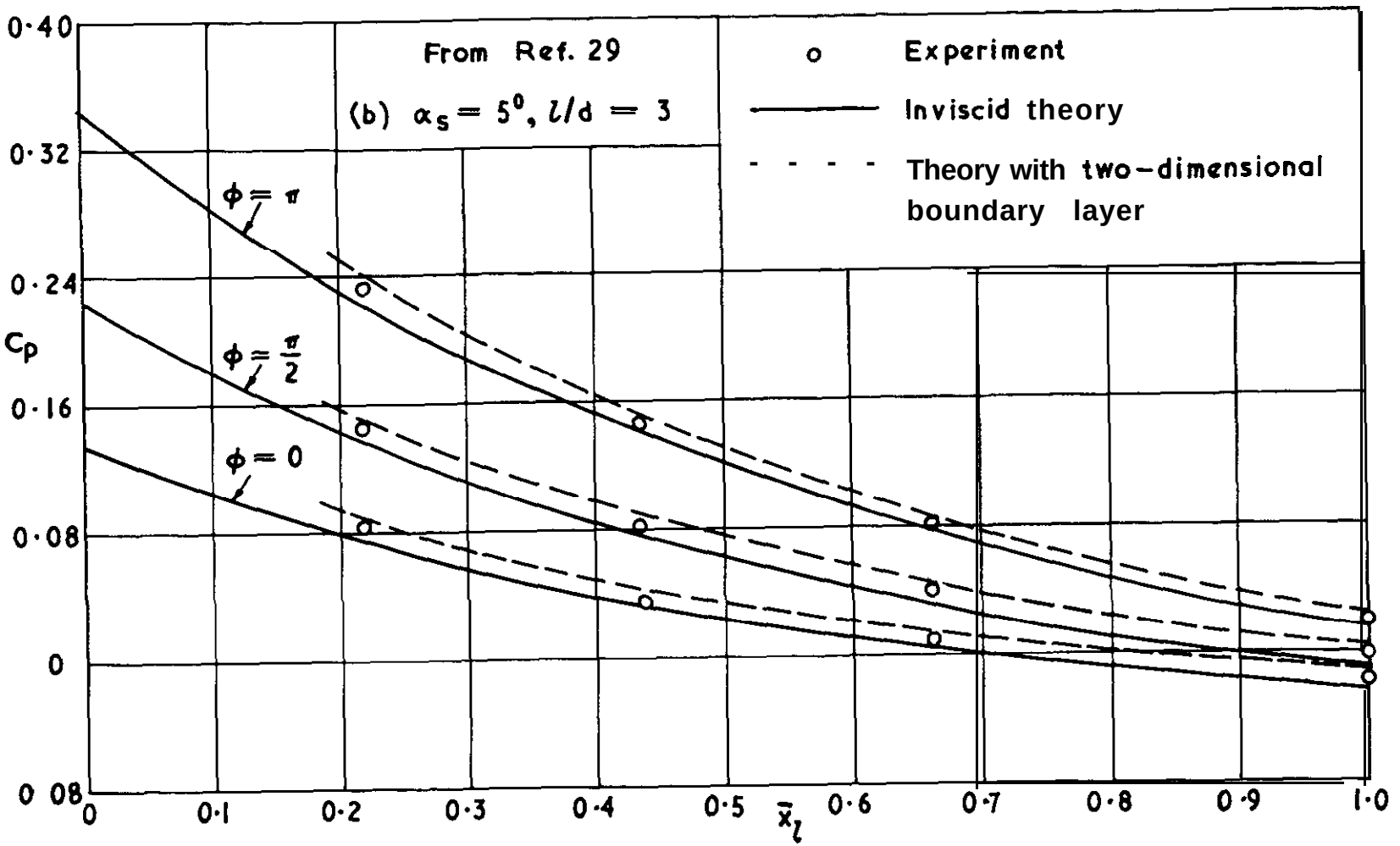

FIG. 17 (b)

Effect of boundary layer on pressures on circular arc oqives at M = 6·30

From Fig. 3·1 of Ref. 26

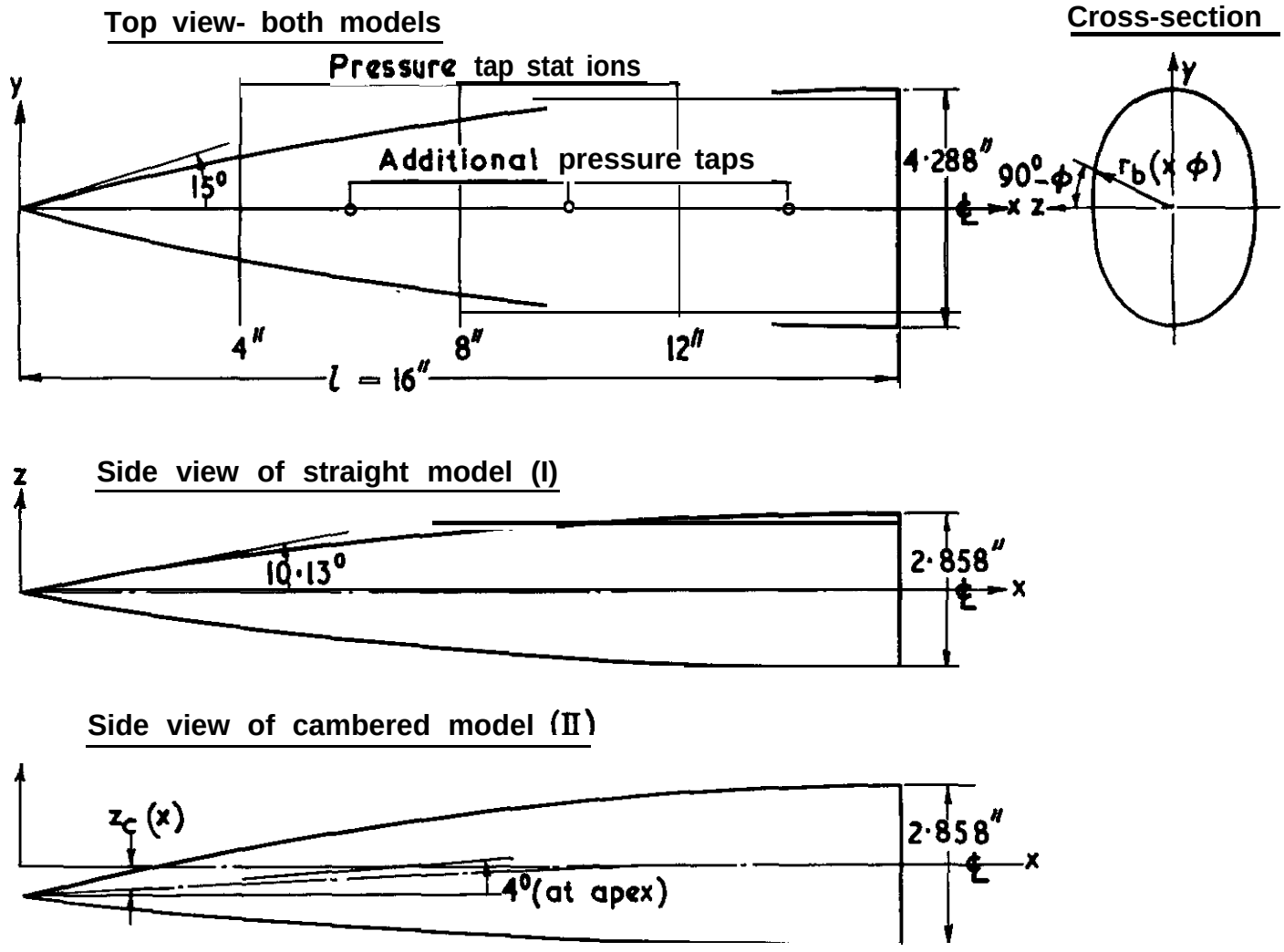

FIG. 18

Geometry of the models for Fias. 19 ~ 23

FIG. 19

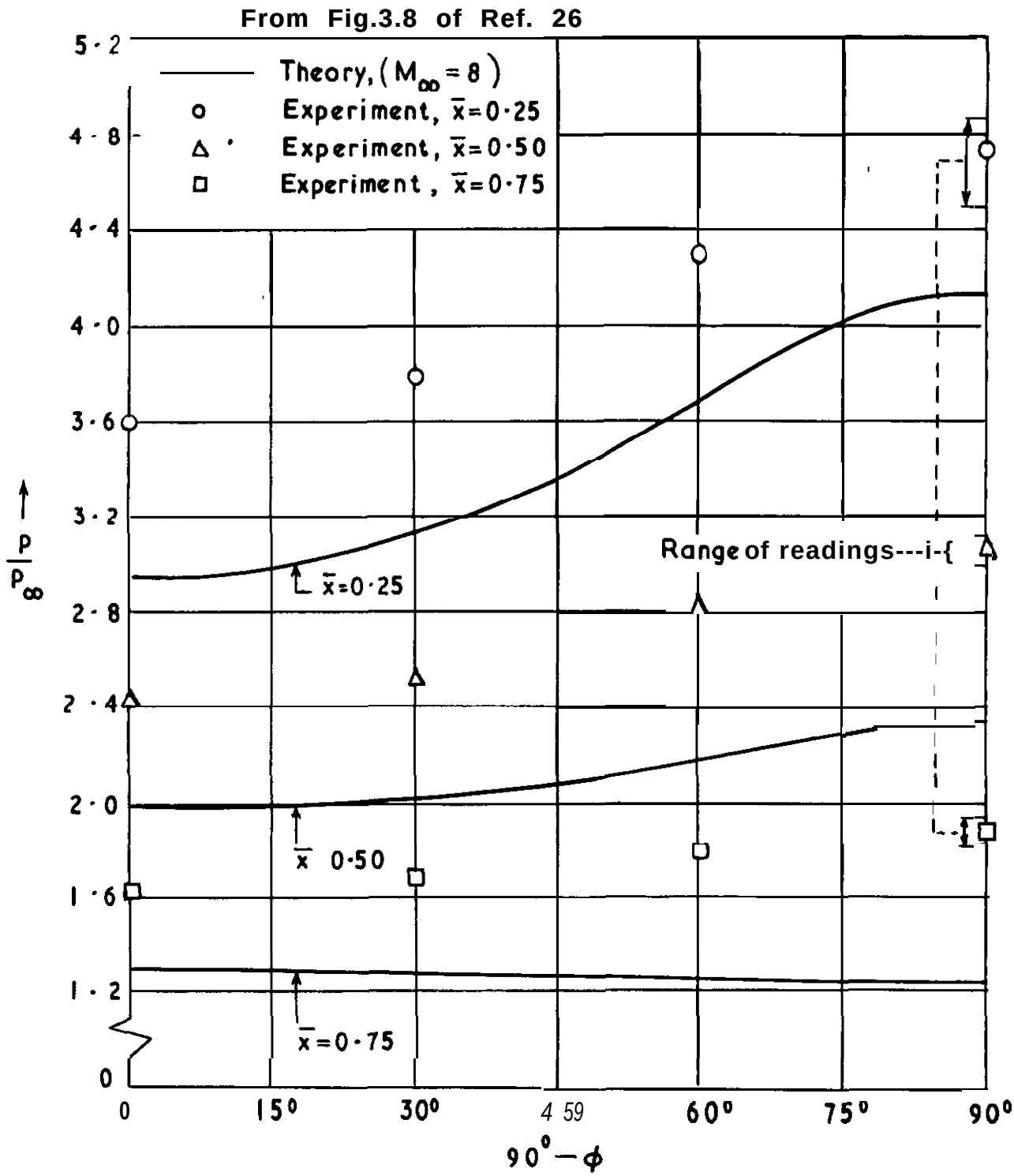

Pressure distributions. Model I, $\alpha=0, M=7\cdot949$, $Re\cong3\cdot0\times10^6$

FIG. 20

From Fig. 3.13 of Ref. 26

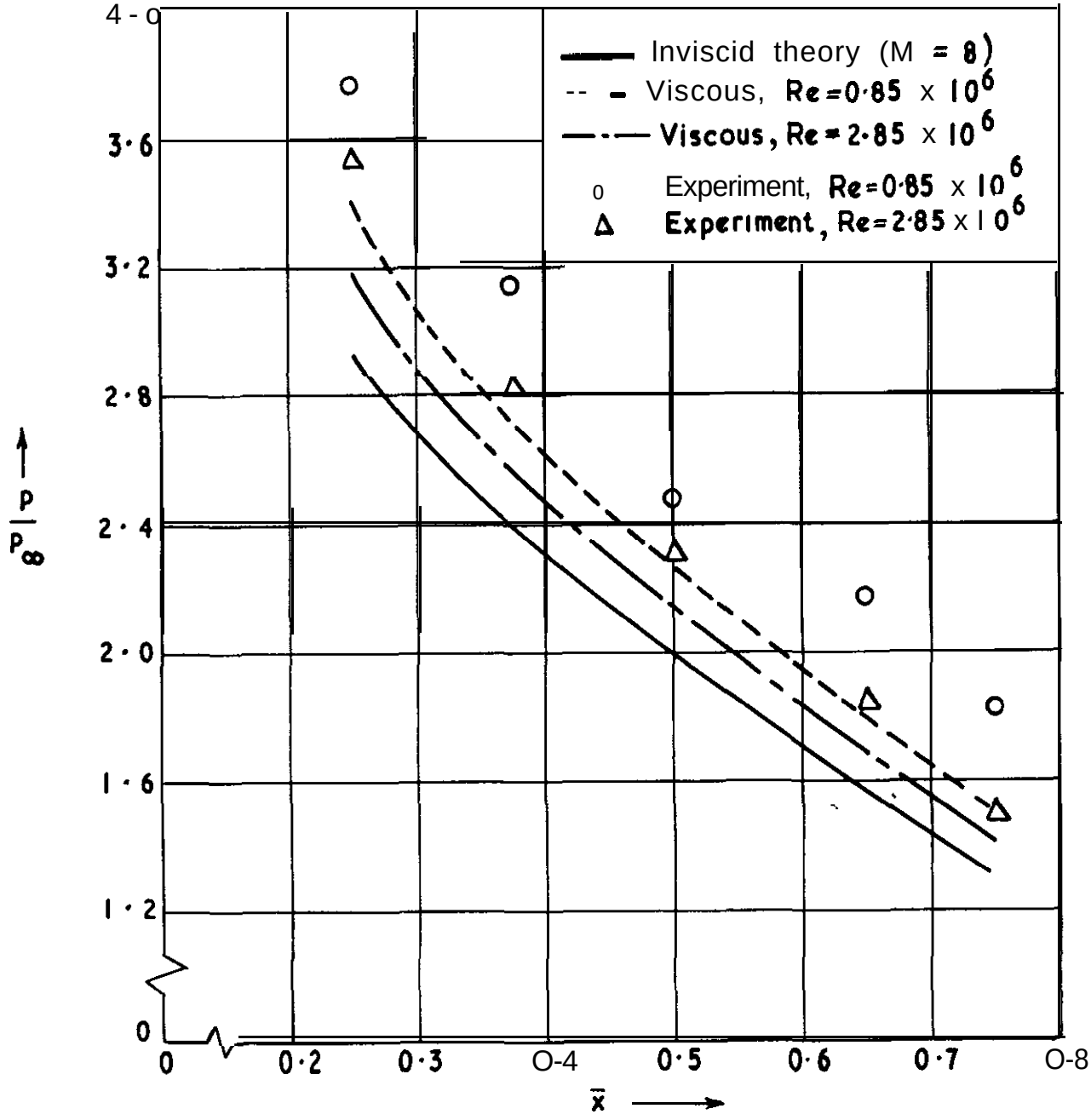

Effect of boundary layer on the pressure distributions along meridian $\phi = 0$. Model I, $\alpha = 0$, M=8

FIG. 21

From Fig. 3.18 of Ref.26

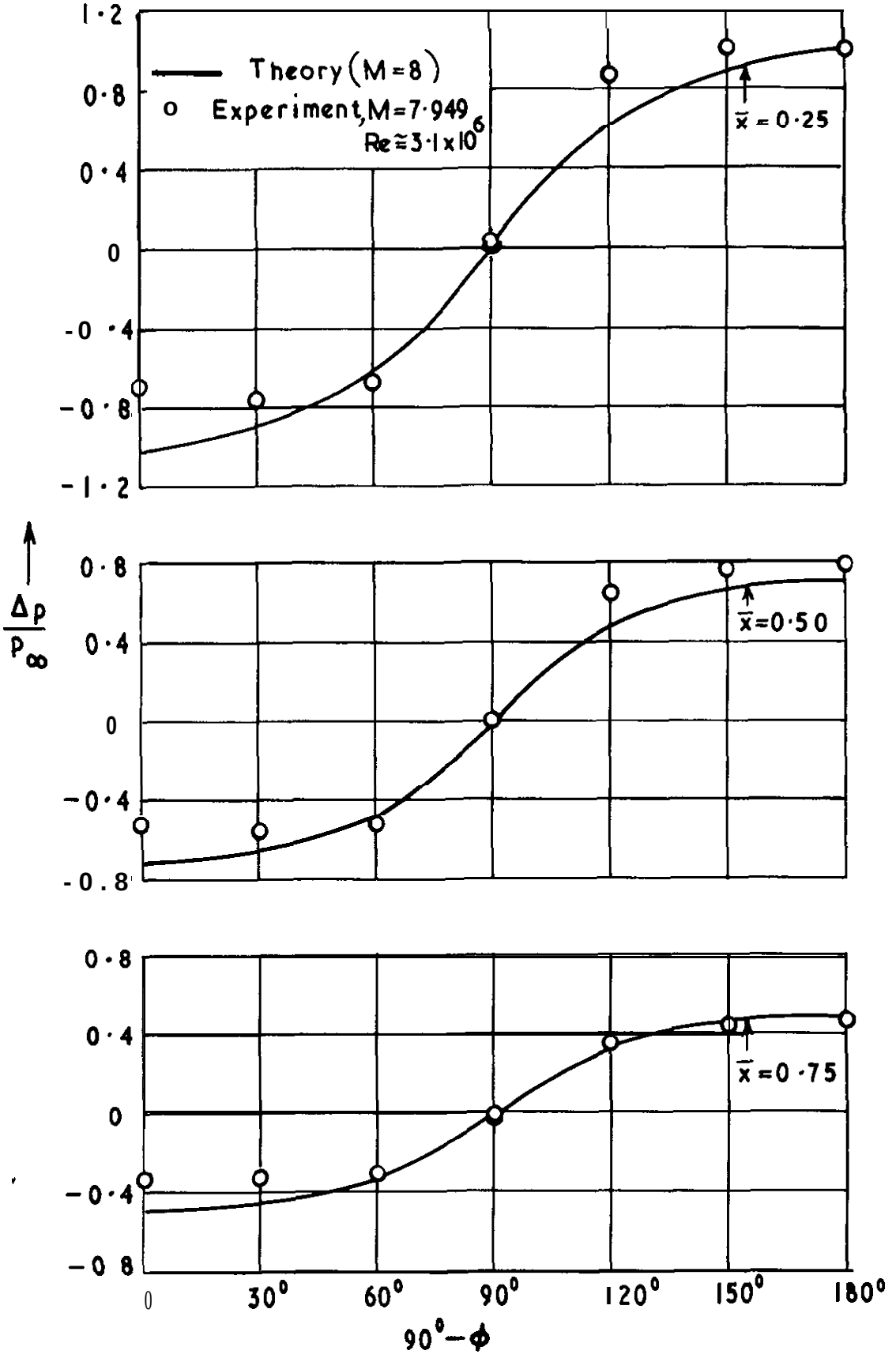

Incremental pressure distributions due to angle of attack. Model I, $\alpha = 2^0$, $M = 7 \cdot 949$, $Re \cong 3 \cdot 1 \times 10^6$

FIG 22

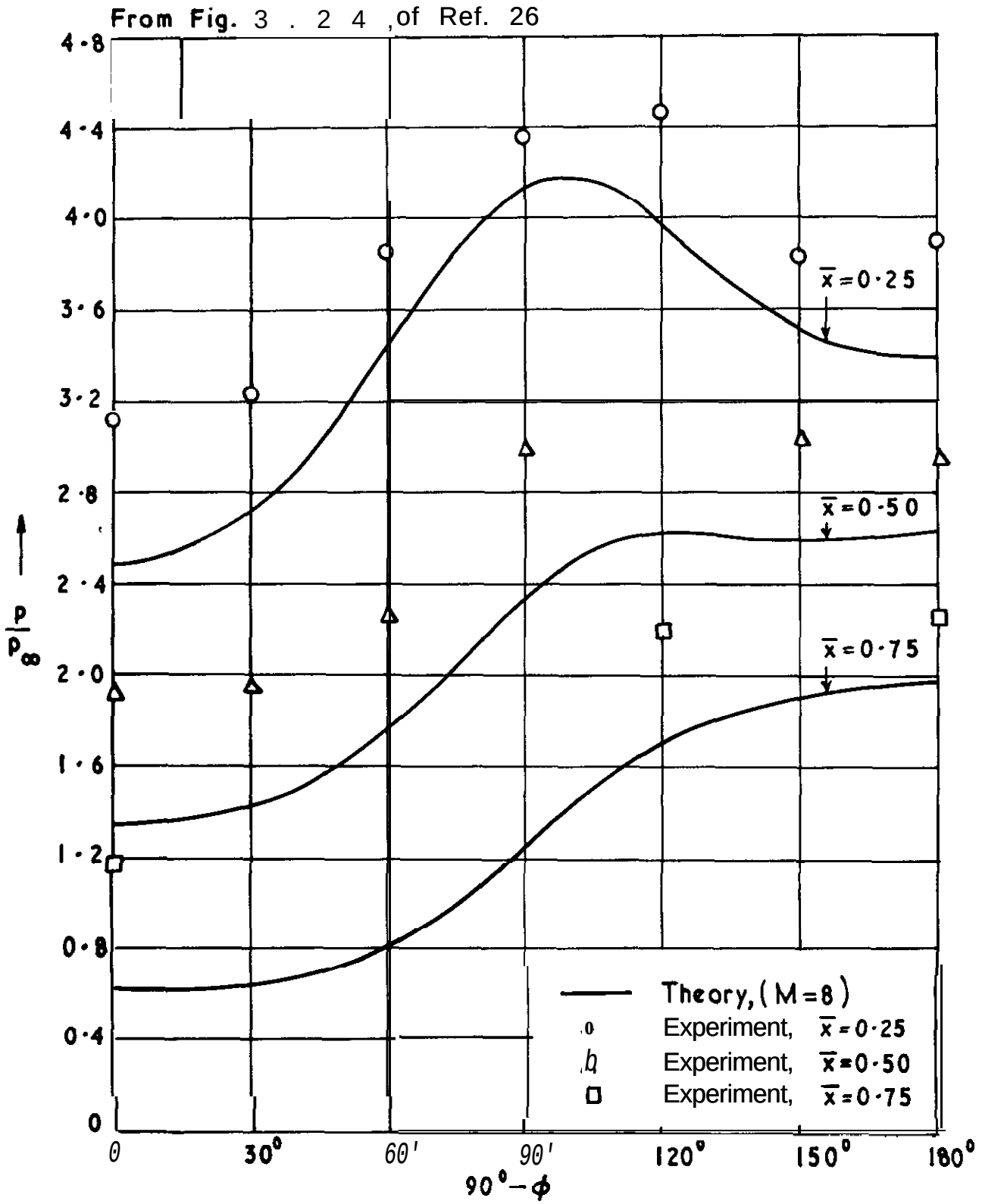

Pressure distributions. Model II, a ≈ 4°, M=7·949, Re ≅ 3 x 10^6

FIG. 23

From Fig. 3.26 of Ref. 26

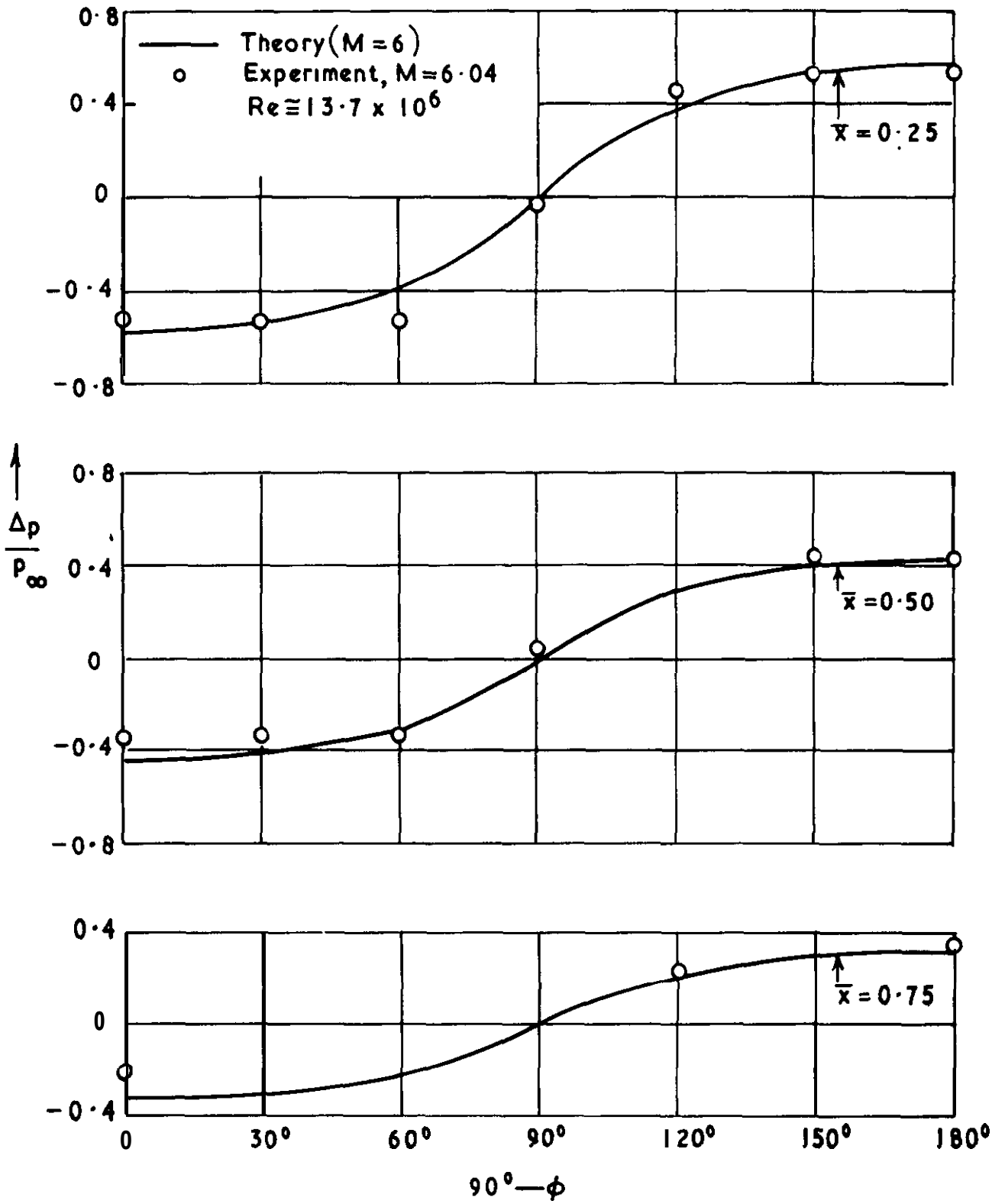

Incremental pressure distributions. Model II, a = 2°, M = 6·04, Re ≅ 13·7 x 10^6

From Fig. 3.2 of Ref. I9

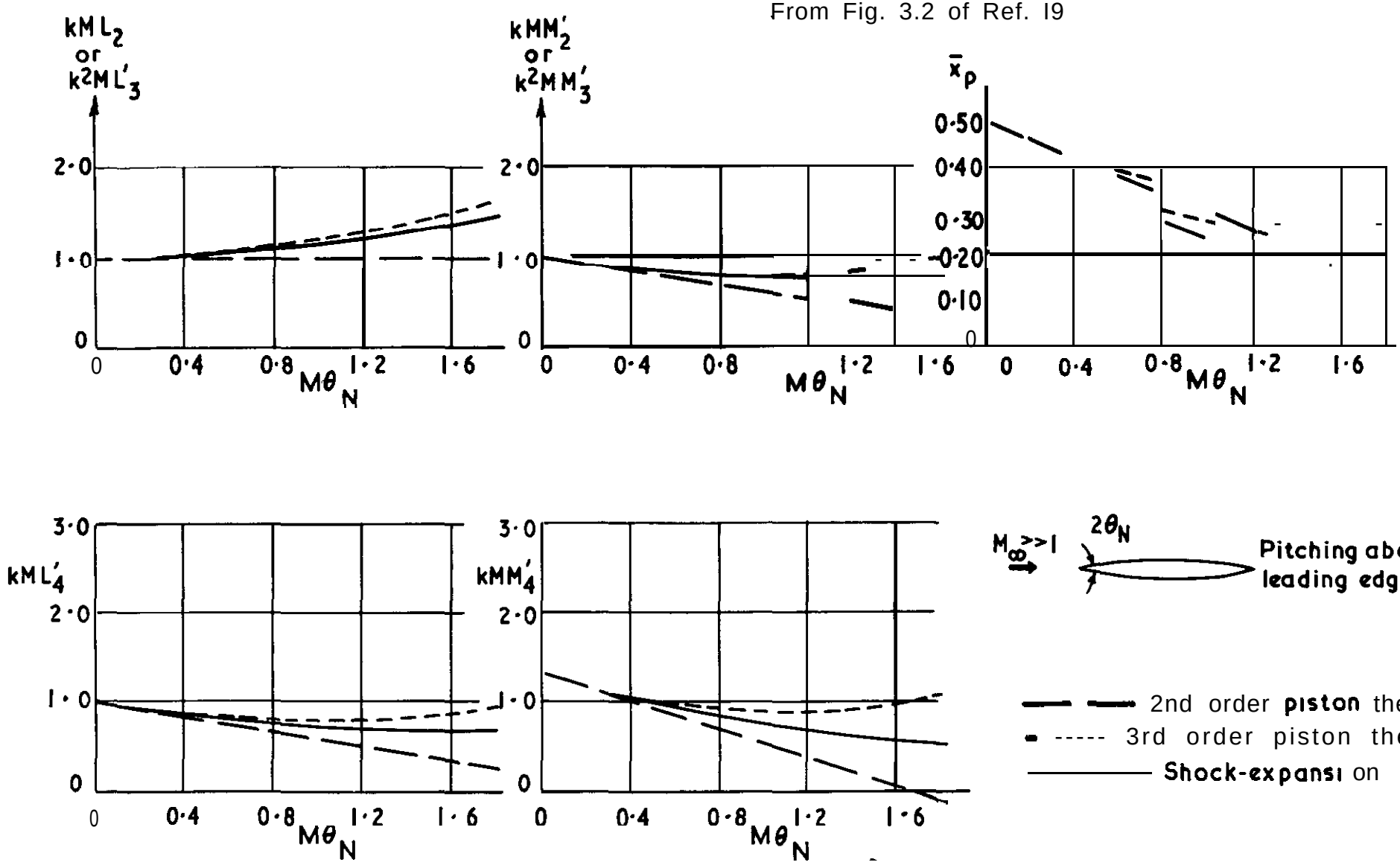

FIG. 24

Low frequency flutter derivatives for a biconvex airfoil — comparison of piston theory with shock-expanston method

From Fig. 3.3 of Ret. 19

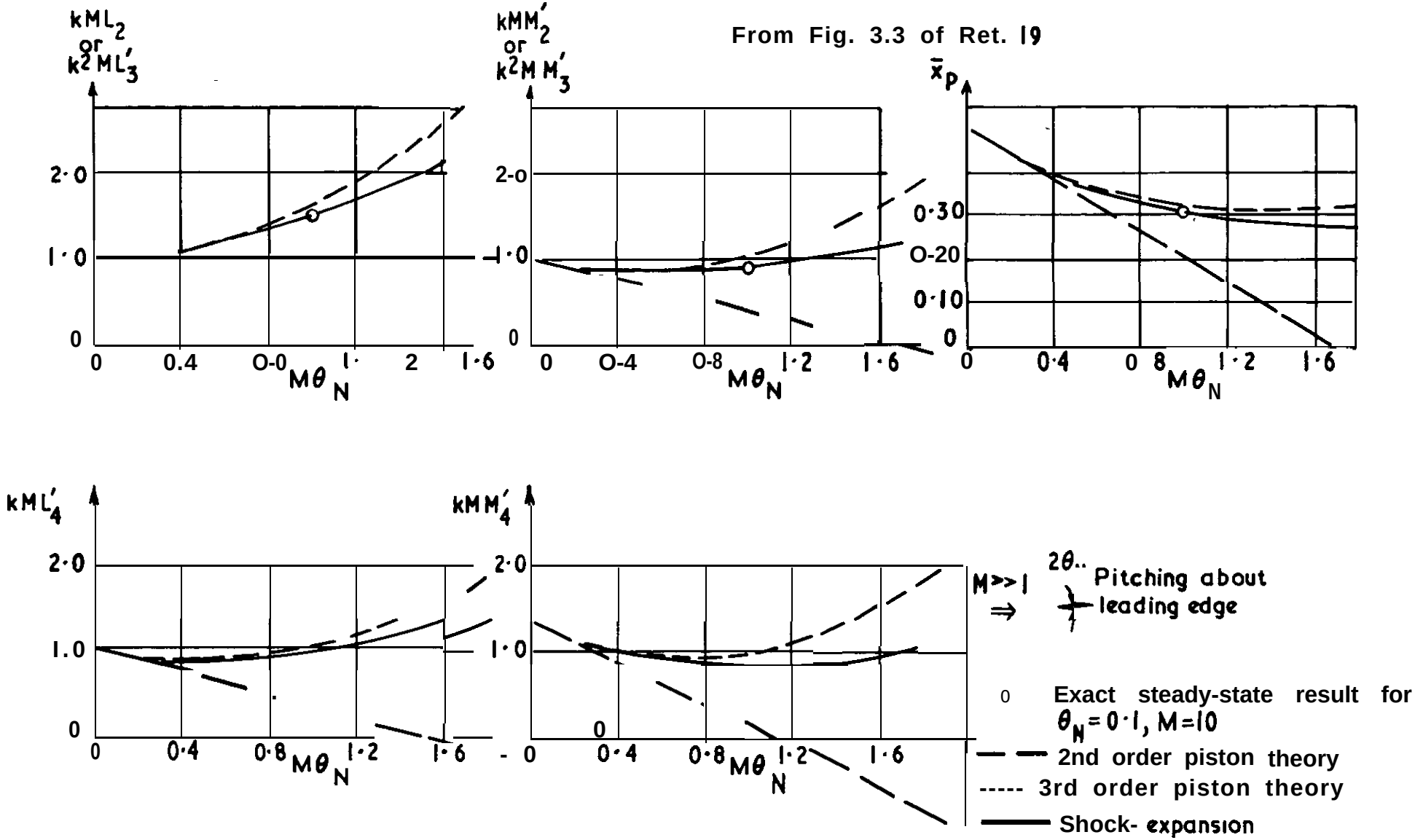

FIG. 25

Low frequency flutter derivatives for a double wedge airfoil -comparison of piston theory with shock-expansion method

FIG.26

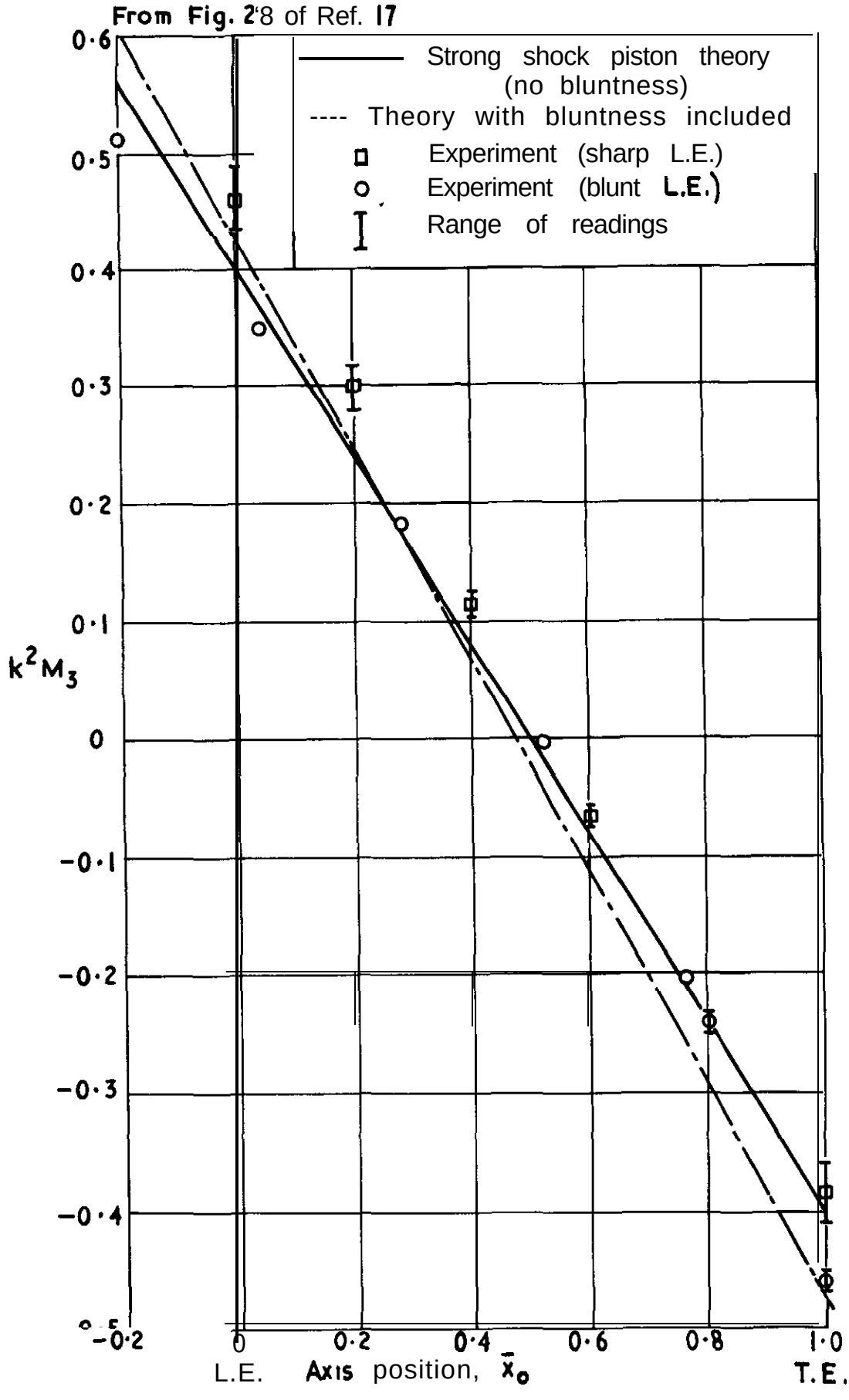

Aerodynamic stiffness for blunt and sharp leading edges

FIG. 27

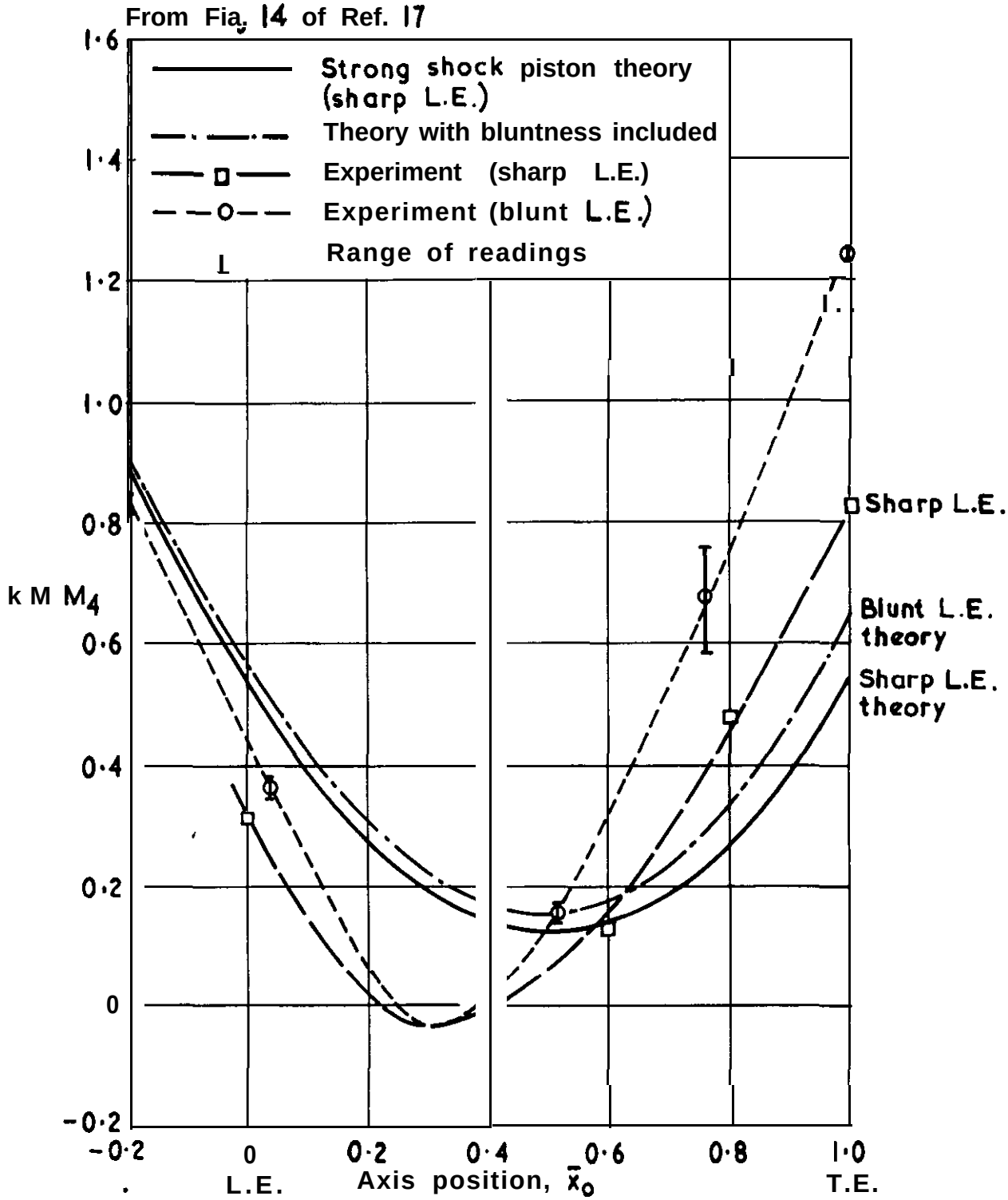

Aerodynamic damping for blunt and sharp leading edges

FIG. 20

From Fig. I2 of Ref. 37

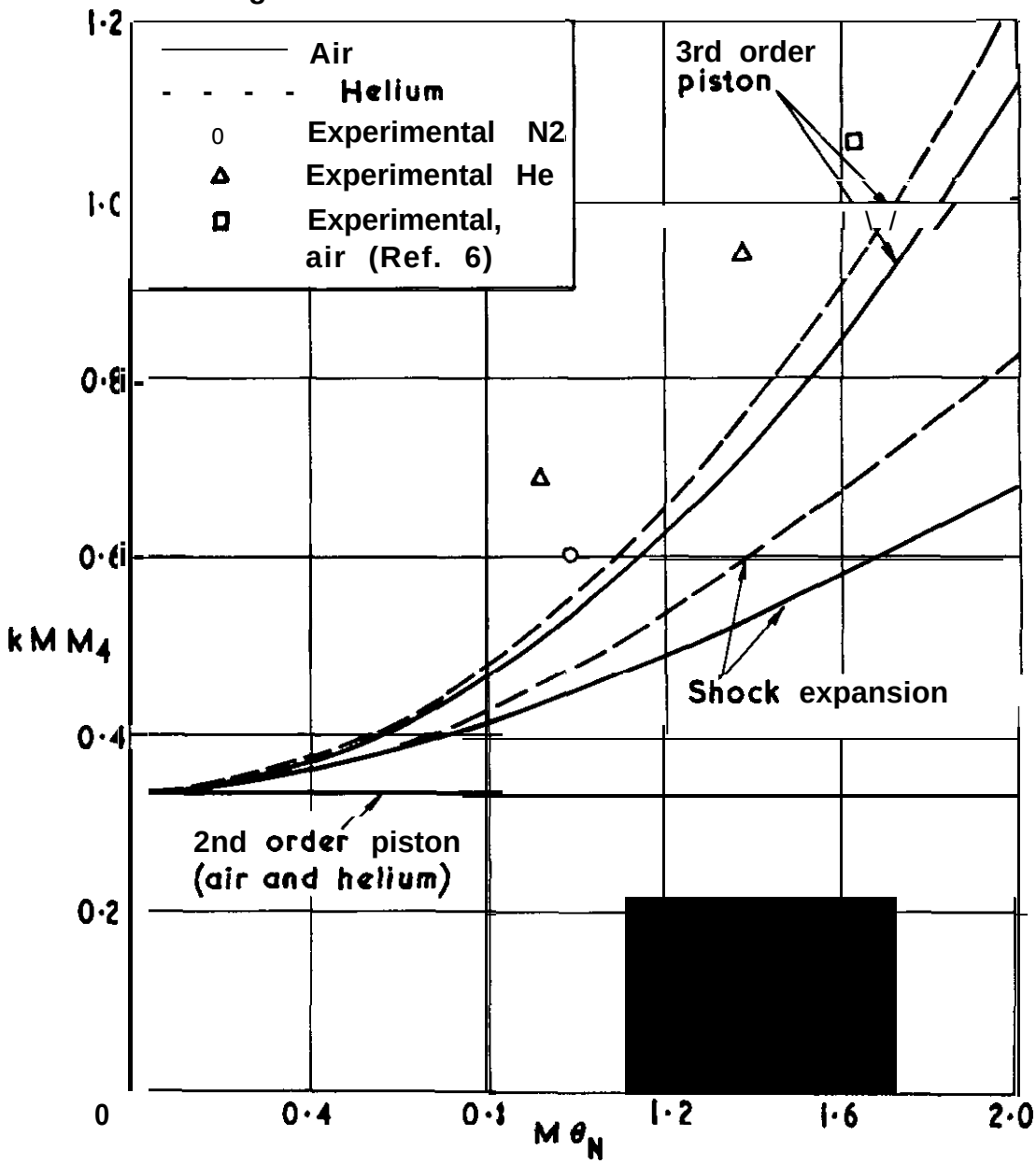

Comparison of experimental results with theory

Symmetrical double wedge aerofoil oscillating about mid-chord

From Ref. 38

FIG. 29

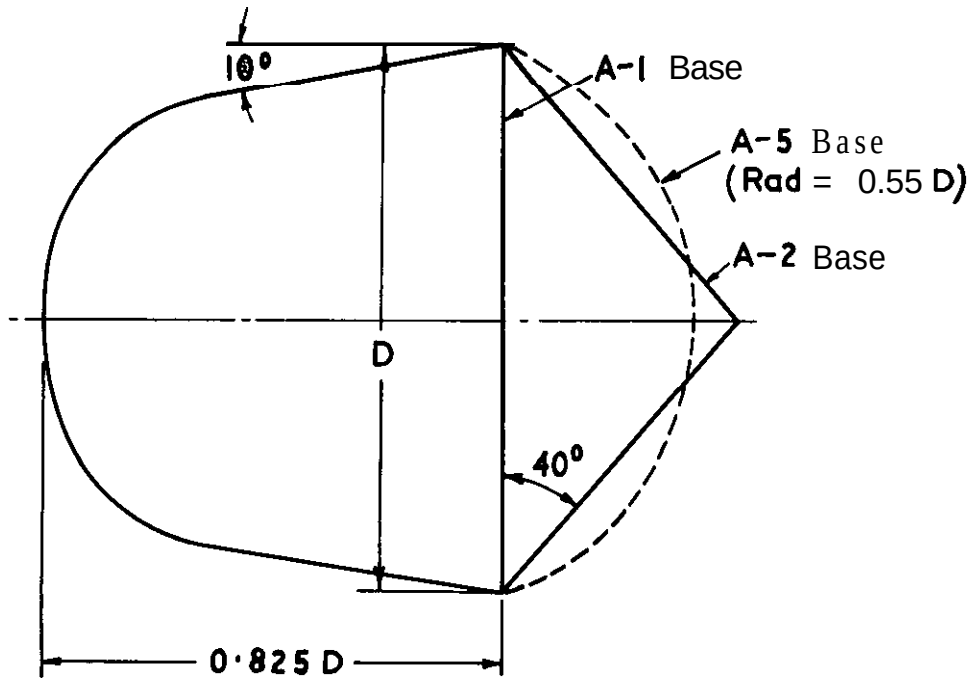

(a) Details of models

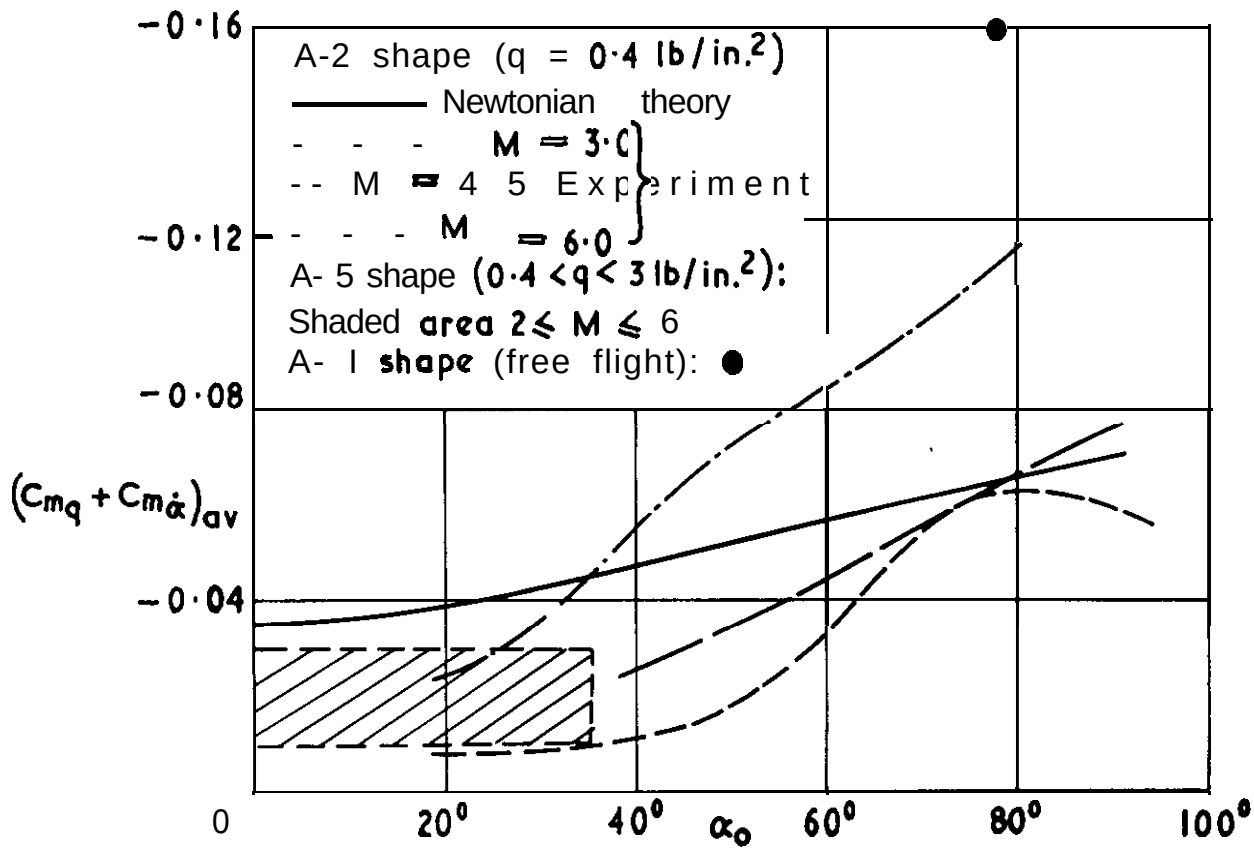

(b) Average effective pitch damping against oscillation amplitude

Comparison of experimental pitching damping and Newtonian theory values for a bluff body

FIG. 30 (a)

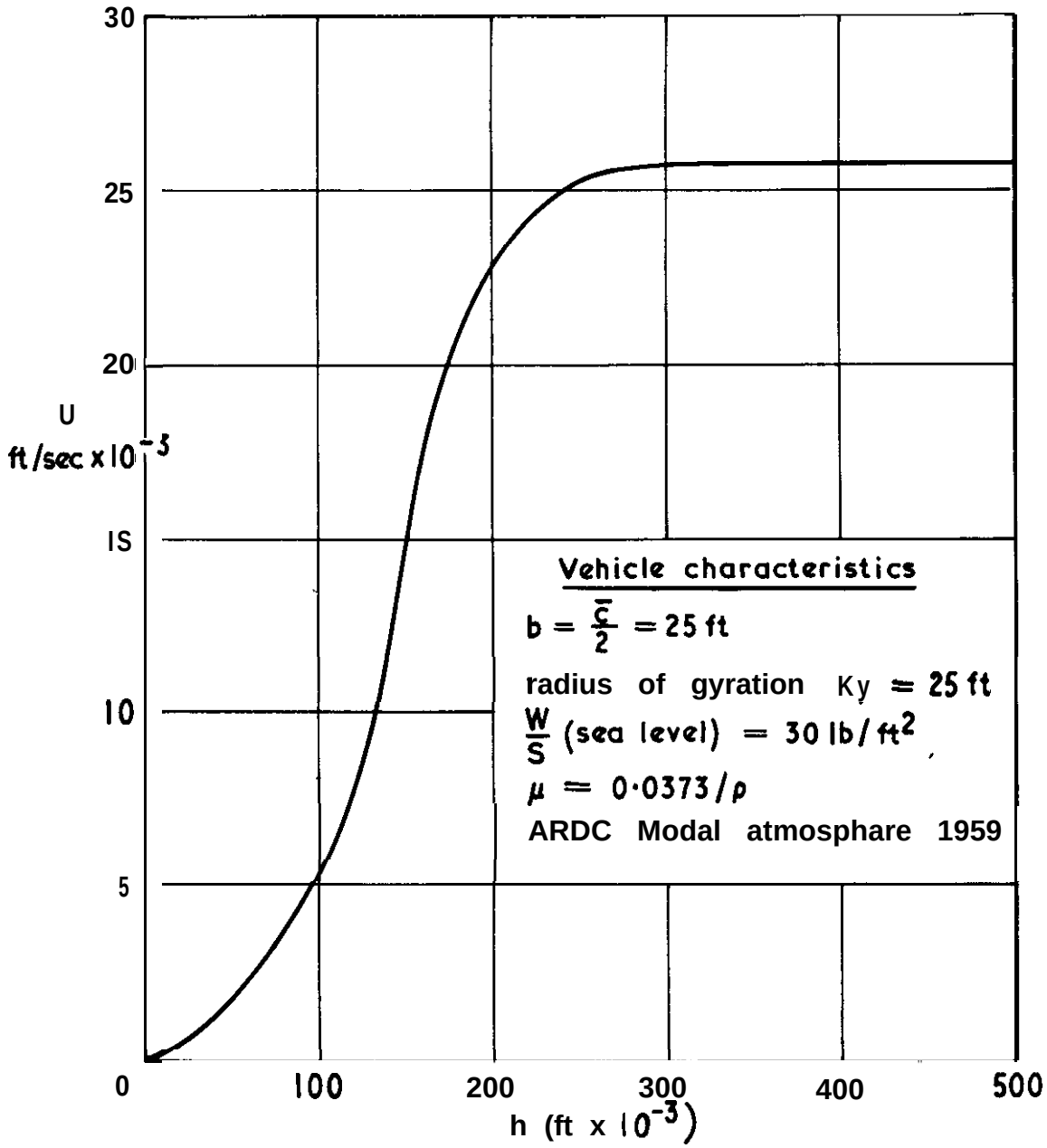

(a) Speed of flight C_L (mean) = 0·05

Oscillatory motion of a lifting vehicle in steady flight at constant altitude

FIG. 30 (b)

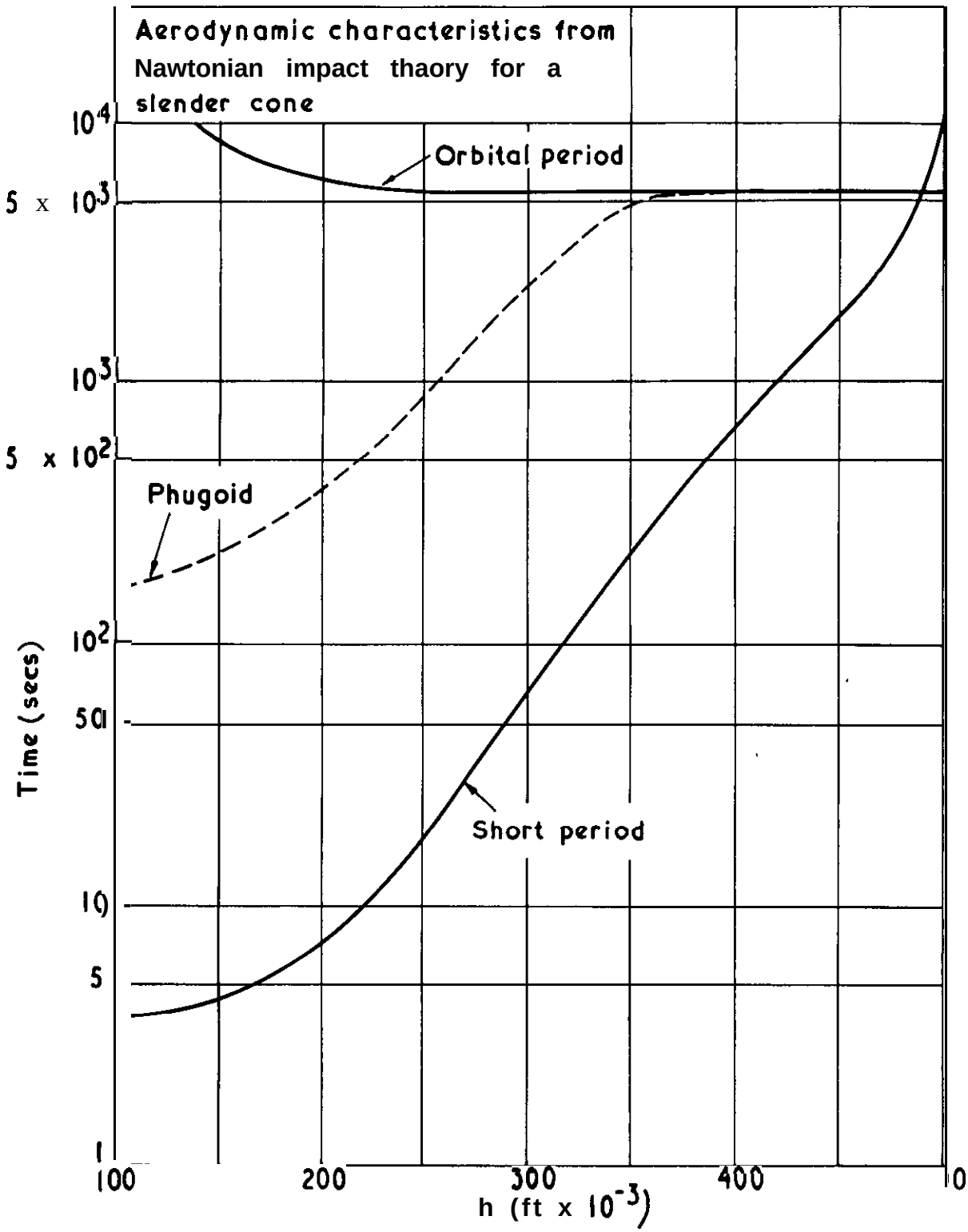

(b) Pariod of longitudinal oscillations From Fig.8 of Raf.43

Oscillatory motion of a lifting vahicla in steady flight at constant altitude

FIG. 30 (c)

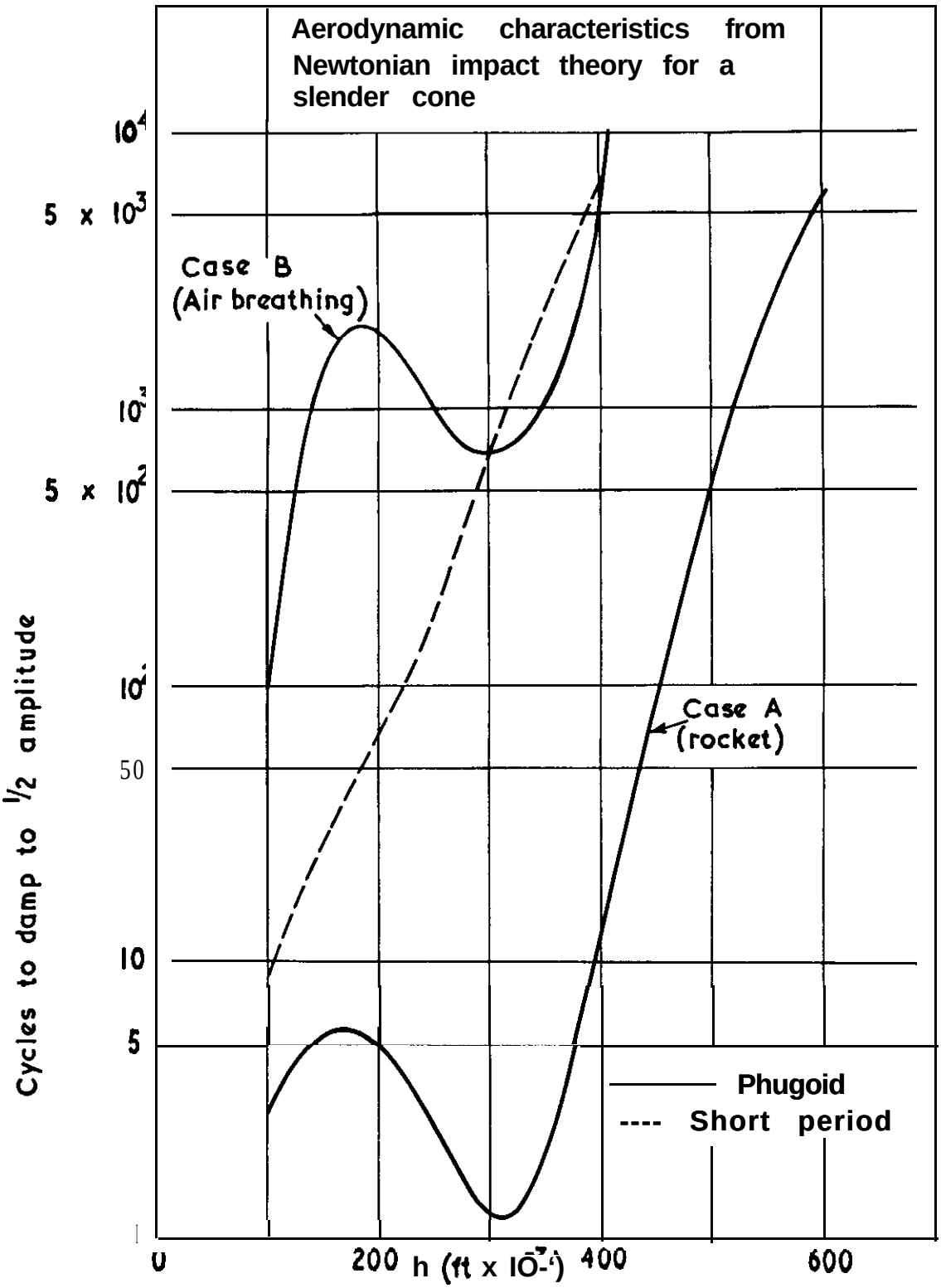

(c) Damping of longitudinal oscillations from Fig. 9 of Ref. 43

Oscillatory motion of a lifting vehicle in steady flight at constant altitude

FIG. 31

From Fig. 2 of Ref. 48

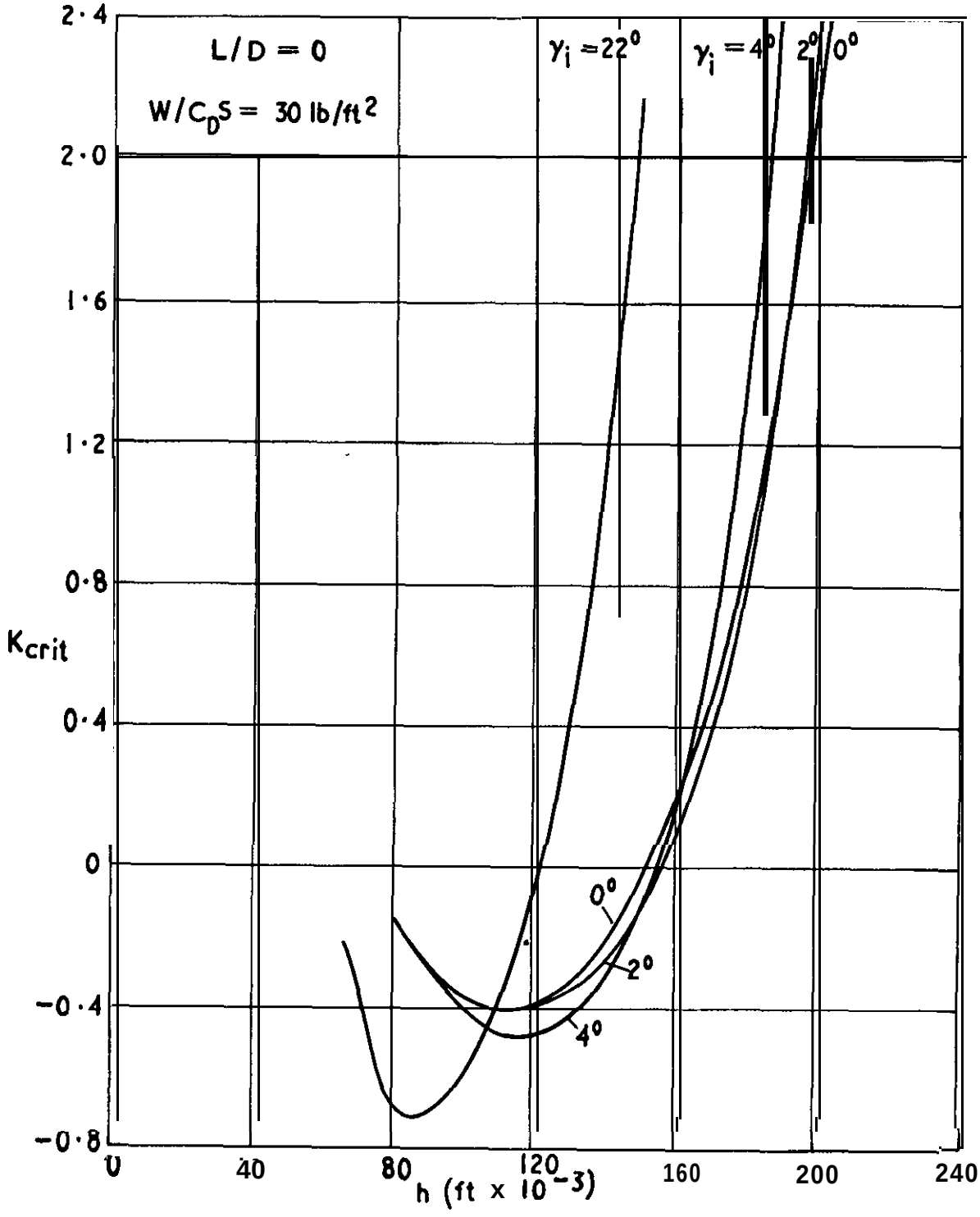

Convergence – boundary curves for non-lifting vehicles with various Initial flight path angles

From Ref.48

FIG. 32

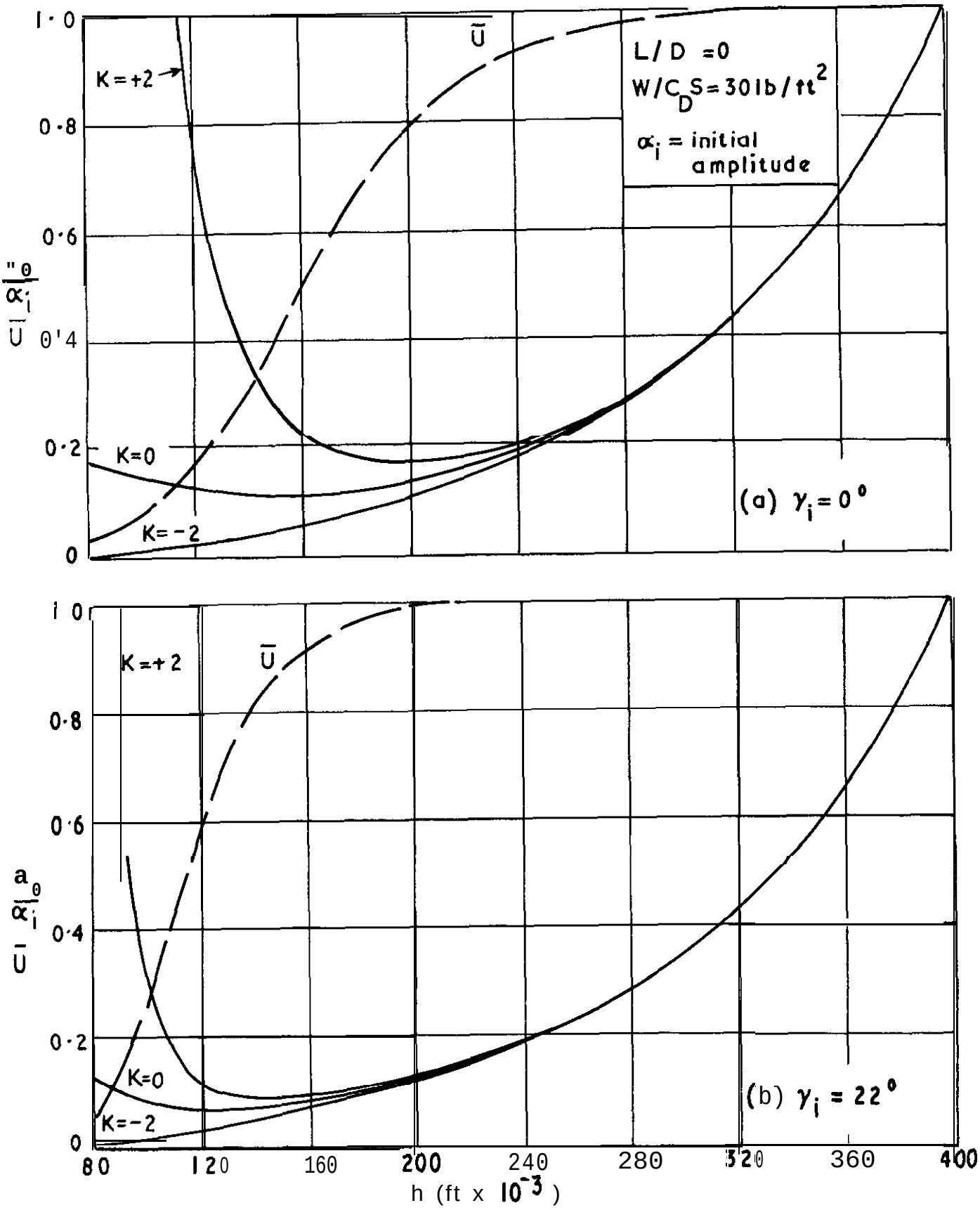

Oscillation-amplitude histories for non-lifting vehicles

FIG. 33

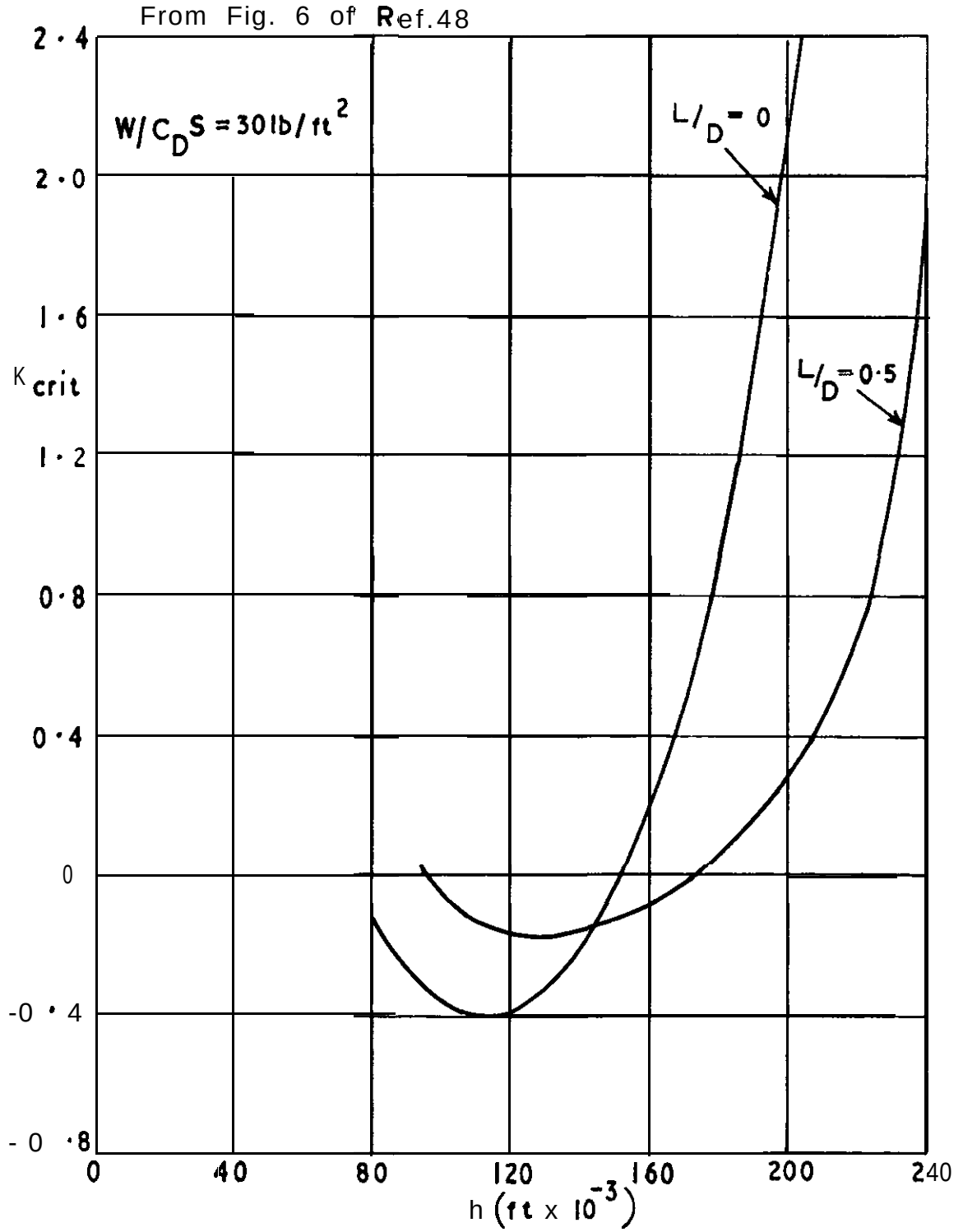

Comparison of convergence-boundary curves for lifting and non-lifting vehicles with zero initial fliaht-oath anales

From Fig.7 of Ref. 48

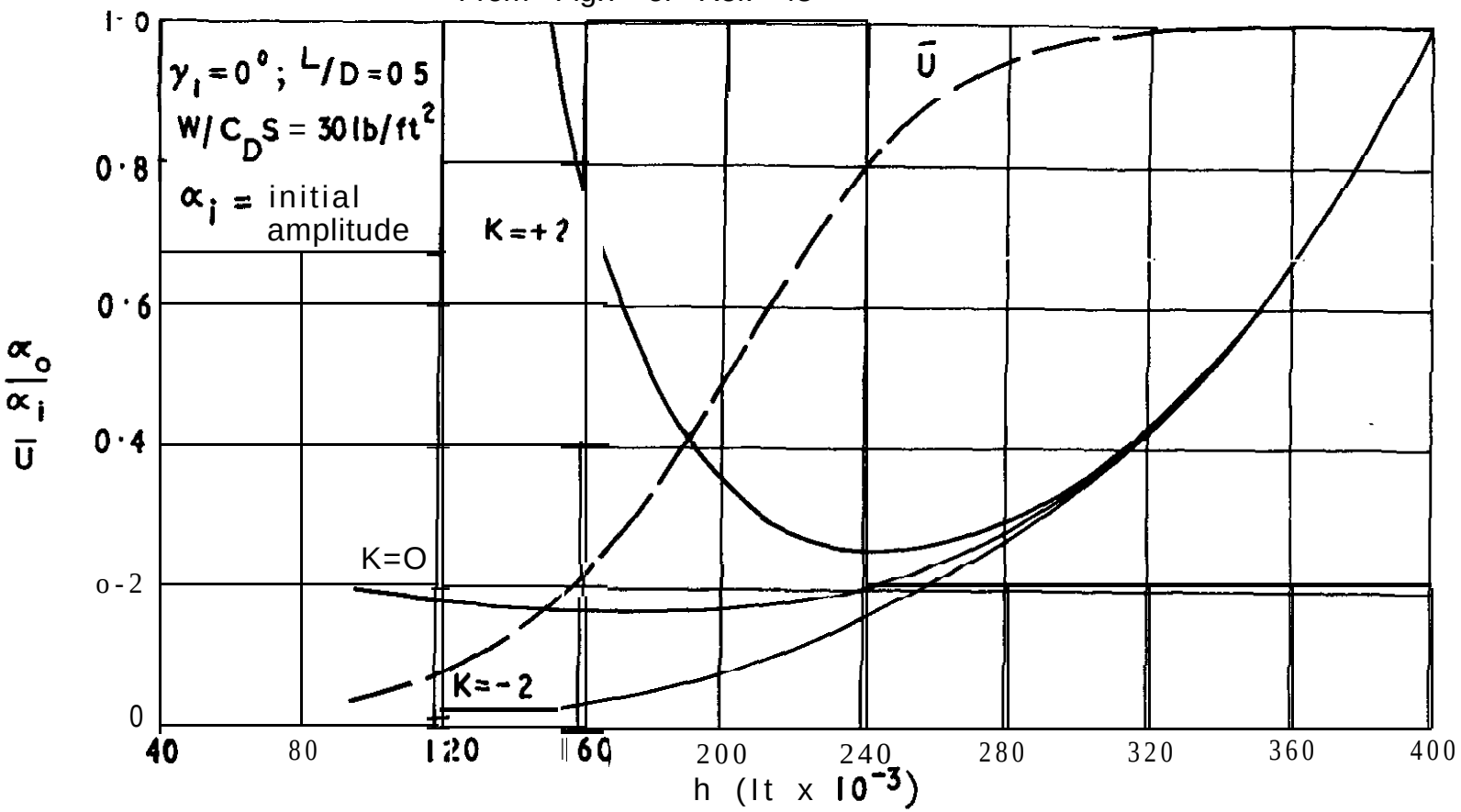

FIG. 34

Oscillation- amplitude histories for lifting vehicles with zero initial flight -path angle

FIG. 35 (a & b)

From Ref. 55

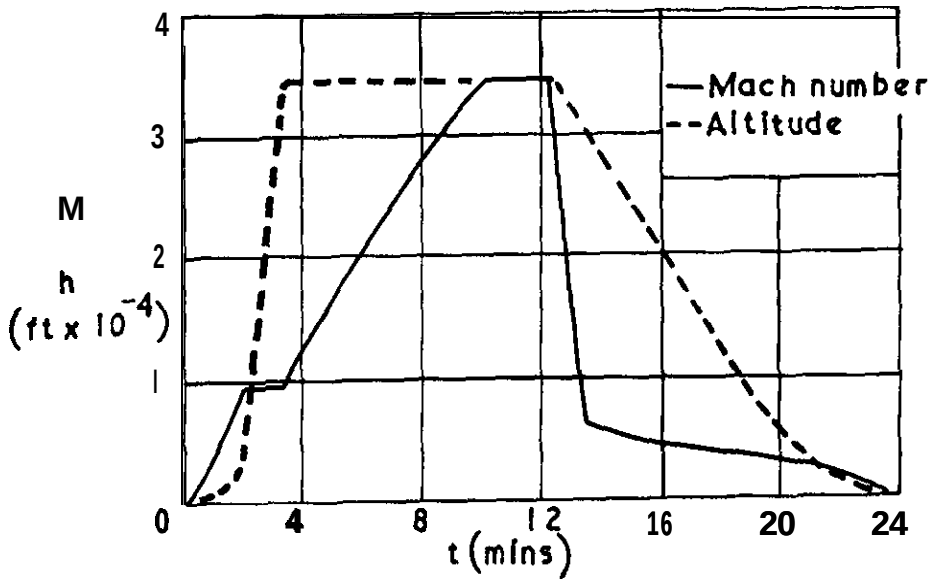

(a) Mission profile of hypothetical fighter

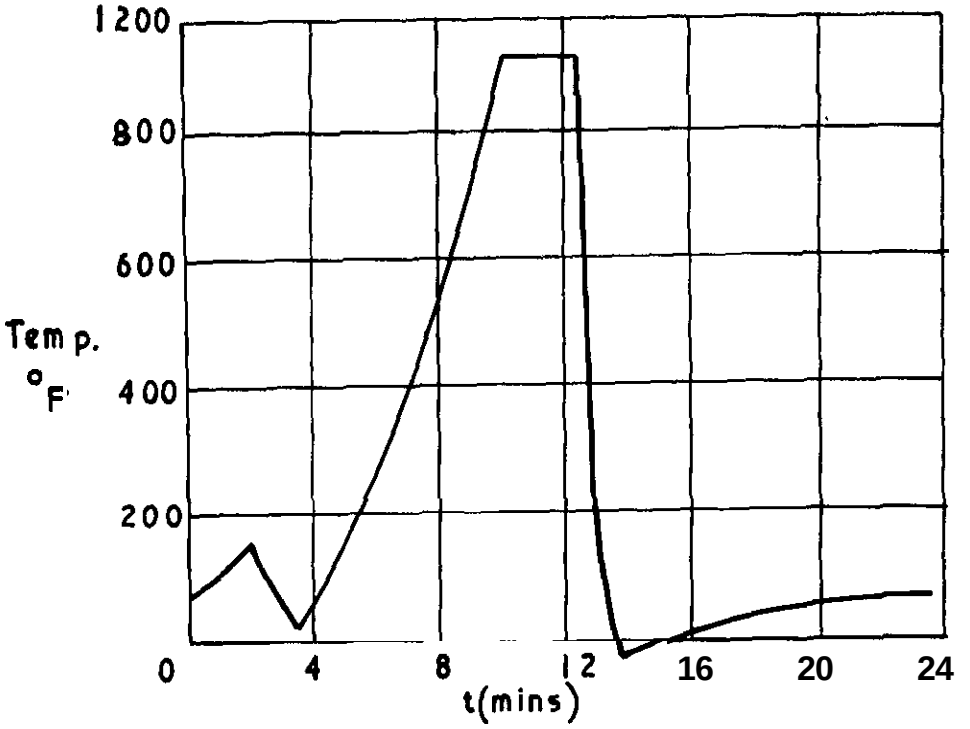

(b) Average adiabatic wall temperature

Influence of thermal effects on wing flutter margin for a hypothetical fighter

FIG 35(c)

From Ref. 55

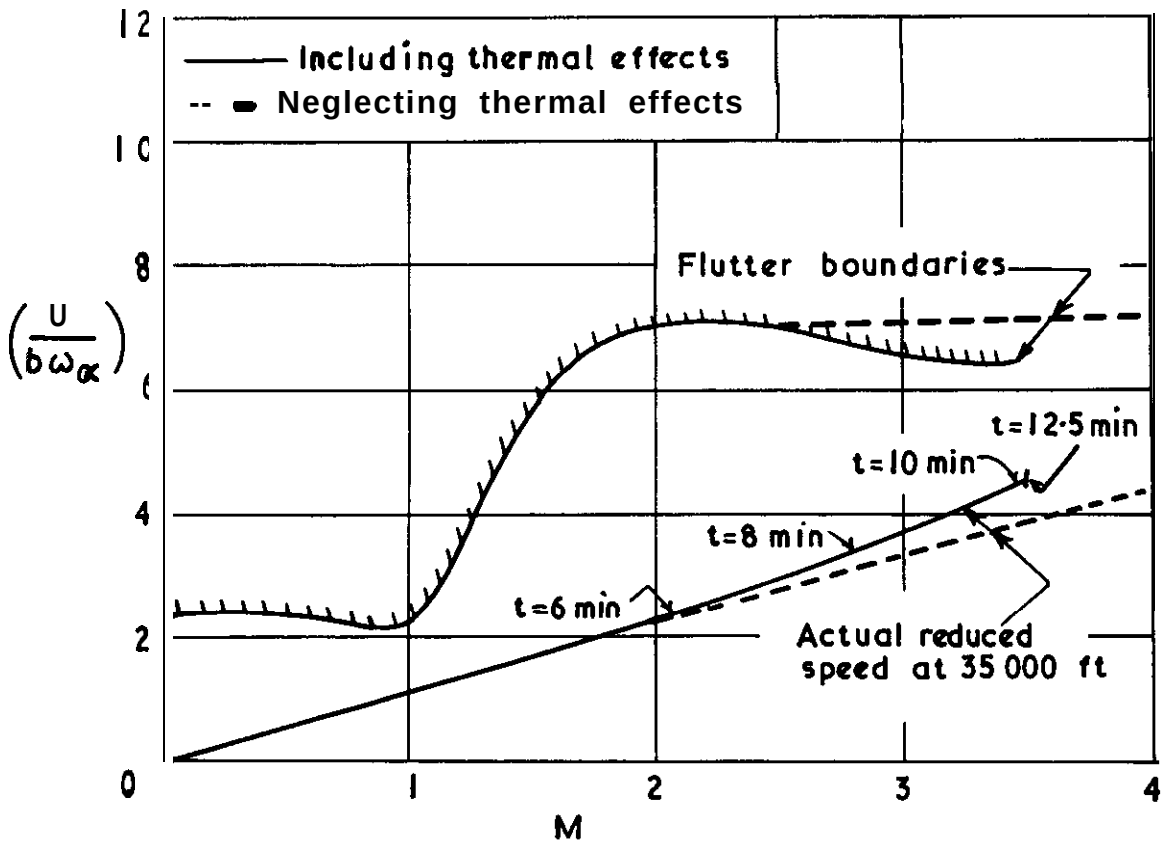

(c) Reduction in wing flutter margin-hypothetical fighter

Influence of thermal effects on wing flutter margins for a hypothetical fighter

FIG. 36

From Fig.8 of Ref. 56

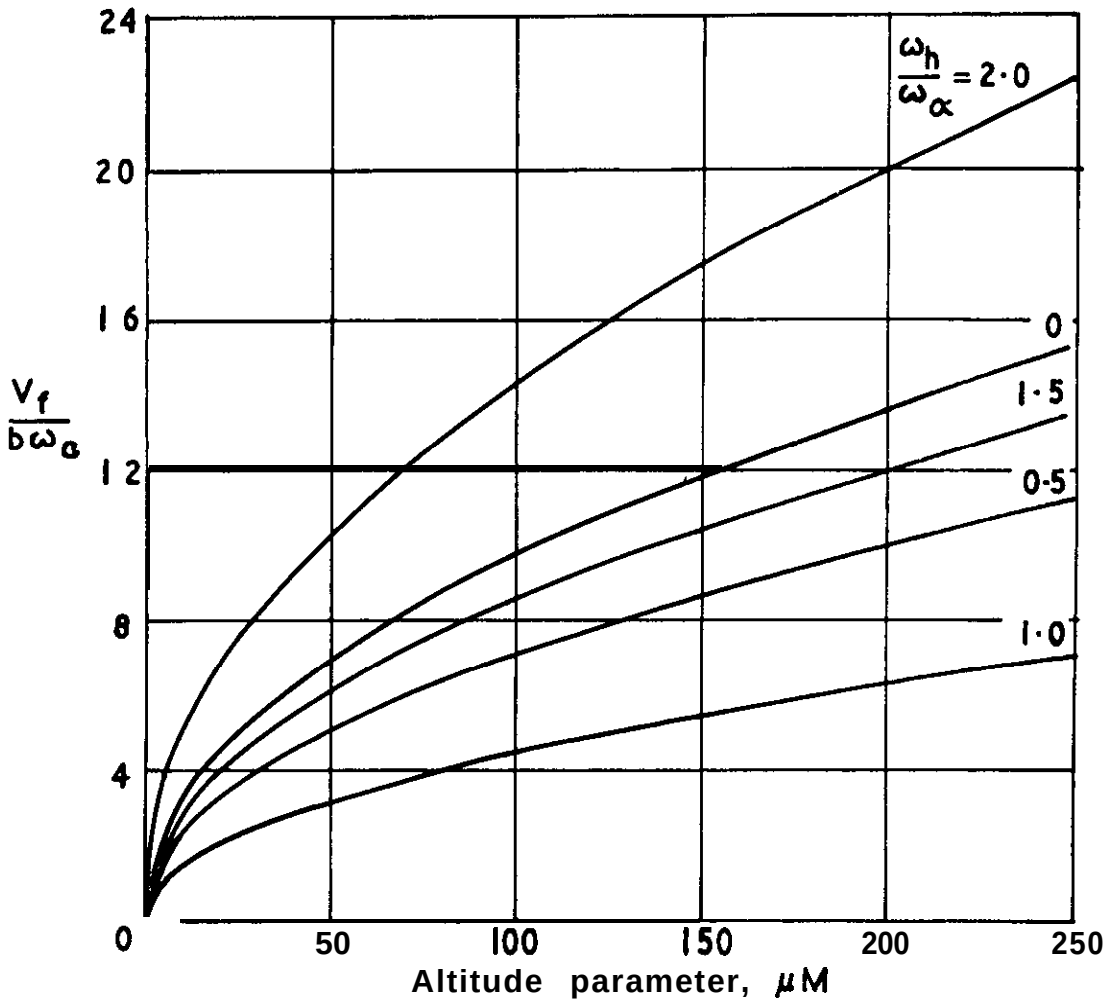

Variation of flutter speed with altitude at fixed frequency ratios

FIG. 37

From Ref. 56

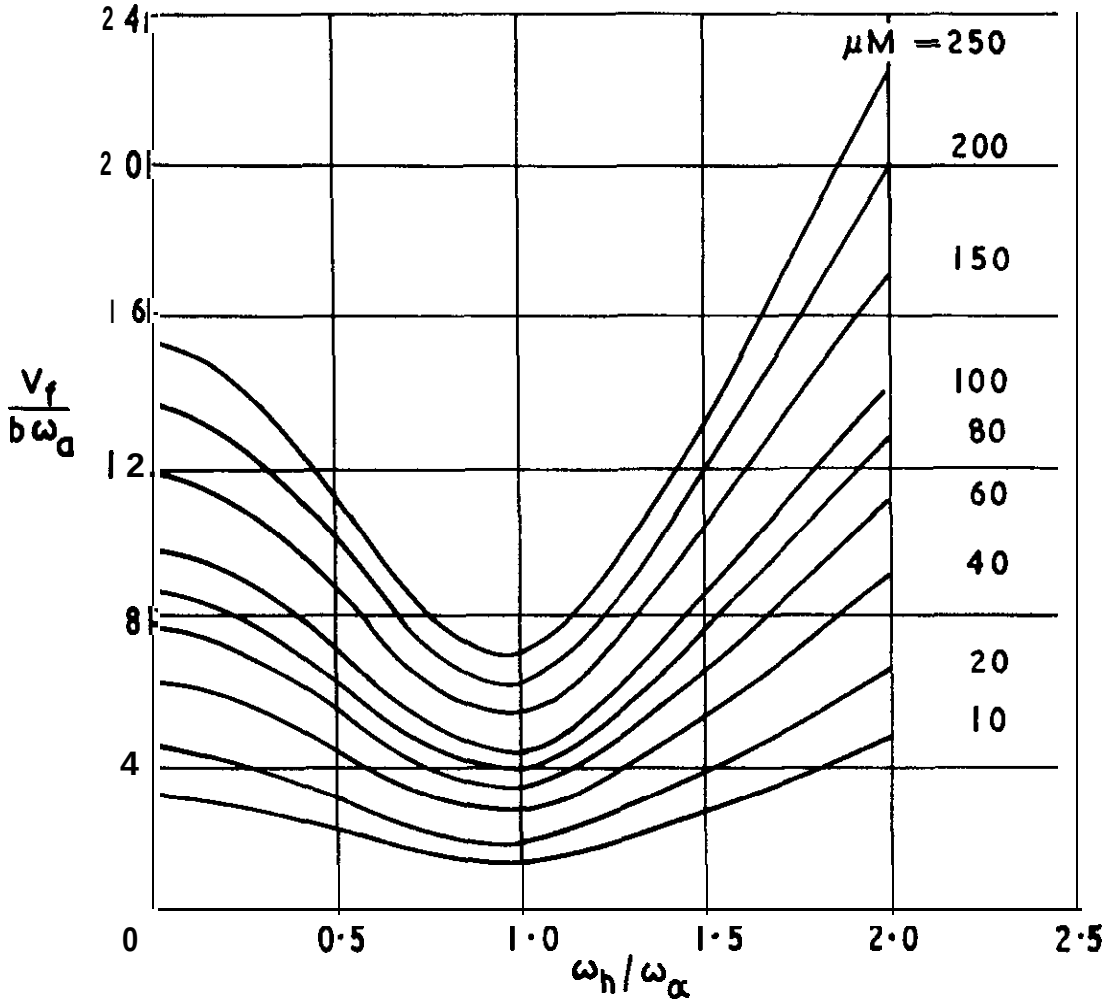

Variation of flutter speed with flexural-torsional frequency ratio and altitude

FIG. 38

From Ref. 56

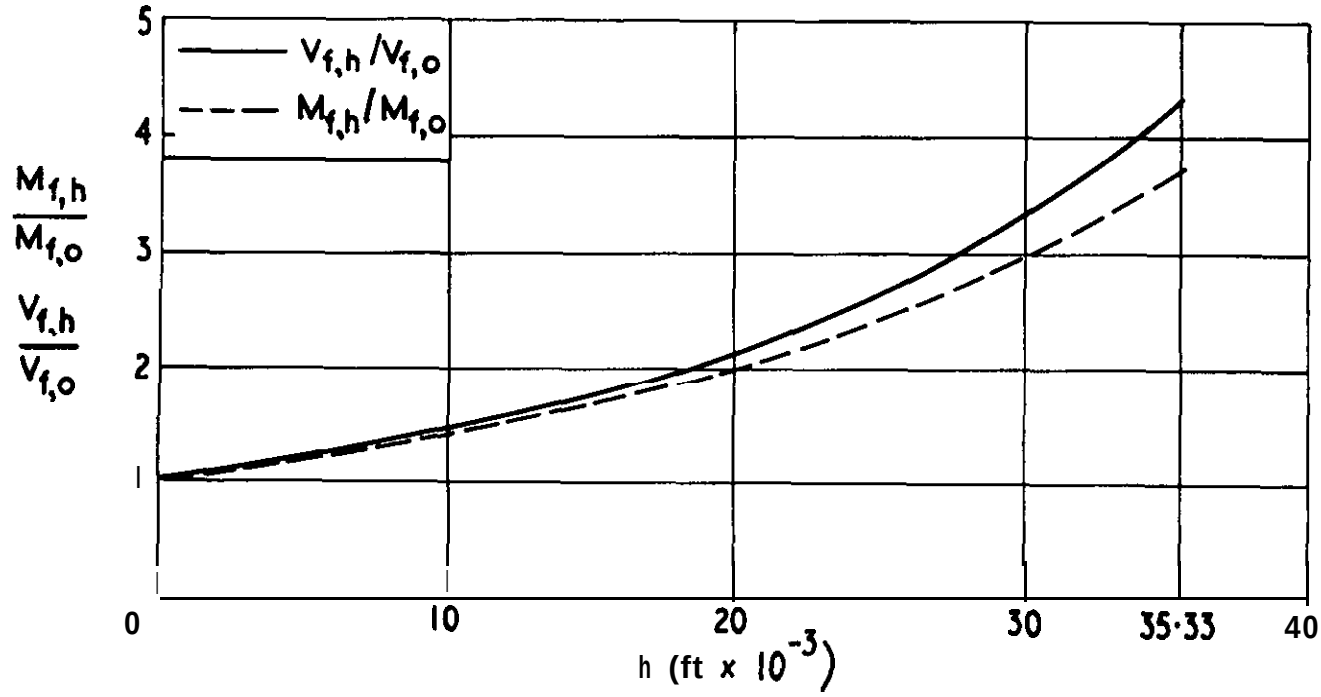

(a) Variation $0 < h < 35{,}330$ ft

Variation of flutter speed and Mach number with altitude

FIG. 38 (b)

From Rof.56

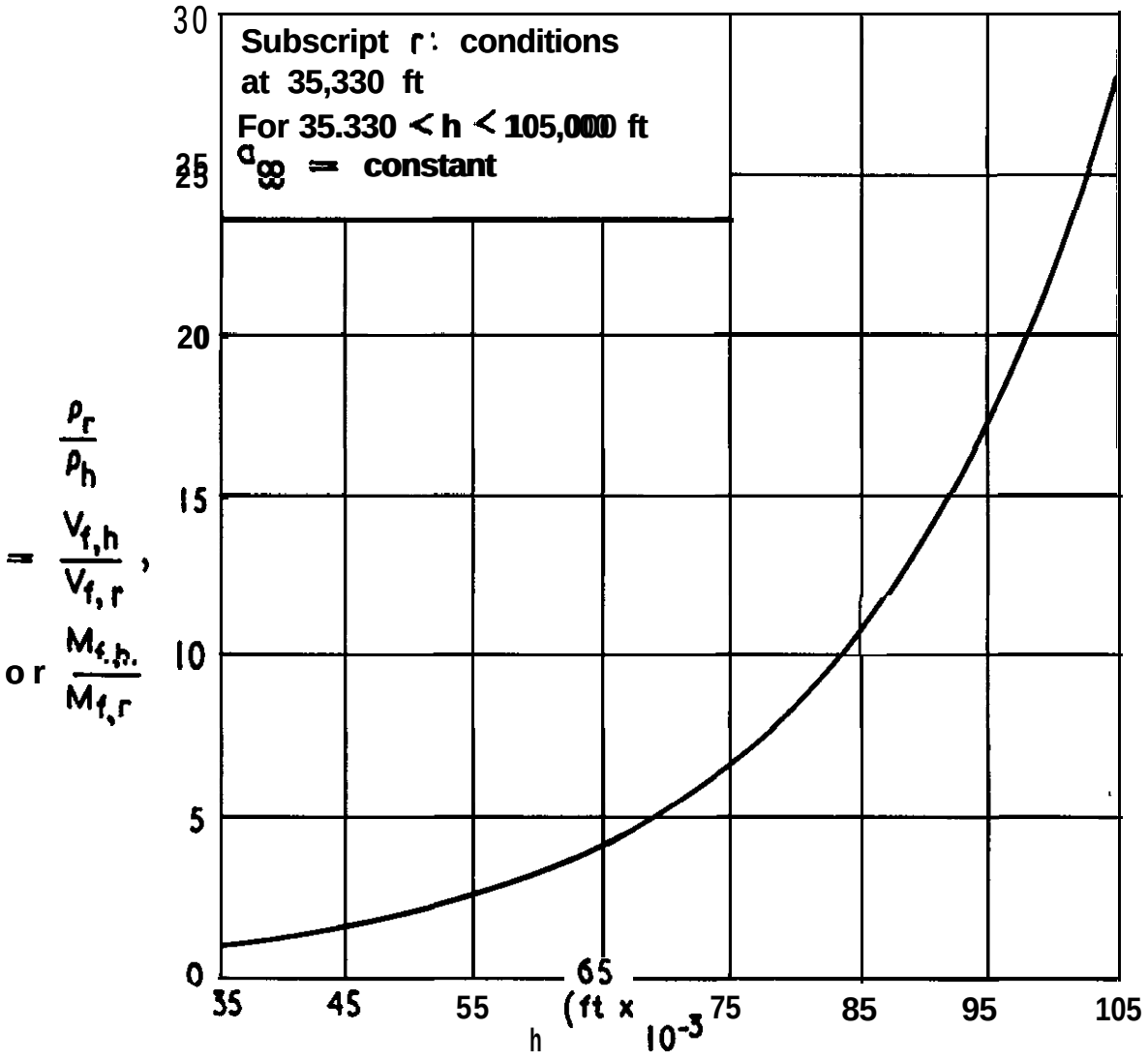

(b) Variation 35,330 < h < 105,000 ft

Variation of flutter speed and Mach number with altitude

FIG. 39

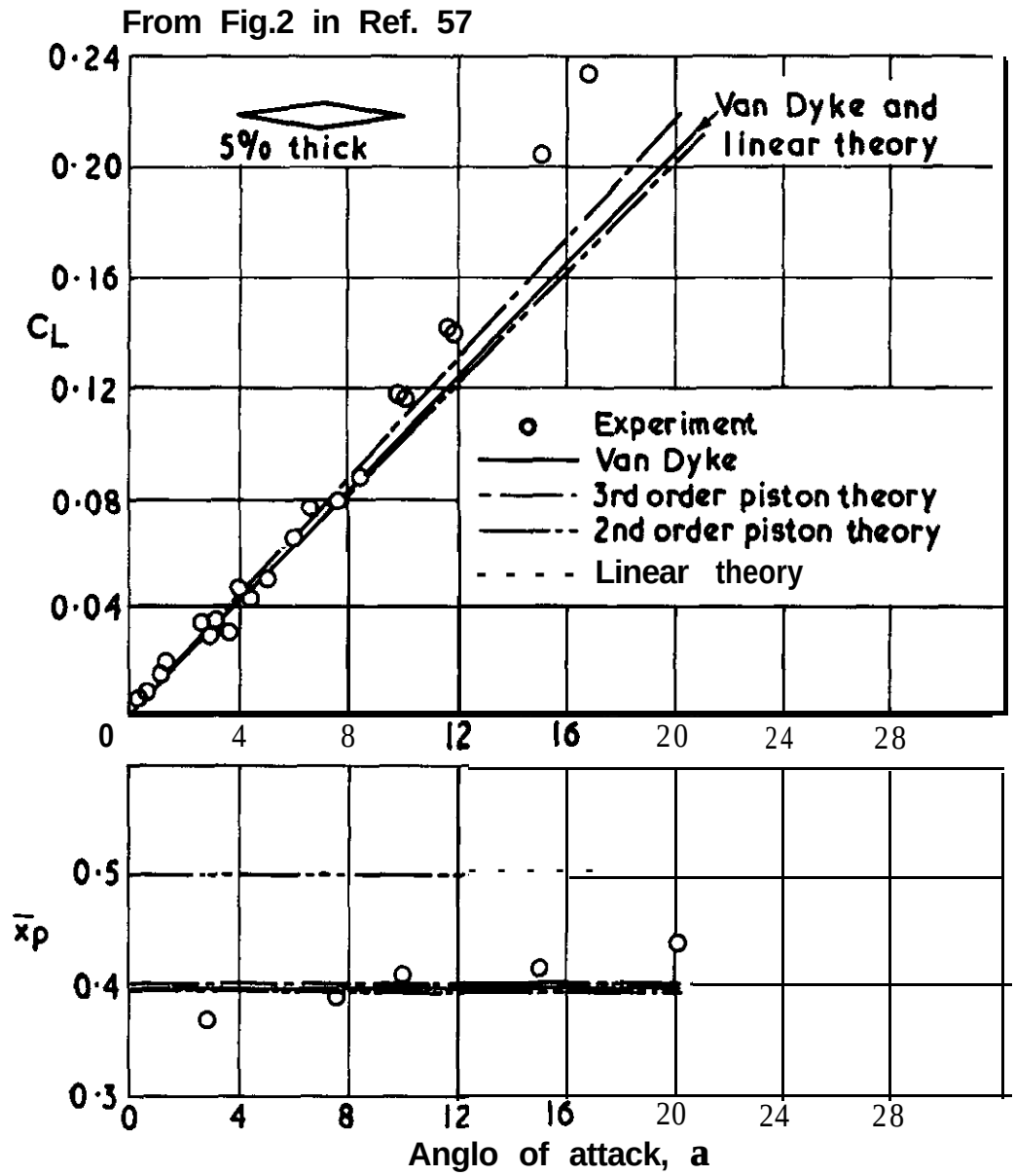

Experimental and theoretical lift and center of pressure in two-dimensional steady flow at $M = 6{\cdot}86$

FIG. 40

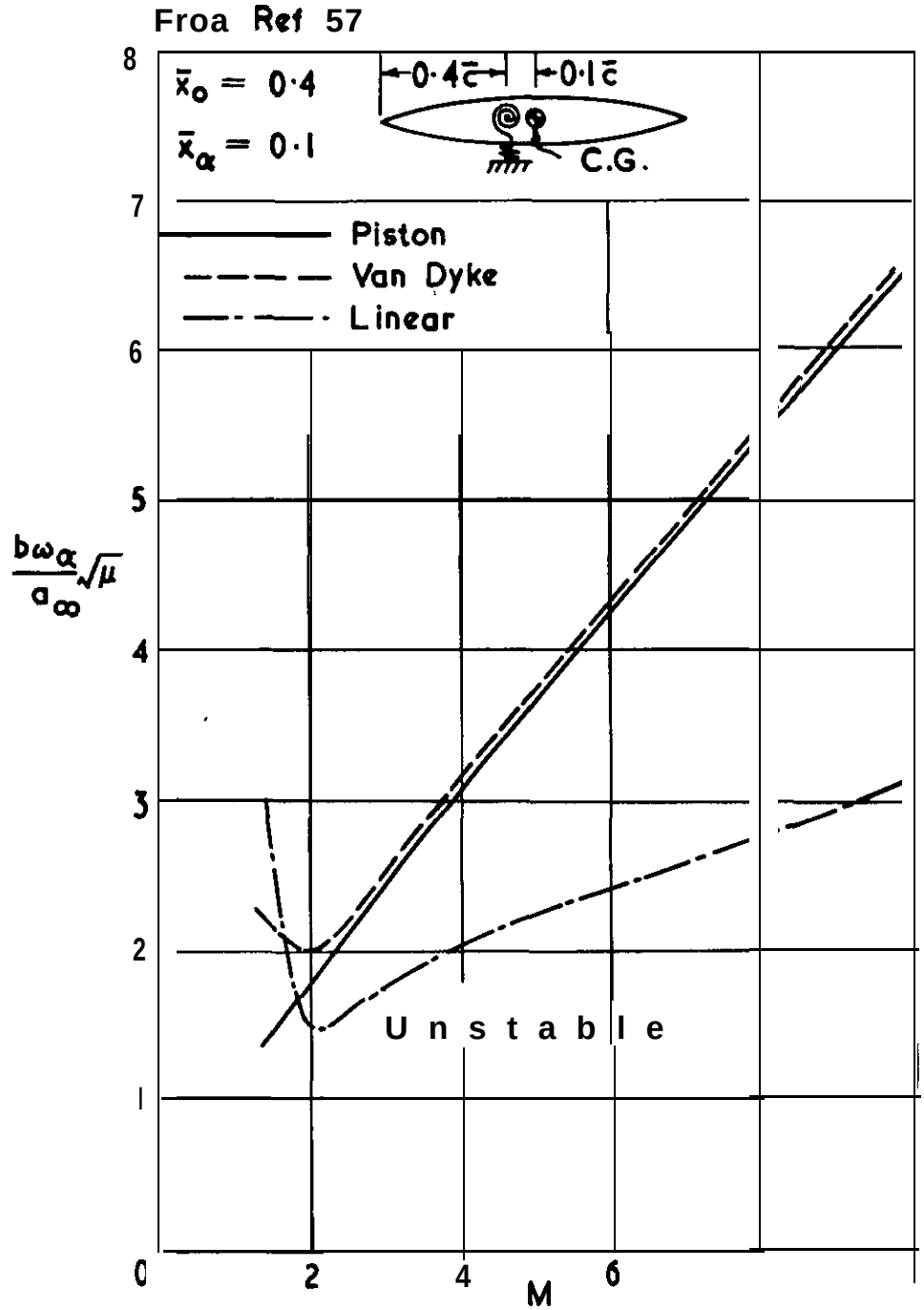

Fluttar boundarias for a 6 par *cant* biconvax airfoil (μ = 250, $\bar{r}_\alpha^2 = 0{\cdot}25$, $\omega_h/\omega_\alpha = 0{\cdot}5$)

FIG. 41(a)

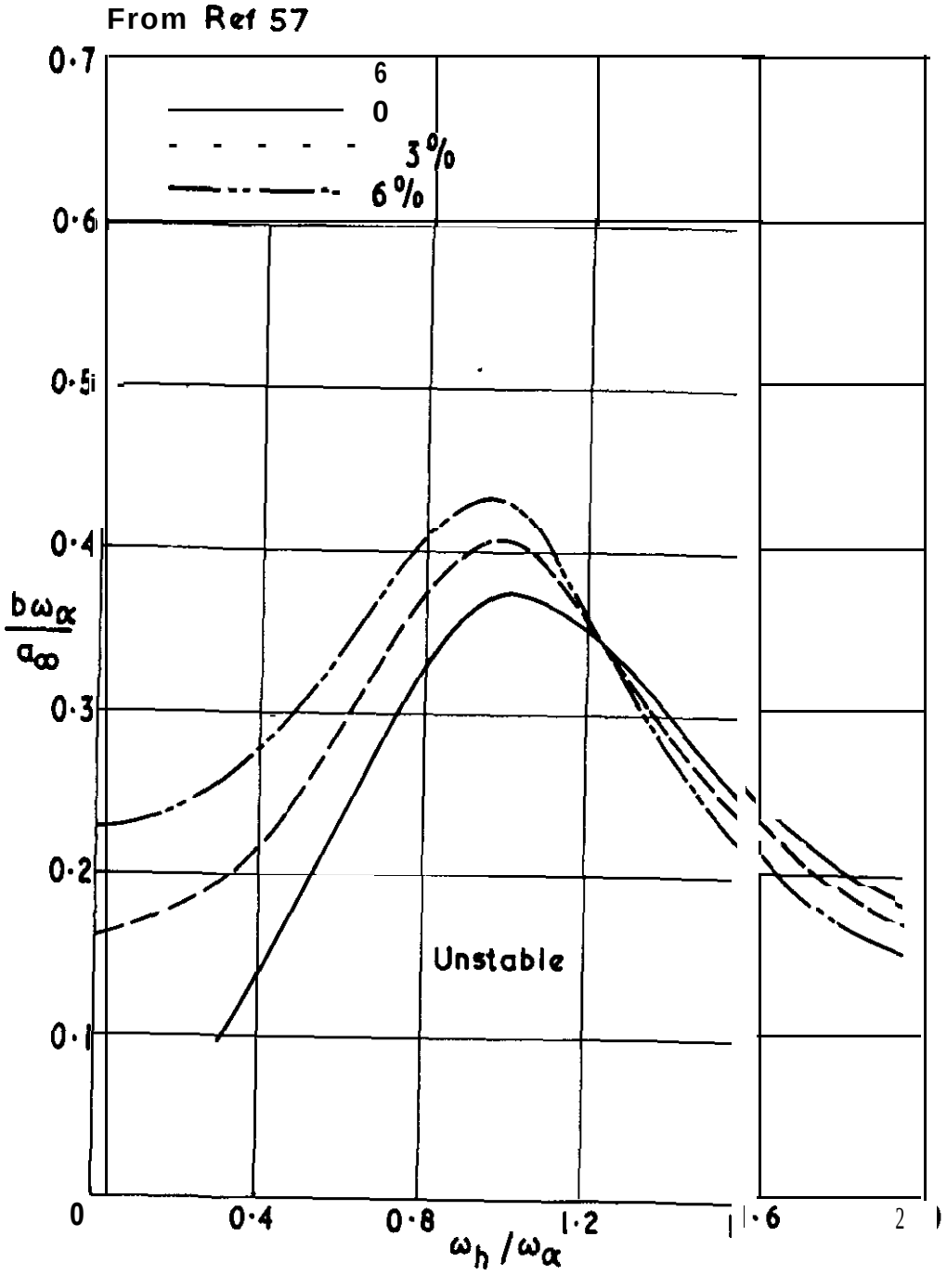

(a) $\bar{x}_0 = 0{\cdot}4$, $\bar{x}_\alpha = 0{\cdot}1$

Flutter boundaries showing thickness effects on biconvex aerofoils (M = 5, μ = 150, $r_\alpha^2 = 0{\cdot}25$)

FIG. 41 (b)

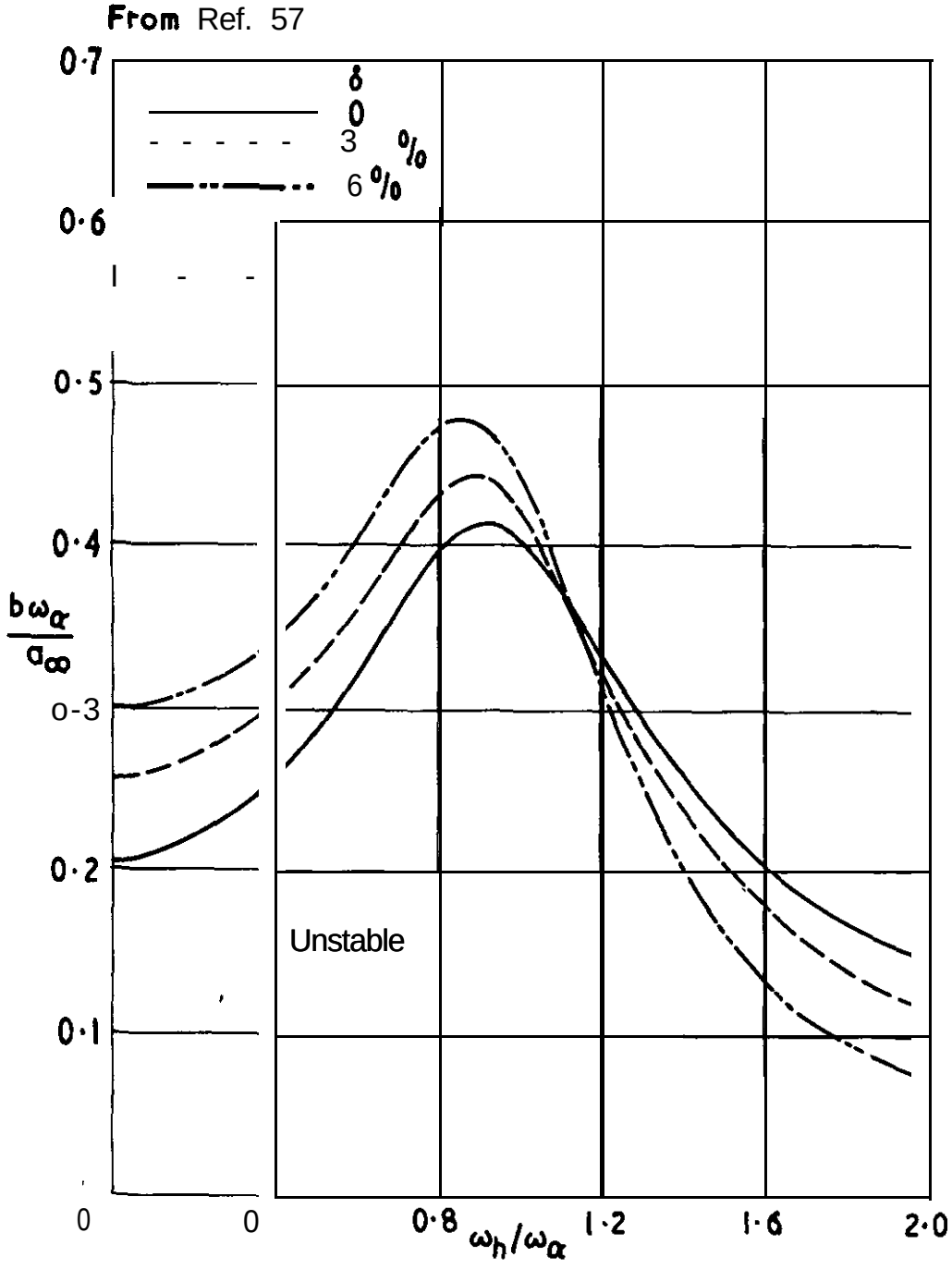

(b) $\bar{x}_o = 0.5$, $\bar{x}_\alpha = 0.1$

Flutter boundaries showing thickness affects on biconvex aarofoils (M = 5. μ = 150, r_α^2 = 0·25

FIG.41 (c)

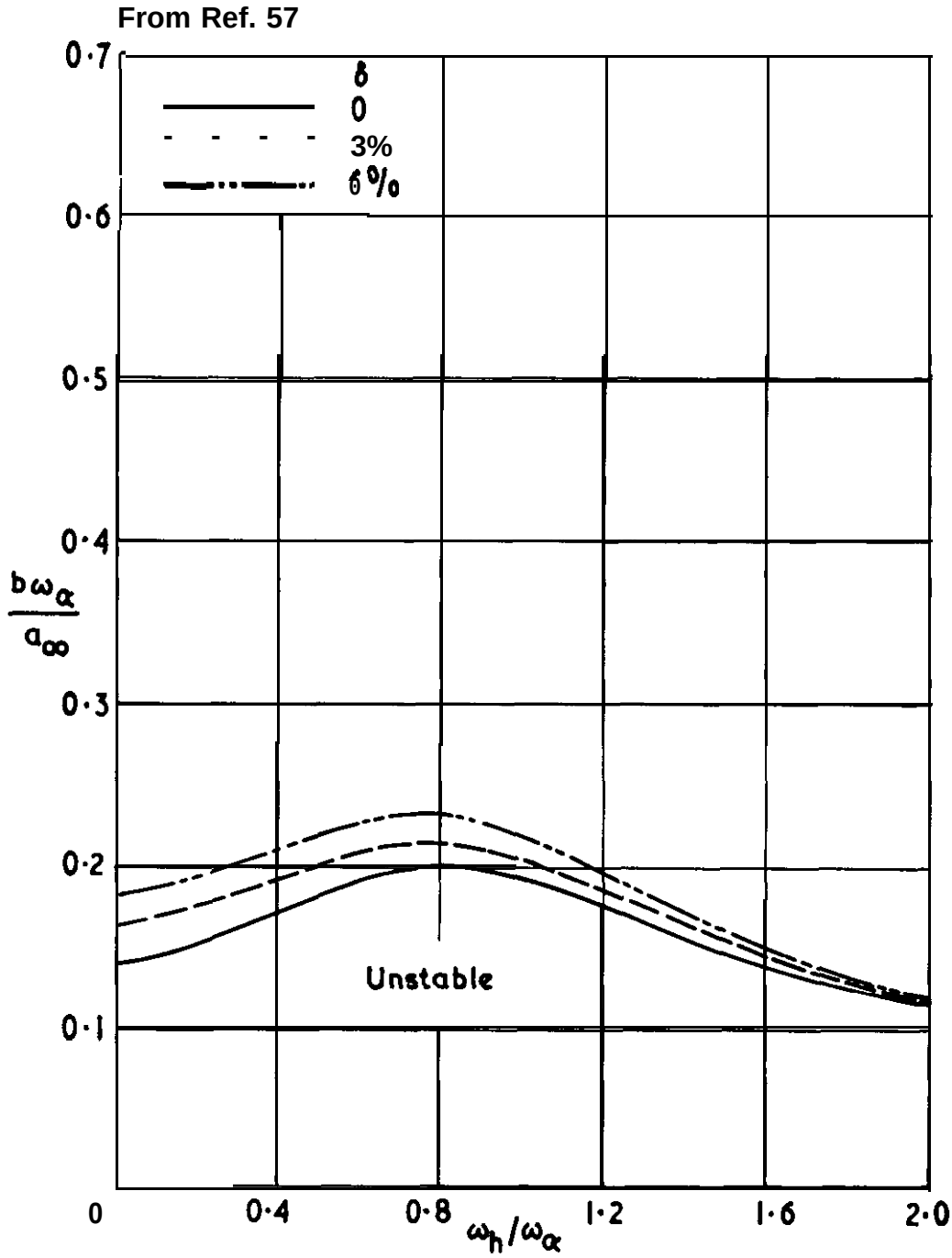

(c) $\bar{x}_0 = 0{\cdot}4$, $\bar{x}_\alpha = 0{\cdot}2$

Flutter boundaries showing thickness effects on biconvex aerofoils

($M = 5$, $\mu = 150$, $r_\alpha^2 = 0{\cdot}25$)

FIG. 41 (d)

From Ref. 57

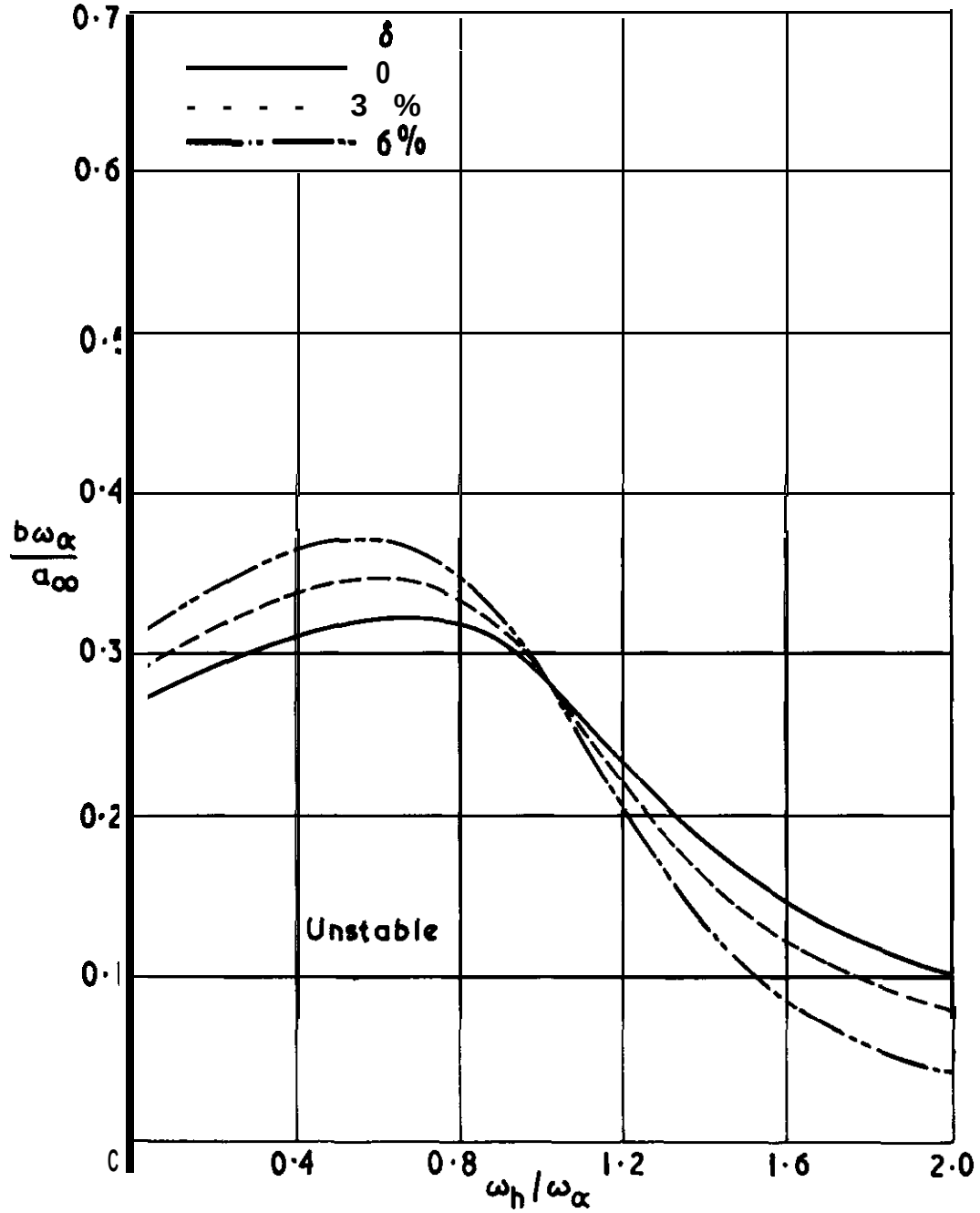

(d) $\bar{x}_o = 0{\cdot}6$ $\bar{x}_\alpha = 0.2$

Flutter boundaries showing thickness off ects on blconvex aerofolls

$(M_\infty = 5, \mu = 150, r_\alpha^2 = 0{\cdot}25)$

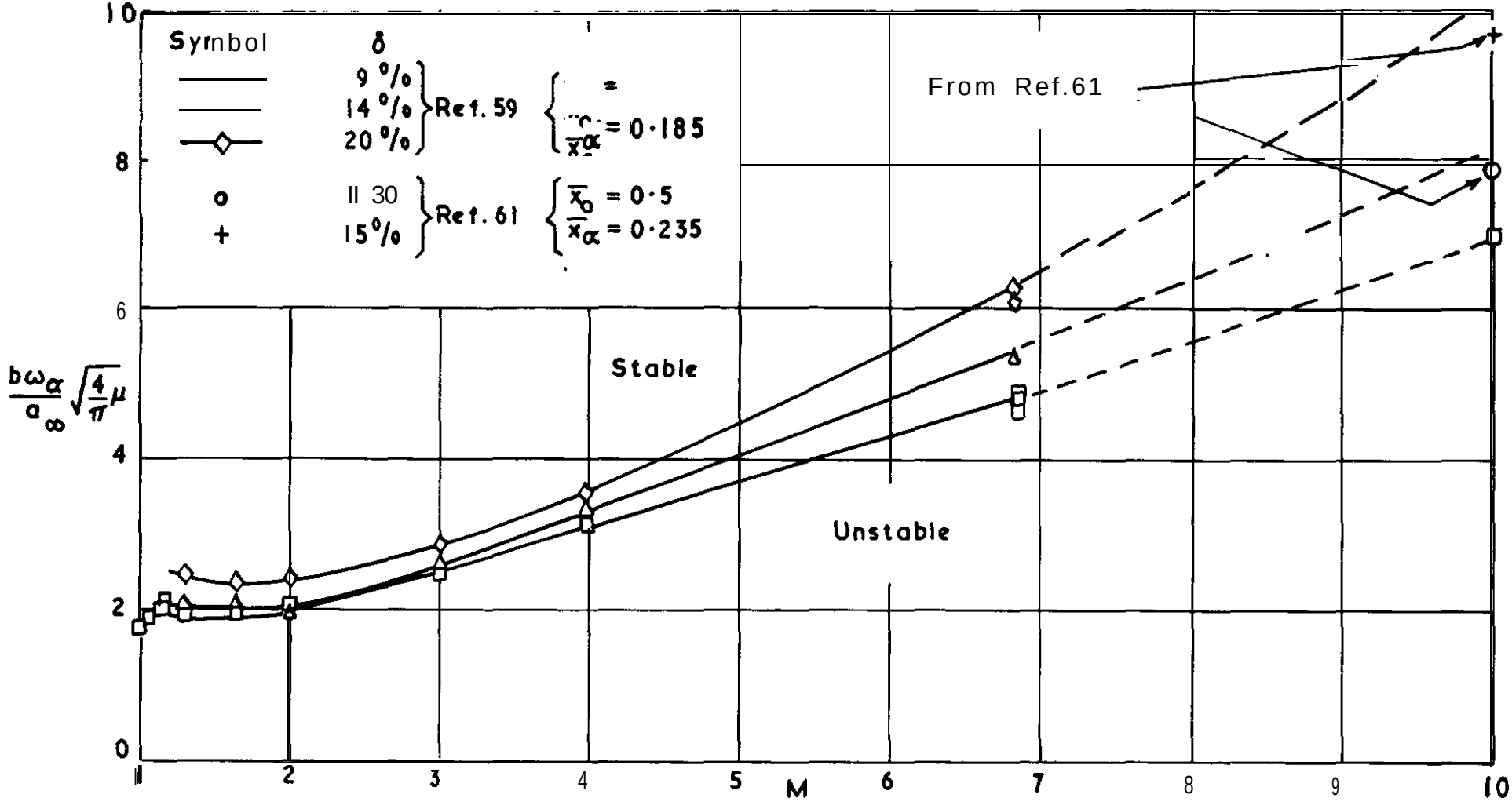

FIG. 42

Experimental variation of sti ffness-altitude parameter with Mach number and thickness for double-wedae models

FIG . 43

From Ref 58

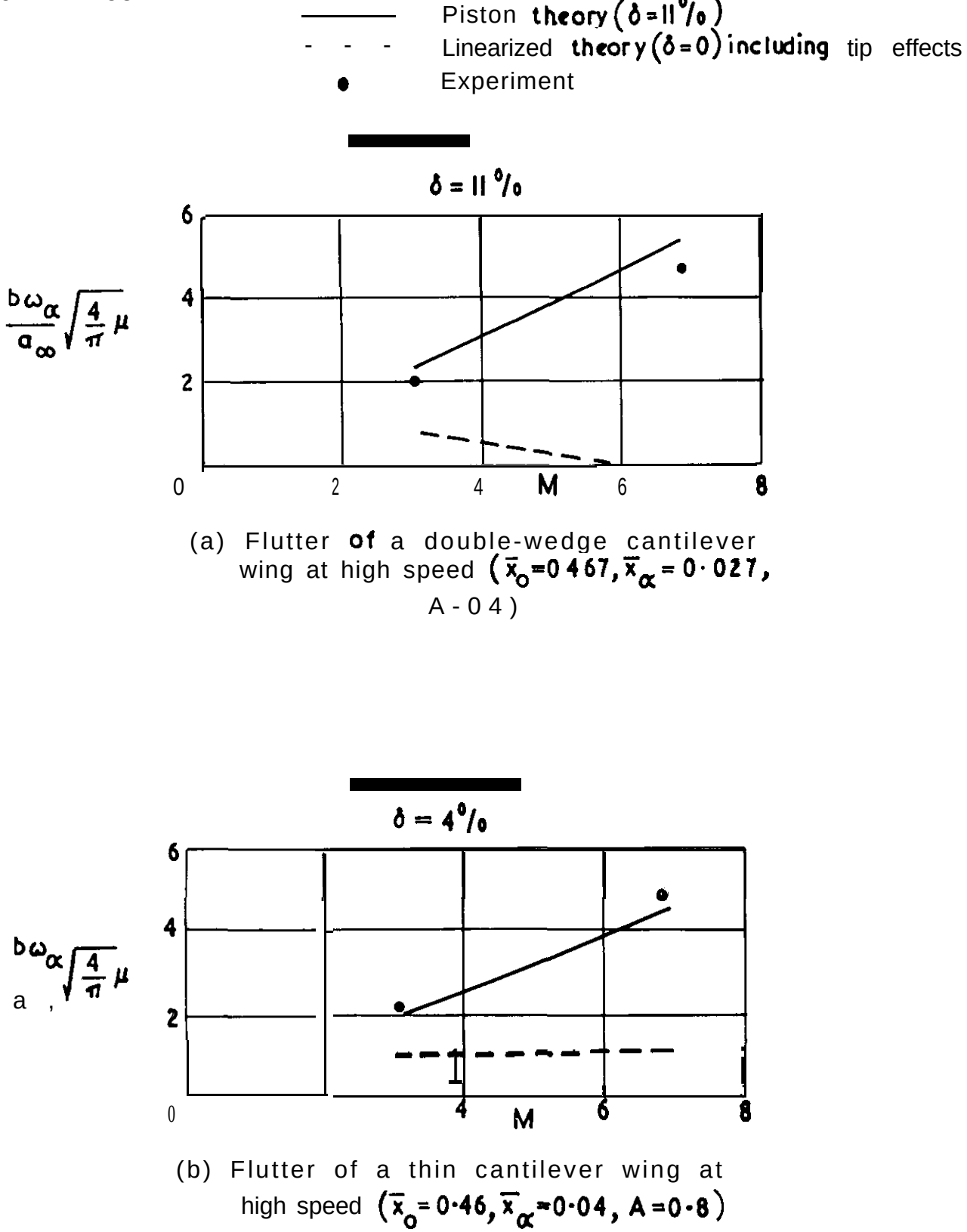

(a) Flutter of a double-wedge cantilever wing at high speed ($\bar{x}_0 = 0467, \bar{x}_\alpha = 0 \cdot 027,$ A - 0 4)

(b) Flutter of a thin cantilever wing at high speed ($\bar{x}_0 = 0 \cdot 46, \bar{x}_\alpha = 0 \cdot 04, A = 0 \cdot 8$)

Comparison of the effect of thickness on the flutter of thin wings from theorv · and experiment

FIG . 44

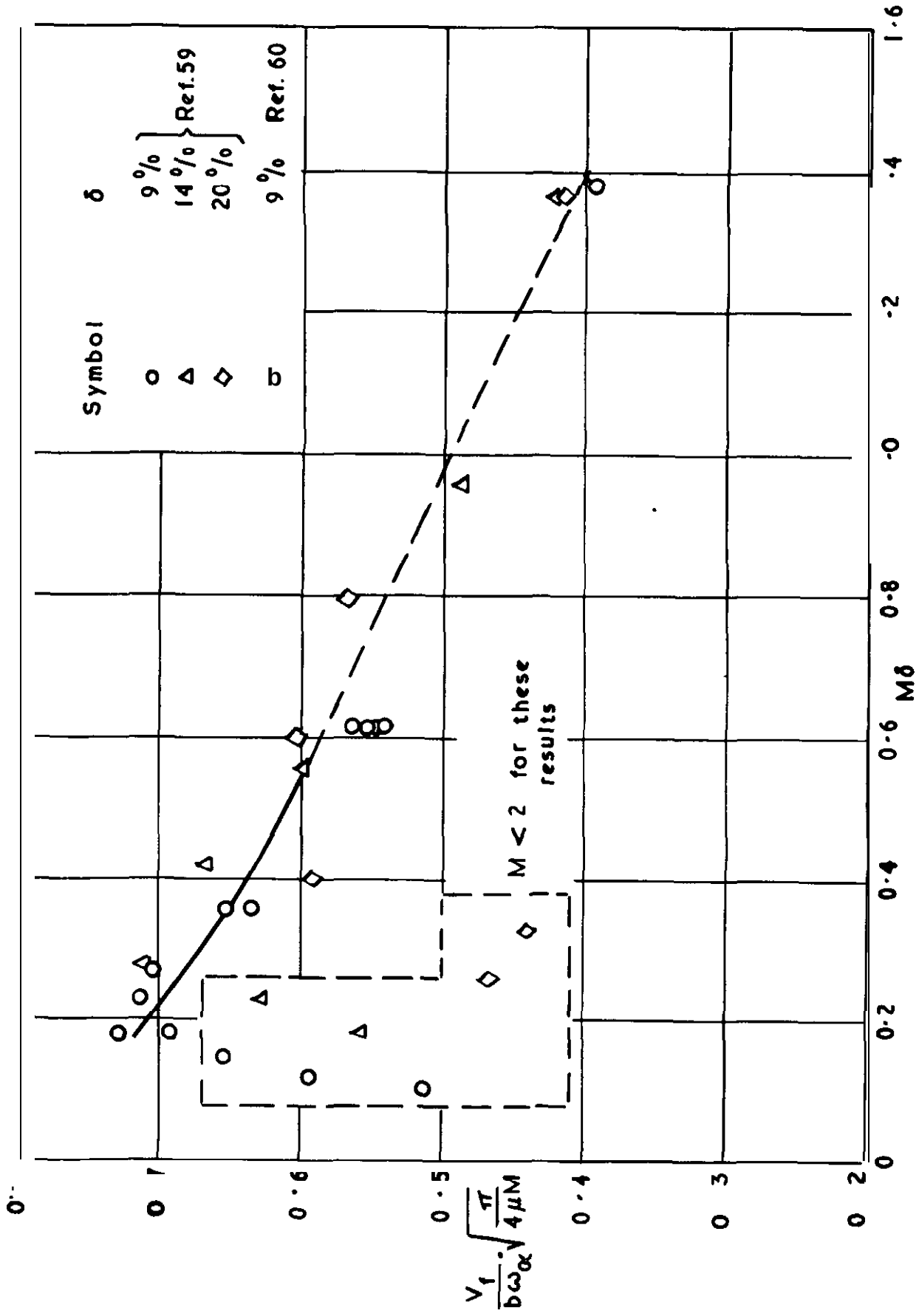

Experimental variation of flutter speed with thickness parameter for double-wedge aerofoil

FIG.43

From Ref. 56

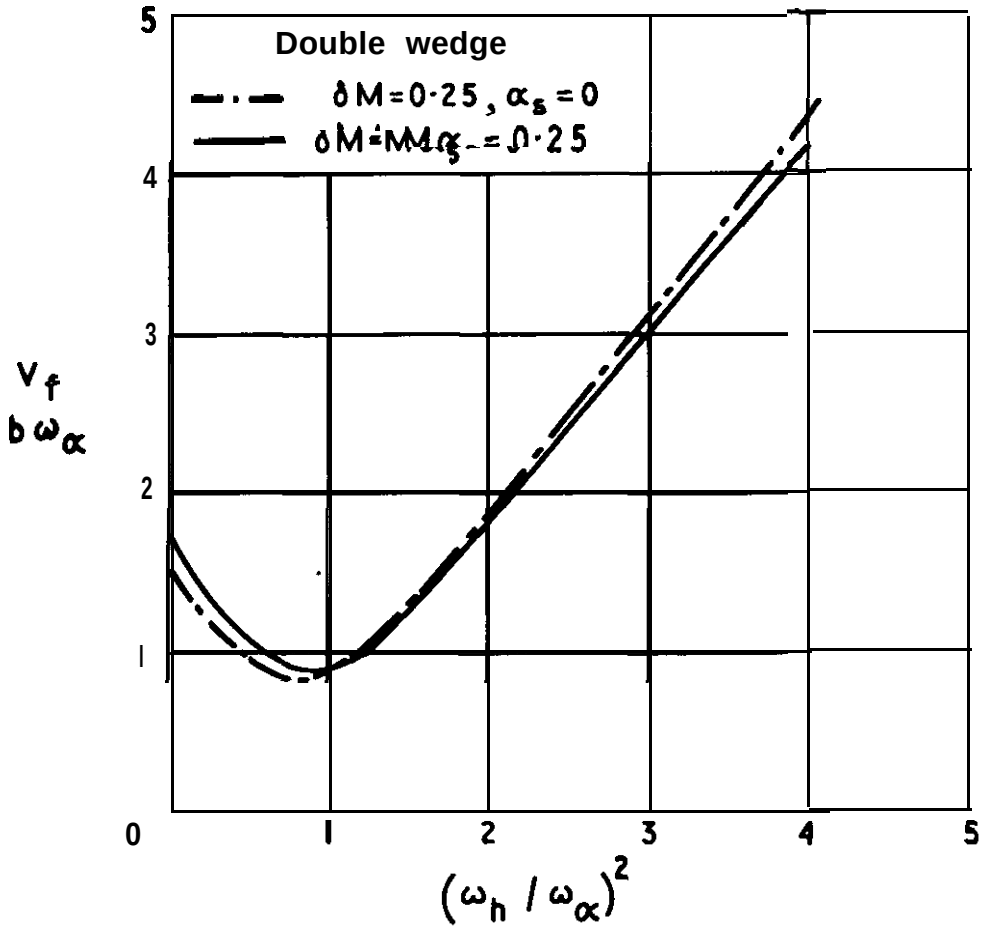

Effect of thickness and mean incidence on flutter speed ($\mu M=250$, $\bar{x}_0=0{\cdot}5$, $\bar{x}_\alpha=0{\cdot}1$)

FIG. 46

From Fig. 5.1 of Ref. 26

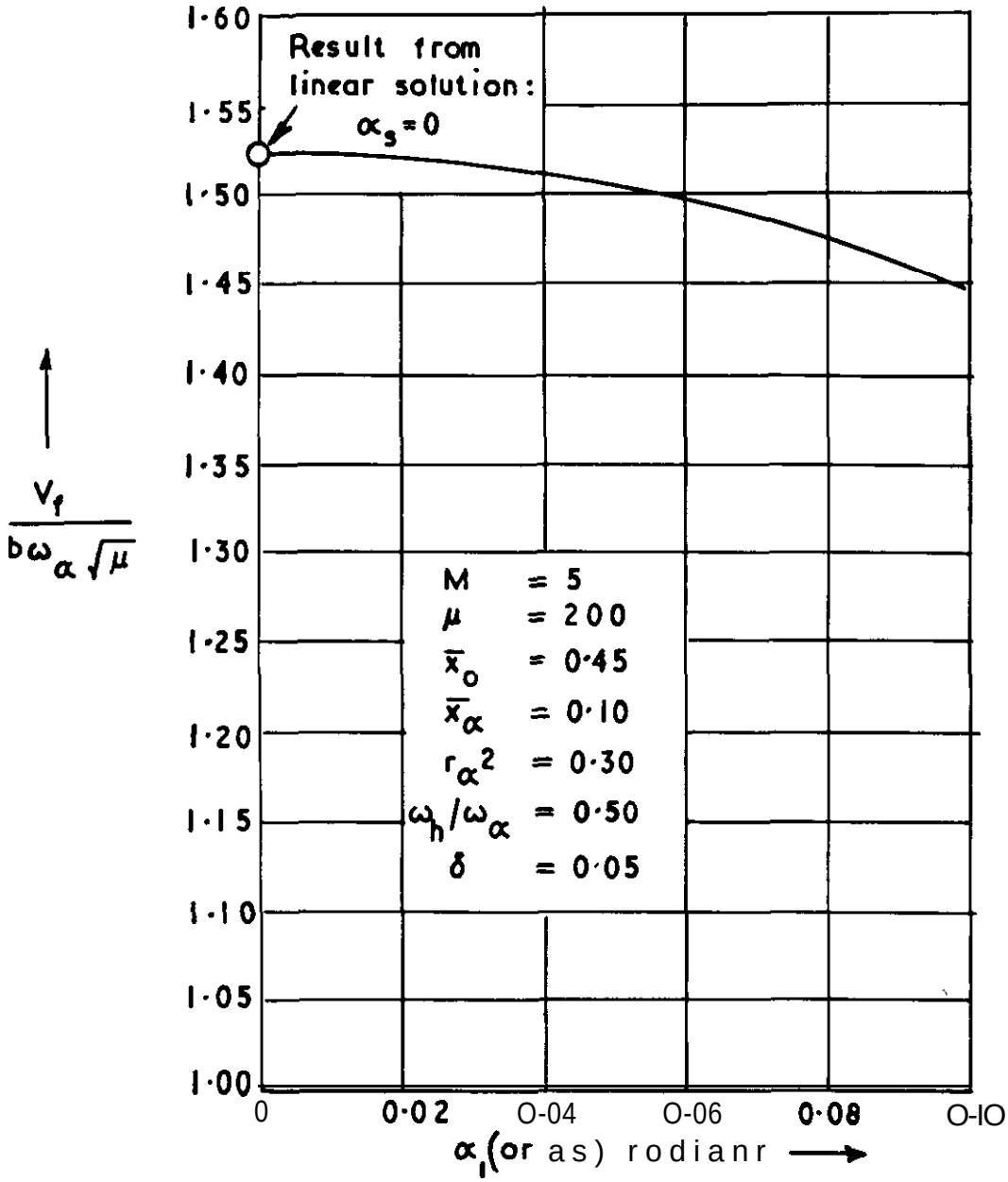

Flutter boundary for a typical wing section. Flutter index $V_f / b\omega_\alpha \sqrt{\mu}$ vs steady mean angle of attack a, or semi-amplitude of torsional oscillations a,

FIG. 47

From Fig. 5 of Ref.61

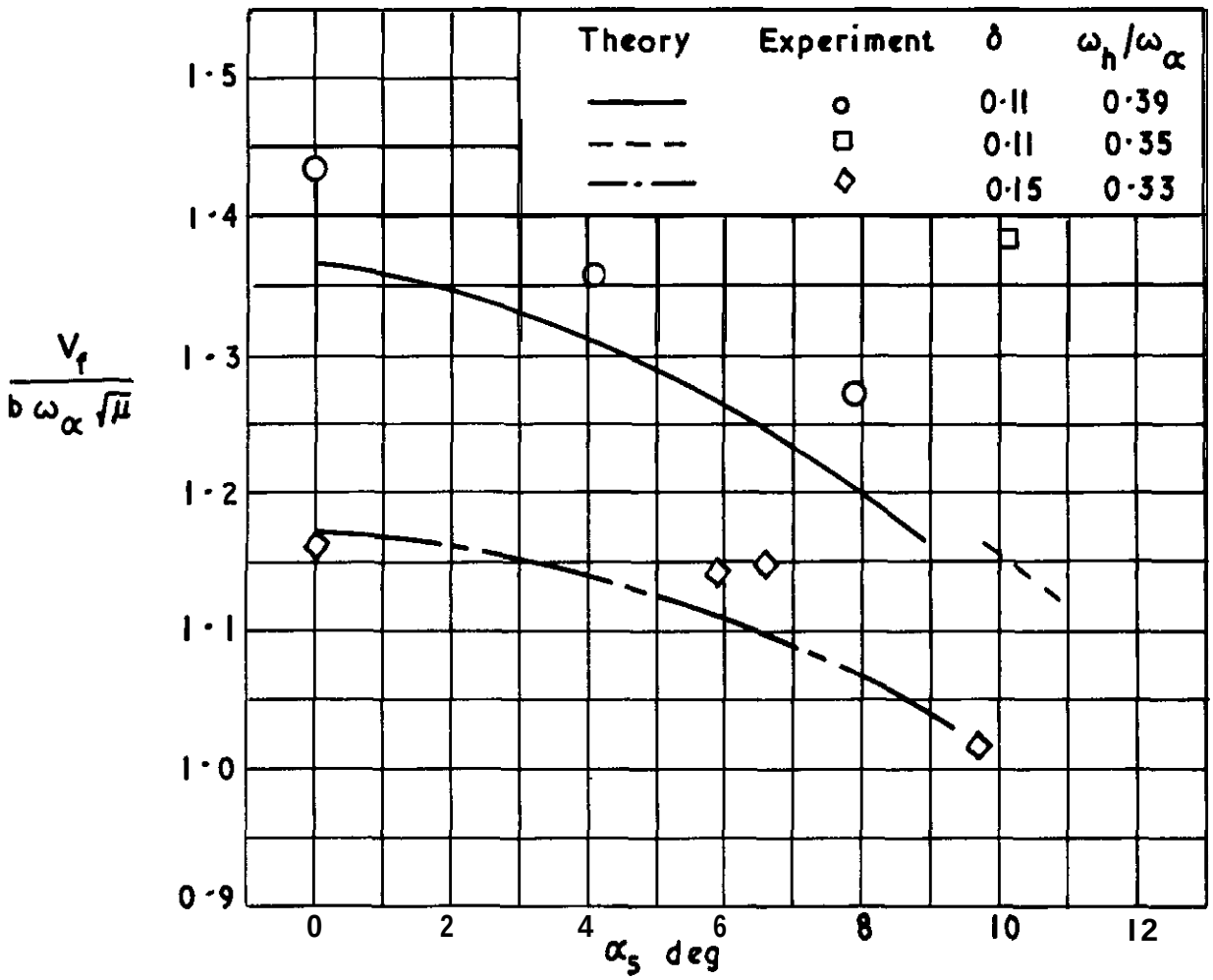

Experimental and calculated flutter results for wedge section at increasing angle of attack (M=10·0)

FIG. 48

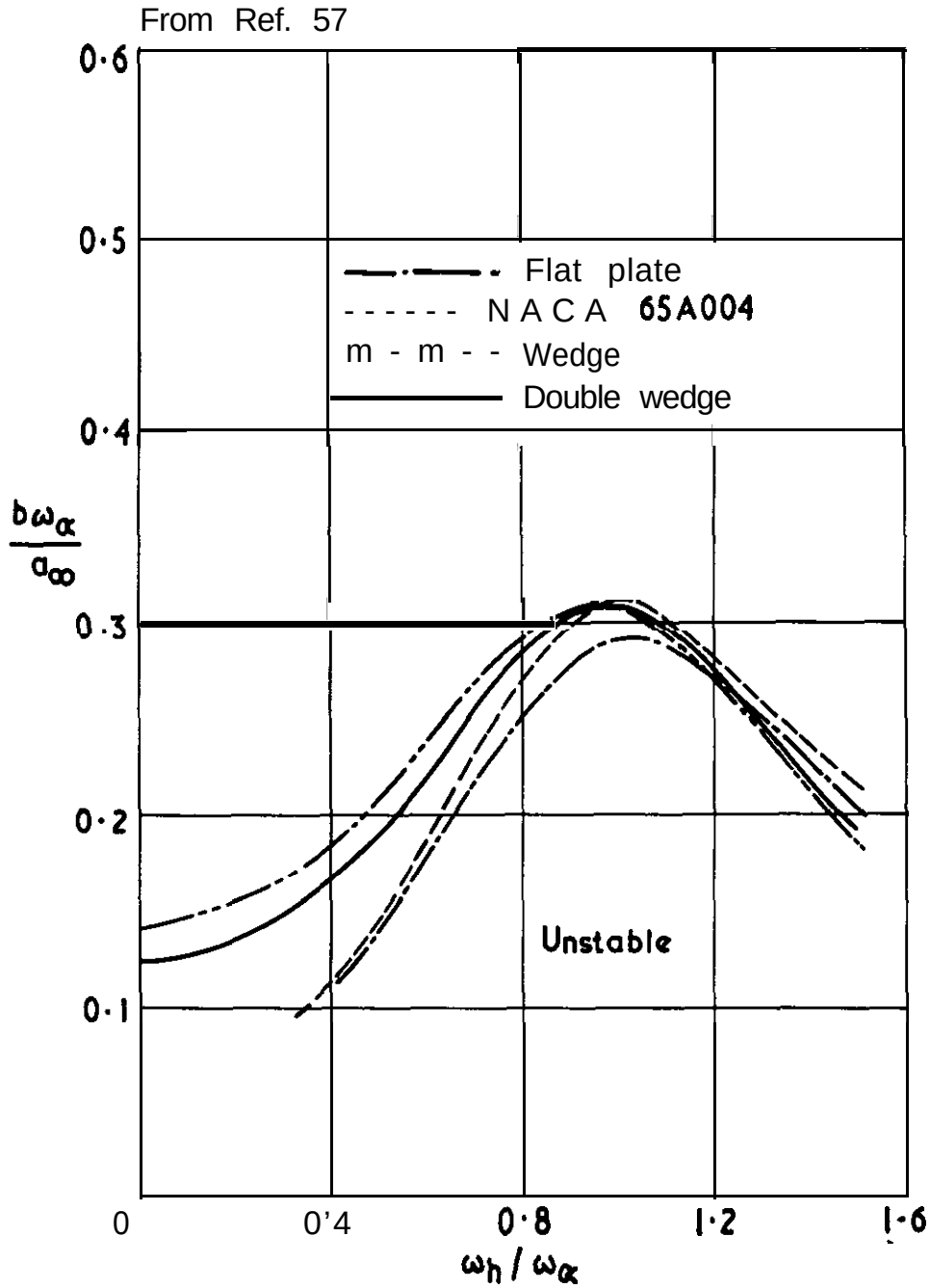

Effect of aerofoil shape on flutter speed of 4 per cent thick aerofoils

($M = 5$, $\mu = 250$, $\bar{r}_\alpha^2 = 0.25$, $\bar{x}_\alpha = 0{\cdot}1$, $\bar{x}_0 = 0.4$)

FIG. 49

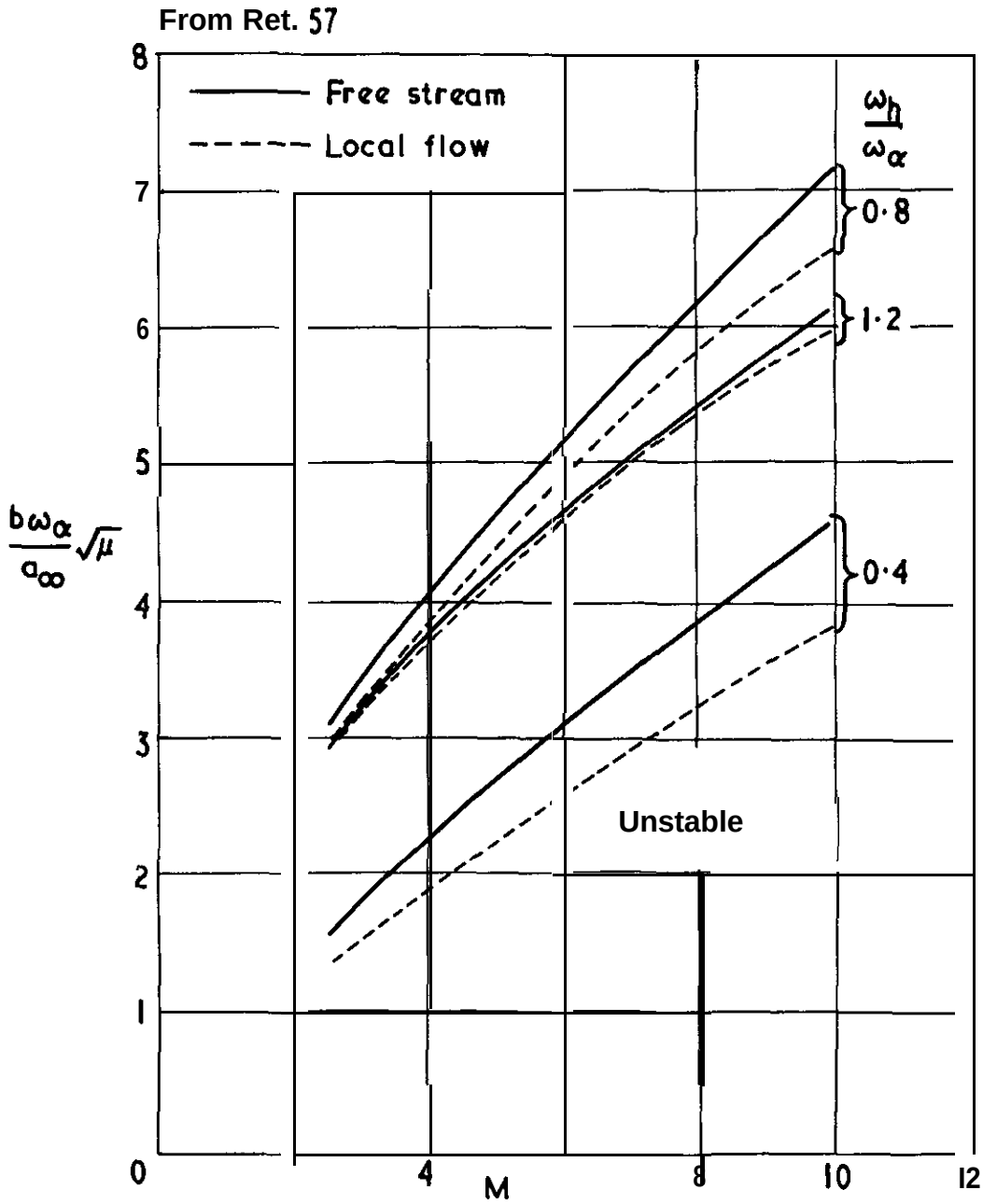

Effect of using local tlow conditions on flutter speed ot a 4 per cent double wedge ($\mu = 250$, $\bar{r}_\alpha^2 = 0{\cdot}25$, $\bar{x}_\alpha = 0{\cdot}1$, $\bar{x}_o = 0\ 4$)

FIG.50

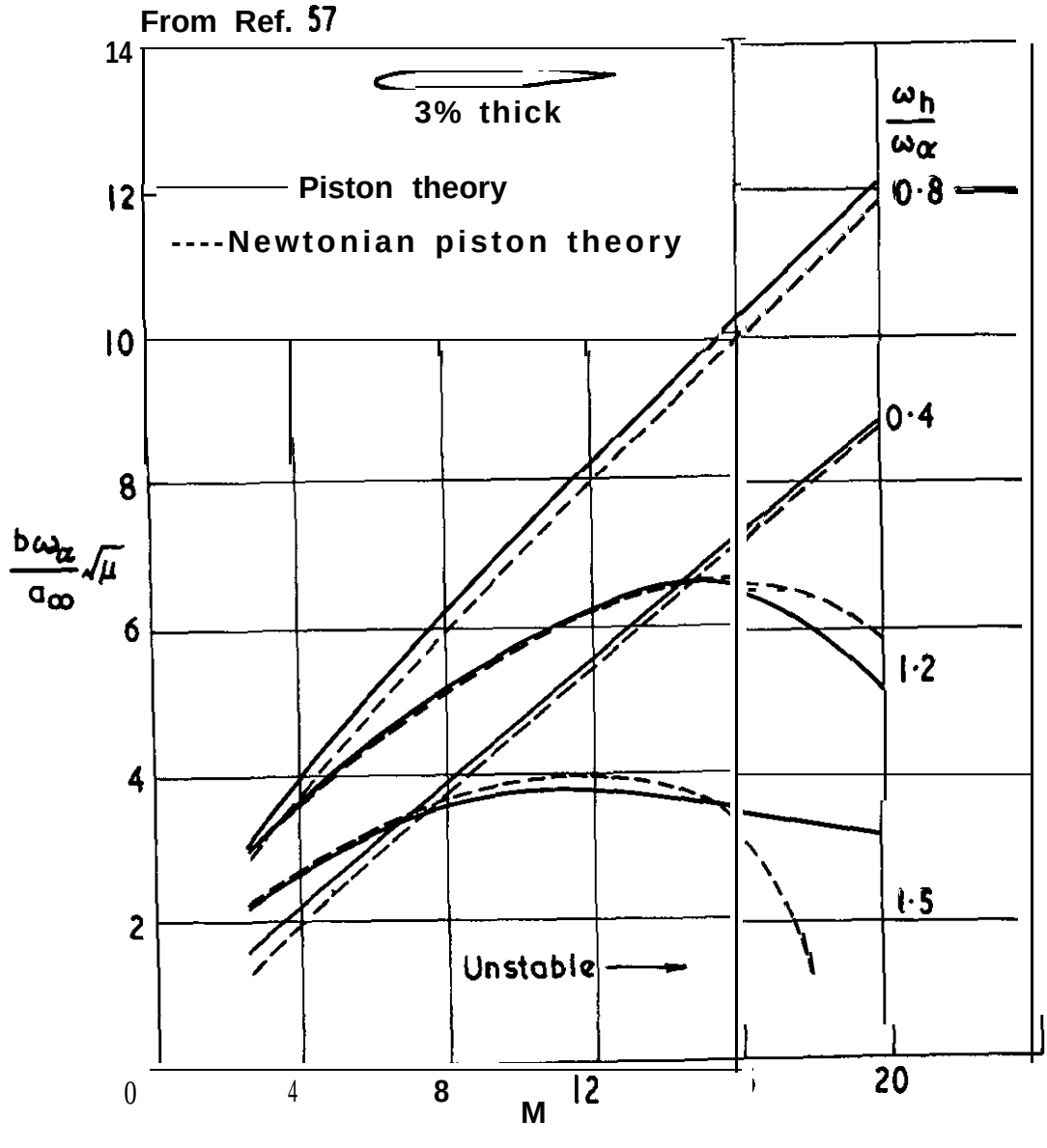

Flutter boundarias using piston theory and Newtonian-piston theory

$(\mu = 250,\ \bar{r}_\alpha^2 = 0{\cdot}25,\ \bar{x}_\alpha = 0{\cdot}1,\ \bar{x}_o = 0{\cdot}4)$

FIG. 51

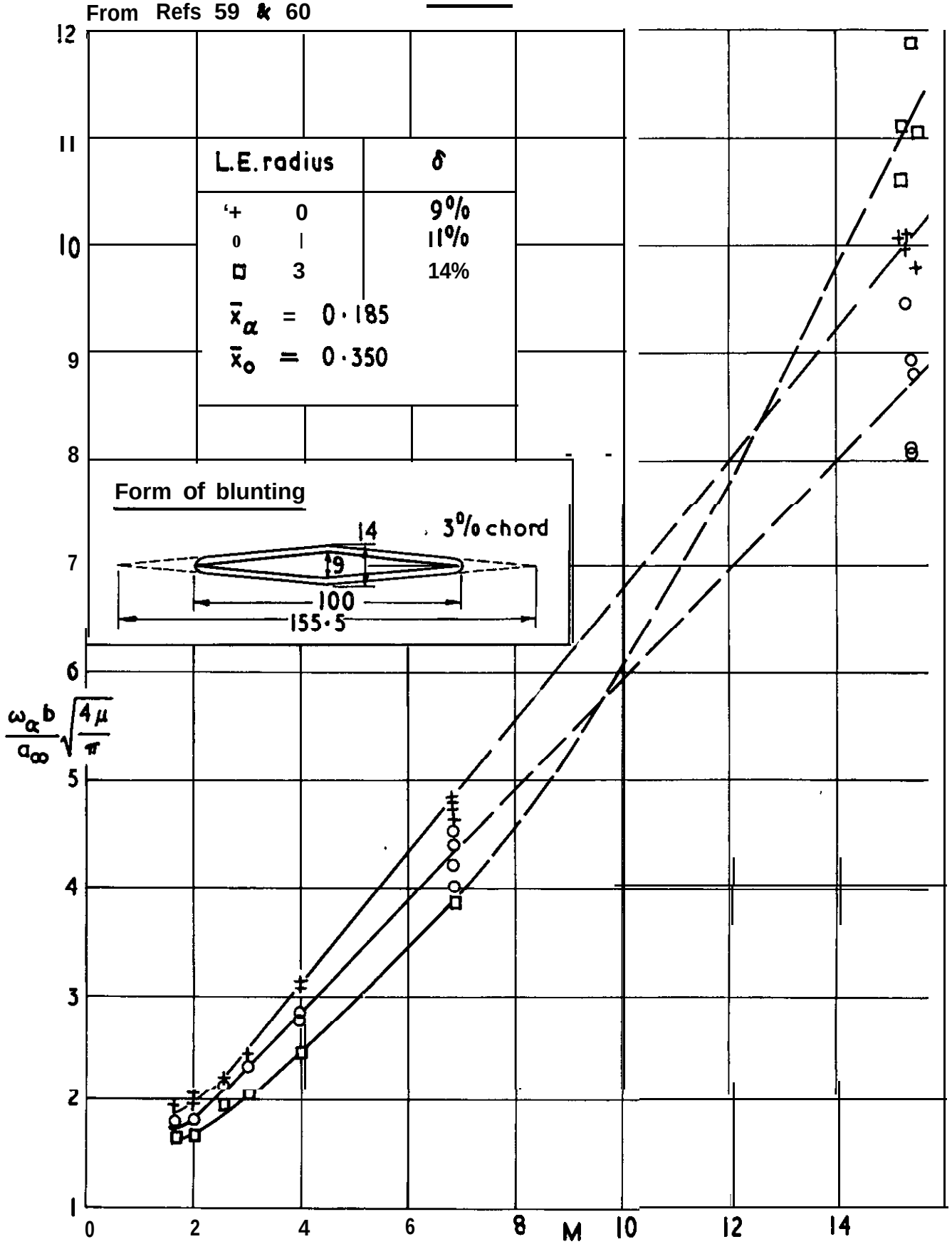

Variation of altitude stiffness parameter with Mach number for double wedge aerofoils with blunt leading edges

FIG. 52

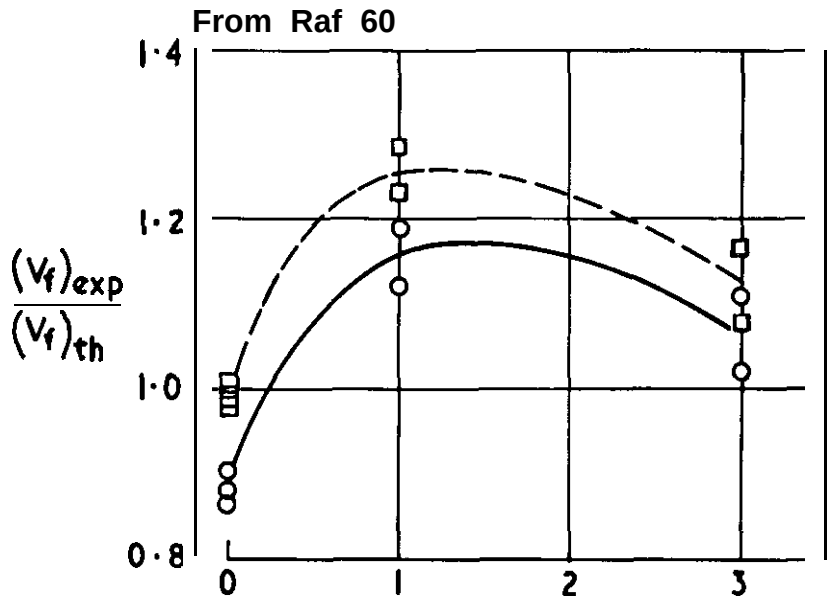

(a) 10 in. span model

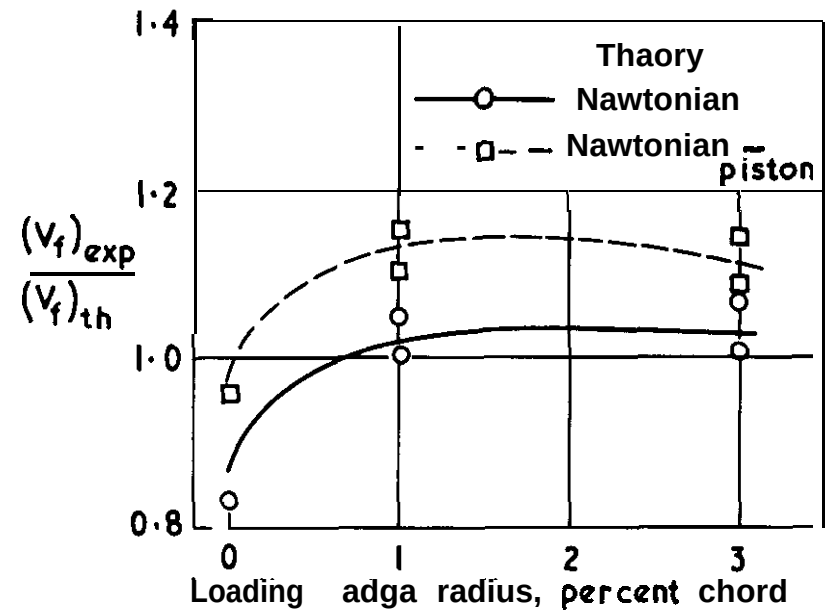

(b) 6in. span modal

Ratio of axparimantal to calculated fluttar velocity as a function of leading-adga radius at M = 15·4 for cantilavar wings (Tha tests show some effect of tunnal intarferenca)

FIG. 53

From Ref. 65

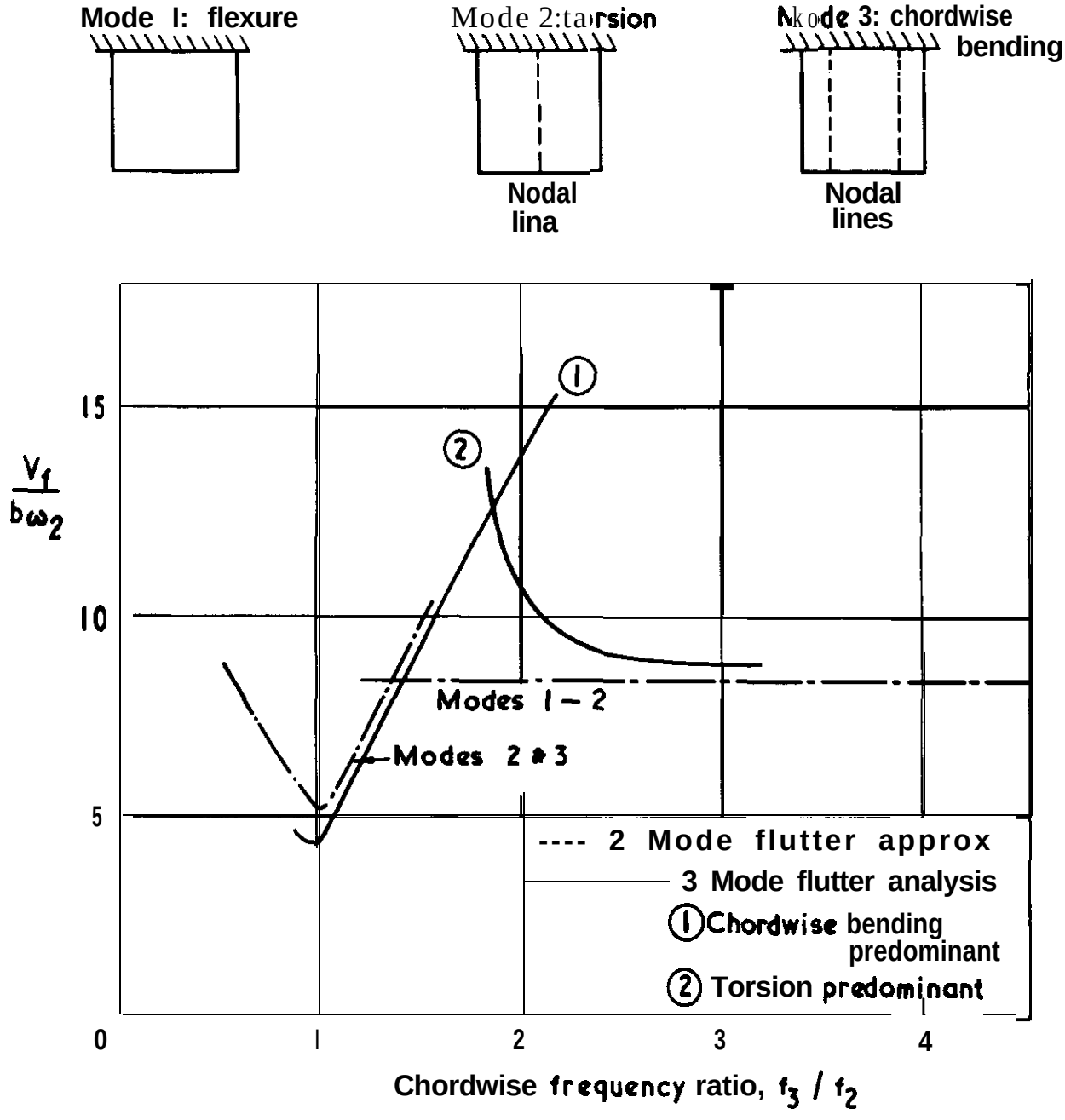

Flutter of hollow rectangular wing with uniform mass distribution

FIG. 54

From Ref. 65

Modes as in FIG.53

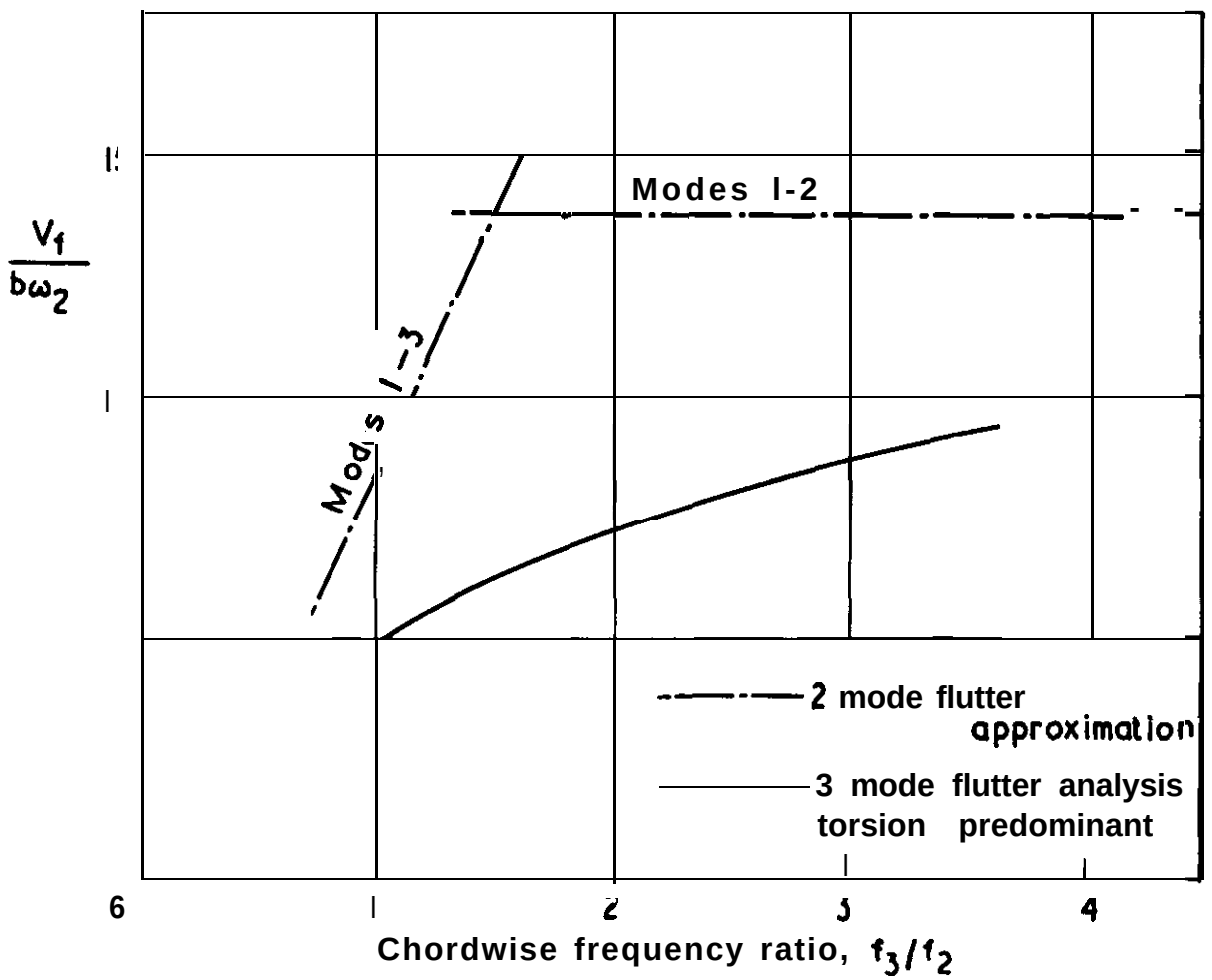

Flutter of solid section rectangular wing

From Fig.5 of Ref 58

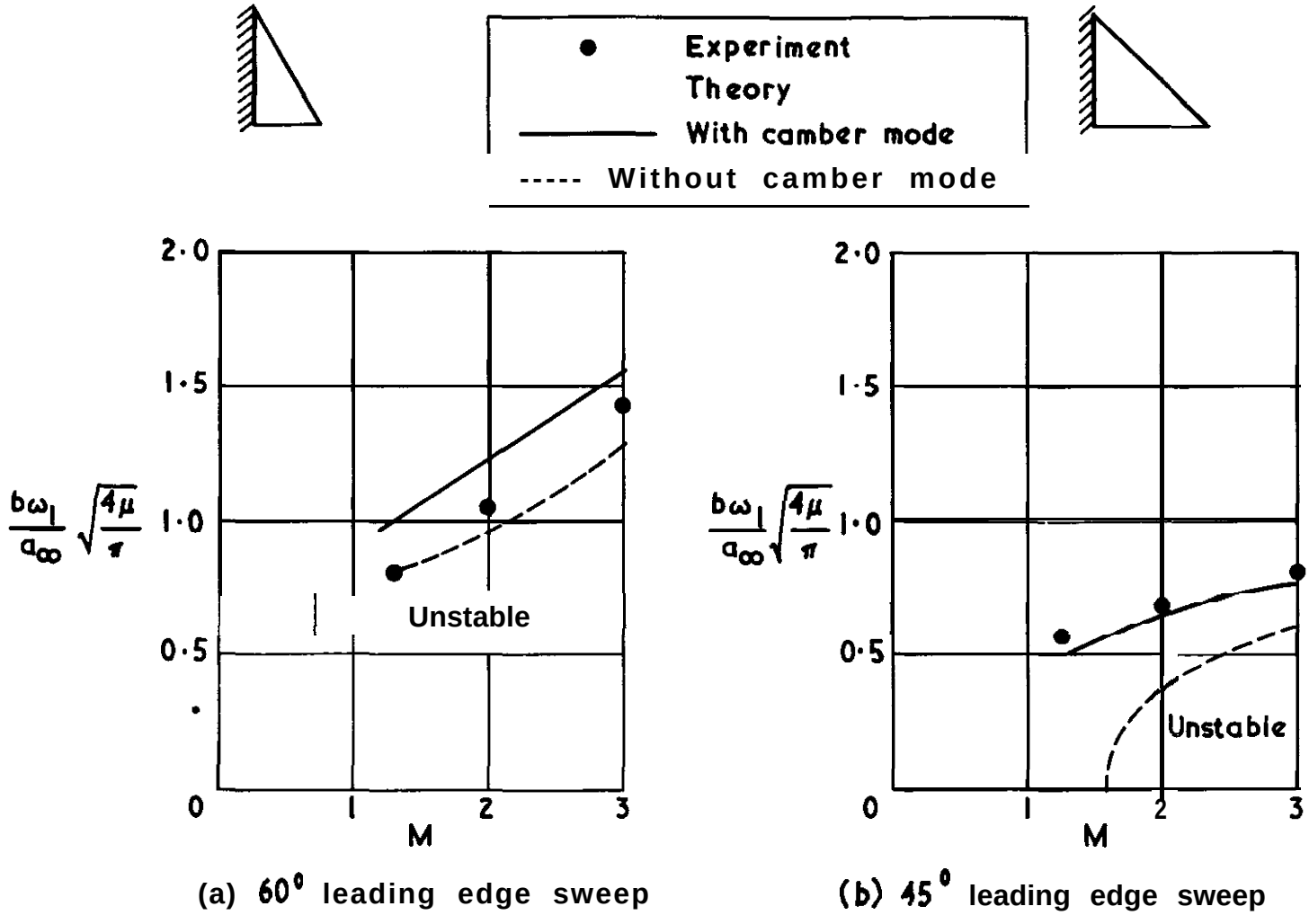

(a) 60° leading edge sweep

(b) 45° leading edge sweep

FIG. 55

Effect of camber modes on the flutter of delta wings

FIG. 56

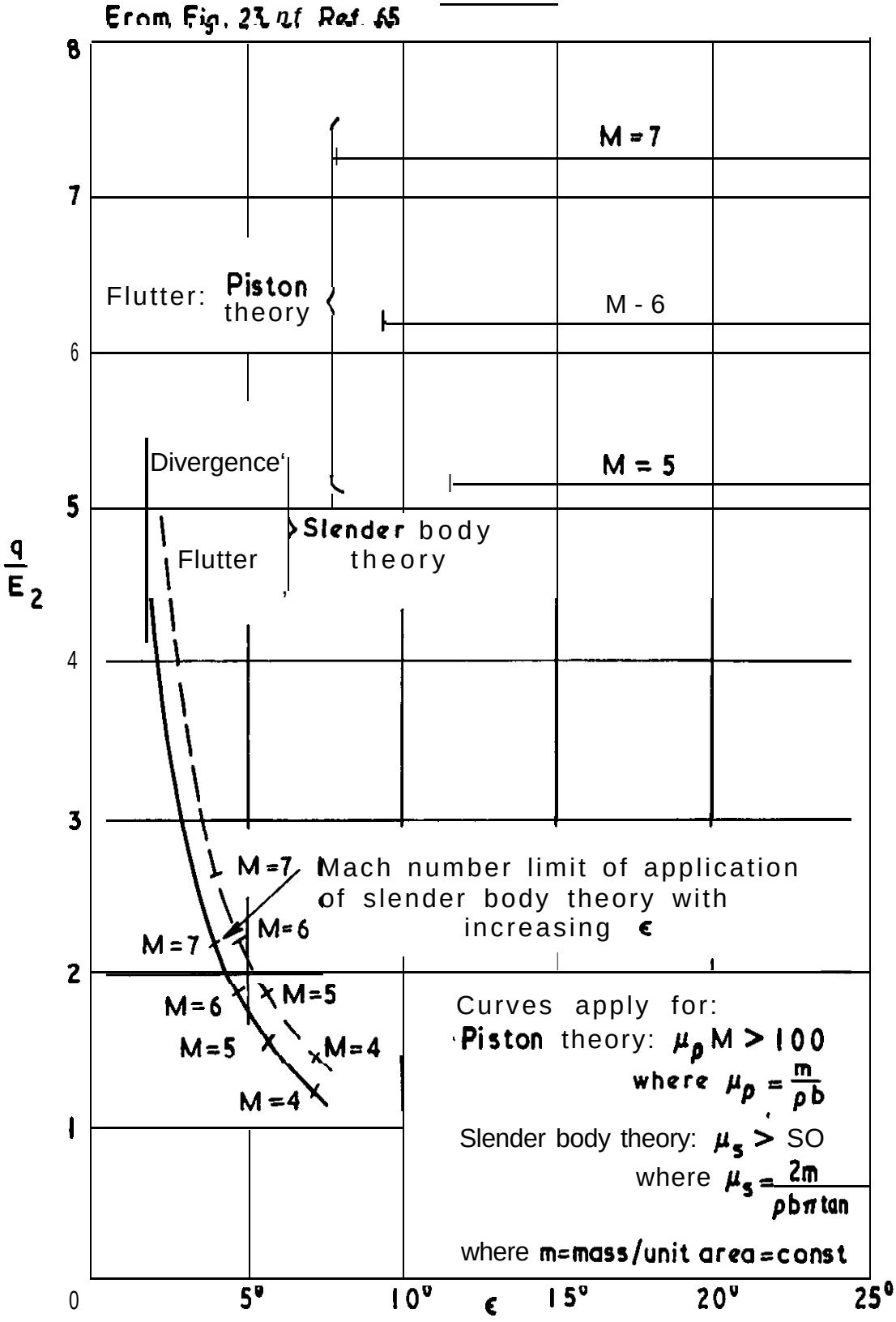

Summary of delta wing aeroelastic characteristics at high density ratios : Chordwise bendina onlv

FIG . 57

From Ref . 57

$\bar{\mu}(= m/l^3\rho) = 3\cdot0,\ \omega_h/\omega_\alpha = 0\cdot5,\ \bar{r}_\alpha^2 = (1-2\bar{x}_0)^2 + [(7/5)-2\bar{x}_0],\ \bar{x}_\alpha = (3/4) - \bar{x}_0$

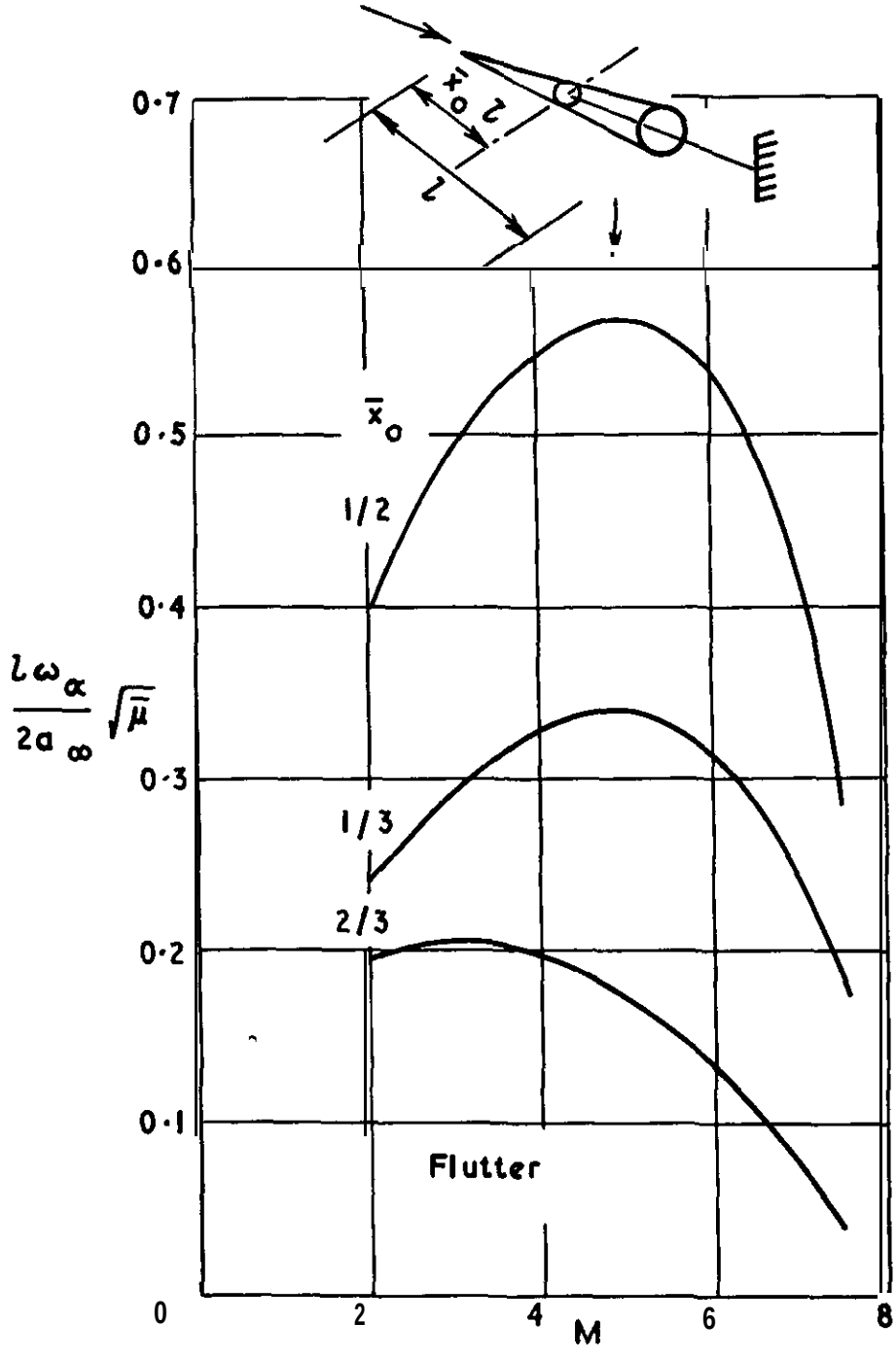

Effect of axis location on the flutter of a cone

FIG. 58

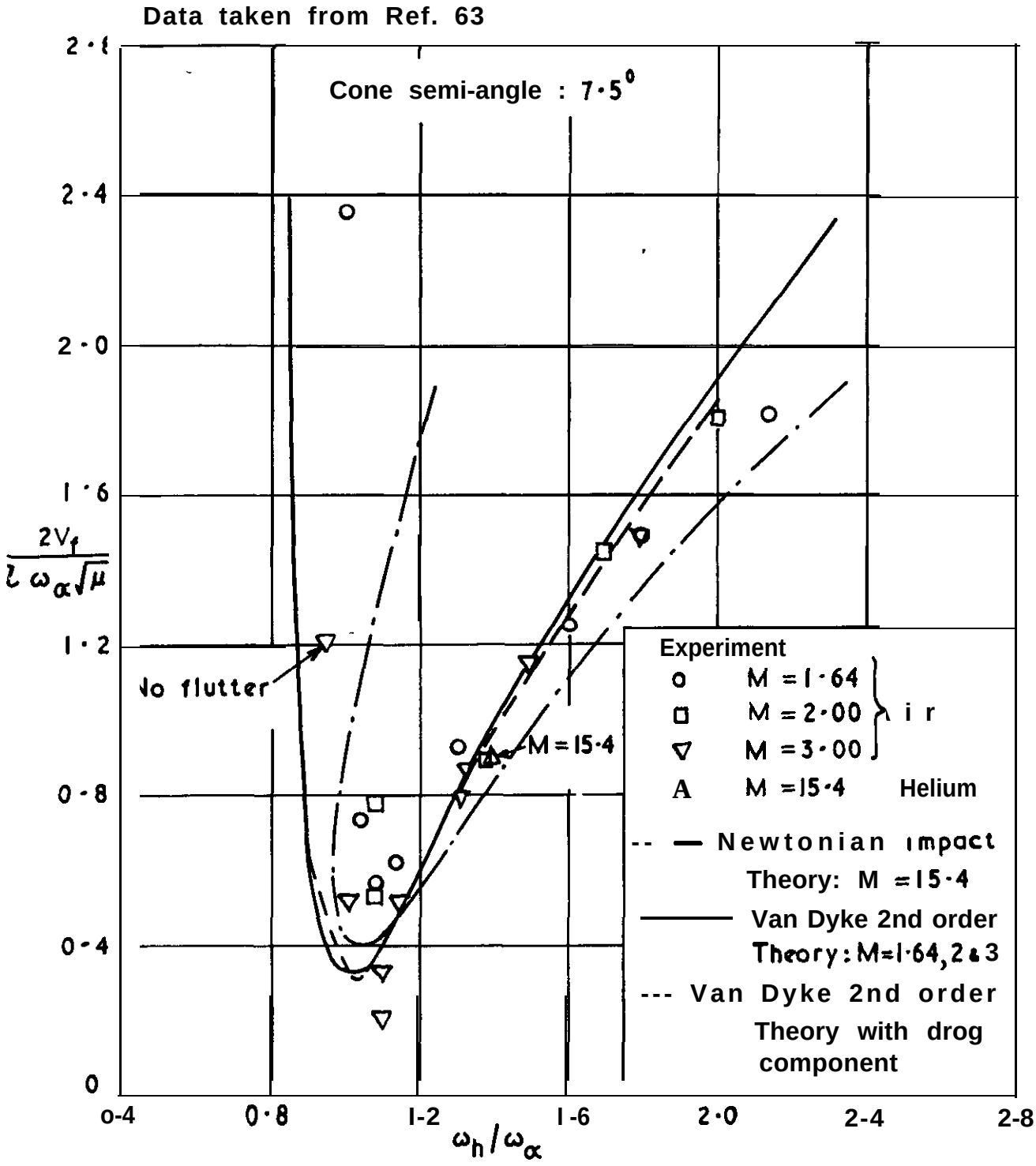

Flutter boundaries for slender cone at Mach numbers of 1·64, 2, 3 and 15·4

FIG. 59

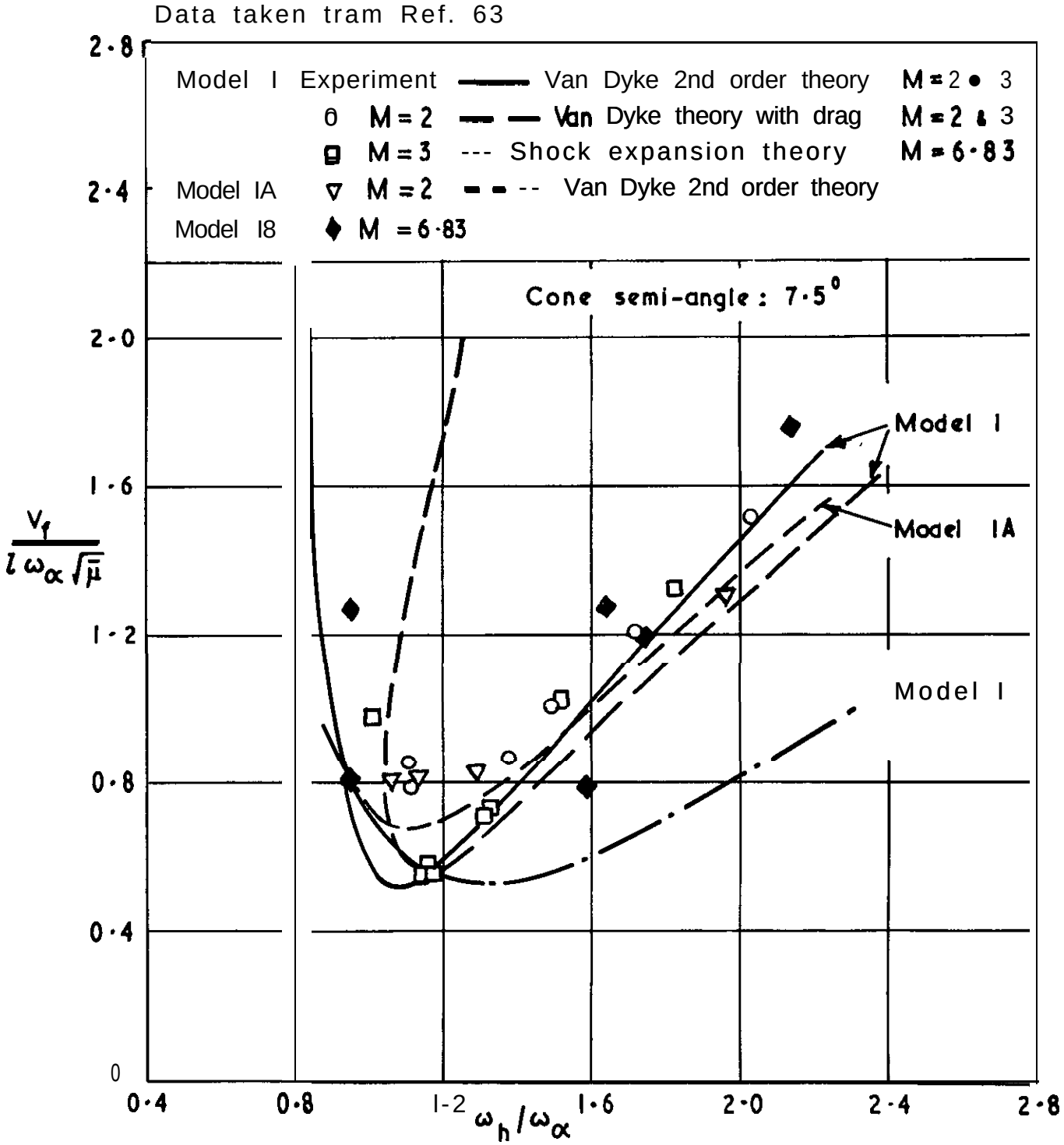

Note: Models similar geometrically differ slightly in mass, C.G. position and M.I. Flutter boundary for Model 1B from Van Dyke's theory lies between Models I and I A

Flutter boundaries for a slender cone at Mach numbers of 2, 3 and 6-83

FIG. 60

From Fig. I2 of Ref. 69

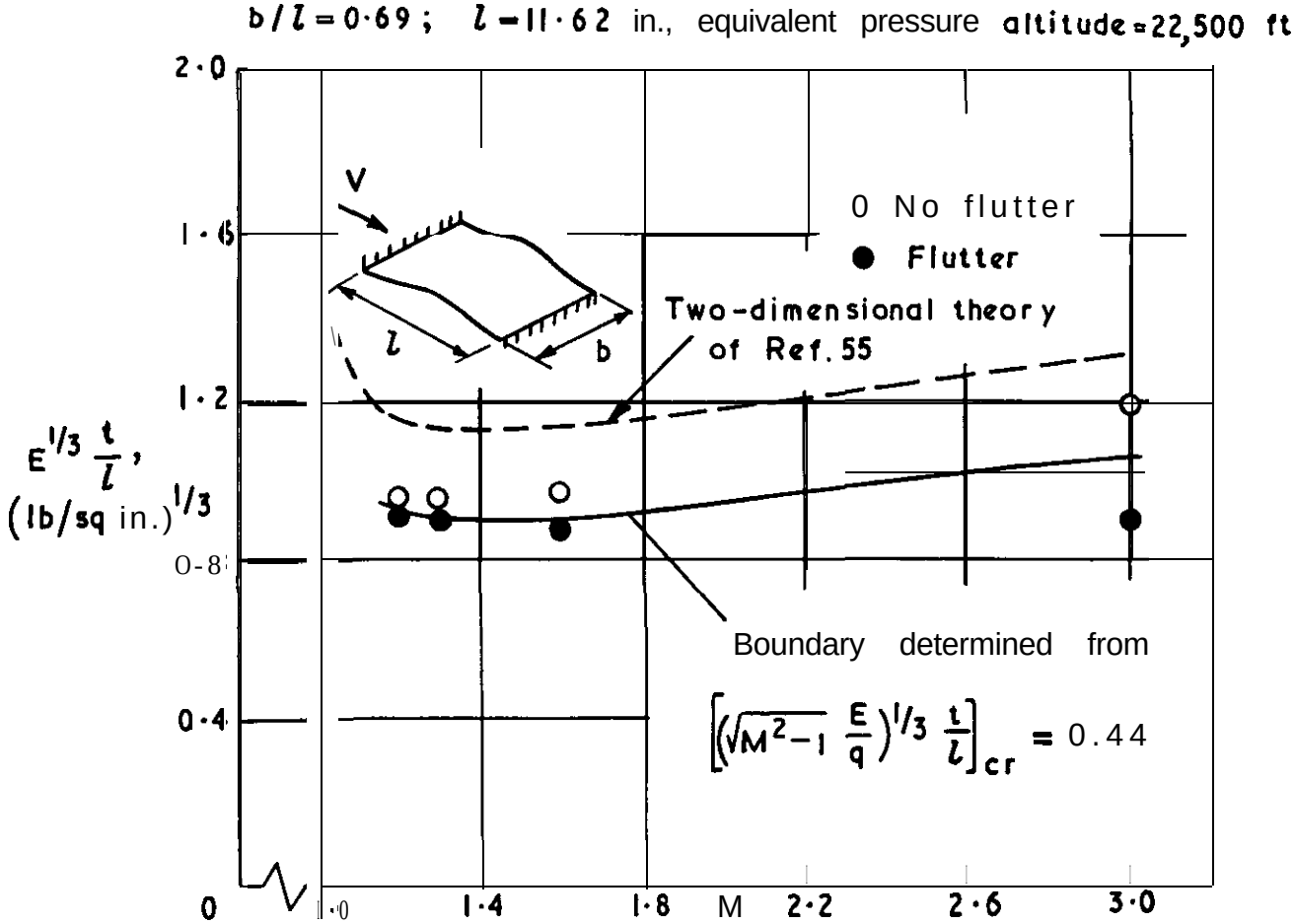

Effect of Mach number on panel flutter at zero pressure differential. Buckled panels clamped on the front and rear edges

FIG. 61

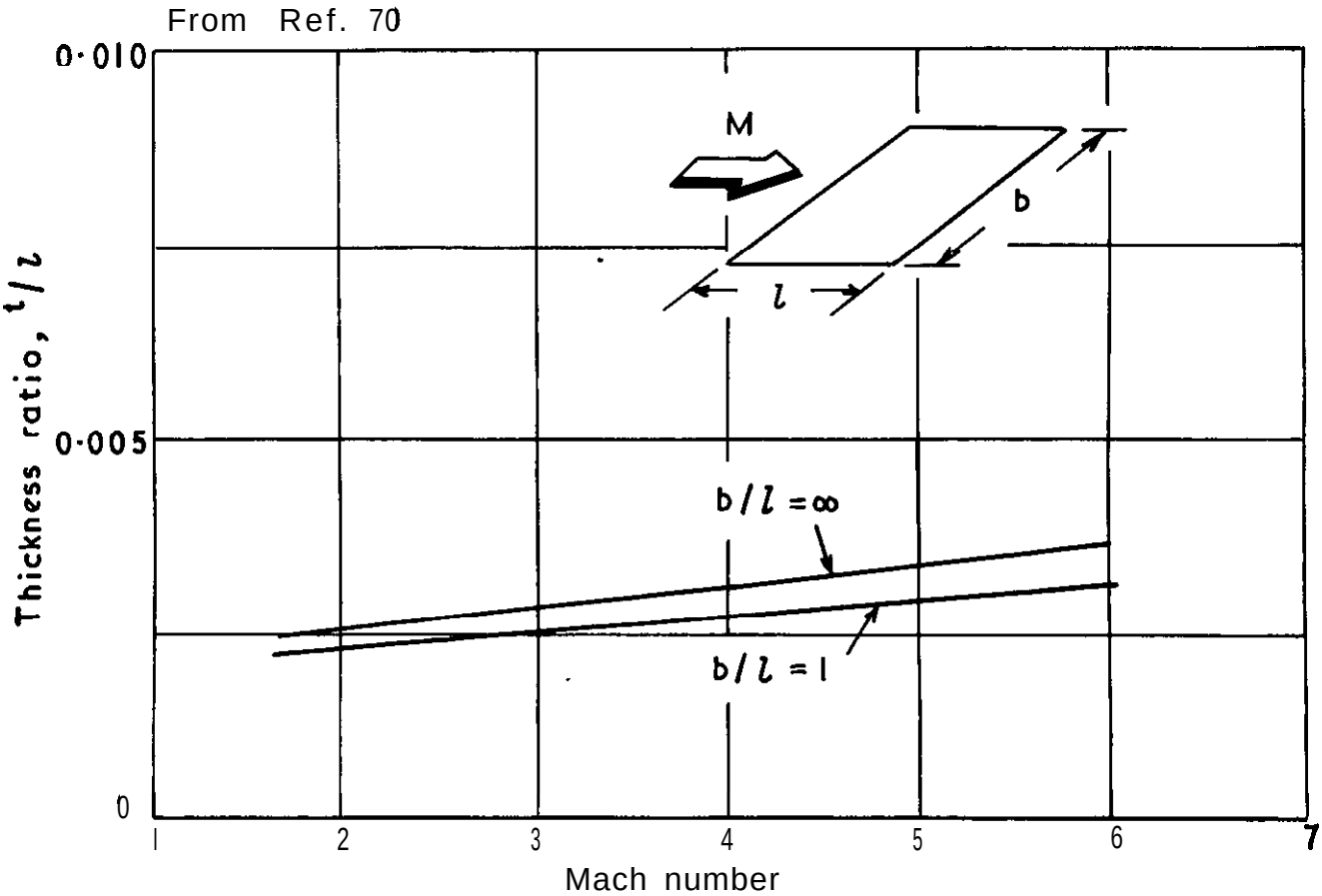

Thickness requirement for unstressed aluminum panels at 50,000 feet, Ref. 70

FIG. 62

From Ref.71

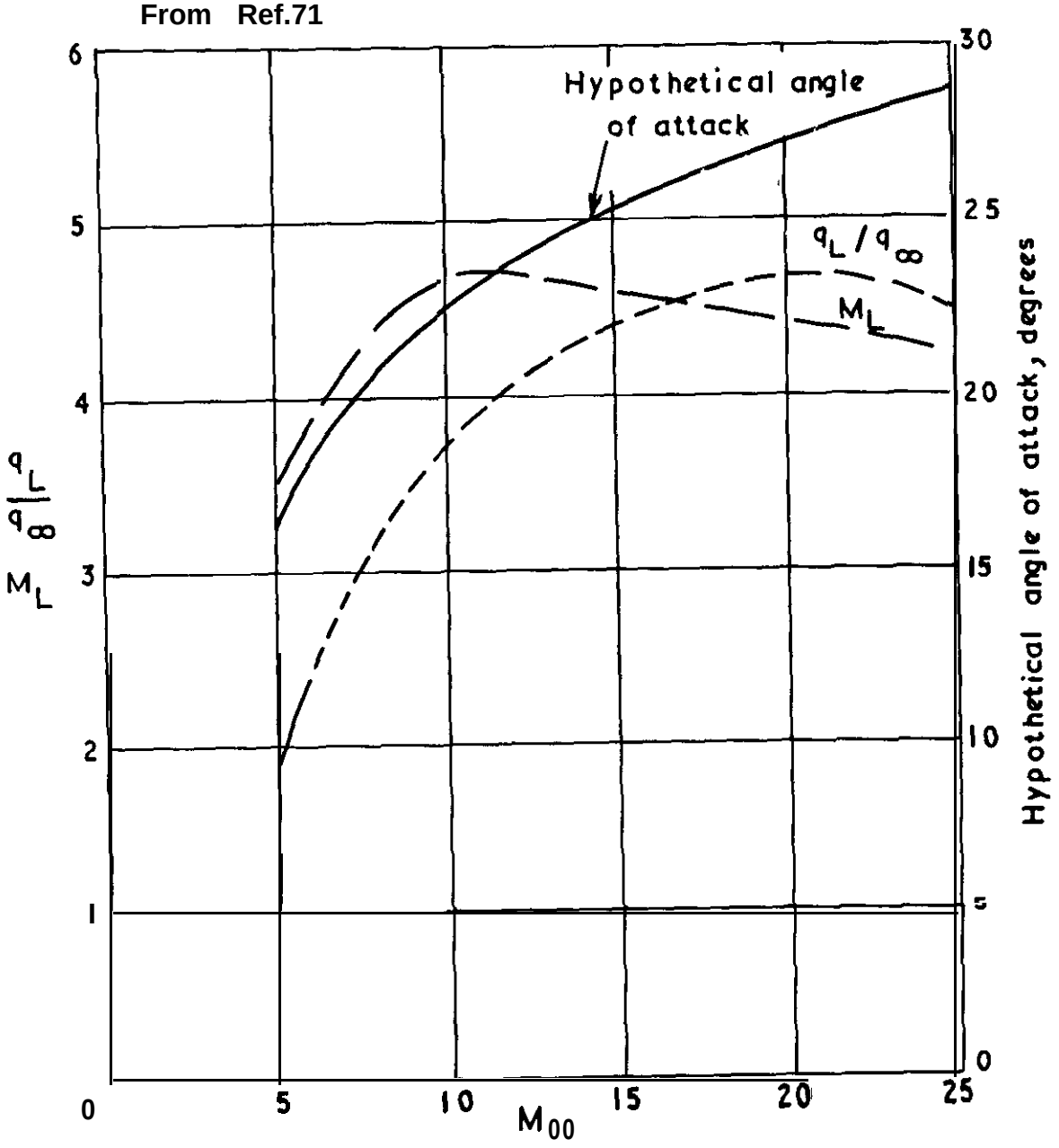

Local Mach number and dynamic pressure for a hypothetical trajectory

FIG.63

From Ref. 70

Panel parameter $= \frac{-N_x l^2}{\pi^2 D} - 2\left(\frac{l}{b}\right)^2$ where $D = \frac{12(1-\nu^2)}{Et^3}$

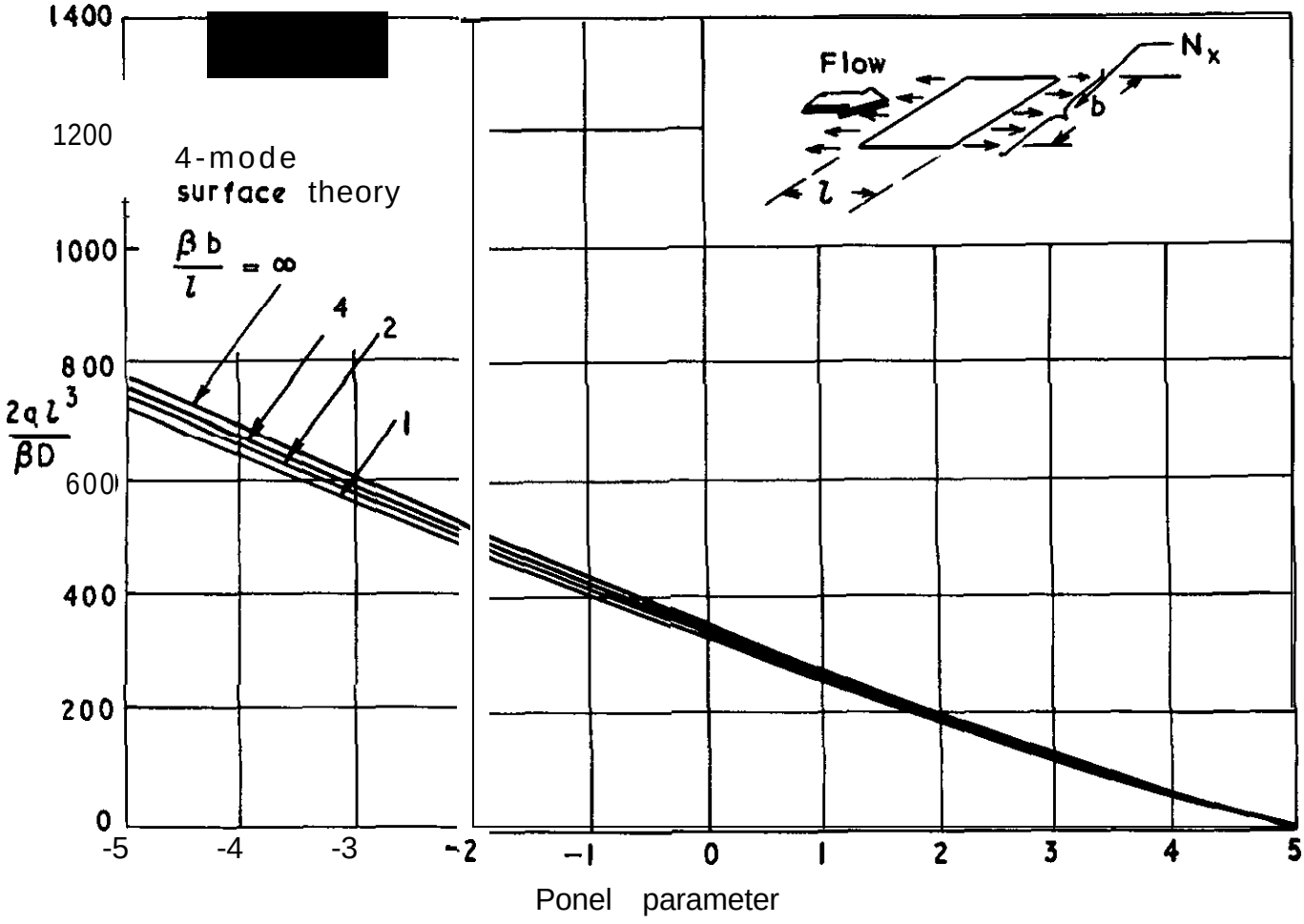

Variation of the ratio of critical dynamic pressure to bending rigidity with the parameter $-N_x l^2/(\pi^2 D) - 2(l/b^2)$

FIG. 64

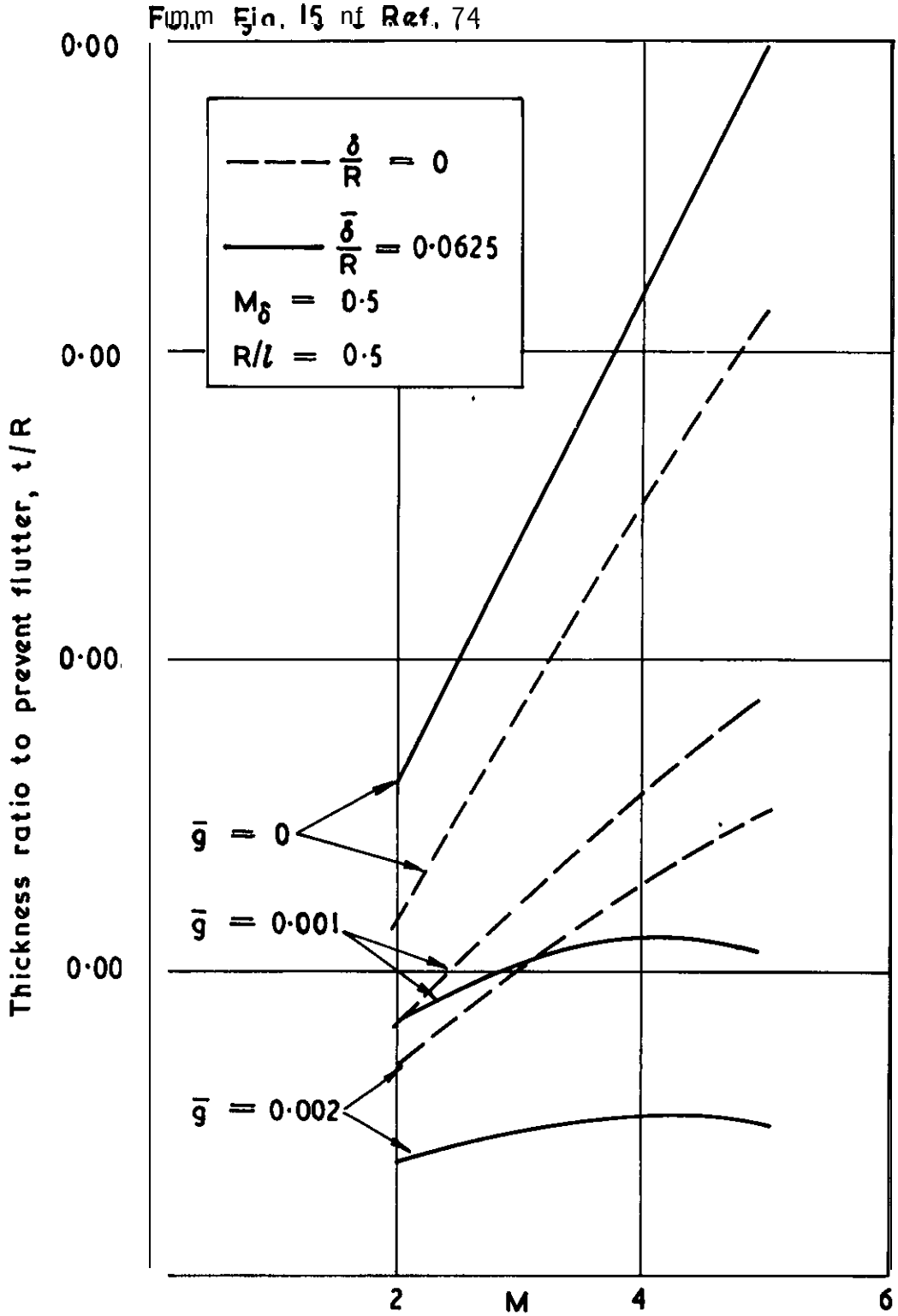

Effect of material damping $\bar{g}$ and boundary layer thickness δ on shell thickness required to prevent symmetric flutter. Cooper cylinder at altitude 50 000 ft

FIG.6.5.

Fig. 18 for Ref. 74

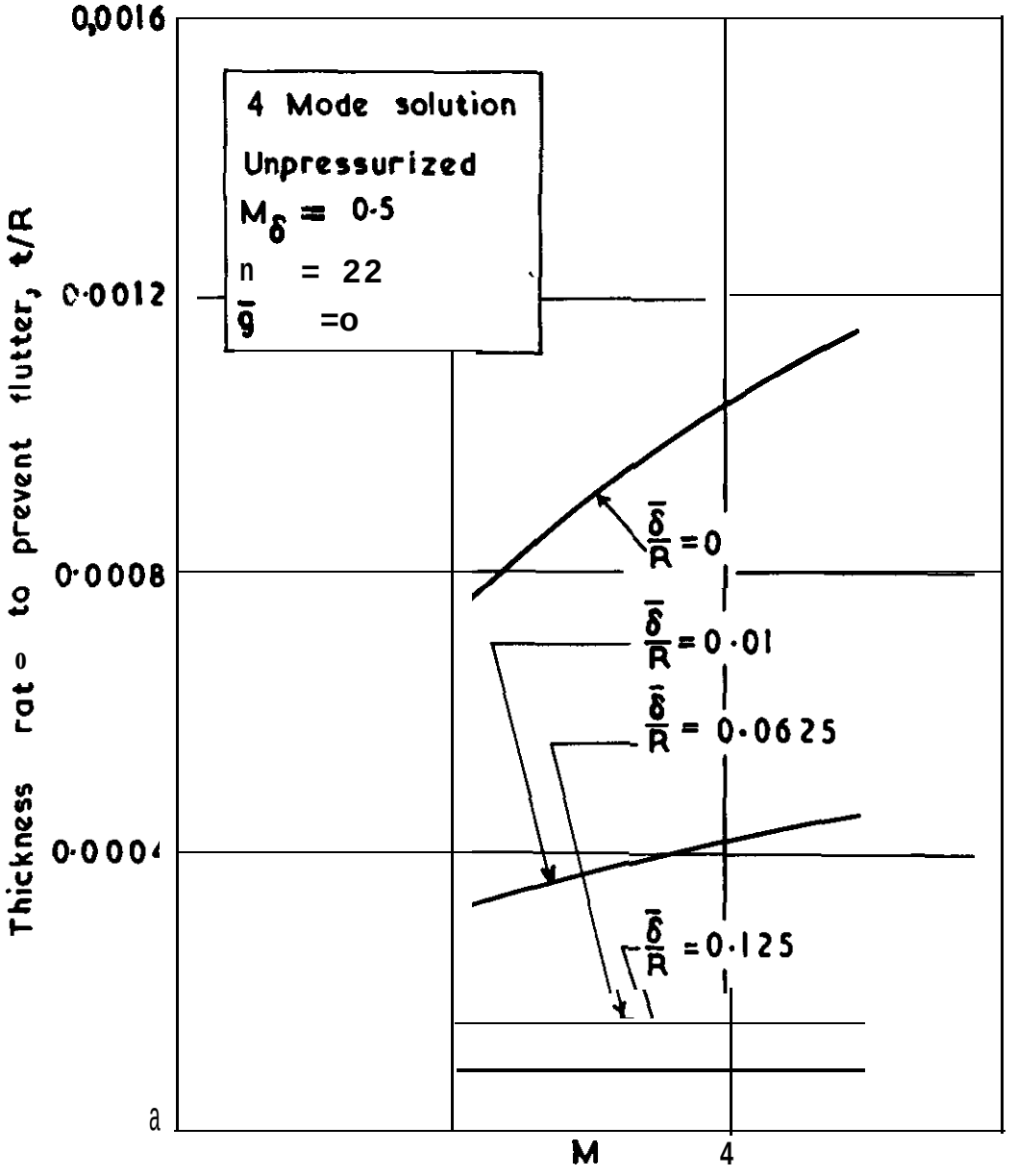

Effect of boundary layer thickness on the shell thickness required to prevent flutter in scallop mode. Copper cylinder at 50,000 ft. altitude.

A.R.C. C.P. No.901
March, 1965
Wood, B. M.

A SURVEY OF UNSTEADY HYPERSONIC FLOW PROBLEMS

After giving general information on hypersonic flows, flight conditions and vehicles, the report reviews work on the analysis of unsteady hypersonic flows, analytical studies of the dynamic stablllty of hypersonic vehicles, and experimental and analytical work on flutter at hypersonic speeds. 0" this basis it then examines the need for research and suggests lines that research should follow.

The chief conclusion is that the quasi-steady analysis of unsteady hypersonic flows may be adequate for the practical purposes of dynamic stablllty and flutter analysis. It is suggested that research should be directed to finding the degree or inaccuracy involved I" quasi-steady estimates of the unsteady aerodynamic forces, and the sensitivity or dynamic stablllty and flutter analyses to inaccuracies I" these forces.

P.T.O.

A.R.C. C.P. No.901
March, 1965
Wood, B. M.

A SURVEY OF UNSTEADY HYPERSONIC FLOW PROBLEMS

After giving general information on hypersonic flows, flight conditions and vehicles, the report reviews work on the analysis of unsteady hypersonic flows, analytical studies of the dynamic stablllty of hypersonic vehicles, and experimental and analytical work on flutter at hypersonic speeds. On thls basis it then examines the need for research and suggests lines that research should follow.

The chief conclusion 18 that the quasi-steady analysis of unsteady hypersonic flows may be adequate for the practical purposes of dynamic stability and flutter analysis. It is suggested that research should be directed to finding the degree Or inaccuracy Involved 1" quasi-steady estimates of the ""steady aerodynamic forces, and the sensitivity or dynamic stablllty and flutter analyses to inaccuracies I" these forces.

P.T.O.

A.R.C. C.P. No.901
March, 1965
Wood, B. M.

A SURVEY OF UNSTEADY HYPERSONIC FLOW PROBLEMS

After giving general information on hypersonic flows, flight conditions and vehicles, the report reviews work on the analysis of unsteady hypersonic flows, analytical studies of the dynamic stability of hypersonic vehicles, and experimental and analytical work on flutter at hypersonic speeds. On this basis it then examines the need for research and suggests lines that research should follow.

The chief conclusion 18 that the quasi-steady analysis or unsteady hypersonic flows may be adequate for the practical purposes of dynamic stability end flutter analysis. It is suggested that research should be directed to finding the degree or inaccuracy involved 1" quasi-steady estimates of the unsteady aerodynamic forces, and the sensitivity of dynamic stablllty and rlutter analyses to inaccuracies in these forces.

P.T.O.

In structure, the report consists of the general survey and conclusions, together with a number of Appendices which review various aspects in detail end which give the information and references on which Lhe statements in the general survey are based.

In structure, the report consists ot the general survey end conclusions, together with a number of Appendices which review various aspects in detail end which give the information and references on which the statements in the general survey are based.

In structure, the report cons ists of the general survey and conclusions, together wlth a number of Appendices which review various aspects in detail and which give the information and references on which the statements in the general survey are based.

Printed and published by
HER MAJESTY'S STATIONERY OFFICE

To be purchased from
49 High Holborn, London W C I
423 Oxford Street, London W I
13A Castle Street, Edinburgh 2
109 St Mary Street, Cardiff
Brazennose Street, Manchester 2
50 Fairfax Street, Bristol 1
35 Smallbrook, Ringway, Birmingham 5
80 Chichester Street, Belfast 1
or through any bookseller

Printed in England

S.O. Code No. 23.9017